Doctoral Dissertations 1896 - February 2014

1-1-1990

# Radio observations of several interstellar molecules.

Y. C. Minh
*University of Massachusetts Amherst*

Recommended Citation

RADIO OBSERVATIONS OF SEVERAL INTERSTELLAR MOLECULES

A Dissertation Presented

by

YOUNG CHOL MINH

Submitted to the Graduate School of the
University of Massachusetts in partial fulfillment
of the requirements for the degree of

DOCTOR OF PHILOSOPHY

February 1990

Department of Physics and Astronomy
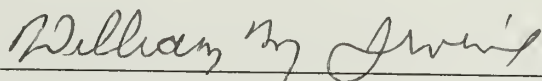
RADIO OBSERVATIONS OF SEVERAL INTERSTELLAR MOLECULES
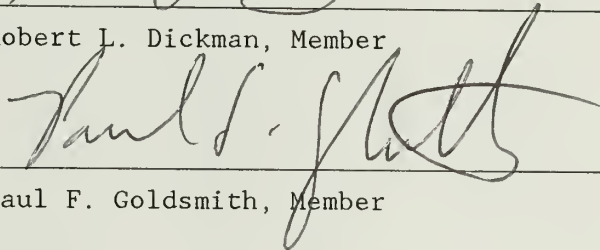
A Dissertation Presented

by

YOUNG CHOL MINH

Approved as to style and content by:

_____

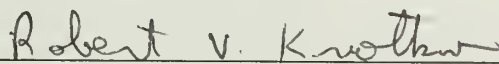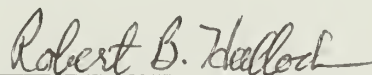William M. Irvine, Chairman of Committee

_____

Robert L. Dickman, Member

_____

Paul F. Goldsmith, Member

_____

Robert V. Krotkov, Outside Member

_____

Robert B. Hallock, Department Head
Department of Physics and Astronomy

# ACKNOWLEDGEMENTS

their support, nothing would have worked properly to finish my degree successfully and smoothly.

I thank my parents for their love, support, and encouragement they have given me throughout the entire span of my life. I really don't know how to express my appreciation to them. "Thank you, Mom and Dad !" I also thank my mother-in-law who has prayed for our health and happiness with constant love. I thank my brothers and sisters for their love and encouragement. I thank my son, Hyun-Sik, who has been a constant source of joy during our living at Amherst. I would like to express a special appreciation to my wife, Kyung-Sun, who has sacrificed her achievements in Korea and endured tough time at Amherst, from my heart for her love and faith in me.

Although it is a pleasure to say "*it's done !*", I know it is not the end but just a start. Good-bye everybody and good-bye Amherst ! Thank you !

ABSTRACT

RADIO OBSERVATIONS OF SEVERAL INTERSTELLAR MOLECULES

FEBRUARY 1990

YOUNG CHOL MINH

B.S., M.S., SEOUL NATIONAL UNIVERSITY

Ph.D., UNIVERSITY OF MASSACHUSETTS

Directed by Professor William M. Irvine


We present observations of rotational transitions for several interstellar molecules whose formation may be related to grain processes and discuss their implications for interstellar chemistry.

Interstellar hydrogen sulfide has been observed at fractional abundances $f(H_2S) \sim 10^{-9}$ relative to $H_2$ towards cold, dark clouds, while its abundance is enhanced by a factor of 1000 in the Orion hot core and the plateau. $H_2S$ may be evaporating from the grain mantles in the hot core, and even in the cold, dark clouds, grain surface reactions may be responsible for the gas-phase $H_2S$ abundances. We also derive an upper limit for the HDS abundance $[HDS]/[H_2S] \leq 6 \times 10^{-4}$ in the Orion hot core.

$H_2CS$ ortho-to-para ratios have been observed to be $\sim 1.8$ towards TMC-1, which may suggest that $H_2CS$ is in equilibrium with the expected grain temperaure (10 K) and gas-grain exchanges are taking place effectively in cold, dark clouds. We derive a ratio of $\sim 3$, the statistical value, for Orion(3NlE) and NGC7538, and $\sim 2$ for Orion(KL).

We derive upper limits of the ethyl cyanide column densities of $\sim 3 \times 10^{12}$ cm$^{-2}$ towards TMC-1 and L134N. Together with the detection for vinyl cyanide, there may be no necessity of invoking grain surface synthesis for these highly saturated species in cold clouds, but the desorption processes seem to be quite inefficient for these heavy molecules.

Finally, we have surveyed HOCO$^+$ as a tracer of interstellar CO$_2$ towards many galactic sources, and derive $f(\text{HOCO}^+) \sim 10^{-8} - 10^{-9}$ in the Galactic center and $\leq 10^{-10}$ for cold dark clouds. The observed abundance of HOCO$^+$ in the Galactic center is $\sim 3$ and $\sim 1$ orders of magnitude larger than that predicted by ion-molecule chemistry and shock chemistry, respectively. UV photolysis of grain mantles may produce CO$_2$ efficiently, resulting in a large abundance of HOCO$^+$ in the Galactic center.

Interstellar grains are thought to play crucial roles in the chemistry of interstellar molecular clouds, and our results give some constraints on the *highly uncertain* grain processes, as well as on the gas phase processes.

TABLE OF CONTENTS

LIST OF TABLES

LIST OF FIGURES

CHAPTER 1

INTRODUCTION

1.1 <u>Overview</u>

Interstellar molecules have been used as important probes of
the physical and chemical conditions of various types of objects in
the universe since the first detection of diatomic radicals and ions
in the 1930's and 40's.   The molecules in the interstellar medium
(ISM) are indeed more than probes; they "provide cooling and heating
pathways which govern cloud evolution, including the enhancement or
supression of instabilities leading toward clump formation,
fragmentation, and ultimately the formation of protostars" (Irvine,
Goldsmith, and Hjalmarson 1987).   Thus, the evolution of a cloud
depends on its chemical conditions as well as on its physical
conditions.

Molecular hydrogen, the most abundant and important species in
interstellar space, is believed to form on grain surfaces
(Hollenbach and Salpeter 1971).   The relative contribution of
grains to the trace composition of the gas-phase is largely unknown,
however.   This thesis began as an effort to clarify this issue.
The effects of grains are expected to increase with density.
Interstellar grains may act as a sink for gas-phase molecules and
may also be involved in producing many molecules by surface

1

catalytic reactions, UV photolysis of grain mantles, evaporation of grain mantles, or disruption by shocks. Details of these processes are, however, currently quite uncertain. Even the questions of grain composition and where and how they form are still controversal. Interstellar grains, including materials such as silicates, graphite, polycyclic aromatic hydrocarbons (PAHs), and amorphous carbon, are believed to form in the outflows of the late-type giants or planetary nebulae. Interstellar grains have been observed to have icy mantles or organic refractory components, probably on top of silicate or graphite cores. Grain surface chemistry to produce "dirty ice" mantles had been suggested as early as 1949 by van de Hulst and later considered in detail by Watson and Salpeter (1972). Surface chemistry involving purely thermodynamic driving forces for grain surface reactions has been considered by Allen and Robinson (1975, 1977). The icy mantles, which form by accretion and reaction of gas-phase species, seem to be ubiquitous in all dense clouds, while the organic refractories have been observed only toward diffuse clouds and the Galactic center (Tielens and Allamandola 1987, and Irvine and Knacke 1989 and references therein).

Recent observations increasingly show that gas and dust can be coupled quite closely. For example, enhanced abundances of oxygen-containing molecules in the Orion compact ridge probably result from $H_2O$ released from grain mantles by the interaction between an outflow and the ambient material (Blake et al. 1987), and

$NH_3$ and $H_2O$ in the Orion hot core are thought to evaporate from grain mantles (Walmsley 1987; Plambeck and Wright 1987). In addition, IR observations towards highly obscured sources have identified several grain mantle components, such as $NH_3$, $H_2O$, and CO (Knacke et al. 1982; Tielens et al. 1984; Lacy et al. 1984), that are also present in the gas phase. Recently d'Hendecourt and Muizon (1989) claimed a detection of interstellar carbon dioxide toward three protostars.

Several models have been constructed for the molecular composition of accreting grain mantles (Tielens and Hagen 1982; d'Hendecourt, Allamandola, and Greenberg 1985). One of the most uncertain processes related to grain chemistry is the desorption mechanism. The accretion time scale of the gas-phase species onto the grain ($\sim 3 \times 10^5$ yr for $n \sim 10^4$ $cm^{-3}$) is supposed to be short relative to both probable molecular cloud lifetimes ($\sim 10^7$ yr) and some of the time scales of the gas-phase chemistry ($\sim 10^7$ yr). Therefore, there must be an efficient desorption mechanism to preserve a gas phase ISM in general (Winnewisser and Herbst 1987). In star-forming regions, desorption may occur easily by interstellar shocks, or by an enhanced UV field, which can disrupt grains or evaporate grain mantles (Dopita 1977; Drain and Salpeter 1979). On the other hand, in the quiescent clouds, desorption may be quite inefficient, but might occur as a result of, for example, heat dissipation of surface reactions, heating via grain-grain

collisions, heavy nuclei cosmic ray bombardment, or X-rays (Leger, Jura, and Omont 1985).

Although interstellar grains have been thought to play important roles in chemical processes in molecular clouds, it is rather difficult to determine observationally that grains are actually involved in producing species other than the hydrogen molecule, and there have been very few radio observations which support grain processes. In this thesis we have studied several molecules whose chemistry may be related to grain processes. We present the observational results for interstellar hydrogen sulfide ($H_2S$), thioformaldehyde ($H_2CS$), ethyl cyanide ($CH_3CH_2CN$), and protonated carbon dioxide ($HOCO^+$), and discuss implications for interstellar chemistry. Each chapter has a format as an individual paper to be published separately: Chapter 2: Minh, Y. C., Irvine, W. M., and Ziurys, L. M. (1989), *Ap. J. (Letters)*, 345, L63; Chapter 3: Minh, Y. C., Ziurys, L. M., Irvine, W. M., and McGonagle, D. (1989), in preparation; Chapter 4: Minh, Y. C., Irvine, W. M., McGonagle, D., and Ziurys, L. M. (1989), in preparation; Chapter 5: Minh, Y. C., Irvine, W. M., and Brewer, M. K. (1989), in preparation; Chapter 6: Minh, Y. C. and Irvine, W. M. (1989), in preparation; Chapter 7: Minh, Y. C., Irvine, W. M., and Ziurys, L. M. (1988), *Ap. J.*, 334, 175; Chapter 8: Minh, Y. C., Brewer, M. K., Irvine, W. M., Friberg, P., and Johansson, L. E. B. (1989), in preparation. Finally in Chapter 9, we summarize our conclusions. The Appendices include the results for statistical equilibrium and LVG model calculations

for $H_2CS$ and $HOCO^+$ in Appendix A, and abundances of several molecules observed towards the Sgr A molecular cloud complex in Appendix B.

## 1.2 Observed Molecules

### 1.2.1 Hydrogen sulfide

Interstellar hydrogen sulfide ($H_2S$) has been suggested as a tracer of high-temperature chemistry and/or grain surface chemistry because crucial gas-phase reactions leading to the formation of $H_2S$ are thought to be appreciably endothermic (Watson and Walmsley 1982; Duley, Millar, and Williams 1980). $H_2S$ was first observed in the ISM by Thaddeus *et al*. (1972) in its $1_{10} - 1_{01}$ transition at 169 GHz toward several GMC's, but there have been very few published observations of $H_2S$, at least in part because of the lack of receivers to study the 2 mm region. We have carried out a survey of $H_2S$ at 169 GHz using a new FCRAO 2 mm receiver and present the results in Chapters 2 to 4.

### 1.2.2 Thioformaldehyde

The ortho/para ratio for molecules which exhibit the appropriate symmetry may be an indicator of dust grain temperatures and dust-gas exchange of material, especially in cold, dark clouds.

However, molecular hydrogen, which has no electric dipole moment, is hard to observe in dense molecular clouds with kinetic temperatures of 10 - 100 K, and formaldehyde ($H_2CO$) lines are observed to be very optically thick (Kahane et al. 1984). $H_2CS$ may be a good candidate to study the ortho-to-para ratio, since the optical depths for the $H_2CS$ lines seem to be much less than those of $H_2CO$ (Irvine et al. 1989). In Chapter 5, we discuss the abundances and ortho-to-para ratios for $H_2CS$ observed towards several interstellar clouds.

### 1.2.3 Ethyl cyanide

Ion-molecule reactions leading to the formation of ethyl cyanide are highly endothermic and proceed quite slowly (Herbst, Adams, and Smith 1983). Heavily saturated molecules such as ethyl cyanide and vinyl cyanide have been suggested to form on grains, since hydrogenation may proceed efficiently on grain surfaces (Irvine and Hjalmarson 1984; Blake et al. 1987). We have searched for ethyl cyanide toward TMC-1 in its $2_{02} - 1_{01}$ transition at 18 GHz and present the result in Chapter 6.

### 1.2.4 Protonated carbon dioxide

The $HOCO^+$ molecule, the protonated form of $CO_2$, has been suggested as a tracer of interstellar $CO_2$, which is conceivably an important carbon and oxygen reservoir, but has no electric dipole

moment (Herbst *et al.* 1977). The major formation route for $CO_2$ is a neutral-neutral reaction, CO + OH, which is endothermic and hence only effective in shocks or high temperature regions. Another possible pathway for the formation of $CO_2$ is grain surface reactions. We present our observational results towards many Galactic molecular clouds in Chapters 7 and 8, and discuss chemical implications.

## 1.3 Sources

Observations have been made towards dense molecular clouds, including cold, dark clouds, star-forming regions in the Galactic disk, and also the Galactic center. We have focused the obsevations on a few well known sources: TMC-1/L134N (Chapters 2, 5, and 6), Orion(KL) (Chapters 3 and 5), and the Galactic center clouds (Sgr B2 and Sgr A; Chapters 7 and 8), while we also include the results for an $H_2S$ survey towards galactic star-forming regions (Chapter 4) and for the extensive search for $HOCO^+$ (Chapter 7).

The morphology and chemistry of TMC-1/L134N, Orion(KL), and Sgr B2 have been reviewed in detail by Irvine, Goldsmith, and Hjalmarson (1987).

### 1.3.1 TMC-1 and L134N

The cold, dark clouds TMC-1 and L134N are located at a distance ~ 150 pc and are well studied low mass molecular clouds which lack embedded high-luminosity sources. The kinetic temperature (~ 10 K) and density (~ $10^4$ $cm^{-3}$) appear very similar for TMC-1 and L134N, but they have some interesting chemical differences. Carbon-rich species and CS and $HCS^+$ are more prominant in TMC-1 than in L134N, while some molecular species, including $NH_3$ and such relatively oxygen-rich molecules as SO, $SO_2$, and HCOOH, are more abundant in L134N (Irvine *et al.* 1987; Irvine, Good, and Schloerb 1983). It has been suggested that these variations may result from, for example, different initial elemental abundances or from differing cloud ages (Irvine, Goldsmith, and Hjalmarson 1987).

### 1.3.2 Orion(KL)

The Orion A molecular cloud (OMC-1), where massive star-formation is taking place, is located at a distance ~ 500 pc. Orion(KL), the central core of OMC-1, demonstrates a complex morphology and chemistry (e.g. Plambeck *et al.* 1982; Vogel *et al.* 1984; Blake *et al.* 1987). It contains at least four main components which have distinctive spatial and spectral distributions: the "extended ridge", the "plateau", the "hot core", and the "compact ridge". The extended ridge is a quiescent

8

component ($T_{kin}$ ~ 50 - 60 K), which is, for example, easily visible in the CS and $H_2CO$ emission, and the molecular processes are probably dominated by ion-molecule chemistry. The emission from the plateau component shows evidence of the energetic outflow driven by the highly luminous IRc 2. Sulfur and silicon containing species are prominent, and shock chemistry dominates molecular processes in the plateau ($T_{kin}$ ~ 100 - 200 K). The hot core is a massive clump which is probably a leftover from the formation of IRc 2, whose radiative heating probably induces kinetic temperatures of the hot core to be ~ 300 K. HCN, HDO, $NH_3$, and the heavily hydrogenated molecules $CH_2CHCN$ and $CH_3CH_2CN$ are very prominant, which suggests active gas-grain interactions and grain mantle evaporation. An additional recognizable component is the compact ridge (often referred to as the southern condensation; $T_{kin}$ ~ 100 - 150 K) in which large, oxygen-rich molecules are prominent. The compact ridge represents an area where outflow from IRc 2 is thought to be interacting with the quiescent ambient material.

### 1.3.3 Galactic center clouds

The Sgr B2 molecular cloud is located at a distance ~ 120 - 300 pc from the Galactic center and represents an extreme case of high luminosity star-formation taking place in a very massive giant molecular cloud. A core of 5 - 10 pc diameter contains an extremely rich variety of molecular species. The OH and $H_2O$ masers

9

are grouped into three condensations: north (N), middle (M), and south (S), each separated by approximately 45 arcseconds in declination.   A study of a number of different species shows different distributions; for example, SO strongly peaks at Sgr B2(M), while OCS does at Sgr B2(N) (Goldsmith *et al.* 1987). Because of the large distance and the activities of the Galactic center, however, it is very difficult to disentangle the effects of abundance variations and excitation differences.

The Sgr A molecular complex, situated ~ 100 - 200 pc from the Galactic center, is composed of several condensations of masses greater than $10^5$ $M_\odot$, which appear to be related, but the geometry and dynamics are still controversal (Brown and Liszt 1984).   The molecular abundances and chemistry of the Sgr A region, however, have not been as well characterized as those of Sgr B2.   The total column density toward Sgr A is about a factor of 10 less than that of Sgr B2.

CHAPTER 2


DETECTION OF INTERSTELLAR HYDROGEN SULFIDE IN COLD, DARK CLOUDS

2.1 <u>Summary</u>

We have detected interstellar hydrogen sulfide ($H_2S$) towards the cold, dark clouds L134N and TMC-1. We derive total column densities of $\sim 2.6 \times 10^{13} cm^{-2}$ and $\sim 7.0 \times 10^{12}$ $cm^{-2}$ at the SO peak of L134N and at the $NH_3$ peak of TMC-1, respectively. Since the expected gas phase reactions leading to the formation of $H_2S$ are thought to be endothermic, grain surface reactions may play a major role in the synthesis of this species in cold, dark clouds. If the carbon abundance is high and grain surface reactions are the dominant formation route, $H_2CS$ would be expected to form instead of $H_2S$, and the abundances of $H_2CS$ have been observed to be high where those of $H_2S$ are low in L134N and TMC-1.

2.2 <u>Introduction</u>

Gas phase ion-molecule reactions have not been very successful in explaining the observed abundances of sulfur-bearing molecules in the interstellar medium, because the initiating reactions of $S^+$ or S with $H_2$ are both endothermic (Watson and Walmsley 1982; Smith and Adams 1985). Some species, such as $H_2S$, SO, and $SO_2$, are observed

to be overabundant in massive-star-forming regions relative to predictions, an effect which has been ascribed to the widespread occurrence of shocks or other high temperature processes (Hartquist, Oppenheimer, and Dalgarno 1980; Prasad $et$ $al.$ 1987). In addition, high abudances of sulfur-bearing molecules such as $HCS^+$, $H_2CS$, $C_2S$, and $C_3S$ have been reported in cold, dark clouds (Irvine, Good, and Schloerb 1983; Irvine $et$ $al.$ 1989; Saito $et$ $al.$ 1987; Yamamoto $et$ $al.$ 1987), where high temperature reactions should not be important. In fact, the $C_2S$ and $C_3S$ abundances in TMC-1 are vastly greater than those of the oxygen analogs $C_2O$ and $C_3O$, showing that there are considerable differences between oxygen and sulfur chemistry in cold clouds. Unlike oxygen chemistry, which is thought to be dominated by gas-phase reactions, sulfur chemistry may be dominated by grain surface reactions (e.g. Millar 1982), at least for chemically reduced species. For example, sulfur is expected to react with atomic hydrogen on grain surfaces easily and thereby form the volatile hydride $H_2S$ (Tielens and Alamandola 1987).

$H_2S$ was first observed in the ISM via the lowest frequency ($1_{10}$ - $1_{01}$) transition by Thaddeus $et$ $al.$ (1972), who obtained column densities ~ $10^{14}$ $cm^{-2}$ toward several GMC's. The $2_{20}$ - $2_{11}$ transition at 217 GHz was detected during the OVRO spectral survey of Orion A (Sutton $et$ $al.$ 1985), but, to our knowledge, there have been no other published observations of $H_2S$ in the ISM, at least in part because of the lack of receivers to study the 2 mm region. Using a new FCRAO receiver (Ziurys, Erickson, and Grosslein 1988) to

observe the $1_{10}$ - $1_{01}$ transition which occurs near 169 GHz, we have made a survey of $H_2S$ toward many well known star-forming regions and cold, dark clouds. The results for active star-forming regions will be published elsewhere (Minh *et al.* 1989). In this Chapter, we report the first detection of $H_2S$ in cold, dark clouds, and comment on the implications for chemical models.

## 2.3 Observations

Observations of the lowest frequency transition of $H_2S$ ( $1_{10}$ - $1_{01}$ at $\nu_o$ = 168.762762373 GHz; Cupp, Kempf, and Gallagher 1968) were made using the FCRAO 14 m telescope between 1989 January and March. The receiver employed a cooled Schottky diode mixer, which gave total system temperatures, corrected to outside the atmosphere, of 700 - 1000 K. Data were taken by position switching 20 arcminutes in azimuth, and spectra were obtained using a 256-channel filter bank with 100 kHz resolution. The FWHM beamwidth at 169 GHz is 35 arcsec and the antenna main beam efficiency $\eta_B$ = 0.25. The temperature scale is given as $T_A^*$, the beam-chopper-corrected antenna temperature. We then approximate the radiation temperature $T_R$ by the main beam brightness temperature $T_{MB}$ = $T_A^*/\eta_B$.

13

## 2.4 Results

The observed line parameters are given in Table 2.1, and
spectra observed towards L134N and TMC-1 are shown in Figures 2.1a
and b, respectively.

$H_2S$ is an asymmetric top, which, because of its two hydrogen
spins, possesses both ortho and para species. The $1_{10}$ - $1_{01}$
transition is the lowest line in the ortho ladder (e.g. see Thaddeus
et al. 1972, for an energy level diagram). Therefore, to derive
the $H_2S$ abundance, the column density was calculated for the ortho
levels only, and then extrapolated to a total column density
assuming an ortho-to-para ratio. To estimate the ortho species
population, the column density in the upper level of the $1_{10}$ - $1_{01}$
transition was calculated under the optically thin assumption and
considering the effect of cosmic background radiation, using the
following formula (cf. Irvine, Goldsmith, and Hjalmarson 1987):

$$N_u = \frac{1.94 \times 10^3 \; \nu^2 \; [\text{GHz}] \; \int T_R dV \; [\text{K km s}^{-1}]}{A \; [\text{s}^{-1}] \; [1 - J_\nu(T_{bg})/J_\nu(T_{ex})]}$$

In this expression $J_\nu(T) = (h\nu/k)[\exp(h\nu/kT)-1]^{-1}$, A is the Einstein
A-coefficient, which for the $H_2S$ $1_{10}$ - $1_{01}$ transition equals 2.65 $\times$
$10^{-5}$ s$^{-1}$, and $\nu$ is the frequency of the transition, while $T_{bg}$ is the
2.7 K cosmic background temperature and $T_{ex}$ the excitation
temperature of the line involved. Although the $H_2S$ emission was

14

TABLE 2.1

Summary of Hydrogen Sulfide Observations

| Source | $T_A^*$ (K) | $V_{LSR}$ (km s$^{-1}$) | $\Delta V$ (km s$^{-1}$) | $\int T_A^* dV$ (K km s$^{-1}$) | $N_{tot}$ (cm$^{-2}$) |
|---|---|---|---|---|---|
| L134N | $0.13\pm.03$[a] | 2.16 | 0.71 | 0.09 | 7.8(12)[c] |
| L134N(SO) | $0.40\pm.07$[a] | 2.33 | 0.74 | 0.30 | 2.6(13) |
| L134N(0,-2) | $\leq 0.15$[b] | — | — | — | $\leq 9.5(12)$[d] |
| L134N(-2.3,2) | $\leq 0.21$[b] | — | — | — | $\leq 1.3(13)$[d] |
| TMC-1 | $\leq 0.09$[b] | — | — | — | $\leq 4.7(12)$[e] |
| TMC-1(NH$_3$) | $0.17\pm.03$[a] | 5.73 | 0.50 | 0.08 | 7.0(12) |

[a] 1 $\sigma$ uncertainty.

[b] 3 $\sigma$ upper limit.

[c] A(B) signifies A x 10$^B$.

[d] $\Delta V = 0.7$ km s$^{-1}$ was assumed.

[e] $\Delta V = 0.5$ km s$^{-1}$ was assumed.

Positions: L134N: RA(1950)= $15^h51^m30\overset{s}{.}0$, Dec(1950)= $-2°43'31''$; L134N(SO): RA(1950)= $15^h51^m26\overset{s}{.}0$, Dec(1950)= $-2°43'31''$; L134N(0,-2): RA(1950)= $15^h51^m22\overset{s}{.}0$, Dec(1950)= $-2°43'31''$; L134N(-2.3,2): RA(1950)= $15^h51^m20\overset{s}{.}8$, Dec(1950)= $-2°41'31''$; TMC-1: RA(1950)= $4^h38^m38\overset{s}{.}6$, Dec(1950)= $25°35'45''$; TMC-1(NH$_3$): RA(1950)= $4^h38^m22\overset{s}{.}0$, Dec(1950)= $25°41'45''$.

Figure 2.1a - b   Spectra of the $1_{10} - 1_{01}$ transition of $H_2S$ taken with the FCRAO 14 m telescope at 100 kHz resolution toward the positions given in Table 2.1 for the dark clouds (a) L134N and (b) TMC-1.

17
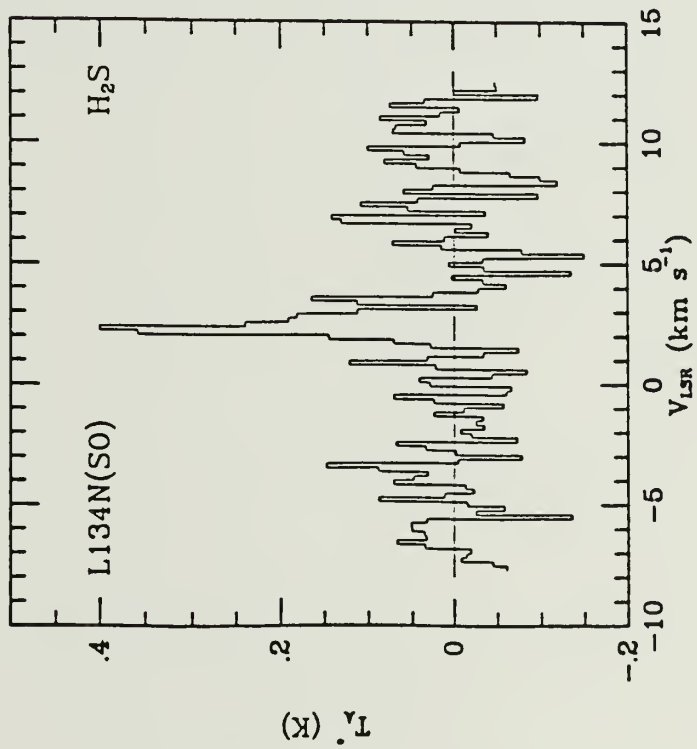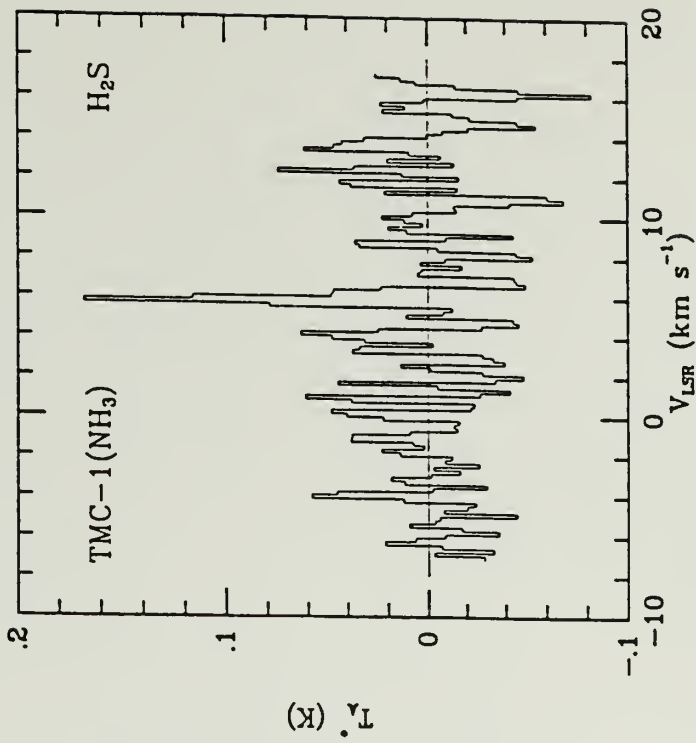
observed to vary in intensity on an angular scale of an arcmin, it was at least somewhat extended relative to our 35" beam, making the use of $T_R \approx T_{MB}$ appropriate.

The total ortho column density was then derived from $N_u$ by summing over the partition function, assuming a rotational temperature of $T_{rot} = T_{ex} = 5$ K for L134N and TMC-1. Excitation temperatures of about 5 K have been found by Swade (1987) in L134N for several molecules whose fundamental transitions have A-coefficients similar to that for the $1_{10} - 1_{01}$ $H_2S$ line. The partition function for the ortho states was calculated by an explicit summation, using the energy levels given by Helminger, De Lucia, and Kirchoff (1973). As it turns out, for a rotational temperature of 5 K almost all the population for ortho-$H_2S$ is contained in the lowest two levels; i.e., $1_{10}$ and $1_{01}$.

Using this assumptions, a column density of $\sim 2 \times 10^{13}$ cm$^{-2}$ was derived for the ortho species of $H_2S$ at the SO peak position in L134N, which implies a total column density for $H_2S$ of $N_{tot} \sim 2.6 \times 10^{13}$ cm$^{-2}$, assuming an ortho-to-para ratio 3 : 1 (see the last column of Table 2.1 for $N_{tot}$ at other observed positions). The ortho-to-para ratio, however, is uncertain. For example, a value of 2 : 1 was found for this ratio for formaldehyde in dark clouds by Kahane *et al.* (1984), who ascribe this deviation from a ratio of 3 : 1 to ortho/para equilibration on grains at a temperature $\sim 10$ K.

Even if the ratio were as low as 1 : 1 for $H_2S$, the total column density given here would be underestimated by less than a factor of 2.

A column density of $\sim 2.6 \times 10^{13}$ cm$^{-2}$ for $H_2S$ translates into a fractional abundance of $\sim 3 \times 10^{-9}$ at the SO peak of L134N, assuming $N(H_2) \sim 8.2 \times 10^{21}$ cm$^{-2}$ at the same position (Swade 1987; assuming $N(C^{18}O)/N(H_2) = 1.7 \times 10^{-7}$). For TMC-1 we find for the same assumptions $f(H_2S) < 5 \times 10^{-10}$ at the cyanopolyyne peak and $f \sim 7 \times 10^{-10}$ at the $NH_3$ maximum, taking $N(H_2) = 10^{22}$ cm$^{-2}$ at both positions (Irvine *et al.* 1987; Friberg and Hjalmarson 1989).

## 2.5 Discussion

Our detections of hydrogen sulfide in cold, dark clouds are quite interesting, because the most significant gas phase reactions to produce $H_2S$ are appreciably endothermic; consequently, the presence of $H_2S$ has been regarded as an indicator of either shock chemistry or grain surface chemistry (Watson and Walmsley 1982; Smith and Adams 1985; Duley, Millar, and Williams 1980). Since there are no known embedded heating sources in the clouds observed, high temperature chemistry and shock chemistry are presumably unimportant in these regions.

The ion-molecule reactions related to hydrogen sulfide have not been well studied in the laboratory. The radiative association reaction between $HS^+$ and $H_2$ has been employed by chemical modelers

as a principal formation route in dense clouds (cf. Herbst, DeFrees, and Koch 1989), but the predicted $H_2S$ abundance is less than that observed at the SO peak of L134N by a factor of 10 - 100 for the models which match the observed abundances of other species (Herbst and Leung 1986; Leung, Herbst, and Huebner 1984). However, given the lack of experimental data, particularly at temperatures ~ 10 K appropriate to dark clouds, ion-molecule reactions cannot be ruled out entirely as a source of $H_2S$. Other routes that lead to the production of $H_2S$, for example the reaction between $S^+$ and $H_2CO$ (Prasad and Huntress 1982), should be studied further.

Nonetheless, grain surface reactions may be a more promising pathway to explain the observed $H_2S$ abundance. It has been suggested that such reactions may greatly alter the abundances of gas phase molecules, especially for sulfur- and nitrogen-bearing species (e.g. Tielens and Allamandola 1987). If sulfur has been depleted onto grains in a dense region, ions like $C^+$ or $H^+$ are likely to find $SH^-$ or $S^-$ sites on the grain surfaces, which may lead to the formation of $H_2CS$ or $H_2S$, respectively (Duley, Millar, and Williams 1980). $H_2S$ has been identified tentatively in the grain mantles toward the compact radio source W33A (Geballe *et al.* 1986). $H_2S$ is relatively volatile and might be easily desorbed in processes such as those described by Greenberg *et al.* (e.g. 1980).

Our failure to detect $H_2S$ towards the cyanopolyyne peak of TMC-1 is of significant chemical interest in this regard. TMC-1 consists of an elongated series of condensations in Taurus; the

cyanopolyyne peak position has the highest column densities among dark clouds for many molecular species, including particularly many chemically unsaturated organic molecules such as the cyanopolyynes ($HC_{2n}CN$, $n = 0, \ldots, 5$), the hydrocarbon radicals $C_nH$ ($n = 1, \ldots, 6$), the rings $C_3H_2$ and $c-C_3H$, and methylated carbon chains (e.g. Irvine *et al*. 1987; Guélin and Cernicharo 1989). In fact, TMC-1 has become a standard source for comparison of observational results with those of models of ion-molecule chemistry (*e.g*. Millar and Nejad 1985). Nontheless, it has been previously pointed out that some molecular species, including $NH_3$ and such relatively oxygen-rich molecules as SO, $SO_2$, and HCOOH, are more abundant in L134N than in TMC-1 (Irvine *et al*. 1987; Irvine, Good, and Schloerb 1983). It has been suggested that these variations might reflect differences in the gas phase carbon/oxygen ratio between these clouds. Compared to L134N, TMC-1 at the cyanopolyyne peak has a $H_2CS$ abundance ~ 5 times larger than that found in L134N (Irvine *et al*. 1989) and a $H_2S$ abundance at least ~ 4 times less (see Table 2.1). A higher carbon abundance in TMC-1 versus L134N may lead to the formation of $H_2CS$ instead of $H_2S$, as well as to the abundant carbon-chain molecules in TMC-1. Indeed, observations of $H_2CS$ in these two cold clouds indicate an anti-correlation between $H_2S$ and $H_2CS$ (Minh and Irvine 1989).

The question also arises as to whether the chemical differences between TMC-1 and L134N may be partly mirrored by chemical gradients *within* each of these clouds. A gradient in the $NH_3$/cyanopolyyne

abundance seems to be well established in TMC-1 (e.g. Olano, Walmsley, and Wilson 1988), where we detect $H_2S$ only towards the $NH_3$ maximum. Swade (1987; 1989) has shown that the location of peak column density of SO and $SO_2$ in L134N differs from the position of maximum intensity for $C_3H_2$, $HCO^+$ and the cyanopolyynes, and has speculated that this may be a result of differential depletion of oxygen relative to carbon in the latter region. Such an effect could result from the differing volatility of $H_2O$ and $CH_4$ (cf. Blake *et al.* 1987). Note that the fractional abundance of $H_2S$ which we determine in L134N appears to correlate with SO and $SO_2$, rather that with *either* $NH_3$ or $C_3H_2$ and the cyanopolyynes. Clearly more data is needed on the relative distribution of these species in cold clouds.

CHAPTER 3


OBSERVATIONS OF $H_2S$ TOWARDS OMC-1


3.1 <u>Summary</u>

Interstellar hydrogen sulfide ($H_2S$) and its isotopic variant ($H_2^{34}S$) have been observed toward several positions in OMC-1 via their $1_{10} - 1_{01}$ transitions near 168 GHz.  We derive total column densities towards Orion(KL) of $\sim 2 \times 10^{14}$ $cm^{-2}$ for the Orion extended ridge, $\sim 10^{17}$ $cm^{-2}$ for the plateau, and $\sim 10^{18}$ $cm^{-2}$ for the compact ridge, in addition to values for other positions in OMC-1. The fractional abundance of $H_2S \sim 10^{-9}$ in the quiescent regions of OMC-1, as well as in cold dark clouds (Minh, Irvine, and Ziurys 1989), seems to be difficult to explain by currently known ion-molecule reactions.  The fractional abundance of $H_2S$ relative to $H_2$ is enhanced by a further factor of 1000 in the hot core and the plateau (to $\sim 10^{-6}$) relative to the quiescent clouds.  We suggest that $H_2S$ in the hot core may be evaporating from grain mantles, while $H_2S$ in the plateau may result from either high-temperature gas phase chemistry or grain surface chemistry. From the non-detection of HDS in its $2_{11} - 2_{12}$ transition, we estimate the abundance ratio $[HDS]/[H_2S] \leq 5 \times 10^{-3}$ in the hot core by assuming the same excitation conditions and emission regions for both species.

## 3.2 Introduction

The abundances of most interstellar molecules can be reproduced via gas-phase ion-molecule reactions which usually have no activation energy barriers and are simple two body processes. Gas-phase ion-molecule reactions, however, have not been very successful in explaining the observed abundances of some sulfur-bearing molecules in the interstellar medium. Species such as SO and $SO_2$ appear to be unusually abundant in clouds where high mass star-formation is occuring, accompanied by shock waves and high temperatures. Such observations have led to the suggestion that "shock" or "high temperature" chemistry, i.e. chemistry involving gas-phase reactions with activation energies, may be taking place in hot regions and subsequently producing these species (e.g. Hartquist, Oppenheimer, and Dargarno 1980).

Along with elevated temperatures, shocks can also cause the partial or complete destruction of dust grains. Such grain destruction could also contribute to the formation of many of these so-called "high temperature" molecules, since they often contain refractory elements. Also, the UV radiation field from the newly formed massive stars can evaporate grain mantles and consequently release molecules into the gas phase. It is, however, often very difficult to differentiate between gas-phase reactions and grain related processes in the formation of interstellar molecules in shocked regions.

Interstellar hydrogen sulfide ($H_2S$) has been suggested as a tracer of high-temperature chemistry and/or grain surface chemistry because crucial gas phase reactions leading to the formation of $H_2S$ are thought to be appreciably endothermic (Watson and Walmsley 1982; Smith and Adams 1985; Duley, Millar, and Williams 1980). $H_2S$ was first observed in the ISM via the lowest frequency ortho transition ($1_{10}$ - $1_{01}$) by Thaddeus $et$ $al.$ (1972), who obtained column densities $\sim 10^{14}$ cm$^{-2}$ toward several GMC's. This transition has recently been detected towards the cold, dark clouds L134N and TMC-1 as well (Minh, Irvine, and Ziurys 1989; Paper 1), where high temperature processes should not be important. Although ion-molecule reactions cannot be ruled out entirely as a source of $H_2S$, grain surface reactions may be a more promising pathway to explain the observed abundance in cold, dark clouds (Paper 1). $H_2S$ has also been identified tentatively in the grain mantles toward the compact radio source W33A (Geballe $et$ $al.$ 1986).

The Orion A molecular cloud (OMC-1), where massive star-formation is taking place, is about 500 pc from the sun, and is one of the most extensively studied sources in the sky. The central core, known as Orion(KL), demonstrates a complex morphology (e.g. Plambeck $et$ $al.$ 1982; Vogel $et$ $al.$ 1984) and chemistry (e.g. Blake $et$ $al.$ 1987). It contains at least three main components which have distinctive spatial and spectral distributions: the "extended ridge", the "hot core", and the "plateau". Their characteristic features have been reviewed in detail by Irvine, Goldsmith, and

Hjalmarson (1987) and Prasad *et al.* (1987). Since regions characterized by outflows and elevated temperatures and also extended cooler, quiescent material are present, Orion(KL) serves as an important test object for grain and shock chemistry as well as for low temperature ion-molecule synthesis. We report here observations of the $1_{10}$ - $1_{01}$ transition of interstellar hydrogen sulfide ($H_2S$) and its isotopes towards OMC-1 and comment on the implications for chemical models. Data towards several other star-forming regions for $H_2S$ will be published elsewhere (Minh *et al.* 1989; see also § 4).

## 3.3 Observations

Observations of $H_2S$ and its isotopic species $H_2^{34}S$ and HDS (see transitions and rest frequencies in Table 3.1) were made using the FCRAO 14 m telescope between 1989 January and April. Telescope parameters are also included in Table 3.1. The FCRAO 2 mm receiver (Ziurys, Erickson, and Grosslein 1988) gave total system temperatures, corrected for atmospheric attenuation, of 700 - 1000 K. Data were taken by position switching 30 arcminutes in azimuth, and spectra were obtained using 256-channel filter banks with 250 kHz and 1 MHz resolutions. The temperature scale is given as $T_A^*$, the beam-chopper-corrected antenna temperature. For calculating column densities, we use the main beam brightness temperature $T_{MB} = T_A^*/\eta_B$.

26

TABLE 3.1

Line Frequencies and FCRAO Telescope Parameters

| Molecule | Transition | Rest Frequency[a] (MHz) | FWHP (arcsec) | $\eta_B$ |
|----------|------------|-------------------------|---------------|----------|
| $H_2^{32}S$ | $1_{10} - 1_{01}$ | 168762.76237 | 35 | 0.25 |
| $H_2^{34}S$ | $1_{10} - 1_{01}$ | 167910.516 | 35 | 0.25 |
| HDS | $2_{11} - 2_{12}$ | 153179.160 | 39 | 0.30 |

[a] From Helminger, De Lucia, and Kirchhoff (1973).

## 3.4 Results

### 3.4.1 Spectra

The $1_{10} - 1_{01}$ transitions of $H_2S$ and $H_2^{34}S$ have been observed towards several selected positions in OMC-1, and the observed line parameters are given in Tables 3.2 and 3.3 for $H_2S$ and $H_2^{34}S$, respectively.

The spectra obtained toward the KL position show evidence for three sub-regions, the extended ridge, the plateau, and the hot core. The $H_2S$ spectrum (Figure 3.1) has a "spike" feature at $V_{LSR}$ ~ 9.5 km s$^{-1}$ with FWHP ~ 3.7 km s$^{-1}$, which agrees quite well with other molecular observations for the extended ridge (Blake *et al.* 1987; Johansson *et al.* 1984). There is no apparent counterpart in the $H_2^{34}S$ spectrum, which may indicate that this component is not optically thick. Another ridge component, the compact ridge, has a slightly lower velocity $V_{LSR} \approx 7 - 8$ km s$^{-1}$ and is characterized by a number of large, oxygen-rich species (cf. Irvine, Goldsmith, and Hjalmarson 1987); we find no specific evidence for compact ridge emission in our spectra, and we ignore this component in the analysis. The emission from the plateau is quite visible in the $H_2S$ spectrum, extending from $V_{LSR}$ ~ - 20 to 40 km s$^{-1}$ as shown in Figure 3.1. We regard this component as the "lower velocity" plateau, which is a rather massive disk-like clump in which many molecules have been observed, including sulfur-containing species

TABLE 3.2

Summary of $H_2S$ Observations

| Position | $T_A^*$ (K) | $V_{LSR}$ (km s$^{-1}$) | FWHP (km s$^{-1}$) | $\int T_A^* dV$ (K km s$^{-1}$) | $N_{column}$ [a] ($\times 10^{14}$ cm$^{-2}$) |
|---|---|---|---|---|---|
| KL [b]  Ridge ..... | 1.47 | 9.5 | 3.7 | 5.8 | 2 |
| Hot Core .. | 0.39 | 5.7 | 12.0 | 5.0 | 9000[c] (20000)[d] |
| Plateau ... | 1.06 | 8.0 | 32.9 | 37.1 | 800[c] (3000)[d] |
| Offset ($\Delta\alpha, \Delta\delta$) from KL | | | | | |
| (-0.6,-1.6)($\equiv$ 1.5S) | 1.99 | 7.4 | 4.8 | 9.5 | 5[c] (2)[d] |
| (1, 3)($\equiv$ 3N1E) .. | 1.12 | 9.8 | 2.0 | 2.2 | 0.1[c] (0.7)[d] |
| (0 , 1) ........ | 1.54 | 10.0 | 3.9 | 6.0 | 2 |
| (-0.3,-0.8) .... | 2.01 | 8.7 | 3.8 | 7.6 | 3 |
| (-0.8,-2.4) .... | 1.41 | 9.1 | 2.7 | 3.9 | 1 |
| (-1, 0) ........ | 1.15 | 8.6 | 3.3 | 3.8 | 1 |
| (-2, 0) ........ | $\leq 0.60$[e] | — | — | — | $\leq 0.5$[f] |
| (1 , 0) ........ | 1.06 | 9.7 | 5.4 | 5.7 | 2 |
| (2 , 0) ........ | $\leq 0.53$[e] | — | — | — | $\leq 0.4$[f] |
| (3 , 0) ........ | 0.72 | 10.2 | 2.7 | 1.9 | 0.7 |
| (4 , 0) ........ | $\leq 0.32$[e] | — | — | — | $\leq 0.3$[f] |

NOTE. - Spectral resolution is 250 kHz.

Position of KL: RA(1950)= $5^h32^m47^s.0$, Dec(1950)= $-5°24'23"$.

TABLE 3.2

(Continued)


[a] Optically thin emission and $T_{ROT}$ = 30 K have been assumed unless
otherwise indicated.

[b] From a gaussian fit by assuming $V_{LSR}$(Hot Core) = 8.0 km s$^{-1}$ and
FWHP (Hot Core) = 12.0 km s$^{-1}$, and $V_{LSR}$(Plateau) = 5.7 km s$^{-1}$.

[c] Using $\tau$(H$_2$S) and $T_{ROT}$ from Table 3.5.

[d] Using $\int T_A^*$(H$_2^{34}$S)dV from Table 3.3, and $T_{ROT}$ and the source size
from Table 3.5, assuming $\tau$(H$_2^{34}$S) $\ll$ 1, S/$^{34}$S = 15.

[e] 3 $\sigma$ upper limit.

[f] 3 $\sigma$ upper limit and FWHP = 2 km s$^{-1}$ were used.

TABLE 3.3

Summary of $H_2^{34}S$ Observations[a]

| Position | | $T_A^*$ (K) | $V_{LSR}$ (km s$^{-1}$) | FWHP (km s$^{-1}$) | $\int T_A^* dV$ (K km s$^{-1}$) |
|---|---|---|---|---|---|
| KL[b] | Ridge ....... | — | — | — | — |
| | Hot Core .... | 0.30 | 5.7 | 12.0 | 3.8 |
| | Plateau ..... | 0.22 | 8.0 | 33.2 | 7.8 |
| 1.5S ............ | | 0.15 | 6.6 | 4.3 | 0.7 |
| 3N1E ............ | | 0.09 | 9.6 | 1.1 | 0.1 |

NOTE. - Positions in Table 3.2. Spectral resolution is 250 kHz.

[a] Line parameters derived from the gaussian fits.

[b] From a gaussian fit by assuming $V_{LSR}$(Hot Core) = 5.7 km s$^{-1}$ and
FWHP (Hot Core) = 12.0 km s$^{-1}$, and $V_{LSR}$(Plateau) = 8.0 km s$^{-1}$.

Figure 3.1 Spectra of the $1_{10} - 1_{01}$ transitions of $H_2S$ and $H_2^{34}S$ taken towards Orion(KL) at a spectral resolution of 250 kHz (position given in Table 3.2). Dotted lines are gaussian fit results and line parameters are included in Tables 3.2 and 3.3.

33
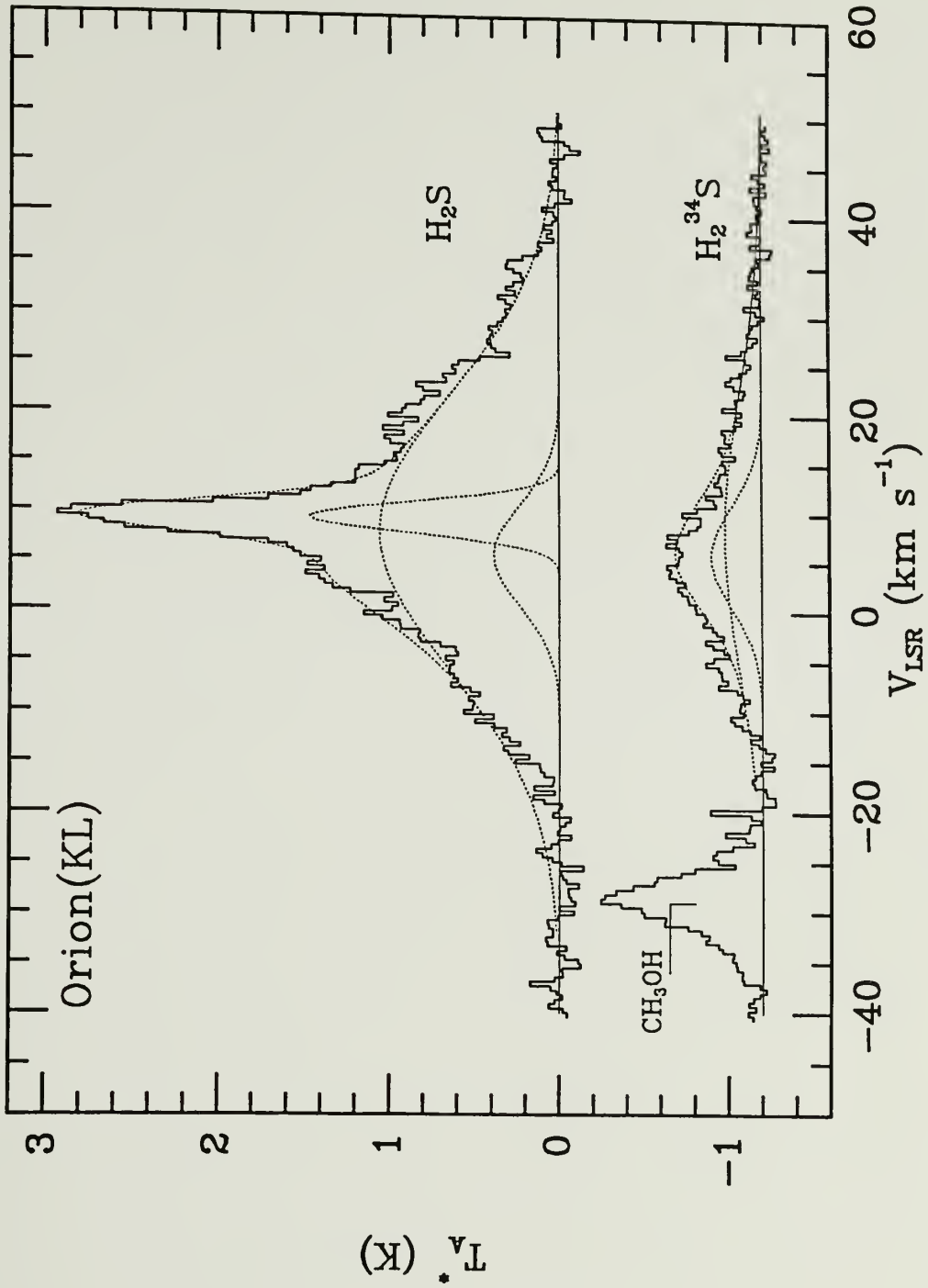
and HDO. The hot core, which may be the most massive clump left over from the formation of IRc 2, is characterized by $V_{LSR} \sim 5$ km s$^{-1}$ and $\Delta V \sim 5 - 10$ km s$^{-1}$ with large abundances of highly saturated molecules, such as $H_2O$ and $NH_3$. The $H_2^{34}S$ spectrum in Figure 3.1 peaks at $V_{LSR} \sim 6$ km s$^{-1}$, which is close to the LSR velocity of the hot core. It therefore appears that $H_2S$ is very prominent in the hot core and probably optically very thick in the $H_2S$ spectrum.

In Figure 3.2, we have shown the spectra obtained towards the 1.5S and the 3N1E positions. At the 1.5S position, there is clear evidence for an outflow distinct from that associated with IRc 2 (Ziurys and Friberg 1987; Schmid-Burgk et al. 1989; Ziurys, Wilson, and Mauersberger 1989). The broad $H_2S$ line (full width at zero power $\sim 12$ km s$^{-1}$) shows some evidence of this. The 3N1E position is a dense and quiescent region, toward which a number of radicals and ions show an emission peak (Turner and Thaddeus 1977; Harris et al. 1982).

The $^{34}SO$ $4_3 - 3_3$ line and presumably the $CH_3OH$ $9_1 - 9_0$ E1 line have been detected in these observations towards KL and 1.5S. Line parameters for both these species are listed in Table 3.4. The LSR velocity of $\sim 8$ km s$^{-1}$ of the $CH_3OH$ $9_1 - 9_0$ E1 line in KL agrees well with other methanol observations (Johansson et al. 1984; Blake et al. 1987) of compact ridge molecules. The methanol line is shown in Figure 3.1 together with the $H_2^{34}S$ spectrum.

Figure 3.2    Spectra of the $1_{10} - 1_{01}$ transitions of $H_2S$ and $H_2^{34}S$ towards Orion 1.5S and 3N1E at a resolution of 250 kHz (positions given in Table 3.2).

36
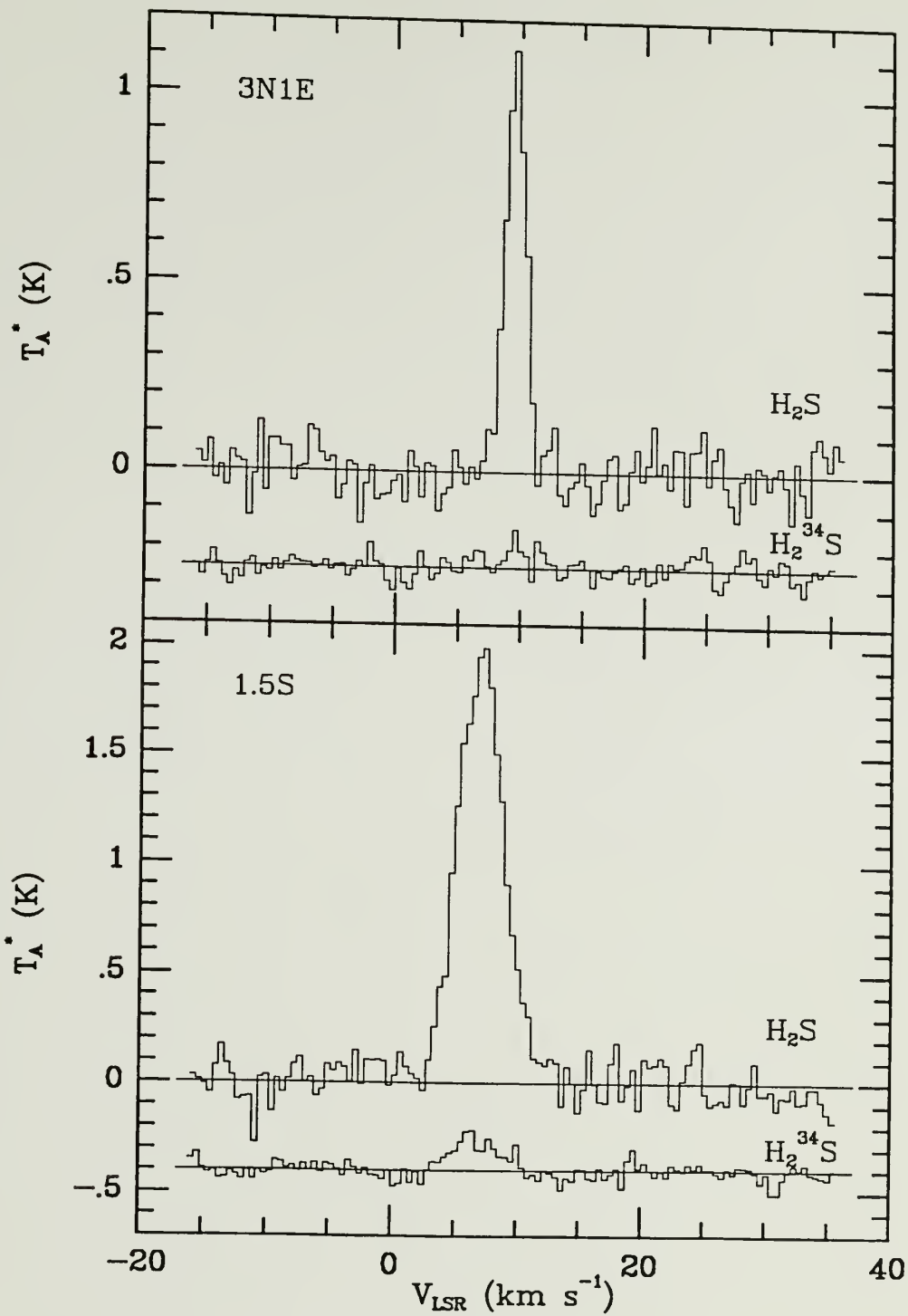
TABLE 3.4

Line Parameters for $^{34}$SO and CH$_3$OH

| Position | $T_A^*$ (K) | $V_{peak}$ (km s$^{-1}$) | FWHP (km s$^{-1}$) | $\int T_A^* dV$ (K km s$^{-1}$) |
|----------|-------------|--------------------------|--------------------|-------------------------------|
| $^{34}$SO $4_3$ - $3_3$ Transition | | | | |
| KL | 0.39 | 6.9 | 18.9 | 7.4 |
| 1.5S | 0.10 | 3.3 | 3.9 | 0.4 |
| CH$_3$OH $9_1$ - $9_0$ E1 Transition | | | | |
| KL | 0.96 | 8.0 | 6.6 | 6.3 |
| 1.5S | 0.10 | 8.9 | 3.8 | 0.4 |

NOTE. - Spectral resolutions are 1 MHz for $^{34}$SO and 250 kHz for CH$_3$OH. Positions for KL and 1.5S are in Table 3.2.

Rest frequency: $^{34}$SO $4_3$- $3_3$ Transition:168.815101 (Hollis *et al.* 1981); CH$_3$OH $9_1$ - $9_0$ E1 Transition: 167.93113 (Lovas 1989).

## 3.4.2 $H_2S$ Abundances

$H_2S$ abundances for each sub-region in KL have been derived by gaussian fitting the spectra. As discussed above, the extended ridge is apparent as a "spike" in the $H_2S$ spectrum, while it has no counterpart in the $H_2^{34}S$ spectrum. This suggest that the $H_2S$ emission of the extended ridge is optically thin. A gaussian fit is straightforward for the "spike" in the $H_2S$ spectrum, and we derive an $H_2S$ total column density $N_{tot}(H_2S) \sim 2 \times 10^{14}$ cm$^{-2}$ by assuming an ortho to para ratio of 3 and evaluating the partition function for $T_{rot} \sim 20 - 50$ K (Johansson *et al.* 1984; Blake *et al.* 1987). This corresponds to a fractional abundance of $H_2S$ relative to $H_2$ of $f(H_2S) \sim 10^{-9}$, taking $N(H_2) \sim 1 - 3 \times 10^{23}$ cm$^{-2}$ for the extended ridge (Blake *et al.* 1987).

Because of the asymmetry of the spectra shown in Figure 3.1, it is difficult to fit to unique components for the plateau and the hot core. So we have set the center velocities for the plateau and the hot core and the line width for the hot core, on the basis of results for other molecules (Johansson *et al.* 1984; Blake *et al.* 1987). Fit results are shown in dotted lines in Figure 3.1, and line parameters are included in Tables 3.2 and 3.3. The emission, of course, does not need to be gaussian, especially for the plateau, but the observed line profiles for both $H_2S$ and $H_2^{34}S$ are matched quite well by this procedure. In addition, since the $H_2^{34}S$ emission may be assumed to be optically thin and the hot core

38

component is very apparent in the $H_2{}^{34}S$ spectrum, we can derive reasonable column densities for the hot core and the plateau from the $H_2{}^{34}S$ spectrum (the assumptions are included in the Notes to Tables 3.2 and 3.3; cf. the equation in Irvine, Goldsmith, and Hjalmarson 1987). When we compare column densities so derived for the $1_{10}$ state to those found from the optical depths obtained comparing the gaussian fit antenna temperatures of the $H_2S$ and $H_2{}^{34}S$ spectra, both results agree well within a factor of a few by assuming the isotopic ratio of $S/{}^{34}S \sim 15 - 22$ (Schloerb et al. 1983).

The Einstein $A$ coefficient for the $1_{10} - 1_{01}$ transition for both main and isotope lines was taken to be $2.25 \times 10^{-5}$ $s^{-1}$ (Thaddeus et al. 1972). Thus the $1_{10} - 1_{01}$ line becomes thermalized at densities $\geq 5 \times 10^5$ $cm^{-3}$. Although such densities probably do not exist over the extended OMC-1 region, they are most likely present towards the KL, 3N1E, and 1.5'S positions. The fraction of the population in the $1_{10}$ level was evaluated by summing over the partition function for the rotational temperatures indicated in Table 3.2. The resulting total column densities are included in Table 3.2. We derive $N_{tot}(H_2S) \sim 10^{17}$ $cm^{-2}$ and $\sim 10^{18}$ $cm^{-2}$ for the plateau and the hot core, respectively, which corresponds to $f(H_2S) \sim 10^{-6}$ for both components, for $N(H_2) \sim 10^{23}$ $cm^{-2}$ for the plateau and $\sim 10^{24}$ $cm^{-2}$ for the hot core (Blake et al. 1987).

The column densities for the $1_{10}$ state at the 1.5S and 3N1E positions have been derived from the optical depths (Table 3.5) obtained from comparing the $H_2S$ and $H_2^{34}S$ spectra, and then total column densities are then given by assuming Boltzmann population distributions at $T_{rot} \sim 75$ K and 15 - 30 K for 1.5S and 3N1E, respectively (cf. Goldsmith et al. 1986). Since the $1_{10}$ energy level of $H_2S$ is about 28 K above the ground state, total column densities are not very sensitive to $T_{rot}$ for values in the range 10 - 50 K. As towards KL, similar values of $N_{tot}$ are obtained from the $H_2^{34}S$ spectra alone, on the assumptions of optically thin emission and $S/^{34}S \approx 15$. We find $N_{tot}(H_2S) \sim 4 \times 10^{14}$ cm$^{-2}$ and $\sim 4 \times 10^{13}$ cm$^{-2}$ at 1.5S and 3N1E. For the other positions listed in Table 3.2, we assumed optically thin emission and $T_{rot} \sim 30$ K. We derive $N_{tot}(H_2S) \sim 10^{13} - 10^{14}$ cm$^{-2}$ (included in the last column of the Table 3.2). Optical depths may be greater than one at such locations, which would mean that we underestimate the total column densities in some regions. For example, if $\tau(H_2S) \sim 2$, then the total column density is underestimated by a factor of 2 - 3. The fractional abundances at all the positions are on the order of $10^{-9}$ for total hydrogen column densities $\sim 0.5 - 5 \times 10^{23}$ cm$^{-2}$ (Table 3.5; Smith et al. 1979; Batrla et al. 1983).

As a check on our assumptions, we used our derived opacities for the hot core and plateau sources, combined with our measured antenna temperatures and assumed excitation temperatures, to estimate sizes of these regions. The results of these calculations

TABLE 3.5

Abundances of $H_2S$ in OMC-1

| Component | $T_{rot}$[a] (K) | Estimated[b] Source Size (arcsec) | $N(H_2)$[a,c] $(cm^{-2})$ | $\tau(H_2S)$[d] | $N(H_2S)$[c] $(cm^{-2})$ | $f$[e] |
|---|---|---|---|---|---|---|
| Extended Ridge | 30 | extended | 1-3(23) | < 1 | 2(14) | 1(-9) |
| Hot Core | 200 | ~ 3 | 1(24) | 23 | 1(18) | 1(-6) |
| Plateau | 100 | ~ 7 | 1(23) | 3 | 1(17) | 1(-6) |
| 1.5S | 75 | ~ 24 | 5(23) | 0.3 | 4(14) | 1(-9) |
| 3N1E | 15-30 | extended | 7(22) | 0.4 | 4(13) | 6(-10) |

Numbers in parenthesis are powers of 10.

[a] From Blake *et al.* (1987), Batrla *et al.* (1983), and Goldsmith *et al.* (1986).

[b] Using the equation: $T_R = (T_{ex} - 2.7)(1 - e^{-\tau})(D/HPBW)^2$, where D is the source diameter.

[c] Column density corrected for source size.

[d] Optical depth in the line center, from ratio of $H_2S$ and $H_2^{34}S$ data, assuming $S/^{34}S = 15$.

[e] Fractional abundance of $H_2S$ relative to $H_2$.

are given in Table 3.5. As shown in the table, we obtained a source diameter $\theta_s \sim 3''$ for the hot core, and $\theta_s \sim 7''$ for the plateau. Both of these values are less than those derived from other measurements by a factor of $\sim 2$ (e.g. Plambeck et al. 1982; Genzel et al. 1982). This disagreement may result from uncertainties in gaussian fit values and estimations of the excitation temperatures, although it is possible that the $H_2S$ emission is more confined than that of some other species. For the 1.5S position, we obtain $\theta_s \sim 24''$, the same value for the outflow as estimated from SiO observations (Ziurys, Wilson, and Mauersberger 1989). Optical depths and abundances for $H_2S$ are summarized in Table 3.5.

We have also made a search for deutrated $H_2S$ (HDS) at the KL postion, but this species has not been detected to a 1 $\sigma$ level of 33 mK at 250 kHz resolution. Since $H_2S$ seems to be most prominent in the hot core, as we see in the $H_2^{34}S$ spectrum in Figure 3.1, we used an excitation temperature $\sim 200$ K and a source size $\sim 3''$ for the hot core (Table 3.5) to derive an HDS column density. We derive an upper limit $N_{tot}(HDS) \leq 10^{15}$ cm$^{-2}$ in the hot core. Then we estimate the abundance ratio of [HDS]/[$H_2S$] to be less than $\sim 5 \times 10^{-4}$ (see Table 3.2).

## 3.5 Discussion

Recent ion-molecule chemical models employ the radiative association reaction between $SH^+$ and $H_2$ as a principal formation route for the ion $H_3S^+$ in dense clouds, which is the assumed precursor to $H_2S$. The predicted abundance of $H_2S$, therefore, depends on the rate coefficient of the radiative association reaction. Leung, Herbst, and Huebner (1984), following the work of Prasad and Huntress (1982), predicted a fractional abundance of $\sim 10^{-10}$ in quiescent clouds by using a large value of the rate coefficient. Herbst, DeFrees, and Koch (1989) have recalculated the rate coefficient to be about a factor of 2 less than that used by Leung, Herbst, and Huebner (1984). In the quiescent clouds in Orion A, including the extended ridge, our observed fractional abundance is $f(H_2S) \sim 10^{-9}$, which is similar to the value in the cold dark cloud L134N (Paper 1). Thus, the $H_2S$ abundance predicted by standard ion-molecule models is about an order of magnitude less than the observed value. In constrast, Charnley *et al.* (1988) in their dynamical cloud model produce $H_2S$ via the reaction $S^+ + H_2CO \rightarrow H_2S^+ + CO$, followed by $H_2S^+ + e^- \rightarrow H_2S + h\nu$. In this model, the cloud chemistry gets cycled via a collapse/star-formation/expansion sequence. In their slow cycle model, they produce $f(H_2S) \sim 10^{-9}$ in the cloud collapse phase - in good agreement with cold cloud observations. However, as with the other reaction sequence leading

43

to $H_2S$, the rates of the reactions used by Charnley *et al.* (1988) are not well known.

It is consequently difficult to establish whether ion-molecule chemistry can produce sufficient $H_2S$. Given certain assumptions about key rate coefficients, it appears that ion-molecule models can produce $f(H_2S) \sim 10^{-9} - 10^{-10}$, i.e., the values measured for the ambient gas in Orion and for the dark clouds L134N and TMC-1 as well (Minh, Irvine, and Ziurys 1989). However, until such key rate coefficients are determined accurately by experimental methods, the success of ion-molecule synthesis of $H_2S$ remains an open question.

Other processes such as high-temperature chemistry or grain surface chemistry may be important in the Orion hot core and plateau, where the $H_2S$ fractional abundances $f(H_2S) \sim 10^{-6}$ (see Table 3.5). Under high-temperature conditions, the endothermicities or the activation energies can be overcome. Smith and Adams (1985) have suggested that even for moderate increases in the ion velocities relative to $H_2$ (as would occur in MHD shocks), endothermic reactions which lead to the formation of $H_2S$ could be initiated: $S^+ + H_2$, $SH^+ + H_2$, and $H_2S^+ + H_2$. In MHD shocks, $SH^+$ is predicted to be formed in observable quantities (Millar *et al.* 1986; Pineau des Forets *et al.* 1986). $H_2S$ can also be formed from atomic sulfur by hydrogen-abstraction reactions with $H_2$, which have barriers of substantially greater than 7000 K (Hartquist, Oppenheimer, and Dalgarno 1980). The high temperature chemistry models predict a large enhancement of the abundace of sulfur-

containing molecules, including $H_2S$ (e.g. Hartquist, Oppenheimer, and Dargarno 1980; Mitchell 1984), after the passage of shocks, although the final abundances largely depend on the nature of the shock, poorly known reaction rates, and initial abundances.

Grain surface reactions have sometimes been suggested to play an important role in the formation of gas phase interstellar molecules, especially for sulfur- or nitrogen-containing species, although there are a number of serious uncertainties in the grain surface reaction schemes (cf. Prasad et al. 1987). One of the major questions is the desorption process, although this may be less of a problem in star-forming regions because of the intense UV field and the strong shock waves generated from the young stellar objects embedded in the cloud. Duley, Millar, and Williams (1980) have invoked grain surface reactions to synthesize $H_2S$. If sulfur has been depleted onto grain surfaces, ions like $C^+$ or $H^+$ are likely to find $SH^-$ or $S^-$ sites on the grain surfaces, which may lead to the formation of $H_2CS$ or $H_2S$, respectively. Although this model contains many uncertainties and produces too much $H_2S$, it may be possible that in dense clouds, where sulfur is highly depleted, a variety of sulfur-containing molecules may be formed easily through reactions on the sulphuretted grains (see also Tielens and Alamandola 1987).

The hot core is probably a dense clump or set of clumps in the cavity surrounding IRc 2. The heating mechanism of the hot core is probably radiative (Goldsmith et al. 1983), which may warm up the

45

grains and induce the thermal evaporation of their icy mantles. The large $H_2S$ abundance is consistent with release from the grain mantles directly, such as, for example, has been postulated for $NH_3$ and HDO, whose abundances are significuantly enhanced in the hot core (Sweitzer 1978; Plambeck and Wright 1987). Plambeck and Wright also suggest that any species released from the grain mantles will survive ~ 1 x $10^3$ yrs before being destroyed by gas phase reactions, but this is comparable with the outflow age, and such species could still be overabundant. Therefore, we conclude that the high $H_2S$ abundance $f(H_2S) \sim 10^{-6}$ in the hot core may result from grain mantle evaporation.

Unlike the large deuterium enhancements of the species such as $[HDO]/[H_2O]$ and $[NH_2D]/[NH_3]$ in the hot core (Plambeck and Wright 1987; Walmsley $et$ $al.$ 1987), we derive $[HDS]/[H_2S] \leq 5$ x $10^{-4}$. The large deuterium enhancements (as high as ~ 3 x $10^{-3}$ for $[NH_2D]/[NH_3]$) are thought to originate via deuterium fractionation in the gas-phase followed by freeze out onto grain mantles and subsequent evaporation. Grain surface chemistry may, however, also result in a high deuterium fractionation, mainly by the accretion of atomic deuterium in the gas phase (Tielens and Allamandola 1987; Brown and Millar 1989; Millar, Bennett, and Herbst 1989) Our non-detection of HDS may suggest that there are differences in the formation and fractionation of $HDS/H_2S$ relative to the processes that are important for $HDO/H_2O$ and $NH_2D/NH_3$.

The plateau emission comes from a violent region within KL which seems to be powered by IRc 2. Shock chemistry may be dominant in the plateau, and is thought to be responsible for the large abundances of SO, $SO_2$, and SiO. These species may be easily formed in the heated gas because of the enhancements of S, Si, and OH following grain disruption in the shocked region. The large abundance of the fragile molecule $H_2CO$ in the plateau (Blake et al. 1987) strongly suggests that small dense condensations also exist in the outflow region, and the high abundance of HDO in the plateau probably suggests that grain surface chemistry may be still important in the plateau. Therefore $H_2S$ may form either in the high-temperature shocked gas or on the grain surfaces in the plateau, and it is difficult to discriminate which chemistry actually plays the major role in producing the observed large abundance of $H_2S$, $f(H_2S) \sim 10^{-6}$. However, the small condensations in the plateau would contain grains similar to those in the hot core, and the evaporation of grain mantles by UV radiation or shocks would be expected to produce $H_2S$ in the gas phase.

In summary, the $H_2S$ abundances are enhanced by a factor of 1000 in the hot core and the plateau ($f(H_2S) \sim 10^{-6}$) relative to quiescent clouds. The large abundance of $H_2S$ in the hot core may result from grain mantle evaporation, while the large abundance in the plateau could result from high-temperature gas phase chemistry and/or grain-surface chemistry. $f(H_2S) \sim 10^{-9}$ for the quiescent region of OMC-1, which is similar to the value for L134N (Paper 1),

which seems to be difficult to explain by currently known ion-molecule reactions, at least under static cloud conditions. Higher spatial resolution observations should be useful, especially in a region like Orion(KL).

CHAPTER 4


HYDROGEN SULFIDE IN STAR-FORMING REGIONS


4.1 Summary

Interstellar hydrogen sulfide ($H_2S$) and its isotopic variant $H_2^{34}S$ have been observed towards several star-forming regions via their $1_{10}$ - $1_{01}$ transitions. Where both $H_2S$ and $H_2^{34}S$ were observed, the $H_2S$ lines are typically optically thick and $H_2S$ column densities $\sim 10^{15}$ cm$^{-2}$ are found. We set lower limits for the $H_2S$ column densities of $\sim 10^{14}$ cm$^{-2}$ for other sources observed with only the $H_2S$ line. The fractional abundances of $H_2S$ relative to molecular hydrogen are in the range of $10^{-8}$ to $10^{-9}$. $H_2S$ has been searched for unsuccesfully only towards the supernova remnant IC443B, where we set an upper limit 6 x $10^{13}$ cm$^{-2}$ for the $H_2S$ total column density.

4.2 Introduction


Interstellar hydrogen sulfide ($H_2S$) was first observed in the ISM via its $1_{10}$ - $1_{01}$ transition towards several GMCs by Thaddeus *et al.* (1972). Recently, Minh, Irvine, and Ziurys (1989; Paper 1; cf. Chapter 2), and Minh *et al.* (1989; Paper 2; cf. Chapter 3) have observed this transition towards cold dark clouds and towards OMC-1,

and discussed the relative importance of grain-surface reactions, high-temperature shock chemistry, and ion-molecule reactions for the formation of $H_2S$. Indeed, it is very difficult to differentiate between gas- phase reactions and grain-related processes in the formation of interstellar molecules such as $H_2S$, although there are clearly large enhancements in the fractional abundance of $H_2S$ in regions of massive star formations (by factors up to $10^3$). Even in quiescent regions, the observed fractional abundances of $\sim 10^{-9}$ seems to be difficult to explain with currently known ion-molecule models. $H_2S$ has been suggested as a tracer of high-temperature chemistry or grain surface chemistry because the expected gas phase reactions leading to the formation of $H_2S$ are thought to be appreciably endothermic (Watson and Walmsley 1982; Smith and Adams 1985; Duley, Millar, and Williams 1980). $H_2S$ has been identified tentatively in the grain mantles toward the compact radio source W33A (Geballe *et al*. 1986).

Sulfur-containing molecules appear to be fairly abundant in star formation regions, accompanied by shock waves and high temperatures. Such observations have lead to the postulation that "shock" or "high temperature" chemistry, i.e. chemistry involving gas-phase reactions with activation energies, may be taking place in hot regions and producing these species. Along with elevated temperatures shocks can also cause the partial or complete destruction of dust grains, which would return molecules in the grains to the gas-phase. Also, the UV radiation field from the

newly formed massive stars can evaporate grain mantles and consequently release volatile molecules into the gas phase. Although the strong UV field also can disscociate molecules released from the grain mantles, the high density of gas and dust grains may strongly inhibit such destruction and thus enhance these species in the gas component in star-forming regions.

$H_2S$ abundances in the active regions of Orion(KL), which are enhanced by a factor of 1000 relative to those in quiescent clouds, strongly suggest that the increased $H_2S$ production is related to activities in star formation regions, and possibly to grain-related processes. In this Chapter, we report the results of $H_2S$ and $H_2^{34}S$ observations toward several other star forming regions.

### 4.3 Observations

Observations of the $1_{10} - 1_{01}$ transitions of $H_2S$ and its isotope species $H_2^{34}S$ (rest frequencies: 168.76276237 GHz and 167.910516 GHz, respectively, Helminger, De Lucia, and Kirchhoff 1973) were made using the FCRAO 14 m telescope between 1989 January and April. The HPBW and the beam efficiency of the telescope are 35 arcseconds and 0.25 at these frequencies, respectively. The receiver and the observing method are described in § 3.3. The temperature scale is given as $T_A^*$, the beam-chopper-corrected antenna temperature. We approximate the brightness temperature by main beam brightness temperature $T_{MB} = T_A^*/\eta_B$.

51

## 4.4 Results

### 4.4.1 Sgr B2

The Sgr B2 molecular cloud, situated $\sim 120$ pc from the Galactic Center, represents a relatively extreme case in terms of mass and column density. A variety of different molecules has been observed in this core, probably because of the large column density and the existence of many different excitation conditions (cf. Irvine, Goldsmith, and Hjalmarson 1987). The $H_2S$ and $H_2{}^{34}S$ spectra obtained at the center (M) and 1N positions are shown in Figure 4.1, and the observed line parameters at these locations and towards more quiescent gas at the position labeled 2N are given in Table 4.1. The $H_2S$ spectra show two peaks at $V_{LSR} \sim 50$ km s$^{-1}$ and $\sim 80$ km s$^{-1}$, which coincide with two peaks of strongly self-absorbed $^{13}CO$ J=2-1 (Lis 1989). The $H_2{}^{34}S$ spectra, however, may indicate that the $H_2S$ emission in Sgr B2 is not self-absorbed, but traces two different components inside this molecular cloud. Based on the $H_2{}^{34}S$ spectra, we regard the $H_2S$ emission as coming from two different regions, but higher spatial resolution observations would be useful to discriminate the velocity components in Sgr B2 unambiguously.

An estimate of the optical depth can be derived by comparing the antenna temperatures of the same transition of two isotopic variants such as $H_2S$ and $H_2{}^{34}S$. We derive optical depths by assuming the cosmic value of the $S/{}^{34}S$ ratio $\sim 22$ and the

52

TABLE 4.1

$H_2S$ and $H_2^{34}S$ Line Parameters Observed towards Sgr B2

| Position | $T_A^*$ | $V_{LSR}$ | $\Delta V$ | $\int T_A^* dV$ |
|---|---|---|---|---|
| | (K) | (km s$^{-1}$) | (km s$^{-1}$) | (K km s$^{-1}$) |
| SgrB2(M) | 0.36 | 50 | 10 | 3.6 |
| | (0.14) | (51) | (13) | (1.9) |
| | 0.18 | 76 | 18 | 3.3 |
| SgrB2(N) | 0.30 | 48 | 16 | 5.0 |
| | (0.24)(?) | (56) | (3) | (0.9) |
| | 0.17 | 84 | 22 | 3.9 |
| SgrB2(2N) | 0.23 | 52 | 7 | 1.5 |
| | 0.15 | 84 | 9 | 1.3 |

Numbers in parenthesis are for the $H_2^{34}S$ $(1_{10} - 1_{01})$ line.

Spectral resolution is 1 MHz.

Line parameters are derived from gaussian fit.

<u>Positions</u>: SgrB2(M): RA(1950) = $17^h44^m11^s.3$, Dec(1950) = $-28^\circ22'30''$;

SgrB2(N): RA(1950) = $17^h44^m11^s.3$, Dec(1950) = $-28^\circ21'30''$; SgrB2(2N):

RA(1950) = $17^h44^m11^s.3$, Dec(1950) = $-28^\circ20'30''$.

Figure 4.1   Spectra of the $1_{10}$ - $1_{01}$ transitions of $H_2S$ and

$H_2^{34}S$ taken towards Sgr B2(M) and (N) at a spectral resolution

of 1 MHz (positions given in Table 4.1).   The $CH_3OH$

$(9_1 - 9_0$ E1) line is shown in the $H_2^{34}S$ spectra.

55
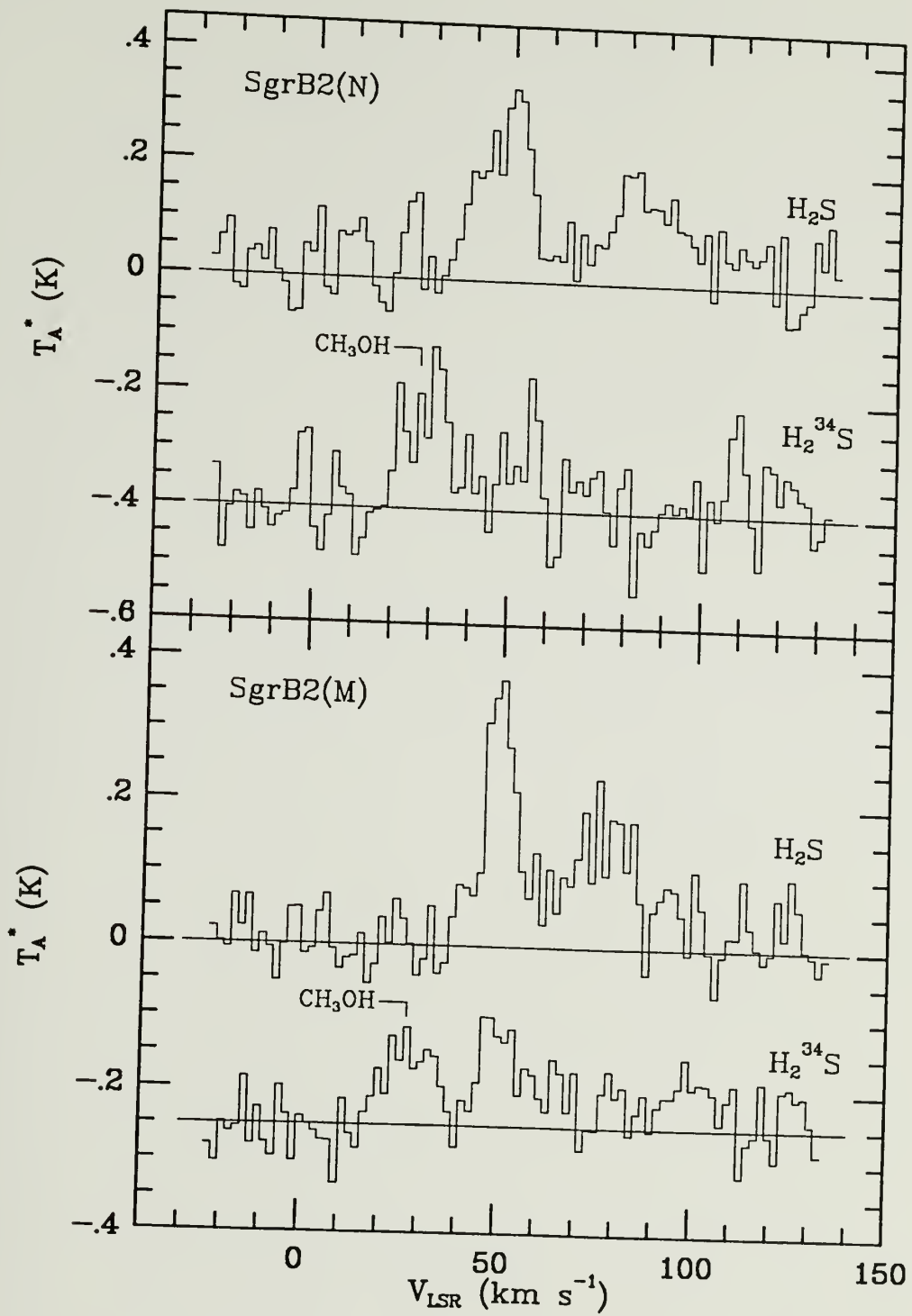
co-existence of the two species in the same region with the same excitation temperature. Results are included in Table 4.6. Adoption instead of $S/^{34}S \sim 15$, which seems to be appropriate to Orion (Paper 2), would result in $\sim 30$ % decrease in the total column density. We have assumed rotational temperatures ($T_{rot}$) of 20 K, and the effects of varying this assumption in calculating total column densities are shown in Figure 4.2. As shown in the figure, total column densities are relatively insensitive to $T_{rot}$. For comparison, total column densities have also been derived from the $H_2^{34}S$ line using the "standard" equation (Irvine, Goldsmith, and Hjalmarson 1987) for optically thin emission, $T_{rot} = 20$ K, and the isotopic abundance ratio given above. We derive similar values of total column density from both methods, and $N_{total}(H_2S) \sim 10^{15}$ cm$^{-2}$ for each component in Sgr B2(M) and (N). For Sgr B2(2N), we assumed the $H_2S$ line was optically thin. The column densities are included in Table 4.6.

4.4.2 W49

W49, at a distance of 14 kpc, is one of the most active star-formation regions in the Galaxy. It contains the most powerful complex of $H_2O$ masers in the Galaxy (Knowles *et al.* 1974; Genzel *et al.* 1978), with hundreds of spectral features. Several positions have been observed, and the $H_2S$ line parameters are given in Table 4.2 and sample spectra in Figure 4.3. The $H_2S$ spectrum

Figure 4.2   Multiplication factors for determining total column densities of $H_2S$ from values calculated with $T_{rot} = 20$ K, as a function of rotational temperatures $(T_{rot})$.   Calculation assumes a Boltzmann population distribution.   Solid line assumes optically thin lines and dashed line corresponds to calculation with the optical depth as found from the ratio of the $H_2S$ and $H_2^{34}S$ transitions.
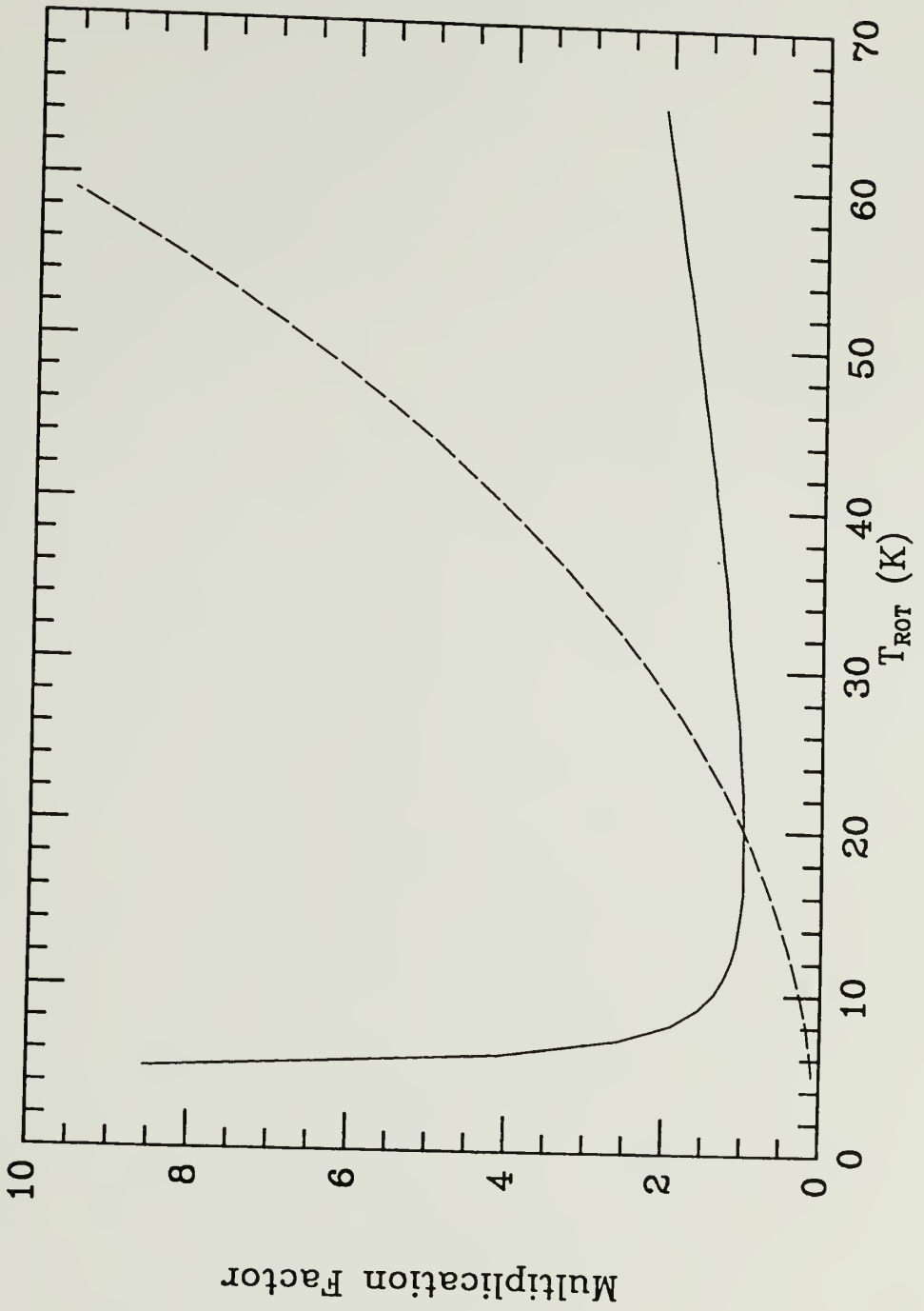
towards W49N is quite similar to the single-dish CO spectrum (HPBW ~ 45"), which shows a strong self-absorption feature (Scoville *et al.* 1986). The $H_2S$ emission is probably self-absorbed, since the $H_2^{34}S$ spectrum obtained toward W49N shows a single peak whose $V_{LSR}$ coincides with the absorption feature of the $H_2S$ spectrum (Figure 4.3). The $H_2S$ emission in W49N is fairly extended, and spatial-velocity maps are shown in Figure 4.4. We derive an optical depth ~ 7 at the line center towards the (0, 0) position in Table 4.2 by comparing the $H_2S$ and $H_2^{34}S$ spectra, and $N_{total}(H_2S)$ ~ $2 \times 10^{15}$ cm$^{-2}$ from both the $H_2S$ optical depth and the $H_2^{34}S$ line itself with the same assumptions described in § 4.4.1.

4.4.3 <u>W51</u>

The W51 molecular complex is located at a distance of 7 kpc and has two infrared and radio continuum sources associated with bright $H_2O$ masers: W51(M) and W51(N). Genzel and Downes (1982) have suggested that W51(N) has a remarkable morphological similarity to Orion(KL), but the total infrared luminosity is much larger than the luminosity of Orion(KL), and the mass and momentum contained in the high velocity gas are also larger than in Orion by about an order of magnitude. W51(M/S) is located ~ 1' to the south of W51(N), and has a group of ultra-compact HII regions, and OH and $H_2O$ maser sources. The observed line parameters are included in Table 4.3. The $H_2S$ spectrum for W51(N) shows a "plateau" emission which seems

TABLE 4.2

$H_2S$ Line Parameters Observed toward W49N

| Offset[a] | | $T_A^{*}$ [b] | $V_{LSR}$ | $\Delta V$ | $\int T_A^{*} dV$ |
|---|---|---|---|---|---|
| $\Delta\alpha$ | $\Delta\delta$ | (K) | (km s$^{-1}$) | (km s$^{-1}$) | (K km s$^{-1}$) |
| 0. | 0. | 0.39 ±.03 | 7.4 | 17.8 | 7.3 |
| | | (0.10 ±.03) | (8.8) | (7.6) | (0.8) |
| 1. | 0. | 0.29 ±.04 | 5.3 | 14.8 | 4.3 |
| 2. | 0. | 0.31 ±.05 | 10.7 | 7.3 | 2.3 |
| 3. | 0. | ≤ 0.15[c] | — | — | — |
| -1. | 0. | 0.36 ±.04 | 7.8 | 14.5 | 5.2 |
| -2. | 0. | ≤ 0.15[c] | — | — | — |
| 0. | 1. | 0.18 ±.06 | 8.9 | 10.9 | 2.0 |
| 0. | 2. | ≤ 0.23[c] | — | — | — |
| 0. | -1. | 0.28 ±.06 | 10.6 | 5.8 | 1.6 |
| 0. | -2. | ≤ 0.16[c] | — | — | — |

NOTE. - Spectral resolution is 1 MHz.

Numbers in parenthesis are for the $H_2^{34}S$ ($1_{10} - 1_{01}$) line.

[a] In arcmin from RA(1950) = $19^h07^m49^s.8$ and Dec(1950) = $9°01'17''$.

[b] Errors are 1 $\sigma$.

[c] 3 $\sigma$ upper limit.

Figure 4.3    Spectra of the $1_{10} - 1_{01}$ transitions of $H_2S$ and $H_2^{34}S$ towards W49N and W49S at a resolution of 1 MHz (positions given in Table 4.2).
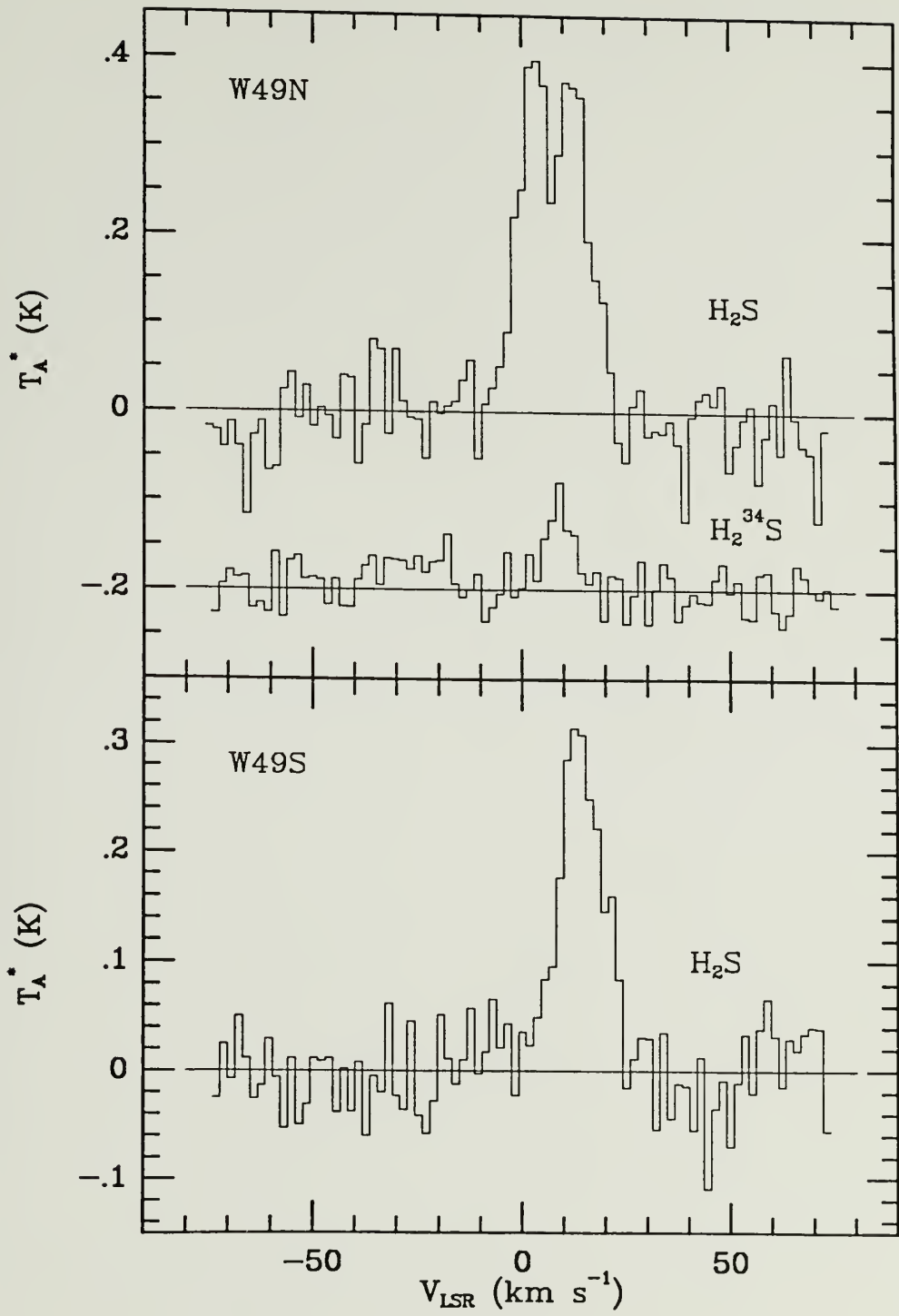
Figure 4.4    Spatial-velocity maps for the observed antenna temperatures obtained toward W49N.    Offsets are from the (0, 0) position of W49N in Table 4.2.    Lowest contour level is 0.05 K and levels increase by 0.03 K for both panels.
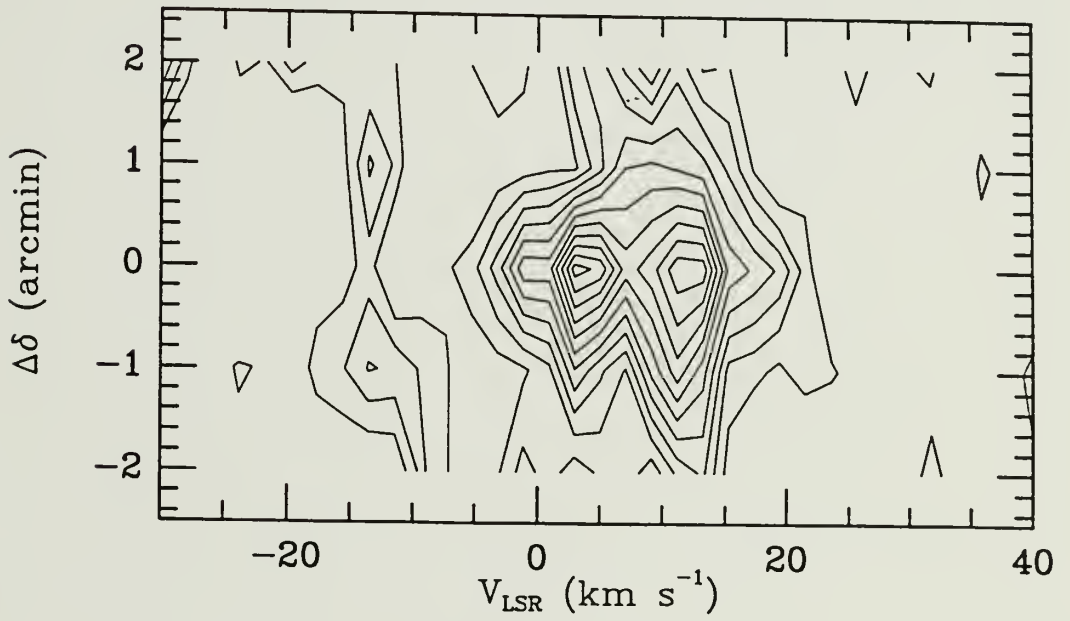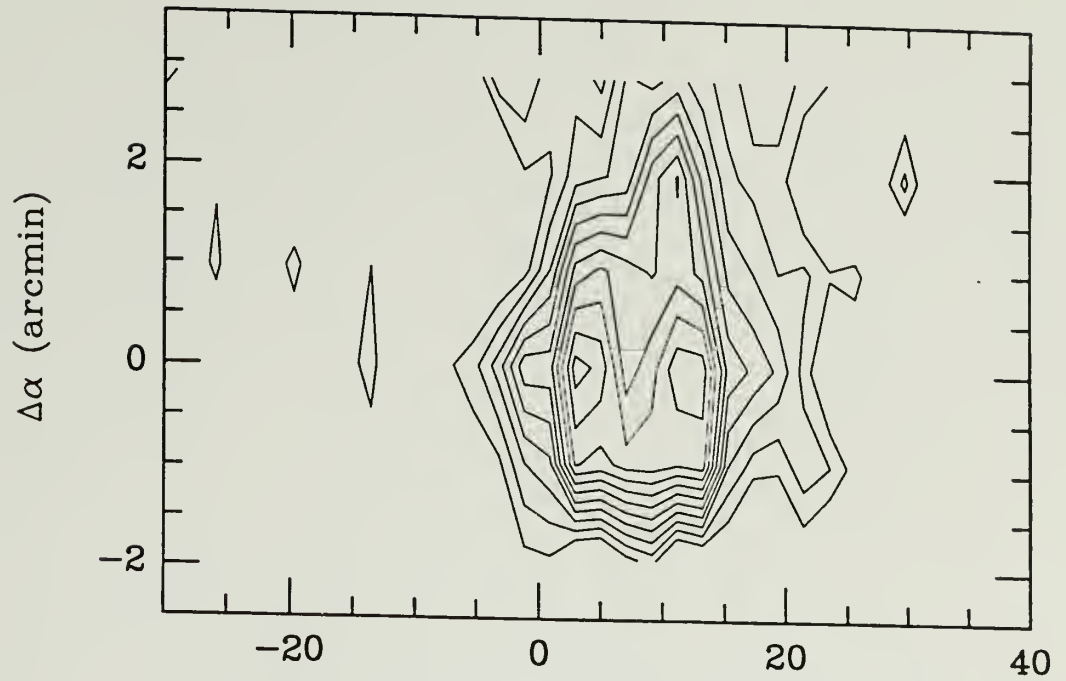
to have a center velocity at ~ 50 km s$^{-1}$ and $\Delta V$ ~ 15 km s$^{-1}$. In Figure 4.5, we show the spectrum and a two component gaussian fit. Since H$_2^{34}$S data was not obtained toward W51(N), we calculated the column density from the integrated intensity of the H$_2$S line by assuming optically thin emission. As a result, the column density may be underestimated by a large factor, because the optical depth could be larger than one and the source size much smaller than the beam size. For W51(M/S), we derive an optical depth of ~ 3 by comparing the H$_2$S and H$_2^{34}$S intensities, leading to N$_{total}$(H$_2$S) ~ $10^{15}$ cm$^{-2}$. We have applied the same assumptions to derive column densities as described in § 4.4.1 (see also Figure 4.2 for the effect of T$_{rot}$ in the calculation of column densities).

4.4.4 <u>W3(IRS5)</u>

W3(IRS5) is located at a distance of ~ 2.5 kpc and has a cluster of infrared sources, H$_2$O masers, and ultra-compact HII regions. The weakness of the radio continuum emission, the lack of high velocity motions and evidence for shock excitation may indicate that W3(IRS5) is in an earlier evolutionary stage than Orion(KL), W51, or W49 (Genzel and Downes 1982). The line parameters are included in Table 4.3 and the spectra in Figure 4.6. We derive an optical depth of ~ 5 for the H$_2$S line from comparison with the H$_2^{34}$S intensity. This corresponds to N$_{total}$(H$_2$S) ~ $10^{15}$ cm$^{-2}$, applying the same arguments as described in § 4.4.1.

TABLE 4.3

Line Parameters Observed in W51 and W3

| Position | $T_A^*$ | $V_{LSR}$ | $\Delta V$ | $\int T_A^* dV$ |
|----------|---------|-----------|------------|-----------------|
| | (K) | (km s$^{-1}$) | (km s$^{-1}$) | (K km s$^{-1}$) |
| W51(N) | 0.14 | 52.9 | 15.0 | 7.9 |
| | 0.92 | 61.1 | 7.2 | 7.1 |
| W51(M/S) | 1.03 | 56.8 | 10.4 | 11.4 |
| | (0.14) | (55.3) | (13.5) | (2.1) |
| W3(IRS5) | 0.64 | -40.8 | 6.9 | 4.7 |
| | (0.13) | (-40.9) | (16.5) | (2.3) |
| W3(OH) | (0.19) | (-43.9) | (4.4) | (0.8) |

Numbers in parenthesis are for the $H_2^{34}S$ ($1_{10} - 1_{01}$) line.

Spectral resolution is 1 MHz.

<u>Positions</u>: W51(N): RA(1950) = $19^h21^m22^s.0$, Dec(1950) = $14°25'20"$;

W51(M/S) = RA(1950) = $19^h21^m26^s.4$, Dec(1950) = $14°24'42"$; W3(IRS5):

RA(1950) = $2^h21^m53^s.0$, Dec(1950) = $61°52'21"$; W3(OH): RA(1950) =

$2^h23^m16^s.8$, Dec(1950) = $61°38'57"$.

66

Figure 4.5    Spectra of the $1_{10}$ - $1_{01}$ transitions of $H_2S$ and $H_2^{34}S$ towards W51(N) and W51(M/S) at a resolution of 1 MHz (positions given in Table 4.3).    Dotted lines in the W51(N) spectrum show gaussian components and line parameters are included in Table 4.3.    The $CH_3OH$ ($9_1$ - $9_0$ E1) line is shown in the $H_2^{34}S$ spectrum.

68
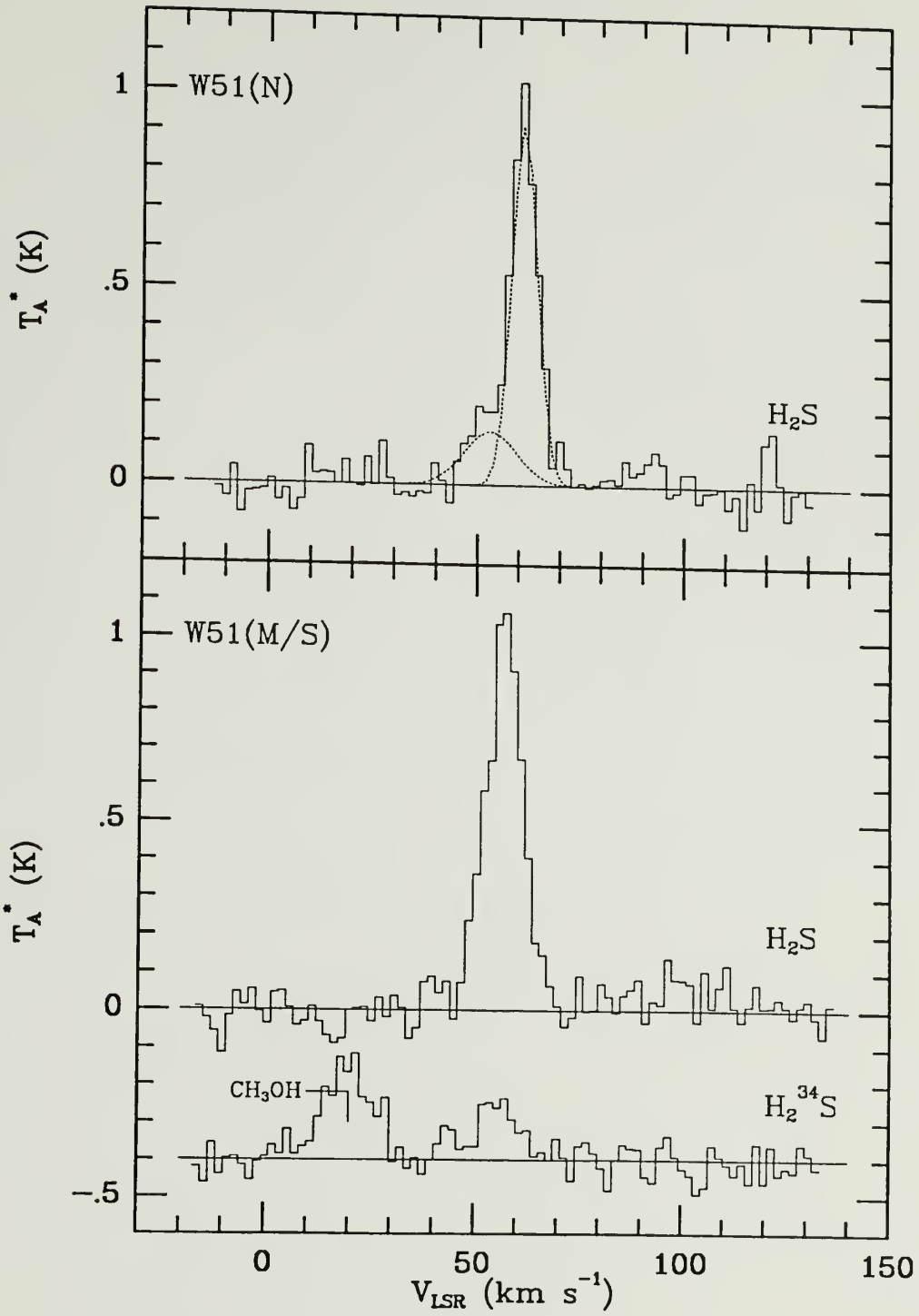
Figure 4.6    Spectra of the $1_{10}$ - $1_{01}$ transitions of $H_2S$ and $H_2{}^{34}S$ towards W3(IRS5) at a resolution of 1 MHz (position given in Table 4.3).

W3(IRS5)

H$_2$S

H$_2^{34}$S

$V_{LSR}$ (km s$^{-1}$)

$T_A^*$ (K)
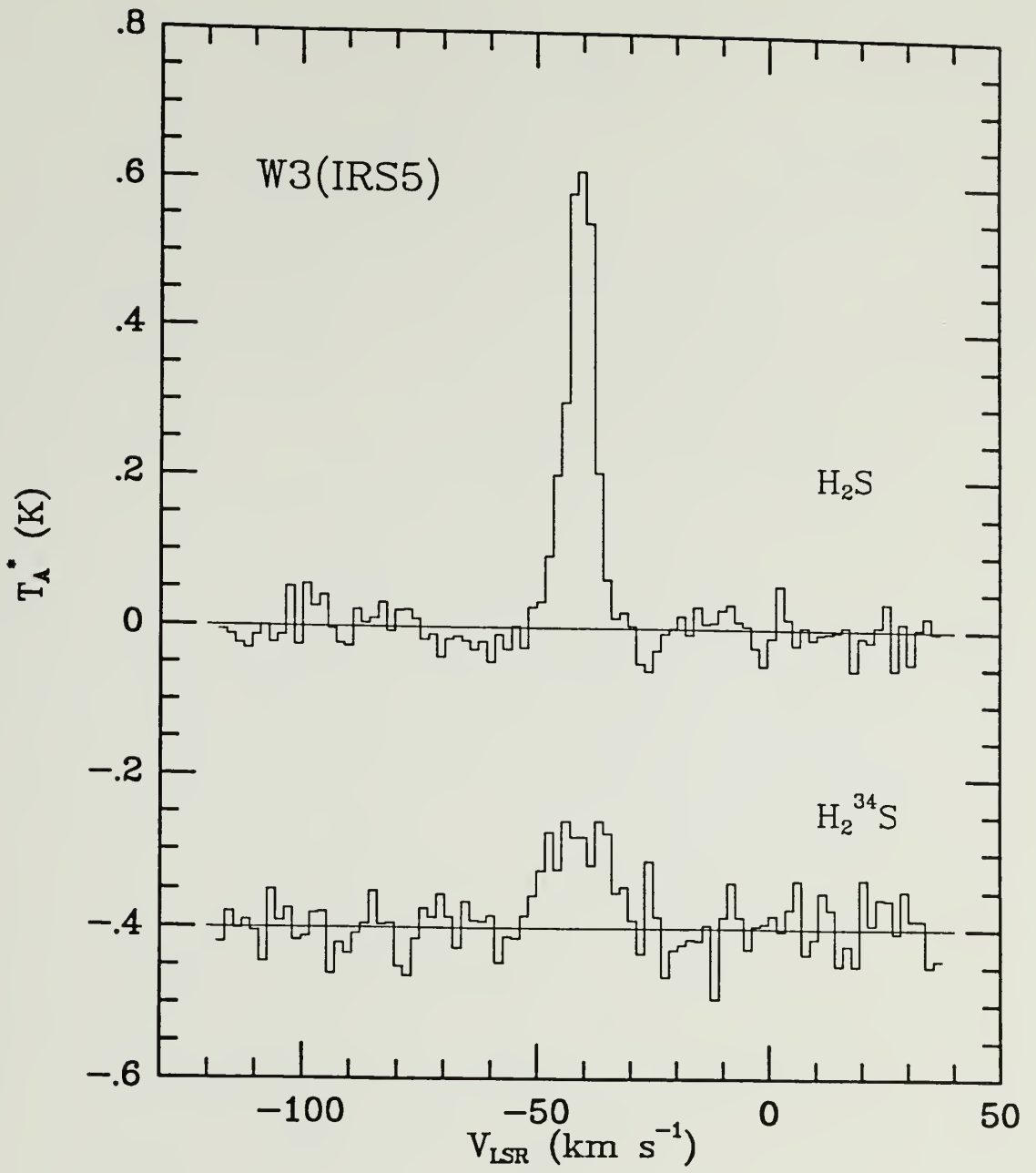
## 4.4.5 Other Sources

The $H_2S$ line parameters for other star-forming regions are included in Table 4.4. Most spectra show somewhat asymmetric line profiles, and sample spectra for NGC7538 are shown in Figure 4.7. The $H_2^{34}S$ line has not been detected toward NGC7538(N) to a 1 $\sigma$ value of 40 mK, which indicates that the optical depth of $H_2S$ is less than 2.6. The $H_2S$ total column densitites for these sources have been derived to be ~ $10^{14}$ $cm^{-2}$ if the $H_2S$ lines are optically thin and the sources fill the antenna beam (see Table 4.6). Most of these sources contain embedded infrared sources, however, and star-formation is probably occuring actively. From the results for the sources in Tables 4.1 - 4.3, it is likely that such regions have optical depths larger than one. The source sizes also could be smaller than the beam size. Therefore, this value of $N_{tot}(H_2S)$ is probably a lower limit.

Among the sources in Table 4.4, the $H_2S$ line has not been detected (to a 3 $\sigma$ limit of 94 mK) only toward IC443B. We derive $N_{total}(H_2S) \leq 6 \times 10^{13}$ $cm^{-2}$. SNR IC443 contains several regions which suggest the recent passage of shocks, as evidenced by unusually broad and asymmetric line profiles observed in CO and OH (e.g. DeNoyer and Frerking 1981; Huang, Dickman, and Snell 1986). In Clump B (IC443B), many molecular species have been detected (cf. Ziurys, Snell, and Dickman 1987), and the SiO abundance is significantly enhanced relative to limits in quiescent clouds.

71

TABLE 4.4

H$_2$S Line Parameters for Other Sources

| Source | $T_A^{*\ a}$ (K) | $V_{LSR}$ (km s$^{-1}$) | $\Delta V$ (km s$^{-1}$) | $\int T_A^* dV$ (K km s$^{-1}$) |
|---|---|---|---|---|
| AFGL4029 | 0.28 ±.04 | -38.8 | 2.7 | 0.8 |
| S235B | 0.85 ±.11 | -17.0 | 4.0 | 3.4 |
| S255 | 0.82 ±.18 | 7.7 | 3.6 | 2.9 |
| W33A | 0.49 ±.05 | 35.9 | 8.4 | 4.2 |
| G34.3+0.2 | 1.14 ±.05 | 56.6 | 4.0 | 4.5 |
| W49S | 0.31 ±.04 | 12.4 | 13.5 | 4.3 |
| S106 | 0.19 ±.04 | -1.4 | 8.4 | 1.6 |
| DR21(OH) | 0.52 ±.09 | -4.2 | 3.2 | 1.7 |
| DR21 | 0.39 ±.13 | -1.3 | 3.9 | 1.6 |
| S140 | 1.15 ±.08 | -6.7 | 3.6 | 4.2 |
| Ceph A | 0.58 ±.04 | -10.9 | 5.6 | 3.3 |
| NGC7538(N) | 1.01 ±.07 | -57.5 | 4.8 | 4.8 |
| NGC7538(S) | 0.81 ±.05 | -57.0 | 5.8 | 4.7 |
| NGC7538(E) | 0.39 ±.04 | -57.0 | 4.6 | 1.8 |
| IC443B | ≤ 0.09[b] | — | — | — |

[a] Errors are 1 $\sigma$.

[b] 3 $\sigma$ upper limit.

TABLE 4.4

(Continued)

NOTE. - Spectral resolutions are 1 MHz for W33A, W49S, S106, and
Ceph A, and 250 kHz for other sources.

Positions: AFGL4029: RA(1950) = $2^h57^m35^s.6$, Dec(1950) = $60°17'22"$;
S235B: RA(1950) = $5^h37^m30^s.4$, Dec(1950) = $35°39'57"$; S255:RA(1950)
= $6^h09^m58^s.3$, Dec(1950) = $18°00'11"$; W33A: RA(1950) = $18^h11^m19^s.0$,
Dec(1950) = $-17°56'46"$; G34.3+0.2: RA(1950) = $18^h50^m46^s.0$,
Dec(1950) = $1°11'10"$; W49S: RA(1950) = $19^h07^m58^s.0$, Dec(1950)
= $9°00'05"$; S106: RA(1950) = $20^h25^m34^s.0$, Dec(1950) = $37°12'52"$;
DR21(OH): RA(1950) = $20^h37^m15^s.0$, Dec(1950) = $42°12'08"$; DR21:
RA(1950) = $20^h37^m07^s.6$, Dec(1950) = $42°08'46"$; S140: RA(1950) =
$22^h17^m41^s.2$, Dec(1950) = $63°03'41"$; Ceph A: RA(1950) = $22^h54^m19^s.0$,
Dec(1950) = $61°45'47"$; NGC7538(N): RA(1950) = $23^h11^m36^s.6$, Dec(1950)
= $61°11'48"$; NGC7538(S): RA(1950) = $23^h11^m36^s.6$, Dec(1950) =
$61°10'48"$; NGC7538(E): RA(1950) = $23^h11^m53^s.0$, Dec(1950) = $61°10'58"$;
IC443B: RA(1950) = $6^h14^m15^s.0$, Dec(1950) = $22°26'50"$.

Figure 4.7    Spectra of the $1_{10}$ - $1_{01}$ transition of $H_2S$

towards NGC7538(N), (S), and (E) at a resolution of 250 kHz

(positions given in Table 4.4).
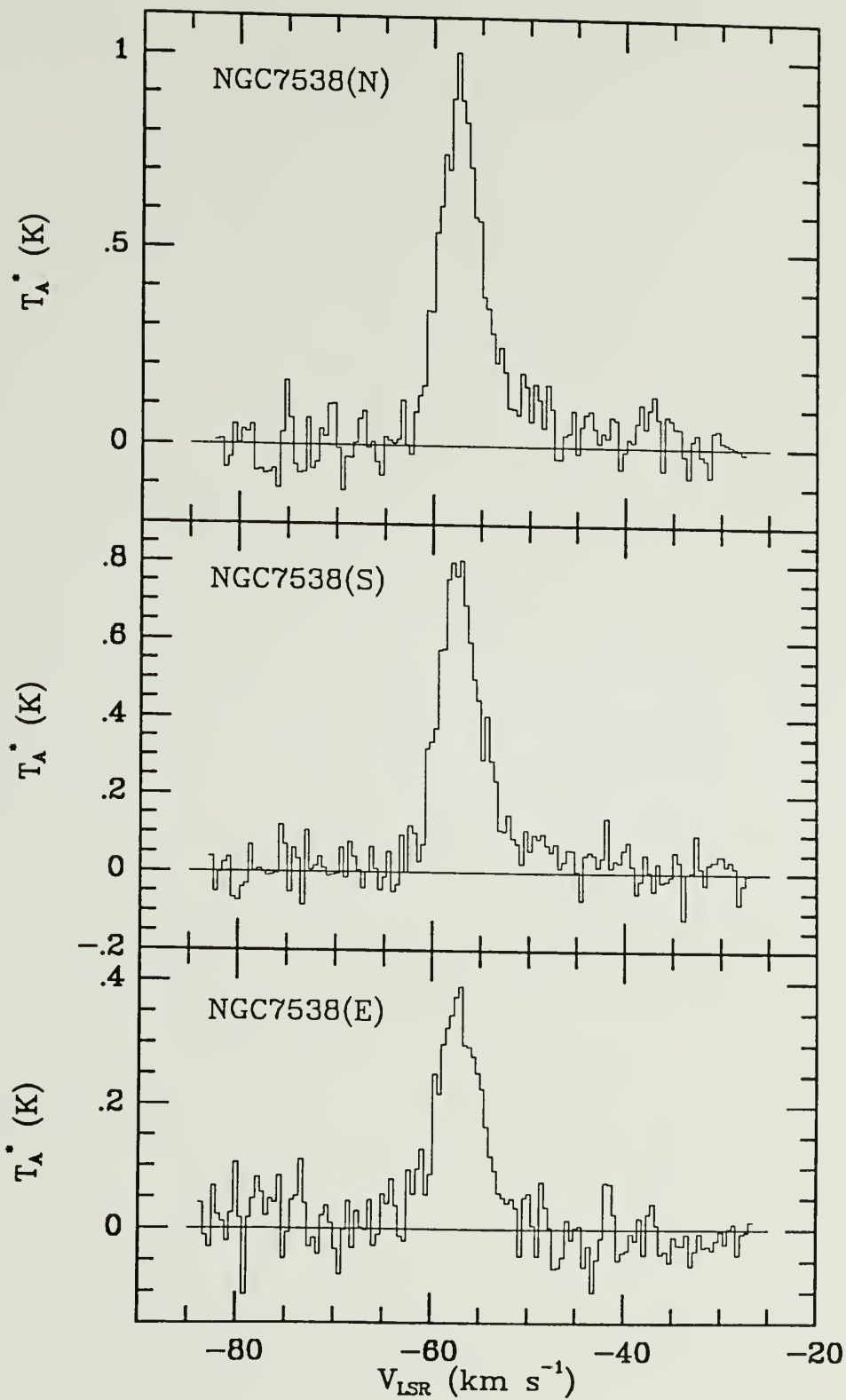
TABLE 4.5

Line Parameters for $^{34}$SO $(4_3 - 3_3)$ and $CH_3OH$ $(9_1 - 9_0$ E1) Lines

| Source | $T_A^{*\ a}$ (K) | $V_{LSR}$ (km s$^{-1}$) | $\Delta V$ (km s$^{-1}$) | $\int T_A^* dV$ (K km s$^{-1}$) |
|---|---|---|---|---|
| $^{34}$SO $(4_3 - 3_3)$ | | | | |
| SgrB2(M) | 0.10 ±.04 | 58.2 | 9.5 | 1.0 |
| W49N(0,0) | 0.10 ±.03 | 7.8 | 7.8 | 0.8 |
| $CH_3OH$ $(9_1 - 9_0$ E1) | | | | |
| SgrB2(M) | 0.13 ±.05 | 64.4 | 12.4 | 1.7 |
| SgrB2(N) | 0.28 ±.07 | 66.4 | 9.1 | 2.6 |
| W51(M/S) | 0.25 ±.05 | 51.4 | 20.2 | 3.8 |

[a] Errors are 1 $\sigma$.

NOTE. - Spectral resolution is 1 MHz.

Rest frequency: $^{34}$SO $(4_3 - 3_3)$ line: 168.815101 GHz (Hollis *et al.* 1981); $CH_3OH$ $(9_1 - 9_0$ E1) line: 167.93113 GHz (Lovas 1989).

TABLE 4.6

H$_2$S Column Densities

| Source | $N_{total}(H_2S)$ (cm$^{-2}$) | Comments |
|---|---|---|
| SgrB2(M) | ~ 2 (15) | Applies to both the 50 km s$^{-1}$ and 80 km s$^{-1}$ components, which have $\tau(H_2S)$ ~ 11 and 7, respectively. |
| SgrB2(N) | ~ 2 (15) | Applies to both the 50 km s$^{-1}$ and 80 km s$^{-1}$ components, which have $\tau(H_2S)$ ~ 6 and 7, respectively. |
| SgrB2(2N) | ≥ 1 (14) | Applies to both the 50 km s$^{-1}$ and 80 km s$^{-1}$ components. From the H$_2$S line, assuming $\tau(H_2S) \ll 1$. |
| W49N (0,0) | 2 (15) | $\tau(H_2S)$ ~ 7 at the line center. |
| W51(N) | ≥ 1 (14) | Applies to both the 50 km s$^{-1}$ and 60 km s$^{-1}$ gaussian fit components. From the H$_2$S line, assuming $\tau(H_2S) \ll 1$. |
| W51(M/S) | 1 (15) | $\tau(H_2S)$ ~ 3 at the line center. |
| W3(IRS5) | 1 (15) | $\tau(H_2S)$ ~ 5 at the line center. |
| IC443B | ≤ 6 (13) | With $3\sigma$ value, $\Delta V$=20 km s$^{-1}$, and $T_{rot}$ = 20K. |
| Other Sources | ≥ 1 (14) | Assuming for the H$_2$S lines $\tau \ll 1$ and $T_{rot}$ = 20 K. |

The $^{34}$SO $4_3$ - $3_3$ line and presumably the $CH_3OH$ $9_1$ - $9_0$ E1 line (Paper 2) have been detected in some sources.  Line parameters for both these species are listed in Table 4.5.

## 4.5 Discussion

We derive $H_2S$ total column densities of ~ $10^{15}$ cm$^{-2}$ towards several star-forming regions observed in the $H_2S$ and $H_2^{34}S$ lines, which is about an order of magnitude larger than suggested by Thaddeus *et al.* (1972), who did not have $H_2^{34}S$ data available.  We find values $\geq 10^{14}$ cm$^{-2}$ in other sources observed only by the $H_2S$ line.  Although total hydrogen column densities are not certain toward many of these locations, the fractional abundances of $H_2S$ relative to $H_2$ may be ~ 0.2 - 1 x $10^{-8}$ in Sgr B2 (for $N(H_2)$ ~ 0.2 - 1 x $10^{24}$ cm$^{-2}$; Irvine, Goldsmith, and Hjalmarson 1987; Lis 1989), ~ $10^{-7}$ - $10^{-8}$ in W49N and W51(M/S) ($N(H_2)$ ~ 1-10 x $10^{22}$ cm$^{-2}$; Scoville and Solomon 1973), and probably in the range $10^{-8}$ - $10^{-9}$ for other sources (assuming $N(H_2)$ ~ 1-10 x $10^{22}$ cm$^{-2}$; e.g. Evans and Blair 1981; Goldsmith and Mao 1983).  However, the $H_2S$ abundances for these other star-forming regions may be regarded as lower limits since these values could be increased very much depending on the source sizes, optical depths, and rotational temperatures.

Most of the star-forming regions observed here have infrared sources, compact HII regions, radio continuum sources, and maser sources.  The $H_2S$ chemistry has been discussed in Paper 1 and 2,

and the possible grain processes for the formation of $H_2S$ could be also important in the sources discussed here. The $H_2S$ abundances in these regions are in between those for quiescent clouds ($\sim 10^{-9}$), and the Orion hot core and the plateau ($\sim 10^{-6}$) (Paper 1 and 2). Therefore, a part of the $H_2S$ emission may also come from small, hot, and dense regions like the Orion hot core or plateau. Higher spatial resolution observations would be very useful to study $H_2S$ in these regions.

In the supernova remnant IC443B, we derive an upper limit for the $H_2S$ column density $N_{total}(H_2S) \leq 6 \times 10^{13}$ cm$^{-2}$, which may correspond to a fractional abundance $f(H_2S) \leq 6 \times 10^{-8}$ assuming the $H_2$ column density estimated from other molecules (Ziurys, Snell, and Dickman 1988). This upper limit is not low enough to determine if the $H_2S$ abundance is significantly enhanced relative to quiescent cloud values, as is predicted in some models of shock chemistry. A better upper limit would be useful to discuss this question.

CHAPTER 5

$H_2CS$ ABUNDANCES AND ORTHO-TO-PARA RATIOS IN INTERSTELLAR CLOUDS

5.1  <u>Summary</u>

Several $H_2CS$ ortho and para transitions have been observed toward interstellar molecular clouds, including cold, dark clouds and star forming regions.   We derive $H_2CS$ fractional abundances $f(H_2CS) \sim 1 - 2 \times 10^{-9}$ relative to molecular hydrogen towards TMC-1, Orion A, and NGC7538, and $\sim 5 \times 10^{-10}$ for L134N.

The $H_2CS$ ortho-to-para ratios in TMC-1 are $\sim 1.8$ towards the cyanopolyyne peak and the ammonia peak, which may indicate the thermalization of $H_2CS$ on 10 K grains.   We derive a ratio of $\sim 3$, the statistical value, for Orion(3N1E) and NGC7538, while we find a value $\sim 2$ for Orion(KL).

5.2 <u>Introduction</u>

Molecules such as $H_2$, $H_2O$, and $H_2CO$, have two distinct states, depending on the spin of the identical hydrogen nuclei: the para and the ortho states for anti-parallel and parallel spins, respectively. Since radiative or collisional conversion from one form to the other is forbidden, the ortho to para abundance ratio would provide information on the effective formation temperature of the molecules

if only gas phase processes were important subsequent to formation (cf. Kahane *et al.* 1984; hereafter KFLEL). Usually molecular formation temperatures are much larger than the energy difference between ortho and para states, and the corresponding abundance ratio would be given by the relative statistical weights of the respective states.

The ortho-to-para ratio for molecular hydrogen has been studied in diffuse regions or very hot regions, and the ratios are considerably different from the statistical value of 3 (e.g. Spitzer *et al.* 1973; Dalgarno, Black, and Weisheit 1973; Davis, Larson, and Smith 1982; Scoville *et al.* 1982; Gately *et al.* 1987; Takayanagi, Sakimoto, and Onda 1987; Hasegawa *et al.* 1987). However, molecular hydrogen, which has no permanent electric dipole moment, is hard to observe in dense molecular clouds with kinetic temperatures of 10 - 100 K, since its transition probabilities are very small and its rotational levels have energies much larger than the cloud kinetic temperature.

KFLEL have derived $H_2CO$ ortho-to-para ratios ~ 3, the statistical weight value, in Orion A, but they find a ratio ~ 1 - 2 in the cold cloud TMC-1. Gas-phase interconversion mechanisms between ortho and para species, such as proton exchange reactions, are probably too slow to be efficient. However, if thermalization on grain surfaces is important, the ortho-to-para ratio for grains at ~ 10 K would be ~ 1.5, while for $T \geq 30$ K, it approaches the statistical value of 3 (KFLEL). Thus, the observations provide

81

evidence for gas-grain interactions in cold clouds. The $H_2CO$ lines observed are, however, severely self-absorbed, especially in the dark clouds.

Thioformaldehyde ($H_2CS$) has been detected in Sgr B2, Orion A, and other star - forming regions (Sinclair *et al.* 1973; Cummins, Linke, and Thaddeus 1986; Loren 1984; Sutton *et al.* 1985; Blake *et al.* 1987; Liszt 1978), and in the cold dark clouds TMC-1 and L134N (Irvine *et al.* 1989). $H_2CS$ is similar to $H_2CO$ in its structure and exists in both ortho and para forms, and $H_2CS$ ortho-to-para ratios ~ 3 have been derived by Gardener *et al.* (1985) in Orion(KL). $H_2CS$ may be a better candidate to study the ortho-to-para ratio than $H_2CO$, especially in cold dark clouds, since the optical depths for the $H_2CS$ lines seem to be much less than those of $H_2CO$ (Irvine *et al.* 1989). In this Chapter, we report the abundances and ortho-to-para ratios of $H_2CS$ observed in the interstellar molecular clouds TMC-1, L134N, Orion A, and NGC7538.


5.3 <u>Observations</u>


Observations were made using the FCRAO 14 m telescope between 1988 December and 1989 June. Observed $H_2CS$ line frequencies are included in the note to Table 5.1. Both the FCRAO 3 mm and 2 mm receivers employed cooled Schottky diode mixers, which gave total system temperatures, corrected to outside the atmosphere, of 400-600 K for the 100 GHz transitions and 800 - 1000 K for the 140 GHz

TABLE 5.1

H$_2$CS Line Parameters[a]

| Transition | T$_A^*$ [b] (K) | $\Delta V$ (km s$^{-1}$) | V$_{LSR}$ (km s$^{-1}$) | $\int T_A^* dV$ (K km s$^{-1}$) |
|---|---|---|---|---|
| | | TMC-1 | | |
| $3_{03} - 2_{02}$ | 0.52 ±.03 | 0.61 | 5.7 | 0.34 |
| $4_{04} - 3_{03}$ | 0.34 ±.07 | 0.55 | 5.6 | 0.20 |
| $3_{13} - 2_{12}$ | 0.54 ±.04 | 0.55 | 5.6 | 0.32 |
| $3_{12} - 2_{11}$ | 0.51 ±.04 | 0.67 | 5.6 | 0.39 |
| $4_{13} - 3_{12}$ | 0.16 ±.05 | 0.79 | 5.7 | 0.13 |
| | | L134N | | |
| $3_{13} - 2_{12}$ | 0.08 ±.02 | 0.61 | 2.2 | 0.05 |
| | | Orion(KL) | | |
| $3_{03} - 2_{02}$ [d] | 0.41 ±.02 | 3.94 | 8.6 | 1.62 |
| $3_{13} - 2_{12}$ | 0.69 ±.06 | 3.13 | 8.5 | 2.17 |
| $3_{12} - 2_{11}$ | 0.52 ±.05 | 3.18 | 7.9 | 1.67 |
| $3_{21} - 2_{20}$ | 0.11 ±.02 | 3.45 | 7.6 | 0.39 |
| | | NGC7538(N) | | |
| $3_{03} - 2_{02}$ | 0.18 ±.02 | 2.99 | -57.1 | 0.54 |
| $3_{13} - 2_{12}$ | 0.27 ±.03 | 3.29 | -57.1 | 0.90 |
| $3_{12} - 2_{11}$ | 0.31 ±.06 | 2.99 | -58.2 | 0.92 |

TABLE 5.1

(Continued)

| Transition | $T_A^{*\ b}$ (K) | $\Delta V$ (km s$^{-1}$) | $V_{LSR}$ (km s$^{-1}$) | $\int T_A^* dV$ (K km s$^{-1}$) |
|---|---|---|---|---|
| TMC-1(NH$_3$) | | | | |
| $3_{03} - 2_{02}$ | $0.22 \pm .05$ | 0.97 | 5.5 | 0.23 |
| $4_{04} - 3_{03}$ | — | — | — | — |
| $3_{13} - 2_{12}$ | $0.24 \pm .04$ | 0.70 | 5.7 | 0.18 |
| $3_{12} - 2_{11}$ | $0.23 \pm .06$ | 0.56 | 5.4 | 0.14 |
| $4_{13} - 3_{12}$ | — | — | — | — |
| L134N(SO) | | | | |
| $3_{13} - 2_{12}$ | $\leq 0.09^c$ | — | — | — |
| Orion(3N1E) | | | | |
| $3_{03} - 2_{02}{}^d$ | $0.40 \pm .04$ | 1.59 | 9.4 | 0.64 |
| $3_{13} - 2_{12}$ | $0.53 \pm .05$ | 1.70 | 9.3 | 0.90 |
| $3_{12} - 2_{11}$ | $0.70 \pm .10$ | 1.19 | 9.4 | 0.84 |
| $3_{21} - 2_{20}$ | $\leq 0.11^c$ | — | — | — |
| NGC7538(S) | | | | |
| $3_{03} - 2_{02}$ | $0.27 \pm .03$ | 3.84 | -56.4 | 1.03 |
| $3_{13} - 2_{12}$ | $0.44 \pm .04$ | 4.63 | -56.4 | 2.03 |
| $3_{12} - 2_{11}$ | $0.43 \pm .10$ | 4.78 | -57.5 | 2.08 |

TABLE 5.1

(Continued)

[a] Spectral resolutions are 100 kHz for TMC-1 and L134N, and 250 kHz
   for Orion and NGC7538.

[b] Errors are 1 $\sigma$ values.

[c] 3 $\sigma$ value.

[d] Contaminated by the $3_{22}$ - $2_{21}$ transition ($\Delta\nu$ = 0.55 MHz).

<u>NOTE</u> :

Line parameters for TMC-1 have been derived from gaussian fits.

<u>Rest</u> <u>frequency</u>: $\nu_o(3_{03}$- $2_{02})$ = 103.040399 GHz; $\nu_o(3_{13}$- $2_{12})$ =
101.47753 GHz; $\nu_o(3_{12}$- $2_{11})$ = 104.616975 GHz; $\nu_o(3_{21}$- $2_{20})$ =
103.051785 GHz; $\nu_o(4_{04}$- $3_{03})$ = 137.371043 GHz; $\nu_o(4_{13}$- $3_{12})$ =
139.483466 GHz; $\nu_o(3_{21}$- $2_{20})$ = 103.051785 GHz (Lovas 1986).

<u>Position</u>: TMC-1: RA(1950) = $4^h38^m38^s.6$, Dec(1950) = $25^°35'45"$;
TMC-1(NH$_3$):RA(1950) = $4^h38^m22^s.0$, Dec(1950) = $25^°41'45"$; L134N:
RA(1950) = $15^h51^m30^s.0$, Dec(1950) = $-2^°43'31"$; L134N(SO): RA(1950) =
$15^h51^m26^s.0$, Dec(1950) = $-2^°43'31"$; Orion(KL): RA(1950) = $5^h32^m47^s.0$,
Dec(1950) = $-5^°24'23"$; Orion(3N1E): RA(1950) = $5^h32^m51^s.0$; Dec(1950)
= $-5^°21'23"$; NGC7538(N): RA(1950) = $23^h11^m36^s.6$, Dec(1950) =
$61^°11'48"$; NGC7538(S): RA(1950) = $23^h11^m36^s.6$; Dec(1950) = $61^°10'48"$.

85

transitions.    Data were taken by position switching 30 arcminutes

in azimuth, and spectra were obtained using 256-channel filter banks

with 100 kHz and 250 kHz resolutions.    The FWHP beamwidths are 52

and 43 arcseconds, and the antenna beam efficiencies $\eta_B$ = 0.57 and

0.40 at 100 GHz and 149 GHz, respectively.    The temperature scale

is given as $T_A^*$, the beam-chopper-corrected antenna temperature.    We

then approximate the radiation temperature $T_R$ by the main beam

brightness temperature $T_{MB} = T_A^*/\eta_B$.    The observed line parameters

are given in Table 5.1 and sample spectra obtained towards TMC-1 and

Orion(KL) in Figure 5.1.    The observed antenna temperatures are

also shown in the rotational diagram in Figure 5.2 for TMC-1 and

Orion A.


5.4 <u>Analysis</u>


We have used an LVG statistical equlibrium - radiative transfer

model to calculate the antenna brightness temperatures of the $H_2CS$

lines.    The model is described in Appendix A.    Since the

collisional cross-sections for $H_2CS$ are not available, we used the

$H_2CO$ collisional de-excitation rates (Green $et$ $al.$ 1978) for the

corresponding $H_2CS$ levels as a first approximation (Gardener $et$ $al.$

1985), and the collisional excitation rates have beeen calculated by

assuming detailed balance.    The calculations for TMC-1 (kinetic

temperature $T_{kin}$ ~ 10 K) and Orion(3N1E) ($T_{kin}$ ~ 20 K) include 16

levels for ortho-$H_2CS$ and 15 level for para-$H_2CS$ up to energy levels

Figure 5.1    Sample spectra of $H_2CS$ obtained towards TMC-1 and Orion(KL).    Positions given in Table 5.1.    Spectral resolution is 100 kHz for TMC-1 and 250 kHz for Orion(KL).

TMC−1    Orion(KL)

$3_{03}-2_{02}$    $3_{03}-2_{02}$
$3_{13}-2_{12}$    $3_{13}-2_{12}$
$3_{12}-2_{11}$    $3_{12}-2_{11}$
$4_{04}-3_{03}$    $3_{21}-2_{20}$

$T_A^*$ (K)

$V_{LSR}$ (km s$^{-1}$)

88
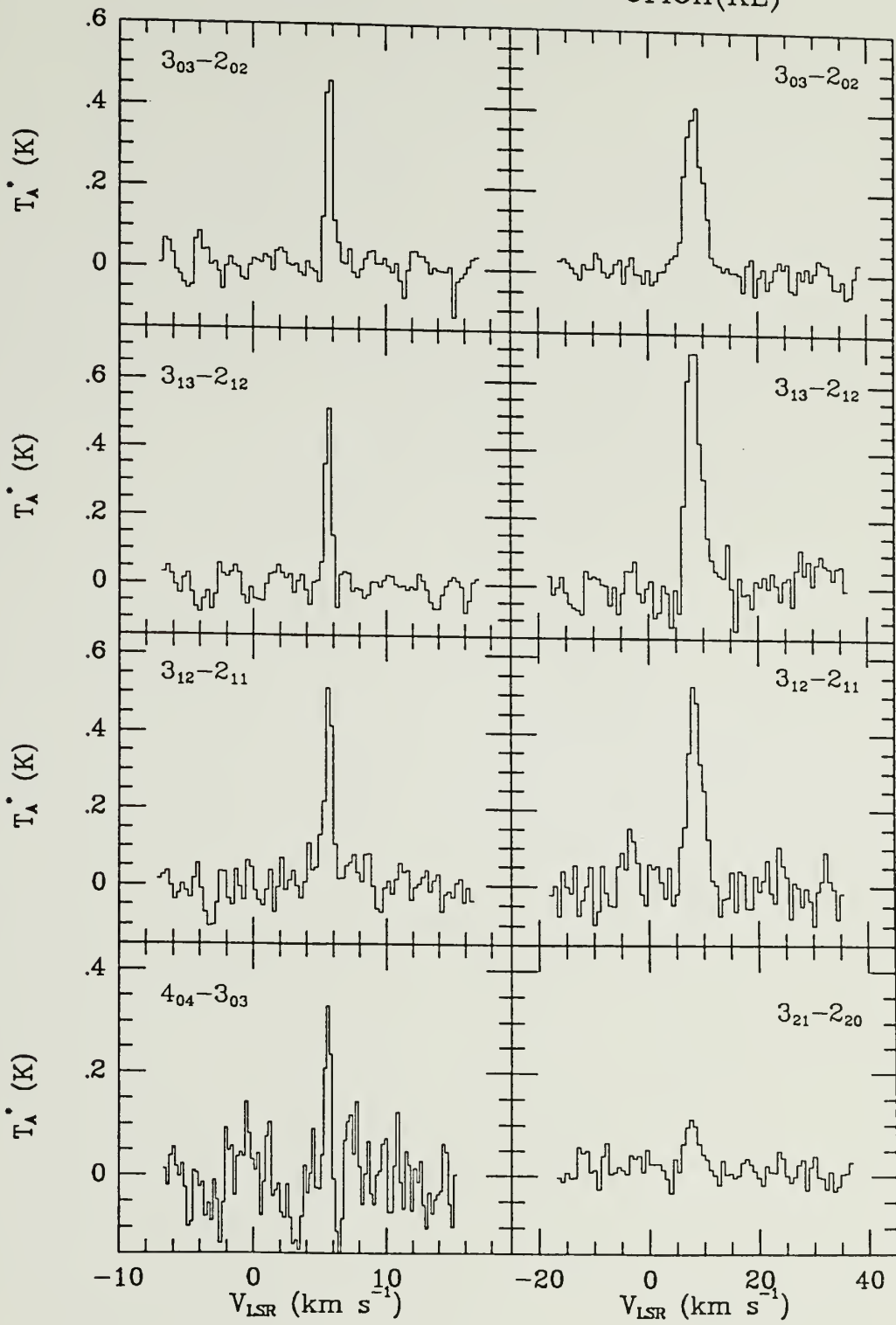
Figure 5.2   Rotation diagram for the observed $H_2CS$ transitions.   In the ordinate, $I = \ln\{1.94\text{x}10^3 \; \nu^2(\text{GHz}) \int T_A^* dV \; (\text{K km s}^{-1}) \; / \; A_{UL} \; g_U \; \eta_B\}$, where $\nu$ is the rest frequency, $A_{UL}$ the spontaneous emission rate, $g_U$ the statistical weight of the upper level, and $\eta_B$ the antenna main beam efficiency.   A correction for the cosmic background has been made for TMC-1 and L134N with the factor, $[1 - J_\nu(T_{BG})/J_\nu(T_{ex})]^{-1}$, where $J_\nu(T) = (h\nu/k)[\exp(h\nu/kT) - 1]^{-1}$, $T_{BG} = 2.7$ K, and $T_{ex} = 5$ K.
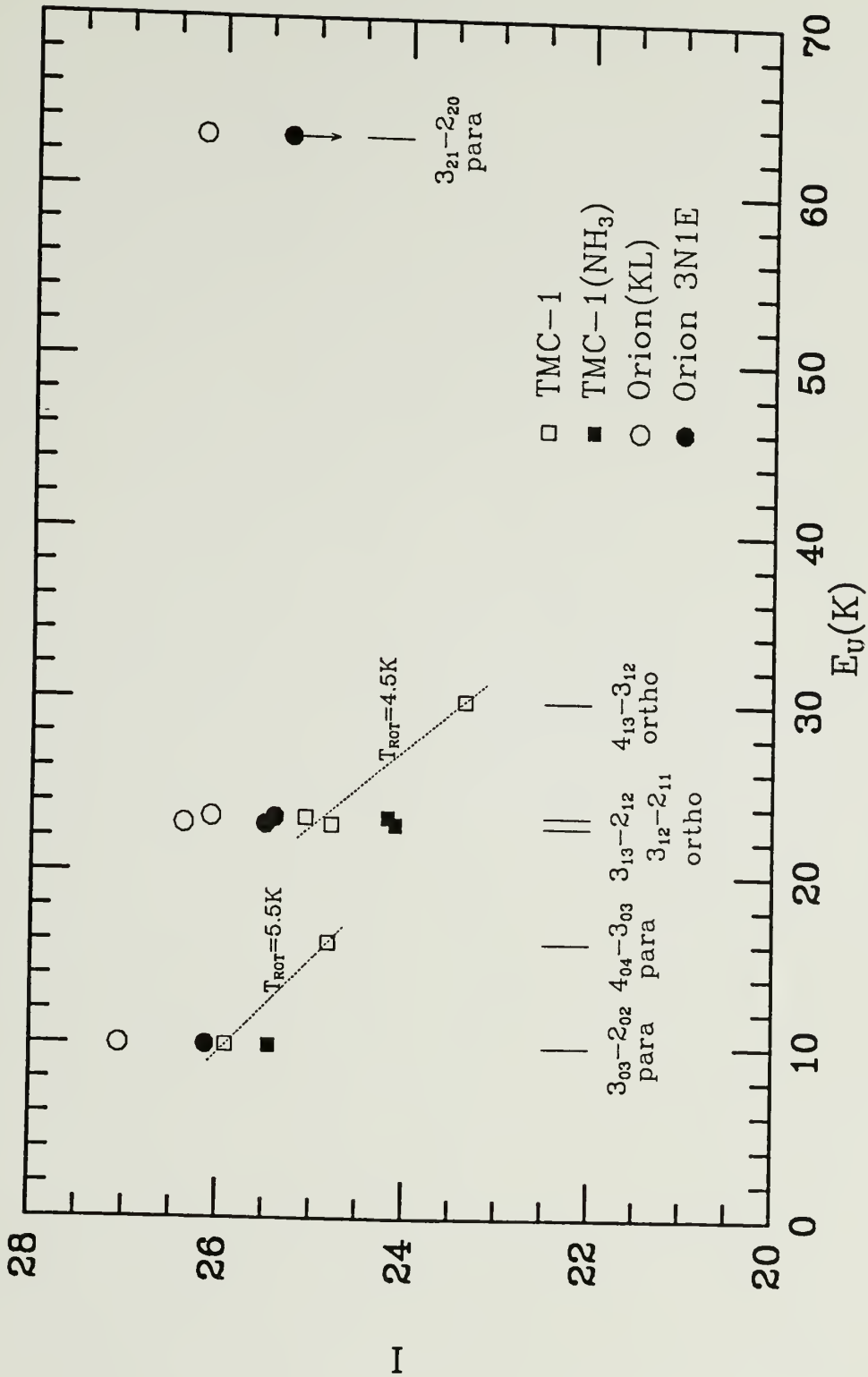
70 K above the ground state for each species. Since the de-excitation rates are not sensitive to kinetic temperatures or $\Delta J$ values, we extrapolate the $H_2CO$ de-excitation rates up to energy levels of 300 K to calculate for the Orion compact ridge, which has $T_{kin} \sim 100$ K. We include 60 levels of ortho-$H_2CS$ and 49 levels of para-$H_2CS$ in the LVG analysis for Orion(KL). Some of the results are shown in Appendix A.

In Figure 5.3 we have shown the calculation results for TMC-1, where the observed brightness temperatures and $3\sigma$ values for each transition are indicated. It was assumed that the emission from all of the observed transitions filled the telescope beam. The shaded region in the left panel of Figure 5.3 is the most probable region confined by the three ortho transitions. We have obtained $n(H_2) \sim 10^5 - 10^6$ cm$^{-3}$ in this analysis, and applied this $H_2$ volume density to also derive the corresponding para abundance. The $H_2$ density, however, has been suggested to be $0.5 - 1 \times 10^5$ cm$^{-3}$ for the whole TMC-1 molecular cloud by Schloerb, Snell, and Young (1983) from observations of $HC_3N$ lines and $\leq 10^5$ cm$^{-3}$ by Bujarrabal et al. (1981) from $HC_3N$ and $HC_5N$ data, which is smaller than our result by a factor of a few. The difference may result from a scaling factor of the collisional cross sections for $H_2CS$ from those of $H_2CO$. The results from the LVG analysis are included in Table 5.3, together with the abundances derived by assuming optically thin emission and a rotational temperature of 5 K (cf. Irvine, Goldsmith, and Hjalmarson 1987), for comparison. The column densities and

Figure 5.3 Curves of constant brightness temperature as a function of molecular hydrogen density $n(H_2)$ and $H_2CS$ abundance, computed from LVG model for observed transitions in TMC-1, with kinetic temperature set to 10 K. Left panel is for the ortho transitions and the right for the para transitions, as indicated in the figure. The center lines for each transition are for the observed brightness temperatures and the other two lines for 3 $\sigma$ rms values. The shaded region in the left panel indicates the most probable region suggested by the LVG analysis.
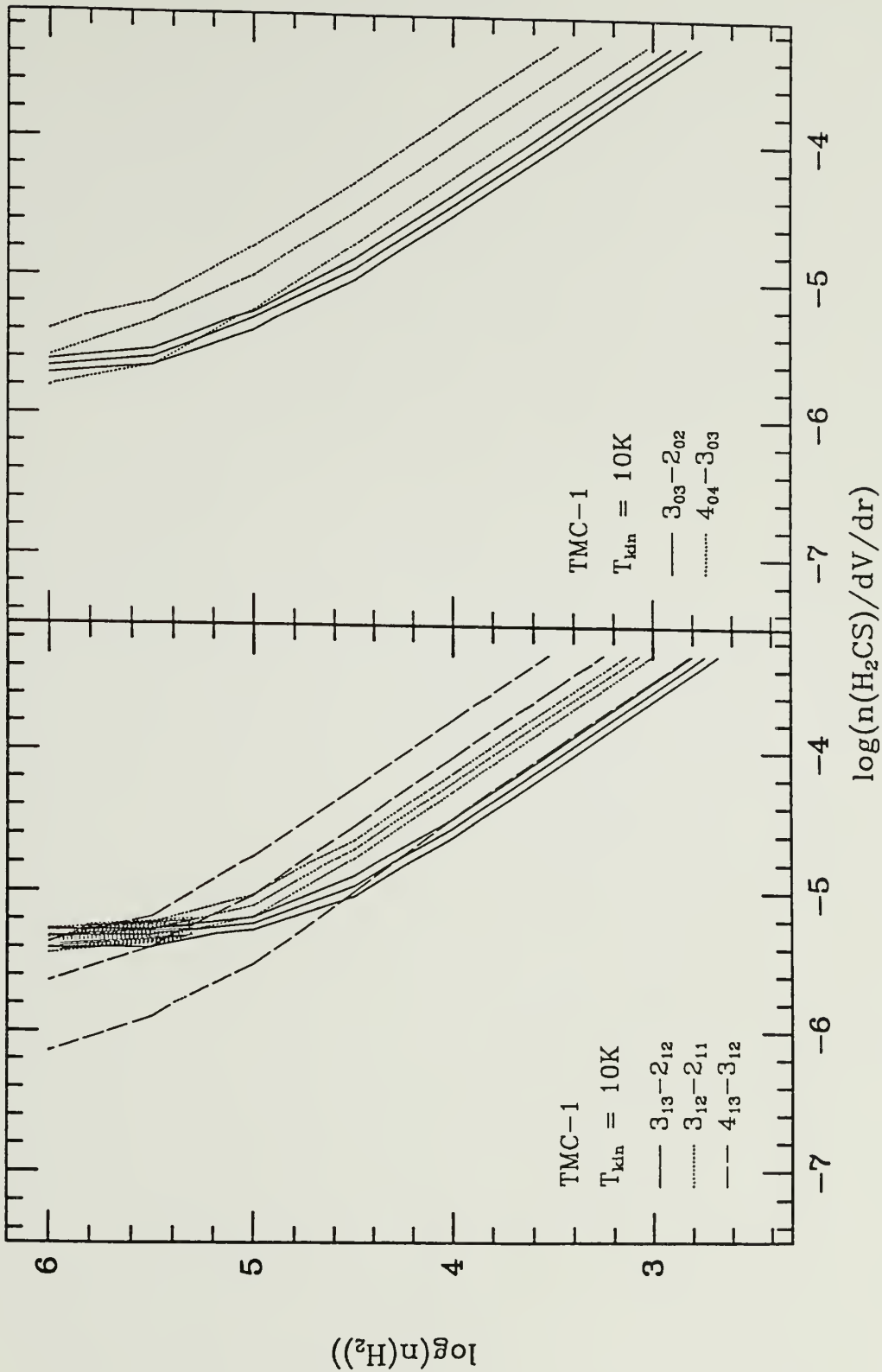
ortho/para ratios found by the two procedures agree quite well. The results for a second position in this cloud, TMC-1($NH_3$), have been calculated in the same way and are also listed in Table 5.3.

In Figure 5.4 we have shown the LVG model results for Orion(KL), and the shaded region in the right panel for para transitions indicates a probable locus for $n(H_2)$ and the abundance parameter. We applied the source size ~ 30", since $H_2CS$ is thought from the $V_{LSR}$ values to be a constituent of the compact ridge (Blake et al. 1987). Although the $3_{03}$ - $2_{02}$ transition may be contaminated by the $3_{22}$ - $2_{21}$ transition ($\Delta\nu$ ~ 0.6 MHz), the constant antenna temperature curve for the $3_{21}$ - $2_{20}$ transition is well confined to a small range of the abundance parameter $n(H_2CS)/dV/dr$, so that the column density of $H_2CS$ is well defined (Figure 5.4). The optical depths and excitation temperatures derived from the LVG analysis are included in Table 5.2 and the column densities and abundances in Table 5.3.

The column densities have also been derived by assuming optically thin emission and a rotational temperature 60 K for both para and ortho $H_2CS$. The rotational diagram in Figure 5.2 gives $T_{rot}$ ~ 63 K for the $3_{03}$ - $2_{02}$ and $3_{21}$ - $2_{20}$ transitions, and we also obtained $T_{rot}$ ~ 62 K and 60 K for para and ortho $H_2CS$, respectively, from the J = 7 - 6 transition data of Sutton et al. (1985). We derived column densities by using the $3_{21}$ - $2_{20}$ transition for para-$H_2CS$ and the $3_{13}$ - $2_{12}$ and $3_{12}$ - $2_{11}$ transitions (by averaging

Figure 5.4   Same as Figure 5.3 for the observed brightness
temperatures for Orion(KL).   Source size of 30" has been assumed
and kinetic temperature hasbeen set to 100 K.

Orion(KL)

$T_{kin} = 100K$

—— $3_{03}-2_{02}$

········ $3_{21}-2_{20}$

Orion(KL)

$T_{kin} = 100K$

—— $3_{13}-2_{12}$

········ $3_{12}-2_{11}$

$\log(n(H_2CS)/dV/dr)$

$\log(n(H_2))$
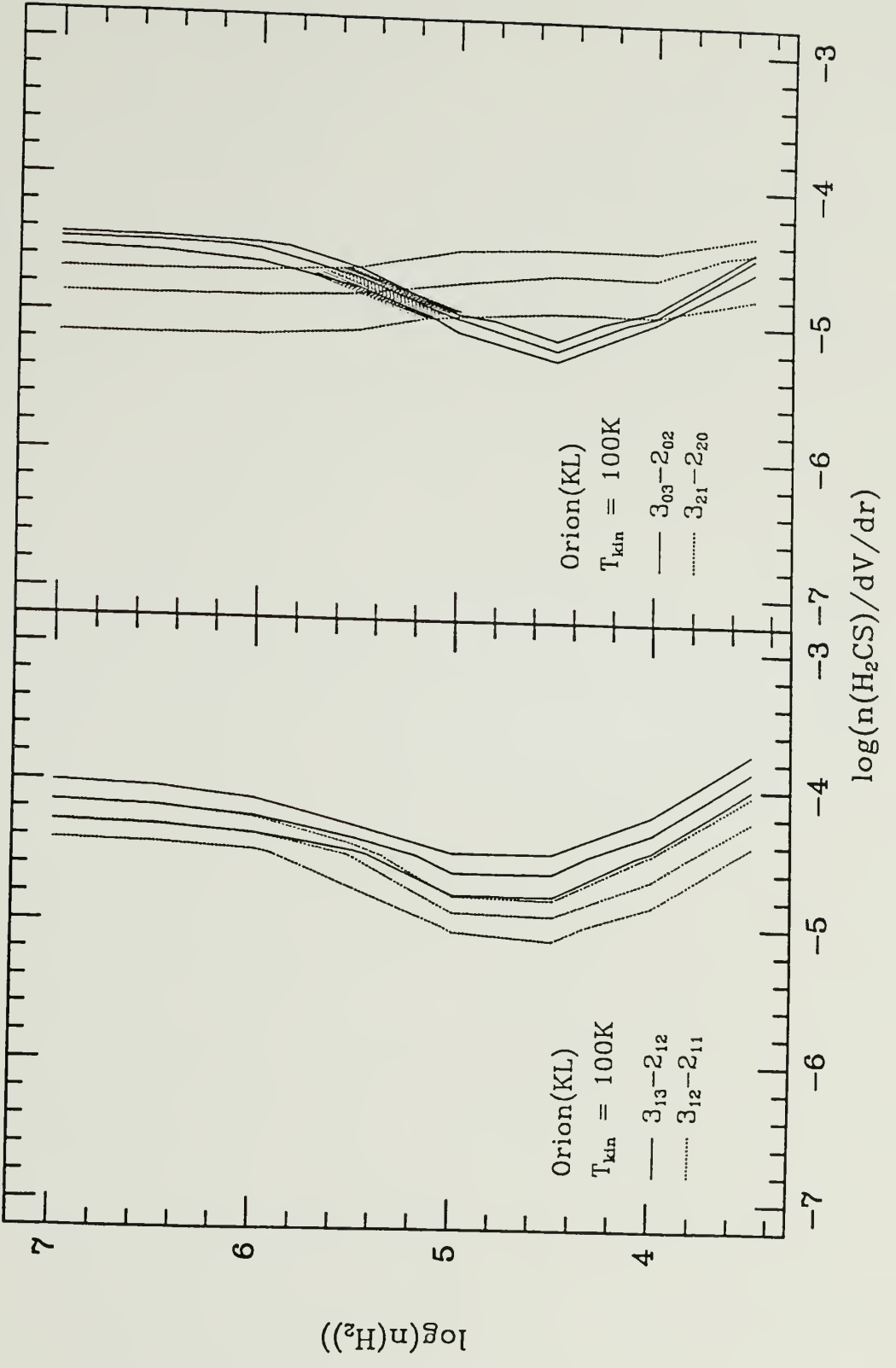
TABLE 5.2

Excitation Temperatures and Optical Depths

Derived from the LVG Analysis

| $T_{kin}$ (K) = | $10^a$ | | $20^b$ | | $100^c$ | |
|---|---|---|---|---|---|---|
| Transition | $T_{ex}$ (K) | Tau | $T_{ex}$ (K) | Tau | $T_{ex}$ (K) | Tau |
| $3_{03} - 2_{02}$ | 4.6 | 0.22 | 6.2 | 0.17 | 79.4 | 0.03 |
| $4_{04} - 3_{03}$ | 4.2 | 0.12 | 5.3 | 0.13 | 26.2 | 0.12 |
| $3_{13} - 2_{12}$ | 6.0 | 0.31 | 8.5 | 0.22 | 63.4 | 0.09 |
| $3_{12} - 2_{11}$ | 5.0 | 0.31 | 7.0 | 0.22 | 37.7 | 0.12 |
| $4_{13} - 3_{12}$ | 4.1 | 0.20 | 5.6 | 0.21 | 20.1 | 0.34 |

[a] For TMC-1 data; at $n(H_2) = 10^5$ $cm^{-3}$, and $n(para-H_2CS)/dV/dr = 1.6$ x $10^{-6}$ $cm^{-3}$ (km $s^{-1}$ $pc^{-1})^{-1}$ and $n(ortho-H_2CS)/dV/dr = 5$ x $10^{-6}$ $cm^{-3}$ (km $s^{-1}$ $pc^{-1})^{-1}$.

[b] For Orion(3N1E) data; at $n(H_2) = 10^5$ $cm^{-3}$, and $n(para-H_2CS)/dV/dr = 1.6$ x $10^{-6}$ $cm^{-3}$ (km $s^{-1}$ $pc^{-1})^{-1}$ and $n(ortho-H_2CS)/dV/dr = 5$ x $10^{-6}$ $cm^{-3}$ (km $s^{-1}$ $pc^{-1})^{-1}$.

[c] For Orion(KL) data; at $n(H_2) = 10^5$ $cm^{-3}$, and $n(para-H_2CS)/dV/dr = 10^{-5}$ $cm^{-3}$ (km $s^{-1}$ $pc^{-1})^{-1}$ and $n(ortho-H_2CS)/dV/dr = 3$ x $10^{-5}$ $cm^{-3}$ (km $s^{-1}$ $pc^{-1})^{-1}$.

TABLE 5.3

$H_2CS$ Abundances

| Source | N(para)<br>( $\times 10^{13}$ cm$^{-2}$) | N(ortho)<br>( $\times 10^{13}$ cm$^{-2}$) | $\dfrac{N(ortho)}{N(para)}$ | $f(H_2CS)$ [a] |
|---|---|---|---|---|
| **LVG Model Results** | | | | |
| TMC-1 | 0.54 ± 0.06 | 0.97 ± 0.04 | 1.8 ± 0.3 | 2 (-9) |
| TMC-1(NH$_3$) | 0.29 ± 0.04 | 0.49 ± 0.06 | 1.7 ± 0.4 | 8 (-10) |
| Orion(KL) | 17 ± 2 | 30 ± 4 | 1.8 ± 0.5 | 2-5 (-9) |
| Orion(3N1E) | 0.73 ± 0.04 | 2.2 ± 0.3 | 3.0 ± 0.6 | 4 (-10) |
| **Results by Assuming Optically Thin Emission** | | | | |
| TMC-1 | 0.85 ± 0.06 | 1.6 ± 0.2 | 1.9 ± 0.4 | 3 (-9) |
| TMC-1(NH$_3$) | 0.54 ± 0.12 | 0.71 ± 0.17 | 1.3 ± 0.6 | 1 (-9) |
| L134N | —— | 0.23 ± 0.05 | —— | ~ 5 (-10) [b] |
| L134N(SO) | —— | ≤0.26 | —— | ≤ 5 (-10) [b] |
| Orion(KL) | 27 ± 13 | 45 ± 6 | 1.7 ± 1.0 | 2-7 (-9) |
| Orion(3N1E) | 0.91 ± 0.09 | 2.5 ± 0.3 | 2.8 ± 0.6 | 5 (-10) |
| NGC7538(N) | 0.86 ± 0.10 | 2.8 ± 0.4 | 3.3 ± 0.8 | 5 (-10) |
| NGC7538(S) | 1.6 ± 0.2 | 6.3 ± 0.5 | 3.9 ± 0.8 | 1 (-9) |

[a] Fractional abundance of $H_2CS$ relative to $H_2$. Hydrogen total column densities $N(H_2) \sim 10^{22}$ cm$^{-2}$ for TMC-1 (Irvine *et al.* 1987;

TABLE 5.3

(Continued)

Friberg and Hjalmarson 1989); ~ 1-3 x $10^{23}$ $cm^{-2}$ for Orion(KL)
(Johansson *et al.* 1984; Blake *et al.* 1987; Irvine, Goldsmith, and
Hjalmarson 1987); ~ 0.6-1 x $10^{23}$ $cm^{-2}$ for Orion(3N1E) (Smith *et al.*
1979); ~ 8.2 x $10^{21}$ $cm^{-2}$ for L134N (Swade 1987; assuming
$N(C^{18}O)/N(H_2)$ = 1.7 x $10^{-7}$); ~ 8 x $10^{22}$ $cm^{-2}$ for NGC7538(N) and (S)
(Campbell and Thompson 1984).

[b] Ortho-to-para ratio of 1.5:1 was assumed.

Note: Error values in LVG results are either 1 $\sigma$ values or most
probable regions crossed by the observed brightness temperatures,
while those in results derived by assuming optically thin emission
are 1 $\sigma$ values.; Rotational temperature of 5 K has been assumed for
TMC-1 and L134N, 60 K for Orion(KL), and 15 K for Orion(3N1E) to
derive the abundances from the observed integrated antenna
temperatures in the optically thin case.

their line strengths) for ortho-$H_2CS$, and the results are consistent with those found from the LVG analysis (see Table 5.3).

For the Orion(3N1E) position, we have assumed that the source fills the telescope beam and a kinetic temperature of 20 K (cf. Goldsmith *et al.* 1986; Wilson and Walmsley 1989) for the model calculation. The optical depths and excitation temperatures derived from the LVG analysis are included in Table 5.2 and column densities in Table 5.3, in which we also include the column densities derived by assuming optically thin emission and a rotational temperature of 15 K.

The optical depths for the transitions observed in Orion seem to be very small, as given in Table 5.2. Abundances derived from the LVG analysis for both Orion(KL) and Orion(3N1E) agree quite well with those derived by assuming optically thin emission (within a factor of 2), and the ortho-to-para ratios are very similar.

An ortho-$H_2CS$ column density in L134N has been derived assuming optically thin emission and of a rotational temperature of 5 K (Swade 1987); we assumed an ortho-to-para ratio of 1.5 to derive the total column density, because our observations were limited to one transition.

We include in Table 5.3 data for NGC7538(N) and (S) derived using the optically thin approximation and assuming a rotational temperature of 20 K (Snell and Wootten 1984). The NGC7538 molecular cloud is a very active star-forming region and shows a very complicated structure, including OH and $H_2O$ masers,

high-velocity outflows and several IR sources (e.g. Wynn-Williams, Werner, and Wilson 1974; Werner *et al.* 1979; Campbell and Thompson 1984; Kameya *et al.* 1989; and see referneces therein). The resolution of our $H_2CS$ observations is too poor to discern any relationships with smaller scale structures.

## 5.5 Discussion

The cold dark clouds TMC-1 and L134N have similar temperature, density, and mass, but have some interesting chemical differences. Carbon-rich species and CS and $HCS^+$ are more prominent in TMC-1 than in L134N, while SO and $SO_2$ are higher in L134N, which may result from, for example, different gas phase elemental abundances or from differing cloud ages (Irvine, Goldsmith, and Hjalmarson 1987). This pattern is reflected in our present results.

We derive a total column density $N(H_2CS) \sim 1 - 2 \times 10^{13}$ cm$^{-2}$ for the TMC-1 cyanopolyyne peak and the ammonia peak, which corresponds to a fractional abundance of $H_2CS$ relative to $H_2$, $f(H_2CS) \sim 1 - 2 \times 10^{-9}$ for $n(H_2) \sim 10^{22}$ cm$^{-2}$ (see references in Table 5.3). The $H_2CS$ abundance in L134N is about a factor of 5 less than that in TMC-1. The result for TMC-1 agrees quit well with the prediction of "pseudo-time-dependent" models (Herbst and Leung 1986a,b; Millar and Herbst 1989) at the "early time" which produces best agreement between the model and observations for many heavier organic molecules. The model predicts a lower $H_2CS$

abundance at steady state, which would be consistent with L134N being more chemically evolved than TMC-1.

On the other hand, Duley, Millar, and Williams (1980) have suggested grain surface formation for $H_2CS$ and $H_2S$, and if carbon abundance is high, $H_2CS$ would be expected to form instead of $H_2S$. Indeed, the abundances of $H_2CS$ have been observed to be high where those of $H_2S$ are low in L134N and TMC-1 (this paper and Minh, Irvine, and Ziurys 1989).

The initial ortho-to-para ratios are expected to be the statistical value 3, since gas-phase (or grain-surface) formation reactions release large reaction heats compared to the energy difference between the lowest ortho and para states (~ 15 K for $H_2CS$ and $H_2CO$). We derive instead ~ 1.8 at both the TMC-1 cyanopolyyne peak and the ammonia peak, which may suggest thermalization on 10 K grains and hence an efficient interchange between the grains and the gas phase. Kahane *et al.* (1984) derived essentially the same value for $H_2CO$ in dark clouds, although the observed lines of $H_2CO$ are severely self-absorbed, and had to be interpreted with the aid of a radiative transfer model. It is significant that we confirm their results for the ortho-to-para ratios in cold dark clouds by using $H_2CS$ lines which are optically thin.

In Orion(KL), we derive an ortho-to-para ratio ~ 2, which is much smaller than the statistical value 3, while KFLEL derive ~ 3 for $H_2CO$ after correcting for the radiative transfer effects. Gardner *et al.* (1985) derive ~ 3 in Orion(KL) by using the same $H_2CS$

102

transitions as we use. Gardener *et al.*'s spectra, obtained using the Bell Lab's 7 m telescope, are fairly different compared to ours in Figure 5.1, which may result from the different beam sizes between the two telescopes. The small $H_2CS$ ortho-to-para ratio in the Orion compact ridge cannot be explained by thermalization in the gas phase or on the grains, because the expected kinetic temperature for the Orion compact ridge is on the order of 100 K. We have examined the ortho-to-para ratio with the $H_2CS$ $J = 7 - 6$ transitions observed in the spectral survey of Sutton *et al.* (1985) and derived an ortho-to-para ratio ~ 2.1 from a least square fit of the data, assuming optically thin emission. These data thus support our present result. The reason for small values is not certain. Since the outflow materials from IRc 2 are believed to be interacting with surrounding quiescent clouds in the compact ridge, our small ortho-to-para ratio may result from the non-equlibrium condition of the $H_2CS$ excitation. The physical and chemical conditions for the compact ridge should be studied further.

For the Orion(3N1E) position, if $H_2CS$ is thermalized on grains at ~ 20 K, we expect the ortho-to-para ratio to be ~ 2.7, which is close to the derived values of 2.8 - 3.0. We derive roughly ~ 3 - 4 for the NGC7538(N) and (S) positions.

We may conclude that the $H_2CS$ ortho-to-para ratio is thermalized at ~ 10 K by gas-grain interactions in cold dark clouds, while it becomes the statistical value ~ 3 in warmer regions. These results thus support the idea of exchange of material between

grain surfaces and the gas phase in at least the cold clouds, which must indeed be present to prevent a nearly complete "freeze out" of gas phase molecules during expected cloud life times (e.g. Leger, Jura, and Omont 1985). It is curious that so little other evidence for this expected phenomenon exists.

CHAPTER 6

UPPER LIMITS FOR THE ETHYL CYANIDE ABUNDANCES IN TMC-1 AND L134N

6.1 <u>Summary</u>

We have sought interstellar ethyl cyanide via its $2_{02} - 1_{01}$ transition towards two cold, dark clouds and report upper limits of the total column densities of $3 \times 10^{12}$ cm$^{-2}$ and $2 \times 10^{12}$ cm$^{-2}$ for TMC-1 and L134N, respectively. These values are lower than previous limits. We observed the $2_{02} - 1_{01}$ transition of vinyl cyanide previously identified in TMC-1 by Matthews and Sears (1983b). The detection of vinyl cyanide and the non-detection of ethyl cyanide in TMC-1 are consistent with gas phase ion-molecule chemical models, and there is thus no necessity of invoking grain surface synthesis for vinyl cyanide in cold clouds.

6.2 <u>Introduction</u>

Grain surface reactions have been sometimes suggested to play an important role in the formation of gas-phase interstellar molecules (e.g. Millar 1982). Although there are a number of serious uncertainties in the grain surface reaction schemes, observations between 3 and 12 $\mu$m have identified several molecules in grain mantles (cf. Tielens and Allamandola 1987) which are

typically highly saturated. Large abundances of $NH_3$, HDO, HCN, and $H_2S$ in the Orion hot core have also been regarded as an indication of grain mantle evaporation (Blake *et al.* 1987; Minh *et al.* 1989, see also Chapter 3).

Irvine and Hjalmarson (1984) and Blake *et al.* (1987) have pointed out large abundances of highly saturated molecules such as ethyl cyanide ($CH_3CH_2CN$) and vinyl cyanide ($CH_2CHCN$) in the Orion hot core, and suggested that they might result from hydrogenation of $HC_3N$ on grain surfaces. Ion-molecule processes leading to the formation of $CH_3CH_2CN$ are highly endothermic and proceed quite slowly (Herbst, Adams, and Smith 1983). The hydrogenation of $HC_3N$ may proceed efficiently on the grain surfaces to form vinyl cyanide and ethyl cyanide, especially since there is no rearrangement in the CCCN frame. Blake *et al.* suggest that the observed ratios of $[HC_3N]/[CH_2CHCN]$ and $[HC_3N]/[CH_3CH_2CN]$ in the Orion extended ridge and the hot core indicate that the hydrogenation process prefers to saturate any cyanoacetylene deposited on the grain surface completely.

A detection of vinyl cyanide in the cold dark cloud TMC-1 (Matthews and Sears 1983) raises an interesting question. If vinyl cyanide has formed on the grain surfaces by hydrogenation of $HC_3N$ and then desorbed to the gas-phase, why has ethyl cyanide not been detected in TMC-1 ? Grain surface molecules tend to be saturated, which would lead to an abundance ratio $[CH_3CH_2CN]/[CH_2CHCN] > 1$, as is the case in the Orion hot core. In this Chapter, we report good

upper limits for the ethyl cyanide abundance in TMC-1 and L134N and conclude that ion-molecule reactions may explain observed abundances of vinyl cyanide in cold, dark clouds.

## 6.3 Observations and Results

The observations were made in 1989 January, using the 43 m telescope of the NRAO for the $2_{02} - 1_{01}$ transitions of ethyl cyanide and vinyl cyanide. The half-power beam width was 1.5 arcminutes, and the beam efficiency ($\eta_B$) 0.40 at the observing frequency of 18 GHz. The temperature scale was determined using a noise diode and is given in terms of antenna temperature $T_A$. We approximate the brightness temperature by the main-beam brightness temperature $T_{MB}$, which is defined by $T_{MB} = T_A/\eta_B$. The maser receiver gave a system temperature of typically 70 K. The 1024 channel autocorrelation spectrometer was used with a spectral resolution of 9.8 kHz, and frequency-switching was employed. The observed line frequencies and positions are included in the notes of Table 6.1.

The column densities in the last column of Table 6.1 were determined using the "standard" equation (Irvine, Goldsmith, and Hjalmarson 1987), assuming statistical relative intensities for the hyperfine components, optically thin emission, and equilibrium at a rotational temperature of 5 K for both TMC-1 and L134N (cf. Matthews and Sears 1983b; Swade 1987). A correction for the cosmic background radiation has been included. For a Boltzmann population

TABLE 6.1

A Summary of Observations[a]

| Molecule | Transition | $T_A$ (mK) | $\Delta V$ (km s$^{-1}$) | $V_{LSR}$ (km s$^{-1}$) | $\int T_A dV$ (mK km s$^{-1}$) | $N_{column}$ (cm$^{-2}$) |
|---|---|---|---|---|---|---|
| | | | TMC-1 | | | |
| $CH_3CH_2CN$ | $2_{02}-1_{01}$ F=3-2 | $\leq 14$[b] | — | — | — | $\leq 3.4(12)$[c] |
| $CH_2CHCN$ | $2_{02}-1_{01}$ F=3-2 | 43 | 0.70 | 5.5 | 26 | 6.8(12) |
| | 2-1 | 29 | 0.39 | 5.6 | 15 | |
| | | | L134N | | | |
| $CH_3CH_2CN$ | $2_{02}-1_{01}$ F=3-2 | $\leq 12$[b] | — | — | — | $\leq 2.2(12)$[d] |
| $CH_2CHCN$ | $2_{02}-1_{01}$ F=3-2 | $\leq 33$[b] | — | — | — | $\leq 4.2(12)$[d] |

[a] Spectral resolution is 9.8 kHz.

[b] 3 $\sigma$ upper limit.

[c] 3 $\sigma$ value and $\Delta V = 0.7$ km s$^{-1}$ were used.

[d] 3 $\sigma$ value and $\Delta V = 0.5$ km s$^{-1}$ were used.

NOTE. - Position; TMC-1: RA(1950) = $4^h38^m38^s.6$, Dec(1950) = $25°35'45"$; L134N: RA(1950) = $15^h51^m30^s.0$; Dec(1950) = $-2°43'31"$.

Rest frequency; 17.8910 GHz for the $CH_3CH_2CN$ ($2_{02} - 1_{01}$, F = 3 - 2) line (Lovas 1982); 18.966614 GHz and 18.966534 GHz for $CH_2CHCN$ ($2_{02} - 1_{01}$) F = 3 - 2 and F = 2 - 1, respectively (Gerry, Yamada, and Winnewisser 1979).

distribution the total column density in dark clouds is rather insensitive to the assumed rotational temperature for values in the range 5 - 10 K (the latter being the approximate kinetic temperature in these sources).

Morever, since the dipole moments and molecular constants of ethyl cyanide and vinyl cyanide are quite similar (Poynter and Pickett 1984), we expect that the ratio of these column densities and hence the upper limit on $CH_3CH_2CN$ relative to $CH_2CHCN$ should be quite accurate. The abundances ratios of ethyl cyanide and vinyl cyanide relative to $HC_3N$ are listed in Table 6.2 towards TMC-1, L134N and Orion(KL), including the results of previous publications.

However, the absolute abundances may be slightly affected by the existence of both a- and b-components of the electric dipole moment ($\mu$) for both ethyl and vinyl cyanide. The existence of b-type transitions tends to drain the population from states with $K_a \geq 1$ into lower K-ladders, tending to produce a non-equilibrium population distribution. However, the abundance ratio of these two species is expected to remain essentially unchanged since both $\mu_a$ and $\mu_b$ are very similar.

Matthews and Sears (1983a) obtained an upper limit on the abundance of $CH_3CH_2CN$ ($\leq 5 \times 10^{12}$ cm$^{-3}$) by observing its $1_{10} - 2_{11}$ transition and assuming an LTE population distribution. For the reasons given in the preceding paragraph, we think their result is somewhat uncertain since transitions in the $K_a = 1$ ladder were used.

TABLE 6.2

Abundance Ratios

| Source | $\dfrac{[CH_3CH_2CN]}{[HC_3N]}$ | $\dfrac{[CH_2CHCN]}{[HC_3N]}$ | $\dfrac{[HC_3N]}{[H_2]}$ | References |
|---|---|---|---|---|
| TMC-1 | $\leq 0.02$ | 0.05 | 1 (-8) | 1, 2 |
| L134N | $\leq 0.4$ | $\leq 0.8$ | 7 (-10) | 3 |
| Orion hot core | 6.5 | 1.0 | 2 (-9) | 2, 4 |

References: (1) Irvine and Schloerb (1984), (2) Irvine *et al.*
(1985), (3) Swade (1987), (4) Blake *et al.* (1987)

The vinyl cyanide abundance obtained by Matthews and Sears (1983b) is about a factor of two less for TMC-1 than that in Table 6.1. The reason for this difference is unclear, but conceivably is related to the improved efficiency of the 43 m antenna in recent years (R. Maddalena, private communication).

6.4 Discussion

The large enhancements of ethyl cyanide and vinyl cyanide in the Orion hot core relative to the quiescent ridge have been interpreted as indicating that hydrogenation of $HC_3N$ on grain surfaces must be efficient (Blake et al. 1987). Although the gas-phase reactions leading to the formation of $HC_3N$ are still controversial (Herbst 1988), the large observed abundance of $HC_3N$ in TMC-1 (Irvine and Schloerb 1984) might be expected to produce large abundances of vinyl cyanide and ethyl cyanide after "freezing out" on the grain mantles in TMC-1. Since grain surface molecules tend to be saturated, ethyl cyanide would probably be more abundant than vinyl cyanide, and this is the case for the Orion hot core. Curiously enough, only vinyl cyanide has been detected in TMC-1 (in the gas phase), and the present upper limit for the ethyl cyanide abundance is much less than that for the Orion hot core relative to vinyl cyanide (Table 6.2). Since the molecular weights of ethyl cyanide and vinyl cyanide are very similar, desorption processes should not be so different between these two species. Then we may

111

have to conclude that the vinyl cyanide observed in TMC-1 has not formed on grain surfaces.

Millar and Freeman (1984) have suggested that reactions of $C_3H_5^+$ with N followed by dissociative electron recombination could lead to the formation of vinyl cyanide, and their prediction agrees well with the observed abundance. But gas-phase reactions for the formation of ethyl cyanide are thought to be quite endothermic (Herbst, Adams, and Smith 1983). Therefore, purely gas-phase reactions are sufficient to explain the observed abundance of vinyl cyanide and the failure to detect ethyl cyanide in TMC-1. Moreover, since $HC_3N$ is quite abundant in TMC-1 and would be expected to stick to grains in cold clouds and be hydrogenated, it appears that desorption processes are inefficient in TMC-1, at least for heavy molecules like $CH_3CH_2CN$ and $CH_2CHCN$. This result is quite different than that obtained for $H_2CS$ and $H_2CO$, for which the ortho/para ratio in dark clouds suggests efficient interchange between the grains and the gas phase (Minh, Irvine, and Brewer 1989; Kahane *et al*. 1984).

CHAPTER 7


OBSERVATIONS OF INTERSTELLAR $HOCO^+$:

ABUNDANCE ENHANCEMENTS TOWARDS THE GALACTIC CENTER


7.1 Summary

A survey of the $4_{04} - 3_{03}$ and $1_{01} - 0_{00}$ transitions of $HOCO^+$ has
been made toward several molecular clouds. The $HOCO^+$ molecule was
not observed in any sources except Sgr B2 and Sgr A. The $5_{05} - 4_{04}$
and $4_{14} - 3_{13}$ transitions were also detected toward Sgr B2. The
results indicate that gas phase $CO_2$ is not a major carbon reservoir
in typical molecular clouds. In Sgr B2, the $HOCO^+$ antenna
temperature exhibits a peak ~ 2 arcmin north of the Sgr B2 central
position (Sgr B2[M]) and the $4_{04} - 3_{03}$ line emission is extended
over a ~ 10' x 10' region. The column density of $HOCO^+$ at the
northern peak in Sgr B2 is ~ $3 \times 10^{14}$ $cm^{-2}$, and the fractional
abundance relative to $H_2 \geq 3 \times 10^{-10}$, which is about two orders of
magnitude greater than recent predictions of quiescent cloud ion-
molecule chemistry.

7.2 Introduction


Herbst et al.(1977) have suggested that the abundances of
molecules which lack permanent electric dipole moments and hence

113

rotational transitions in the millimeter spectral region, but which are important to the chemistry of the interstellar medium, may be estimated from observations of their protonated ions. An example of this approach is the investigation of molecular nitrogen from studies of its protonated form, $N_2H^+$ (Turner and Thaddeus 1977; Linke, Guélin, and Langer 1983).

The $HOCO^+$ molecule, the protonated form of $CO_2$, was first identified in the rich molecular cloud Sgr B2 by Thaddeus, Guélin, and Linke (1981), who determined the molecular rotational constants accurately from 3 harmonically related lines. The subsequent laboratory detection of this molecule by Bogey, Demuynck, and Destombes (1984) has confirmed this identification and the values of the rotational constants. The dipole moment of $HOCO^+$ is estimated to be 2 Debyes (Green et al. 1976). According to Herbst et al. (1977), $HOCO^+$ can be formed in molecular clouds via a standard ion-molecule reaction, transfer of a proton from $H_3^+$ to $CO_2$. Therefore, $HOCO^+$ might be widely distributed in interstellar sources if $CO_2$ were relatively abundant. Since only ~ 10 % of the cosmic abundance of carbon is contained in CO (Irvine and Knacke 1988), and simple hydrocarbons such as $CH_4$ are even less abundant (Knacke et al. 1985), $CO_2$ might be an important reservoir of interstellar carbon, and an observational determination of its abundance in molecular clouds is quite important.

The $HOCO^+$ ion has heretofore been observed in only one interstellar cloud, Sgr B2 (Thaddeus, Guélin and Linke 1981;

Cummins, Linke, and Thaddeus 1986), which is an extremely large giant molecular cloud with high mass star formation. The $4_{04} - 3_{03}$ transition of $HOCO^+$ at 85.6 GHz and several higher J transitions were readily detected toward Sgr B2(OH).(No other positions were observed in the cloud). If the chemical abundances in other clouds are similar to Sgr B2, emission lines of $HOCO^+$ should be detectable. Consequently, we conducted a search for $HOCO^+$ toward a variety of interstellar sources, and also mapped the $4_{04} - 3_{03}$ line over Sgr B2. The results of this study are presented here.

7.3 Observations

Observations of the $1_{01} - 0_{00}$ transition of $HOCO^+$ were taken with the NRAO 43 m telescope and K-band maser during January 1987. Telescope parameters are included in Table 7.1. The temperature scale was determined using a noise diode and is given in terms of antenna temperature $T_A$. The 1024 channel autocorrelation spectrometer was used, and either frequency - switching or beam - switching was employed.

Observations of the $4_{04} - 3_{03}$, $4_{14} - 3_{13}$, $4_{13} - 3_{12}$, and $5_{05} - 4_{04}$ transitions were made using the FCRAO 14 m telescope between October 1986 and October 1987. Telescope parameters are included in Table 7.1. The receiver and spectrometers are described in Schloerb, Snell and Young (1983). The temperature scale was

TABLE 7.1

Telescope Parameters

| Transition $J_{K_a K_c} - J'_{K'_a K'_c}$ | Rest freq.[a] (GHz) | Telescope | HPBW[b] (arcsec) | $\eta_A$[c] | $\eta_B$[d] |
|---|---|---|---|---|---|
| $1_{01} - 0_{00}$ | 21.38280 | NRAO 43 m | 84 | 0.23 | 0.29 |
| $4_{04} - 3_{03}$ | 85.53068 | FCRAO 14 m | 60 | 0.47 | 0.56 |
| $4_{14} - 3_{13}$ | 85.231 | FCRAO 14 m | 60 | 0.47 | 0.56 |
| $4_{13} - 3_{12}$ | 85.831 | FCRAO 14 m | 60 | 0.47 | 0.56 |
| $5_{05} - 4_{04}$ | 106.91301 | FCRAO 14 m | 48 | 0.44 | 0.52 |

[a] from Bogey, Demuynck, and Destombes (1984)

[b] half power beam width

[c] aperture efficiency

[d] beam efficiency

determined by the standard chopper wheel method, and is given in terms of $T_A^*$. Observations were made by position switching.

Main beam brightness temperature $T_R$ is then defined for both telescopes by $T_R = T_A/\eta_B$ or $T_A^*/\eta_B$, where $\eta_B$ is the beam efficiency.

## 7.4 Results

### 7.4.1 Galactic Center Region

A study of a number of molecules in Sgr B2 by Goldsmith *et al.*(1987) suggests that the column densities of different species show major variations between two locations of local maxima: Sgr B2(M) at RA(1950) = $17^h44^m10^s.5$; DEC(1950) = $-28°22'05"$, and Sgr B2(N), ~ 45 arcsec north from Sgr B2(M). For example, SO is strongly peaked near Sgr B2(M) and OCS is concentrated around Sgr B2(N).

In contrast, our observations of $HOCO^+$ in the $4_{04} - 3_{03}$ transition show a peak at 2 arcmin north from Sgr B2(M), a position we shall refer to as Sgr B2(2N), with a peak intensity of $T_A^* = 0.82$ K. The spectra observed toward 0, 1, 2, and 3 arcmin north from Sgr B2(M) are shown in Figure 7.1. In all, we detected $HOCO^+$ in a region extended over 10' x 10'. The observed line parameters are given in Table 7.2, which also includes the integrated intensity of the $CH_3CCH$ J = 5 - 4 transition (over all K components), simultaneously observed. Figure 7.2 shows a velocity versus

Figure 7.1    Spectra at 85.5 GHz obtained toward 0, 1, 2, and

3 arcmin north from Sgr B2(M).    Spectral resolution is 1 MHz.

The Sgr B2(M) position is RA(1950) = $17^h44^m9\overset{s}{.}5$ and Dec(1950) =

$-28°22'20"$.    The ordinate is corrected antenna temperature,

$T_A^*$.    The velocity scale assumes the rest frequency of the

$4_{04}$ - $3_{03}$ transition of $HOCO^+$ (Table 7.1).
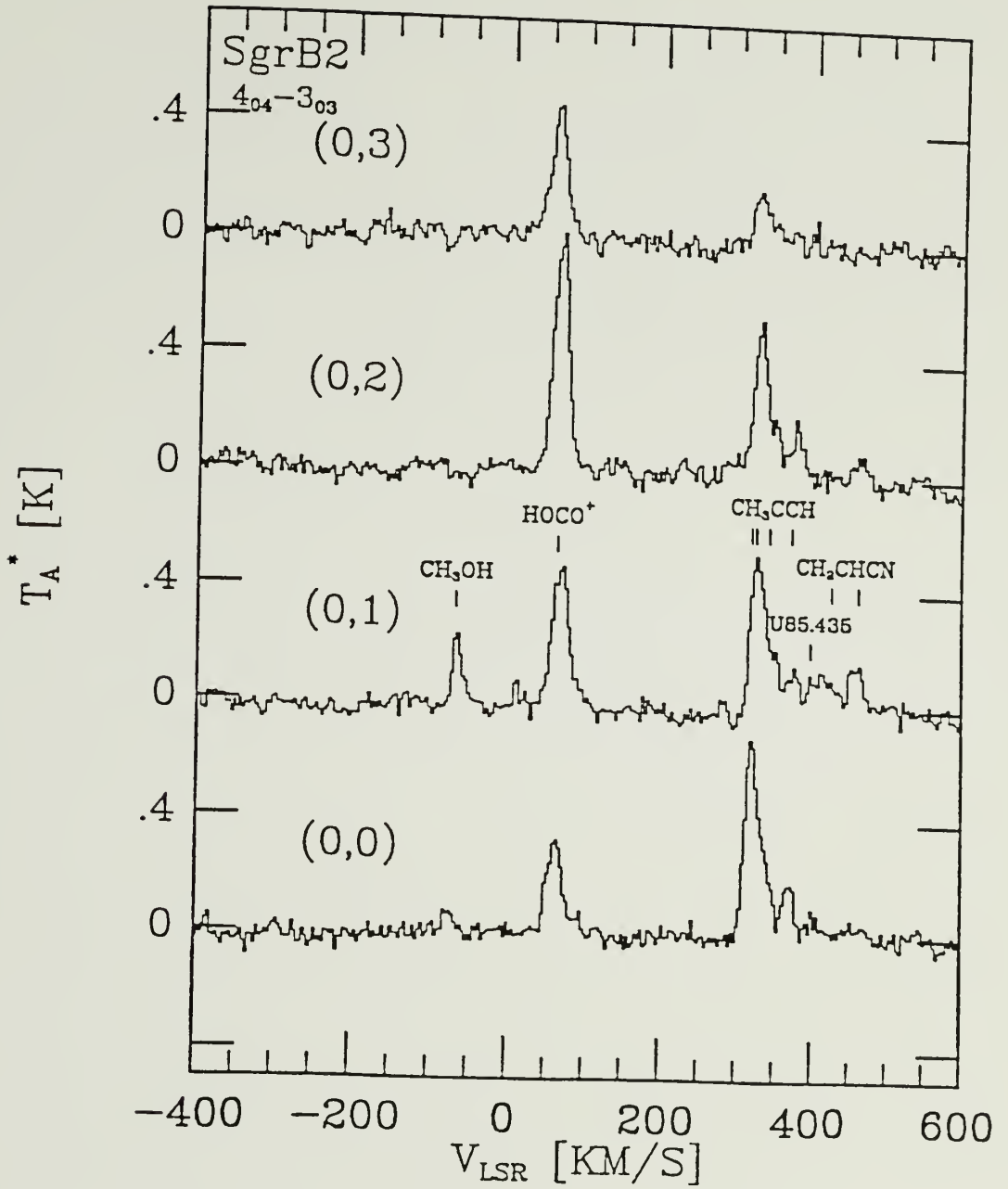
TABLE 7.2

Observed Parameters of the $4_{04} - 3_{03}$ transition at Sgr B2

| Offset | | $T_A^*$ | $\Delta V$ | $V_{LSR}$ | $\int T_A^* \, dV$ | $\int T_A^*(CH_3CCH)dV$ |
|---|---|---|---|---|---|---|
| $\Delta\alpha$ | $\Delta\delta$ | (K) | (km s$^{-1}$) | (km s$^{-1}$) | (K km s$^{-1}$) | (K km s$^{-1}$) |
| 0' | 0' [a] | 0.33 | 27.3 | 63.8 | 9.0 | 24.7 |
| 0 | 1 | 0.48 | 27.4 | 70.8 | 13.0 | 23.9 |
| 0 | 2 | 0.82 | 24.7 | 67.3 | 20.2 | 20.8 |
| 0 | 3 | 0.46 | 27.3 | 60.3 | 12.6 | 5.9 |
| 0 | 4 | 0.25 | 20.1 | 60.3 | 5.0 | 1.0 |
| 0 | 5 | 0.11 | 12.6 | 53.2 | 1.3 | 3.0 |
| 0 | -1 | 0.22 | 25.2 | 49.7 | 5.4 | 14.0 |
| 0 | -2 | 0.23 | 24.9 | 60.3 | 5.7 | 10.2 |
| 0 | -3 | 0.23 | 18.1 | 46.2 | 4.1 | 7.6 |
| 0 | -4 | 0.14 | 24.7 | 53.2 | 3.4 | 6.0 |
| 1 | 0 | 0.25 | 23.2 | 56.7 | 5.9 | 11.6 |
| 1 | 1 | 0.33 | 17.8 | 60.3 | 5.9 | 10.7 |
| 1 | 2 | 0.70 | 23.3 | 60.2 | 16.3 | 17.0 |
| 1 | 3 | 0.37 | 27.9 | 56.7 | 10.3 | 3.7 |
| -1 | 0 | 0.40 | 33.6 | 60.2 | 13.1 | 6.1 |
| -1 | 1 | 0.51 | 30.5 | 67.3 | 15.7 | 9.5 |
| -1 | 2 | 0.70 | 24.3 | 63.8 | 16.9 | 8.5 |
| -1 | 3 | 0.41 | 26.2 | 56.7 | 10.8 | 4.7 |
| 2 | 2 | 0.28 | 21.8 | 60.3 | 6.2 | 3.7 |
| 3 | 2 | 0.21 | 22.3 | 56.7 | 4.7 | 5.7 |
| 4 | 2 | 0.24 | 17.3 | 53.2 | 4.2 | 4.5 |
| 5 | 2 | 0.24 | 17.9 | 49.7 | 4.3 | 2.4 |
| 6 | 2 | 0.13 | 9.7 | 49.7 | 1.3 | 1.8 |
| -2 | 2 | 0.35 | 22.7 | 60.3 | 7.8 | 2.3 |
| -3 | 2 | 0.25 | 21.4 | 42.7 | 5.5 | 3.0 |
| -4 | 2 | 0.25 | 18.1 | 53.2 | 4.5 | 6.8 |
| -5 | 2 | 0.18 | 20.5 | 56.7 | 3.7 | 2.6 |

[a] RA(1950) = $17^h44^m9.5^s$; DEC(1950) = $-28°22'20"$

Figure 7.2   Spatial-velocity map of $HOCO^+$ antenna temperature $(T_A^*)$ for the $4_{04} - 3_{03}$ line along the N-S direction.   The $(0, 0)$ position is given in Figure 7.1.   The contour levels are 0.3, 0.4, 0.5, 0.6, and 0.7 K.
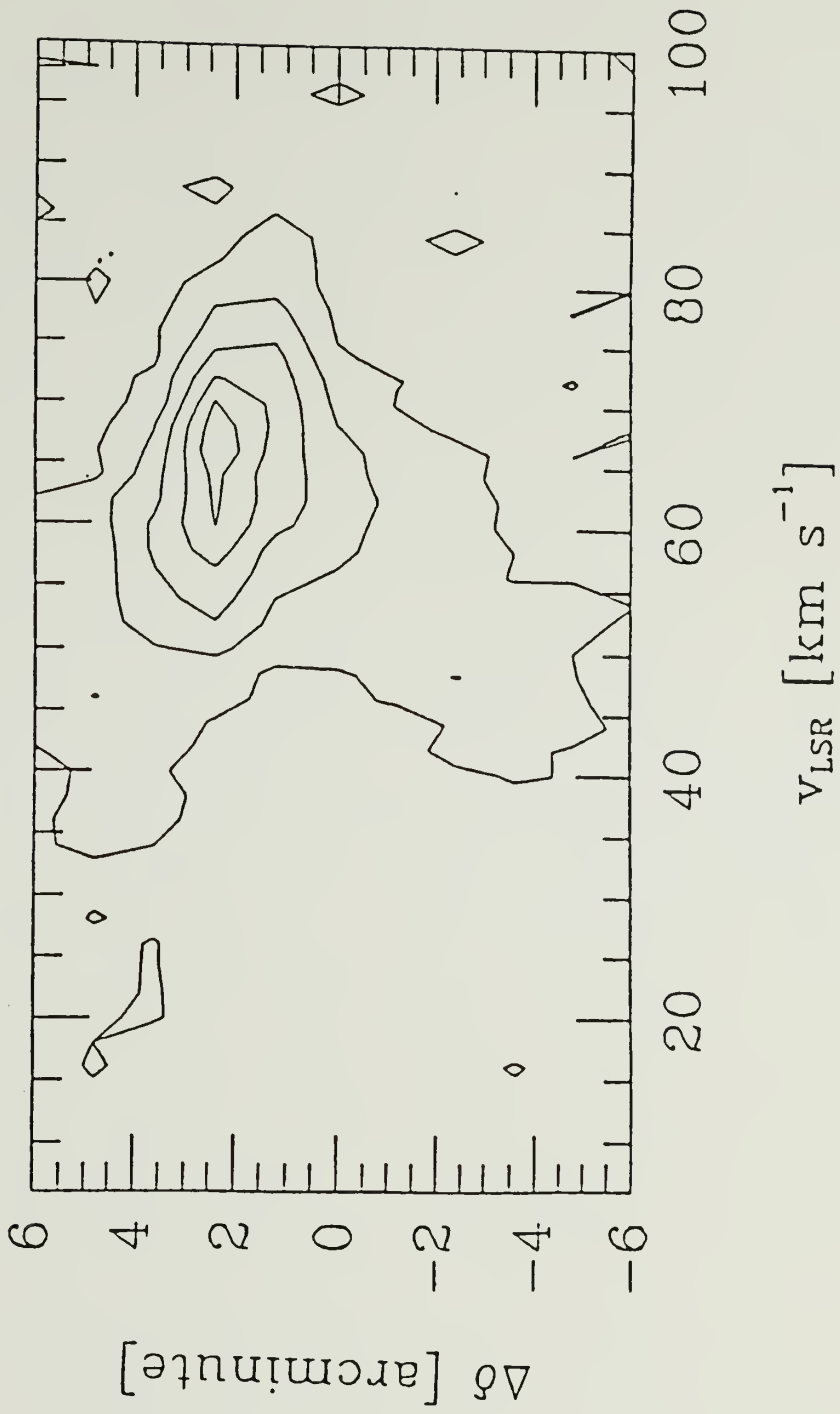
declination map along the N-S direction. There appears to be an increase in the peak velocity around the (2N) position, as well as an extended weak emission at velocities in the range of 40 - 80 km $s^{-1}$.

The $5_{05}$ - $4_{04}$ transition has been observed toward Sgr B2(M) and (2N), and also shows an enhancement at the (2N) position; line parameters are included in Table 7.3. In addition, the $4_{14}$ - $3_{13}$ and $4_{13}$-$3_{12}$ transitions of the $K_a$ = 1 ladder were searched for at Sgr B2(M) and (2N). The frequencies of these transitions differ by only ≈ 300 MHz from the $4_{04}$ - $3_{03}$ transition. The $4_{14}$ - $3_{13}$ transition was detected at Sgr B2(2N), and the spectra observed toward Sgr B2(M) and (2N) are shown in Figure 7.3. The U-line at 85.231 GHz detected by Cummins, Linke, and Thaddeus (1986) seems to be the $4_{14}$ - $3_{13}$ transition of HOCO$^+$. The $4_{13}$- $3_{12}$ transition was not detected down to a 3 $\sigma$ limit of $T_A^*$ = 60 mK.

The $4_{04}$ - $3_{03}$ and $5_{05}$ - $4_{04}$ transitions have been observed toward Sgr A (NH$_3$A), and their line parameters are included in Table 7.3. The $5_{05}$ - $4_{04}$ transition seems to be stronger than the $4_{04}$ - $3_{03}$ transition although the signal-to-noise ratio is not as good.

### 7.4.2 Other Sources

HOCO$^+$ was searched for via its $4_{04}$ - $3_{03}$ and $1_{01}$- $0_{00}$ transitions toward several other molecular clouds, including active star formation regions such as Orion A and W51, and cold dark clouds

123

TABLE 7.3

A Summary of the HOCO$^+$ Survey

| Source | R.A.(1950) | Decl.(1950) | $\Delta V$ [a] $(km\ s^{-1})$ | $T_{rot}$ [a] (K) | Size[b] (pc) |
|---|---|---|---|---|---|
| W3(OH) ..... | $2^h23^m16^s.8$ | $61°38'57"$ | 6.0 | 20 | 1.0 |
| TMC-1 ...... | 4 38 38.6 | 25 35 45 | 1.0 | 6 | 0.2 |
| TMC-2A ..... | 4 28 54.0 | 24 26 27 | 1.0 | 6 | 0.2 |
| Ori-A(KL) .. | 5 32 46.8 | - 5 24 25 | 3.0 | 25 | 0.7 |
|  | 5 32 51.0 | - 5 20 20 | 2.5 | 25 | 0.7 |
| IC443B ..... | 6 14 15.0 | 22 26 50 | 10.0 | 15 | 0.5 |
| NGC2264 .... | 6 38 25.0 | 9 32 29 | 2.0 | 7 | 0.9 |
| L134N ...... | 15 51 32.0 | - 2 40 30 | 0.5 | 5 | 0.3 |
|  | 15 51 26.0 | - 2 43 31 | 0.5 | 5 | 0.3 |
| $\rho$ Oph A .... | 16 23 25.0 | -24 15 49 | 0.6 | 7 | 0.2 |
| $\rho$ Oph B .... | 16 23 25.0 | -24 20 40 | 0.4 | 7 | 0.2 |
| W49 ........ | 19 07 49.0 | 9 01 28 | 15.0 | 25 | 3.0 |
| W51 ........ | 19 21 27.0 | 14 24 30 | 10.0 | 25 | 1.5 |
| B335 ....... | 19 34 35.0 | 7 27 30 | 0.8 | 10 | 1.0 |
| DR 21(OH) .. | 20 37 14.0 | 42 12 00 | 3.0 | 20 | 0.9 |
| Cep MC-1 ... | 22 54 24.4 | 61 45 43 | 4.5 | 25 | 1.0 |
| NGC7538 .... | 23 11 37.0 | 61 10 00 | 4.0 | 20 | 1.0 |
| Sgr A ...... | 17 42 28.0 | -29 01 30 | 18.7 / 24.3 | 15 | 8.0 |
| Sgr B2(M) .. | 17 44 09.5 | -28 22 20 | 27.3 / 22.5 | 13.2 | 10.0 |
| Sgr B2(2N) . | 17 44 09.5 | -28 20 20 | 24.7 / 22.7 | 13.4 | 10.0 |

TABLE 7.3

(Continued)

| Source | $T_A^{*}$ [c,d] $4_{04}-3_{03}$ $5_{05}-4_{04}$ | $T_A$ [c] $1_{01}-0_{00}$ | $N(HOCO^{+})$ [e] $(cm^{-2})$ | $\dfrac{[CO_2]}{[CO]}$ [f] | References |
|---|---|---|---|---|---|
| W3(OH) ..... | ≤ 0.04[g] | — | ≤ 4.7(12) | ≤ 0.01 | 1, 2 |
| TMC-1 ...... | ≤ 0.05[h] | ≤ 0.03 | ≤ 4.3(12) | ≤ 0.04 | 3, 4 |
| TMC-2A ..... | ≤ 0.11[h] | — | ≤ 1.2(12) | ≤ 0.01 | |
| Ori-A(KL) .. | ≤ 0.07[i] ≤ 0.06[i] | — — | ≤ 5.2(12) ≤ 3.7(12) | ≤ 0.02 ≤ 0.01 | 5 5 |
| IC443B ..... | — | ≤ 0.02 | ≤ 5.1(13) | ≤ 0.21 | |
| NGC2264 .... | ≤ 0.11[h] | ≤ 0.02 | ≤ 6.1(12) | ≤ 0.01 | 2, 6, 9 |
| L134N ...... | ≤ 0.06[h] — | ≤ 0.04 ≤ 0.03 | ≤ 2.8(12) ≤ 2.1(12) | ≤ 0.02 ≤ 0.01 | 8 8 |
| $\rho$ Oph A .... | ≤ 0.05[i] | ≤ 0.08 | ≤ 9.8(12) | ≤ 0.10 | 2, 6, 9 |
| $\rho$ Oph B .... | — | ≤ 0.08 | ≤ 6.5(12) | ≤ 0.07 | 2, 6, 9 |
| W49 ........ | ≤ 0.04[g] | — | ≤ 1.9(12) | ≤ 0.001 | 7 |
| W51 ........ | ≤ 0.06[i] | — | ≤ 1.9(12) | ≤ 0.001 | 4 |
| B335 ....... | — | ≤ 0.06 | ≤ 7.6(12) | ≤ 0.02 | 10 |
| DR 21(OH) .. | ≤ 0.03[g] | ≤ 0.02 | ≤ 1.8(12) | ≤ 0.01 | 2, 6, 9 |
| Cep MC-1 ... | ≤ 0.03[g] | — | ≤ 3.3(12) | ≤ 0.01 | 6 |
| NGC7538 .... | ≤ 0.08[g] | ≤ 0.03 | ≤ 6.3(12) | ≤ 0.01 | 1, 2 |
| Sgr A ...... | 0.08[g] 0.23[g,j] | — | 2.3(13) | 0.006 | 9 |
| Sgr B2(M) .. | 0.33[g] 0.39[g] | — | 1.2(14) | 0.02 | 10 |
| Sgr B2(2N) . | 0.82[g] 0.71[g,j] | — | 2.8(14) | 0.06 | |

TABLE 7.3

(Continued)


[a] Values of $\Delta V$ and $T_{rot}$ are assumed, except $\Delta V$ for Sgr A and Sgr B2, and $T_{rot}$ for Sgr B2, which were measured.

[b] Assumed to calculate the volume density of $HOCO^+$ for $[CO_2]/[CO]$.

[c] Upper limits are 3 $\sigma$.

[d] The $4_{04}$ - $3_{03}$ transition except for values indicated by footnote j.

[e] Assumes source fills main beam. Integrated intensities were used for Sgr A and Sgr B2.

[f] $[CO]/[H_2] \sim 8 \times 10^{-5}$ was assumed.

[g] Observed with 1 MHz resolution.

[h] Observed with 100 kHz resolution.

[i] Observed with 250 kHz resolution.

[j] The $5_{05}$ - $4_{04}$ transition.

References. - (1) Andersson 1985; (2) Snell and Wootten 1979; (3) Schloerb, Snell, and Young 1983; (4) Askne et al. 1984; (5) Turner and Thaddeus 1977; (6) Vanden Bout et al. 1983; (7) Scoville and Solomon 1973; (8) Swade 1987; (9) Güsten, Walmsley, and Pauls 1981; (10) Irvine, Goldsmith, and Hjalmarson 1987.

126

Figure 7.3   Spectra observed at 85.2 GHz ($4_{14} - 3_{13}$) toward
Sgr B2(M) and (2N).   The (0,0) position is given in Figure
7.1.   The resolution is 1 MHz.
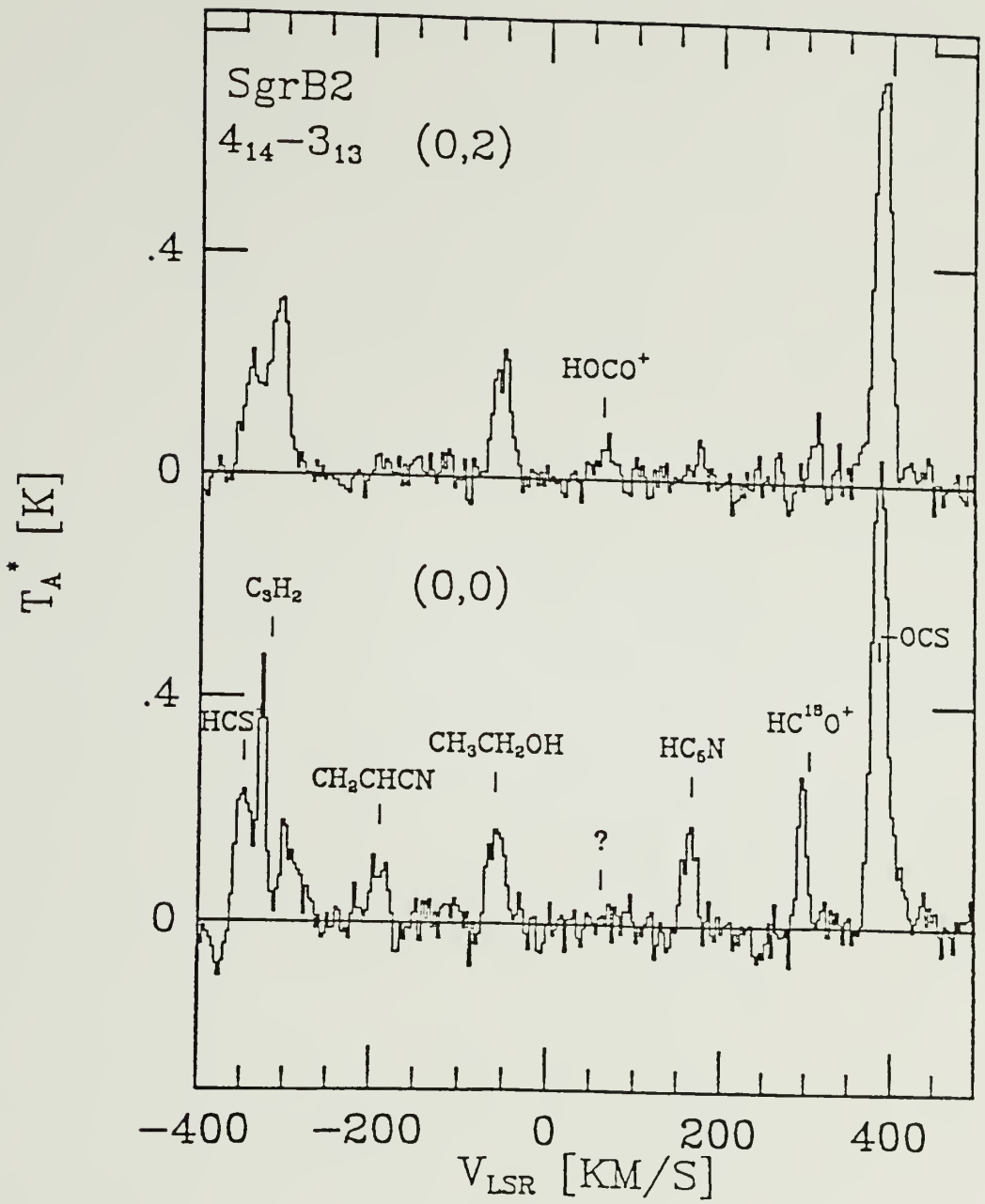
such as TMC-1. However, no lines were detected in any of these
other sources. A summary of the observations is given in Table 7.3.

## 7.5 Discussion

### 7.5.1 Column Densities and Abundances

Values and upper limits of the $HOCO^+$ column density given in
Table 7.3 were determined from the following equation, assuming
optically thin emission,

$$N(HOCO^+) = 2\pi \nu^2 k \Delta V T_R / h c^3 f A$$

where $\nu$ is the line frequency, $f$ the fractional population in the
upper level of the transition, $\Delta V$ the FWHP linewidth, $T_R$ the
brightness temperature assuming the source fills the main beam, and
$A$ the Einstein spontaneous emission coefficient (cf. Irvine,
Goldsmith, and Hjalmarson 1987). The Einstein $A$ coefficient for
the $4_{04} - 3_{03}$ was taken to be $1.31 \times 10^{-5}$ $s^{-1}$ (Herbst $et\ al.$ 1977).
Column densities were calculated using the $4_{04} - 3_{03}$ transition for
"warm" sources , and $1_{01} - 0_{00}$ for cold clouds ($T_{kin} \leq 10$ K) with
the correction term for background radiation, $[1-T_{BG}/T_{EX}]^{-1}$. The
fractional population of the upper level of the transition, $f$, is
estimated using the asymmetric top partition function of $HOCO^+$,
assuming a Boltzmann distribution. The rotational temperature $T_{ROT}$

is assumed to be equal to that found for other large dipole moment
molecules and is given in the 5th column of Table 7.3.  Approximate
upper limits on the $[CO_2]/[CO]$ ratio, given in the last column of
Table 7.3, are derived from equation (4) of Herbst $et$ $al.$ (1977).
This equation results from balancing the expected major formation
and destruction reactions of $HOCO^+$:

$$[CO_2]/[CO] \approx 7.7 \times 10^7 \, [HOCO^+] \, [CO]/[H_2],$$

where the square brackets signify volume density and $[CO]/[H_2]$ has
been assumed to be a constant ($8 \times 10^{-5}$) throughout all clouds in
Table 7.2.  The volume densities of $HOCO^+$ have been calculated from
the assumed source sizes given in column 6 of Table 7.3.

The negative results for $HOCO^+$ in molecular clouds other than
Sgr B2 and Sgr A are consistent with the small fractional abundance
of $HOCO^+$ predicted by quiescent ion-molecule gas-phase chemistry.
For example, Herbst and Leung (1986) predict $f(HOCO^+)$ ~ $10^{-11}$-
$10^{-12}$, for a cloud with n ~ $2 \times 10^3$ $cm^{-3}$ and T ~ 10 - 50 K for their
low metal model.  They find $f(HOCO^+)$ ~ $6 \times 10^{-13}$ for a cloud of n ~
$4 \times 10^5 cm^{-3}$ and T ~ 50 K.  In comparison, we derive a fractional
upper limit to the abundance of $HOCO^+$ of $f < 4 \times 10^{-10}$ for TMC-1,
and $f < 5 \times 10^{-11}$ for Orion(KL) (quiescent component), using values
of $N(H_2)$ from Irvine, Goldsmith, and Hjalmarson (1987).  Such
limits to the $HOCO^+$ fractional abundances typically imply $[CO_2]/[CO]$
< 0.01-0.1 (see Table 7.3).  Thus, $CO_2$ does not appear to be a major

repository for carbon in molecular clouds (usually in quiescent clouds about 10 % of the cosmic complement of carbon is in CO ; cf. van Dishoeck and Black, 1988; Irvine and Knacke, 1988).

In contrast, towards Sgr B2(2N) the column density of $HOCO^+$ is about $2.8 \times 10^{14}$ $cm^{-2}$, derived from the rotational diagram of Figure 7.4. If we assume $N(H_2) < 10^{24}$ $cm^{-2}$ (a likely upper limit; D.Lis, private comm. based on $C^{18}O$ and 1mm continuum data), then $f(HOCO^+) > 3 \times 10^{-10}$, which is about two orders of magnitude greater than the predictions of gas-phase ion-molecule chemistry. This abundance implies a $[CO_2]/[CO]$ ratio of $> 0.06$ using the model of Herbst et al. (1977). Although quite uncertain, this value is about two orders of magnitude larger than those estimated from models of ion-molecule chemistry ($[CO_2]/[CO] \sim 10^{-3}$; Herbst and Leung 1986). Moreover, the average $HOCO^+$ column densities over 3 x 4 arcmin in Sgr B2 are $\sim 1 \times 10^{14}$ $cm^{-2}$ for $T_{ROT} \sim 15$ K, which implies that such high abundances exist over an extended region. One explanation of such a high $[CO_2]/[CO]$ ratio might be an oxygen to carbon abundance that is much larger than the "cosmic" value. Another possible reason might be an increase in the low energy cosmic-ray flux, which is suggested by Güsten, Walmsley, and Pauls (1981) in the galactic center region. This would increase the $H_3^+$ abundance and consequently produce a larger $HOCO^+$ abundance. We note, however, that the chemical abundances for both neutral and ionized species, including those containing oxygen and carbon, appear to be fairly uniform between Sgr B2 and other typical molecular clouds (Irvine,

Figure 7.4    Rotational diagrams for $HOCO^+$ observed toward Sgr

B2(M), Sgr B2(2N) and Sgr A.    In the ordinate (see Irvine,

Goldsmith, and Hjalmarson 1987)

$I = [1.94 \times 10^3 \; \nu^2(GHz)/ \; A_{UL} \; g_U \; \eta_B] \int T_A^* dV(km \; s^{-1})$.    The

rotational temperature of 13.2 K at Sgr B2(M) is derived from

the $4_{04} - 3_{03}$ and $5_{05} - 4_{04}$ transitions, while $T_{ROT} = 13.4$ K at

Sgr B2(2N) is the best least square fit including also the

$4_{14} - 3_{13}$ transition.    Error bars are 3 $\sigma$.
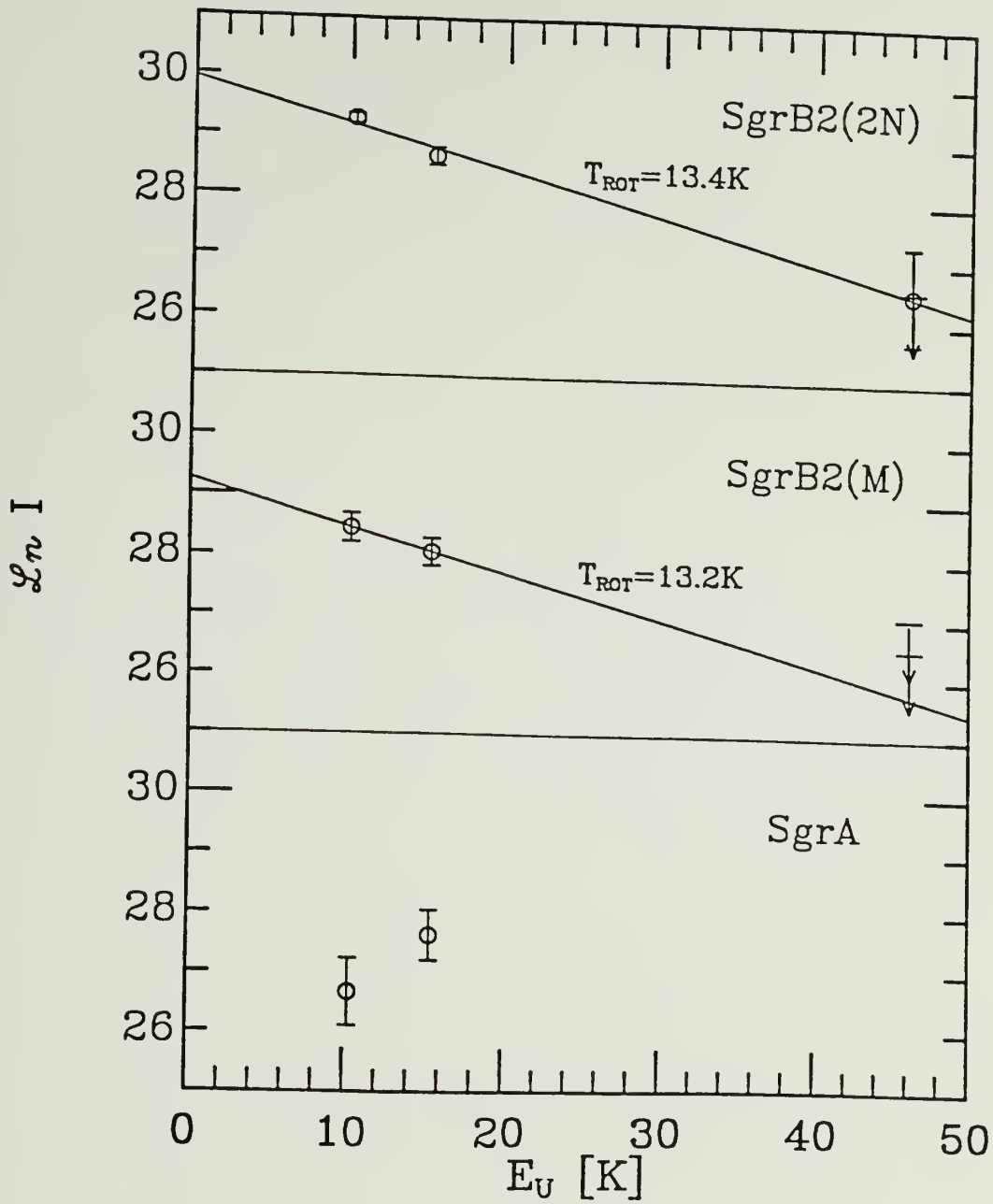
Goldsmith, and Hjalmarson 1987). This is true for example, for both CO and HCO$^+$, as estimated from their $^{18}$O isotopes.

## 7.5.2  Excitation versus Chemistry

Could the enhanced HCO$^+$ emission be an effect of excitation rather than an abundance anomaly ? Indeed, it is interesting that HCO$^+$ peaks at the 2N position, where HNCO is known to have an emission maximum (Churchwell et al. 1986), while most other known molecules tend to peak further south (Goldsmith et al. 1987). HCO$^+$ is similar in structure to HNCO, both species being slightly asymmetric tops with comparable a- and b-dipole moments. It has been suggested by Churchwell et al. (1986) that HNCO emission in Sgr B2 is enhanced by far-infrared excitation and subsequent decay via fast b-type transitions. Perhaps such a mechanism applies to HCO$^+$ as well as HNCO at the Sgr B2(N) position, and accounts for their enhanced emission there. However, at present there is little evidence for an embedded source at the 2N position, such as a compact HII region which might heat the dust and supply the necessary IR radiation (S.N.Vogel, private communication). Also, if we estimate the dust temperature at Sgr B2(2N) from the observed flux at 100 $\mu$m (Gatley et al. 1978) and 350 $\mu$m (Righini, Simon, and Joyce 1976), we find T$_{dust}$ ~ 16 K, which is not particularly hot.

Perhaps the greatest argument against anamolous excitation of HCO$^+$ mimicking an enhanced abundance is the fact that the species

appears to have quite a high concentration at positions extending over several arc minutes. As Table 7.2 shows, even at positions several arc minutes away from Sgr B2(2N) the integrated intensities do not vary more than a factor of two. Therefore, in order to invoke excitation as the cause of the enhanced $HOCO^+$ emission in Sgr B2, a mechanism would have to be found that is fairly general and could occur over extended regions. Infrared excitation is thus unlikely, although some collisional process might conceivably be possible. It is therefore most probable that the large column density of $HOCO^+$ in Sgr B2 is a result of chemistry. Why the physical and chemical conditions favor the production of this ion in this source , and not in other sources, is unknown. Further studies of $HOCO^+$ are certainly necessary in order to answer this question.

CHAPTER 8


ABUNDANCES AND CHEMISTRY OF INTERSTELLAR HOCO$^+$


8.1 <u>Summary</u>

We derive HOCO$^+$ column densities $\sim 10^{15}$ cm$^{-2}$ towards the
Galactic center and $\leq 10^{12}$ cm$^{-2}$ for cold dark clouds using a
statistical equlibrium and LVG model.   A map of HOCO$^+$ in its $4_{04}$ -
$3_{03}$ transition has been obtained toward neutral gas clouds in Sgr A.
The fractional abundance of HOCO$^+$ in the Galactic center region is
found to be about three orders of magnitude larger than that
predicted by quiescent ion-molecule chemistry and about an order of
magnitude larger than predicted by a MHD shock model.   If HOCO$^+$
traces interstellar CO$_2$, the implied high abundance ($[CO_2] \sim [CO]$)
in the Galactic center may result from the UV photolysis of grain
mantles.

8.2 <u>Introduction</u>


The HOCO$^+$ molecule, the protonated form of CO$_2$, has been
suggested as a tracer of interstellar CO$_2$ (Herbst <i>et al.</i> 1977).
Although CO$_2$ is conceivably an important carbon and oxygen reservoir
in the dense interstellar medium, determination of its abundance by
radio astronomical techniques is hindered by its lack of a permanent


136

electric dipole moment. Searches for interstellar HOCO$^+$ have been made by Thaddeus, Guélin, and Linke (1981) and Minh, Irvine, and Ziurys (1988; Paper 1; Chapter 7). HOCO$^+$ has been detected only in the Galactic center region and appears to have quite a high concentration at positions extending over several arcminutes in Sgr B2. The large column density of HOCO$^+$ in Sgr B2 may be a result of chemistry which is peculiar to the Galactic center (Paper 1). In this Chapter we report the results of observations of HOCO$^+$ toward the Sgr A molecular cloud complex, derive HOCO$^+$ abundances using an LVG model for Sgr A and the sources in Paper 1, and discuss the chemical implications.

## 8.3 Observations and Results for Sgr A

Data for the $4_{04}$ - $3_{03}$ and $5_{05}$ - $4_{04}$ transitions of HOCO$^+$ were obtained in 1988 June with the Swedish-ESO 15 m diameter submillimeter wavelength telescope (SEST) on La Silla in the Chilean Andes. A cryogenic Schottky diode mixer receiver with a quasi-optical beam transporting system was employed. The relevant telescope parameters and the system temperatures are included in Table 8.1. Spectra were detected with the wide band acousto-optic spectrometer of 0.69 MHz resolution and 728 channels. Since molecular line emission observed toward Sgr A is well confined and elongated along the Galactic plane, data were obtained by double beam switching with the beam separation being approximately 12' on

TABLE 8.1

Telescope Parameters at SEST [a]

| Parameters | 86 GHz | 110 GHz |
|---|---|---|
| Aperture Efficiency | 0.63 ± 0.04 | 0.58 ± 0.04 |
| Main Beam Efficiency | 0.73 ± 0.04 | 0.68 ± 0.04 |
| HPBW (arcsec) | 55.6 ± 1 | 43.5 ± 1 |
| System Temperature (K SSB)[b] | ~ 340 | ~ 380 |

[a] From Booth *et al.* (1989).

[b] From present observations.

the sky.   The basic calibration was accomplished by the standard chopper wheel method, which provides the antenna temperature, $T_A^*$, corrected for atmospheric attenuation and certain telescope losses. We then approximate the radiation temperature $T_R$ by the main beam brightness temperature $T_{MB} = T_A^*/\eta_B$, where $\eta_B$ is the antenna main beam efficiency.

The Sgr A region shows a complicated structure in both ionized and neutral gas, and is reviewed in detail by Oort (1977) and Brown and Liszt (1984).   The Sgr A molecular complex is composed of several "condensations" of masses greater than $10^5$ $M_\odot$ (Armstrong and Barrett 1984).   Although these "condensations" appear to be related, the geometry and dynamics are still controversal (Brown and Liszt 1984).   The molecular abundances and chemistry of the Sgr A region, however, have not been as well characterized as those of the Sgr B2 molecular cloud complex.   The total column density toward the Sgr A molecular complex is about a factor of 10 less than that toward the Sgr B2 complex.

A map of $T_A^*$ for the HOCO$^+$ $4_{04}$ - $3_{03}$ transition was obtained on a 1' grid, totaling 150 points which are indicated as dots beneath the contour map in Figure 8.1a.   Figure 8.1b shows the corresponding integrated intensity map, and Figure 8.1c shows the velocity contours of the HOCO$^+$ $4_{04}$ - $3_{03}$ transition, superimposed on its integrated intensity map.   The $5_{05}$ - $4_{04}$ transition was observed towards the cores of each condensation.   The general structure of the HOCO$^+$ clouds is quite similar to that of NH$_3$

Figure 8.1a - c   (a) Map of the observed antenna temperature, $T_A^*$, for the $HOCO^+$ $4_{04}$ - $3_{03}$ transition.   Dots indicate observed points, and the cross is the position of Sgr A West.   Contour levels are 0.15, 0.2, 0.25, 0.3, and 0.35 K.   (b) Integrated intensity $(\int T_A^* dV)$ map of the $HOCO^+$ $4_{04}$ - $3_{03}$ transition.   Contour levels are 2.0, 3.5, 5.0, 6.5, and 8.0 K km s$^{-1}$.   (c) Velocity contours of the $HOCO^+$ $4_{04}$ - $3_{03}$ transition (full lines) superimposed upon the integrated intensity map (dashed lines).

$T_A^*(HOCO^+ \, 4_{04}-3_{03})$

Galactic Longitude (arc min)

Galactic Latitude (arc min)

BEAM

(a)

141

$$\int T_A^*(HOCO^+ 4_{04}-3_{03})dV$$

(b)

M$-$0.13$-$0.08

M$-$0.02$-$0.07

M 0.08$-$0.04

M 0.10$-$0.01

M 0.07$-$0.08

M 0.11$-$0.08

M 0.25+0.01

BEAM

Galactic Longitude (arc min)

Galactic Latitude (arc min)

142

$V_{LSR}$ (km/s)

Galactic Longitude (arc min)

Galactic Latitude (arc min)

(c)

143
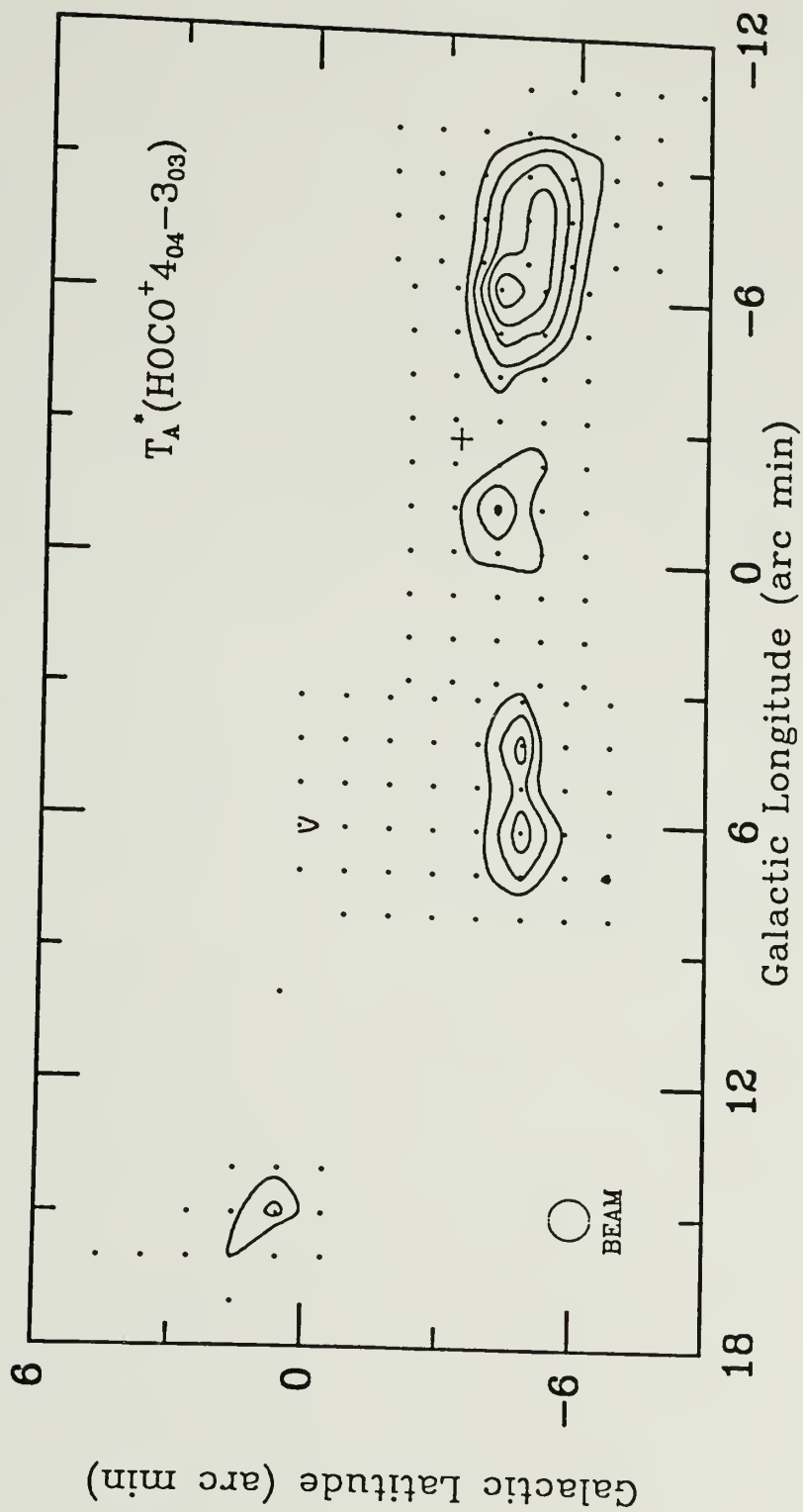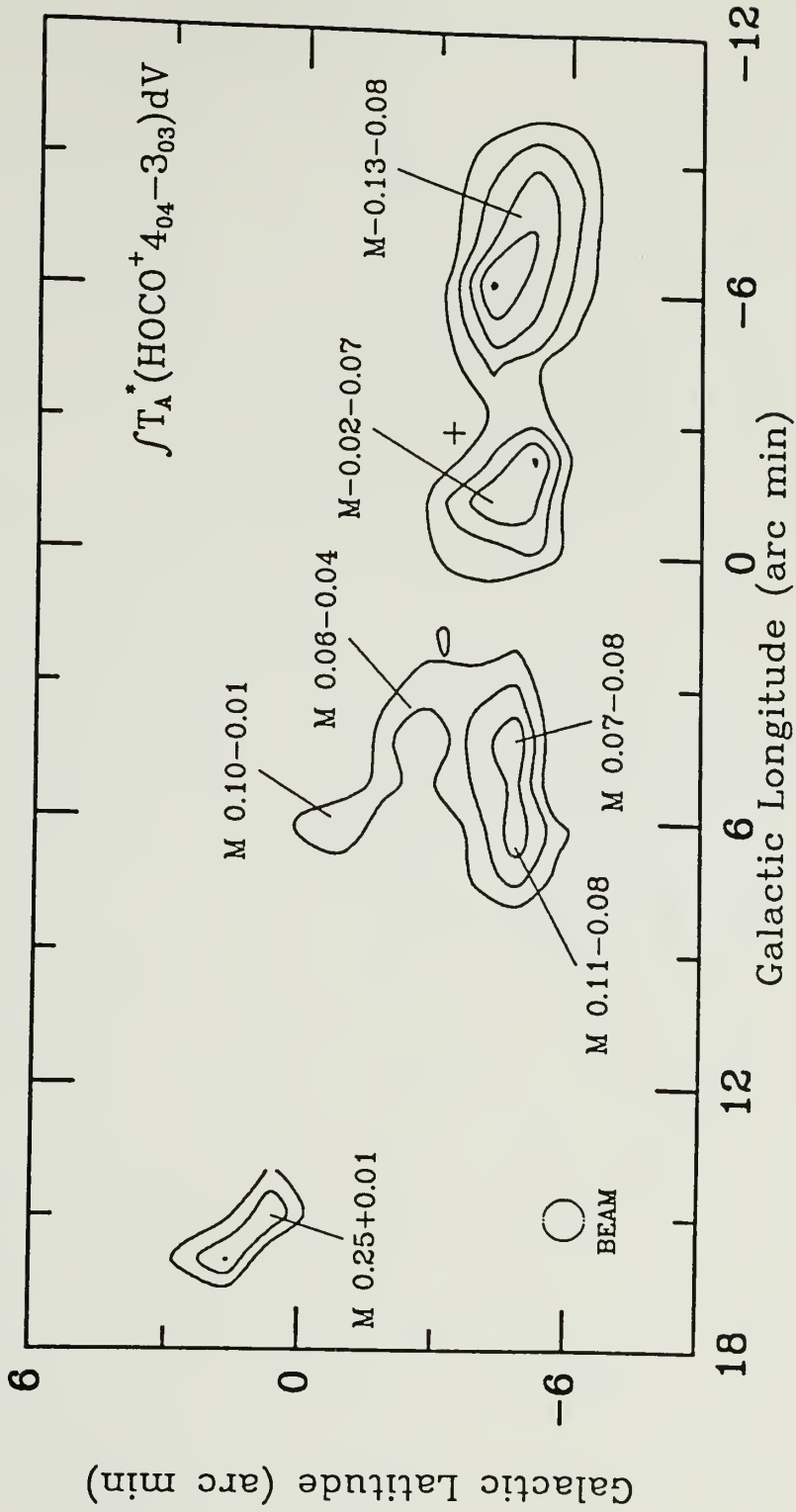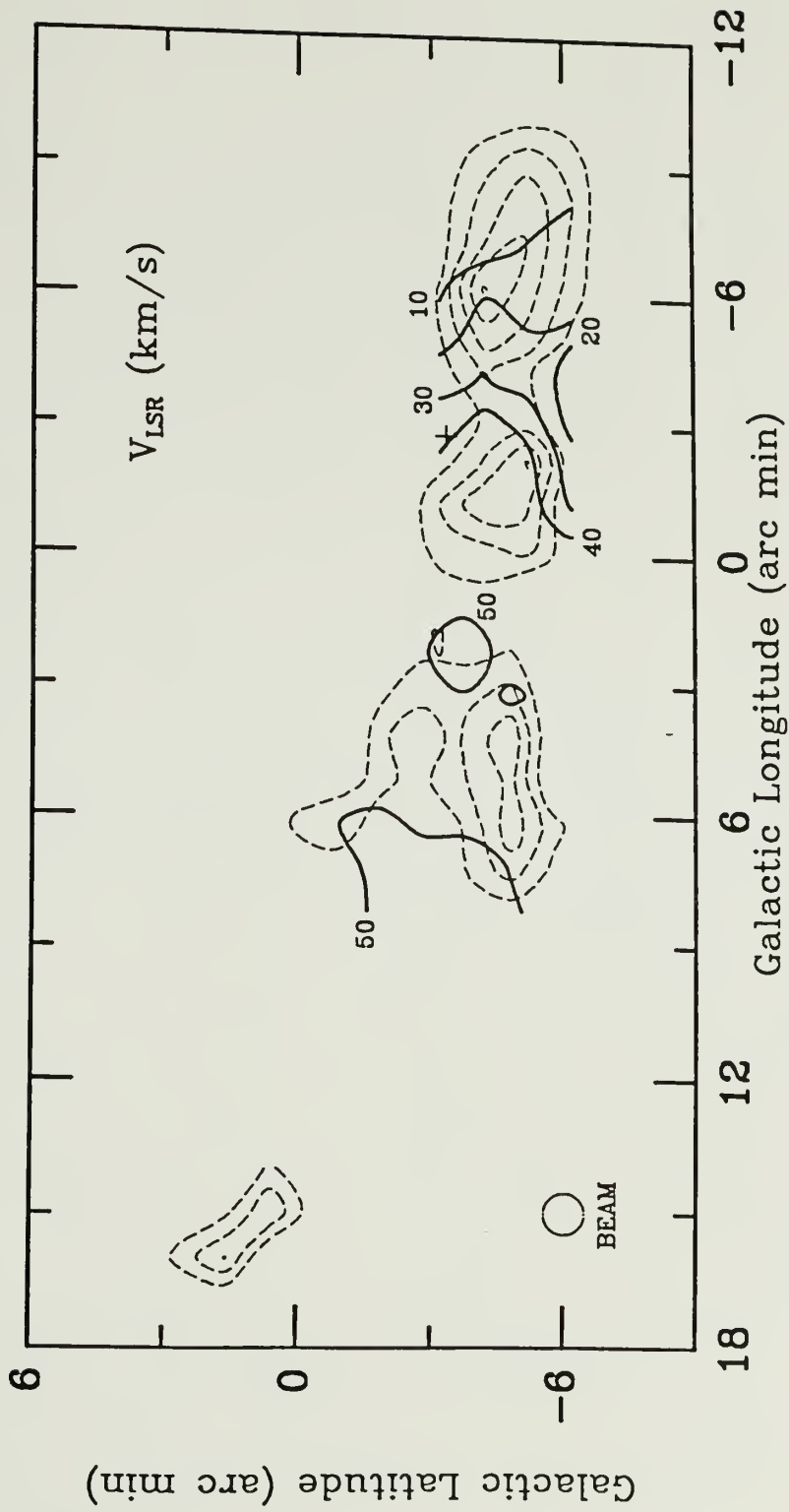
(Güsten, Walmsley, and Pauls 1981).   The clouds M-0.13-0.08 and M-0.02-0.07 seem to be merging or overlapped in the line of sight, as is also shown in the velocity map of Figure 8.1c.   The region of positive longitudes shows a fairly uniform velocity in the range 40 - 50 km s$^{-1}$, while the negative longitude region shows an apparent velocity gradient from $V_{LSR}$ ~ 10 km s$^{-1}$ to ~ 50 km s$^{-1}$ along the Galactic plane.

In Table 8.2, we summarize the HOCO$^+$ observations towards the cores of the condensations observed in ammonia by Güsten, Walmsley, and Pauls (1981) (see Figure 8.1b).   Data towards the condensation M-0.13-0.08 are given at the location of the strongest emission of the HOCO$^+$ $4_{04}$ - $3_{03}$ transition, which is offset ($\Delta l$, $\Delta b$) = (1.4', 0.4') from the nominal position implied by the name.


8.4 Excitation of HOCO$^+$


We have used an LVG model to solve the statistical equilibrium and radiative transfer equations for HOCO$^+$.   The model is described in Appendix A.   HOCO$^+$ is an asymmetric top with a $^1\Sigma$ ground electronic state.   It has both a- and b-components of its electric dipole moment (molecular constants are given in Bogey, Demuynck, and Destombes 1984).   We included in the calculation a total of 72 levels up to energies of ~ 200 K above the ground state in the $K_a$ = 0, 1, and 2 ladders.   We have used HNCO collisional de-excitation rates (S. Green, private communication) for those of HOCO$^+$ as a

TABLE 8.2

Summary of the HOCO$^+$ Observations[a,b] for the Sgr A Molecular Cloud

| Position | Freq.[c] (GHz) | $T_A^*$ (K) | $\int T_A^* dV$ (K km s$^{-1}$) | $V_{peak}$ (km s$^{-1}$) | $\Delta V$ (km s$^{-1}$) |
|---|---|---|---|---|---|
| M-0.13-0.08 | 85 | 0.39 ±.02[d] | 8.2 | 18 | 17 |
|  | 106 | 0.34 ±.03 | 6.5 | 21 | 18 |
| M-0.02-0.07 | 85 | 0.26 ±.05 | 6.3 | 45 | 24 |
|  | 106 | 0.23 ±.02 | 6.0 | 50 | 24 |
| M 0.06-0.04 | 85 | 0.13 ±.05 | 2.3 | 45 | 15 |
|  | 106 | 0.12 ±.02 | 1.1 | 50 | 9 |
| M 0.07-0.08 | 85 | 0.27 ±.06 | 6.1 | 50 | 25 |
|  | 106 | 0.18 ±.02 | 3.8 | 48 | 20 |
| M 0.10-0.01 | 85 | 0.18 ±.05 | 3.9 | 47 | 19 |
|  | 106 | 0.11 ±.02 | 2.6 | 46 | 20 |
| M 0.11-0.08 | 85 | 0.29 ±.06 | 5.9 | 45 | 19 |
|  | 106 | 0.25 ±.02 | 5.8 | 48 | 22 |
| M 0.25+0.01 | 85 | 0.22 ±.04 | 5.0 | 33 | 25 |
|  | 106 | 0.23 ±.02 | 5.0 | 36 | 21 |

[a] At the cores of each condensation.

[b] Spectral resolution is 0.69 MHz.

[c] 85. 53068 GHz for the $4_{04} - 3_{03}$ transition and 106.91336 GHz for the $5_{05} - 4_{04}$ transition (Bogey, Demuynck, and Destombes 1984).

[d] 1 $\sigma$ uncertainty.

145

first approximation, since $HOCO^+$ and HNCO have similar molecular constants and structures. The collisional de-excitation rates are fairly insensitive to kinetic temperature and $\Delta J$. The HNCO excitation has been modelled in Sgr B2 by Churchwell *et al.* (1986), and we might expect that the general features of the $HOCO^+$ excitation would be similar to that for HNCO. Our main purpose for the LVG analysis is to check the effect of the fast b-type transitions and background radiation on the excitation of $HOCO^+$; this should allow us to calculate its abundance more accurately that was done in Paper 1, which assumed optically thin emission and a Boltzmann population distribution. In Figure 8.2, we have shown fractional abundances for each J level in the $K_a = 0$ ladder for several Boltzmann distributions and for the LVG analysis results. The fast b-type transitions drain the populations in $K_a \geq 1$ levels to the $K_a = 0$ ladder, and consequently enhance the populations of the $K_a = 0$ ladder. This enhancement of $K_a = 0$ ladder populations may partly result in the extended emission of the $HOCO^+$ $4_{04} - 3_{03}$ transition observed towards Sgr B2 and Sgr A.

In Figure 8.3, we have plotted the antenna brightness temperature ($T_R$), the optical depth (Tau), and the excitation temperature ($T_{ex}$) as functions of the apparent background radiation temperature ($T_{rad}$), as calculated from the LVG model for the $4_{04} - 3_{03}$ and $5_{05} - 4_{04}$ transitions. $T_{ex} \sim T_{rad}$ for $n(H_2) \leq 10^4$ cm$^{-3}$ and $T_{kin} \geq T_{ex} \geq T_{rad}$ for $n(H_2) > 10^4$ cm$^{-3}$, as shown in the bottom panel of Figure 8.3. The antenna temperatures for the $K_a = 0$

Figure 8.2   Fractional populations of each J level in the $K_a = 0$ ladder of $HOCO^+$. Left panel is for Boltzmann distributions, middle for LVG calculations with volumn density $n(H_2) = 10^4$ cm$^{-3}$, and right for LVG calculations with $n(H_2) = 10^5$ cm$^{-3}$.   Temperatures are indicated in the figure.   No background radiation is included.

147
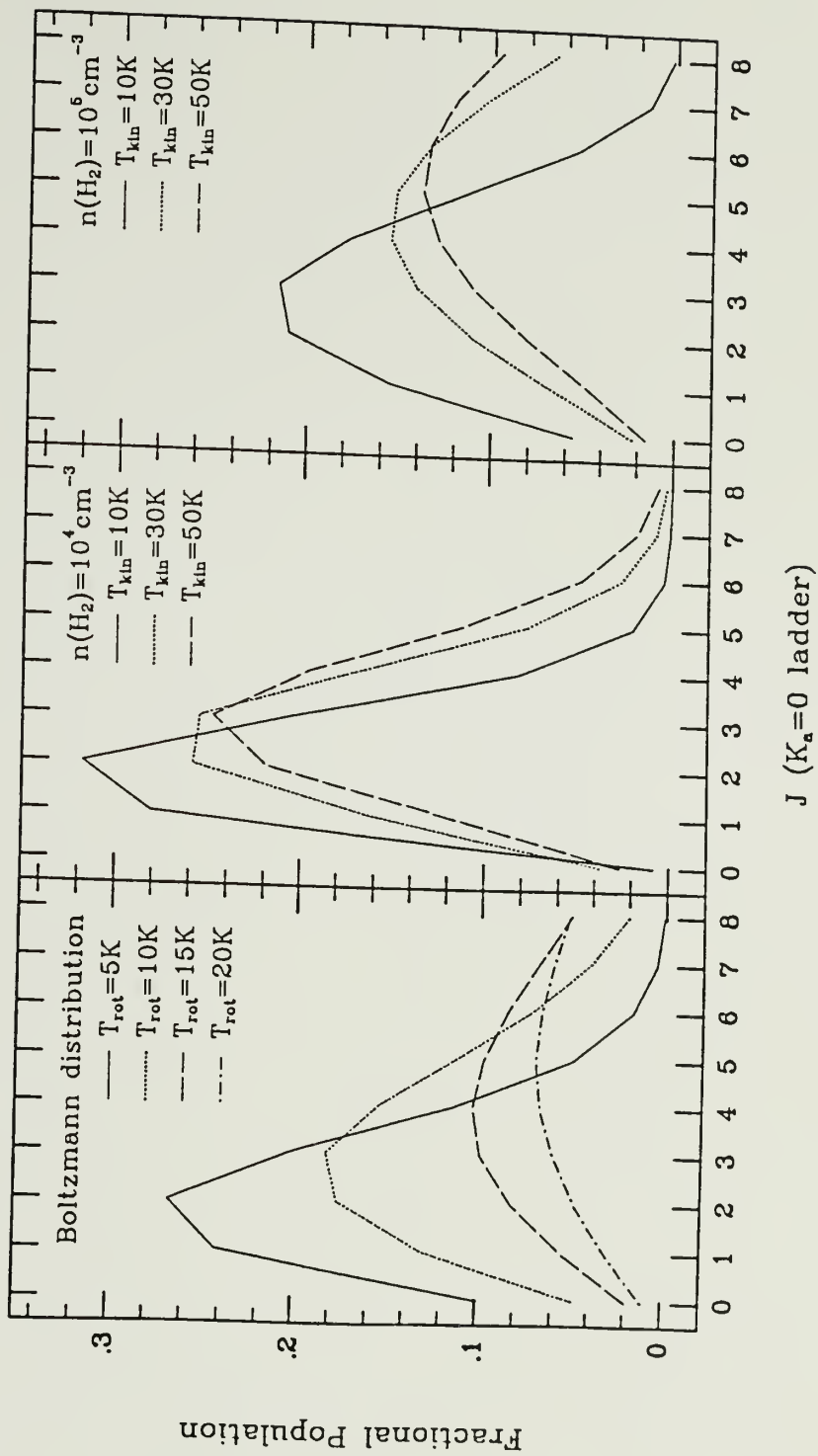
Figure 8.3    Sample of the LVG analysis results for the antenna brightness temperature ($T_R$) for the two observed $HOCO^+$ transitions, the optical depth (Tau), and the excitation temperature ($T_{ex}$), as functions of the apparent background radiation temperature ($T_{rad}$).
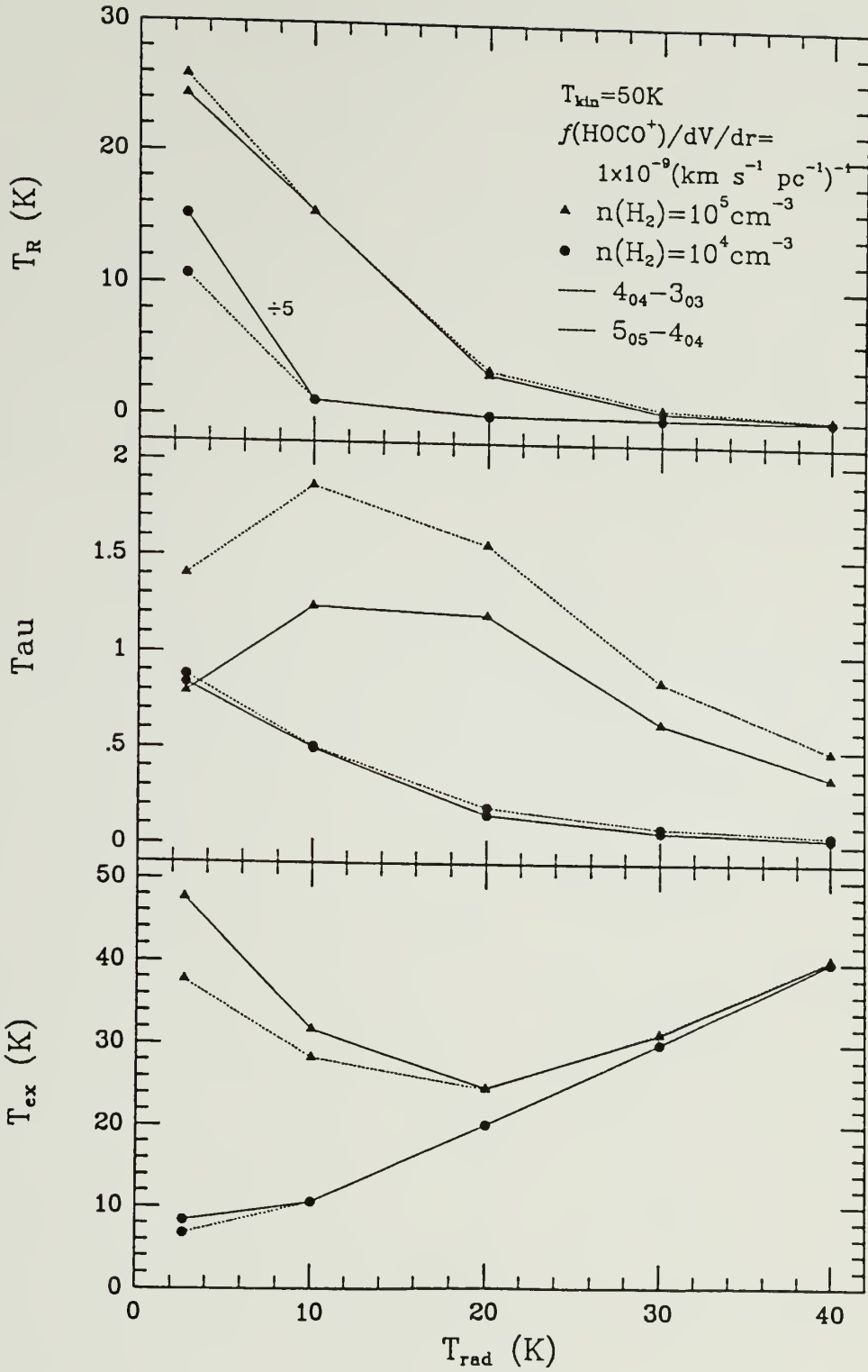
ladder transitions decrease quickly as $T_{rad}$ increases (upper panel of Figure 8.3), because the excitation temperatures between the $K_a$ ladders equilibrate to $T_{rad}$, which increases the populations in the $K_a \geq 1$ ladders, as was discussed by Churchwell *et al.* (1986), and the antenna brightness temperature is proportional to the difference between the excitation temperature and the background radiation temperature.

Churchwell *et al.* (1986) suggest that the strength of the HNCO lines observed in the center of Sgr B2 can be explained best if the excitation includes the effect of a 10 K radiation field with a beam filling factor ~ 0.8 and a 70 K field with a beam filling factor of ~ 0.2, which results in 15 % of the total HNCO column density in $K_a$ $\geq 1$ ladders (see discussion in the reference). We also apply a 10 K radiation field but with a beam filling factor 1 in the $HOCO^+$ LVG analysis for Sgr B2(M) and (2N). If a 70 K radiation field with a beam filling factor 0.2 is included for the model of Sgr B2(M), then the column density is expected to increase by ~ 10 %. In Sgr A, the infrared surface brightness intensities peak around Sgr A (West) at 30 $\mu$m, show a double-lobed structure at 50 $\mu$m and 100 $\mu$m (Becklin, Gatley, and Werner 1982), and peak at the center of M-0.13-0.08 at 540 $\mu$m (Hildebrant *et al.* 1979). Therefore, hot grains ($T_{dust}$ ~ 40 K; Gatley *et al.* (1977); Dent *et al.* (1982)) dominate around Sgr A (West), while the neutral gas clouds which we have observed may be more closely related to relatively cool dust grains. We derive a dust color temperature of ~ 20 K at the center

of M-0.13-0.08 from 100 $\mu$m and 540 $\mu$m data (the energy differences corresponding to the inter-ladder b-type transitions are $\Delta E(K_a = 0-1)$ ~ 390 $\mu$m and $\Delta E(K_a = 1-2)$ ~ 130 $\mu$m). The apparent radiation temperature depends on the actual energy density of the region, which is less than the grain color temperature, and we assume an apparent radiation temperature of 10 K as a lower limit for Sgr A (M-0.13-0.08). Constant brightness temperature curves calculated from the LVG model for the Galactic center sources are shown in Figure 8.4a to c for the observed antenna temperatures of the $4_{04}$ - $3_{03}$ and $5_{05}$ - $4_{04}$ transitions and corresponding 3 $\sigma$ values. Similar curves corresponding to the observed upper limits for the $1_{01}$ - $0_{00}$ and $4_{04}$ - $3_{03}$ transitions for TMC-1 (3 $\sigma$) are indicated in Figure 8.4d.

We have used kinectic temperatures of 50 K and 10 K for the Galactic center clouds and for the cold dark clouds, respectively. Churchwell and Hollis (1983) derive an almost constant kinetic temperature $T_{kin}$ ~ 50 K across Sgr B2 with $CH_3CCH$ data. In Sgr A, Güsten, Walmsley, and Pauls (1981) derive $T_{kin}$ ~ 50 - 120 K, while Morris et al. (1983) derive $T_{kin}$ ~ 30 - 60 K, using $NH_3$ lines. The $HOCO^+$ LVG analysis shows that the excitation is dominated by radiation processes not collisional processes, and we also use $T_{kin}$ ~ 50 K for Sgr A. $T_{kin}$ ~ 10 K may be a typical value for cold, dark clouds (Irvine, Goldsmith, and Hjalmarson 1987), and we use this value for TMC-1 and L134N in the LVG analysis.

Figure 8.4a - d  Constant brightness temperature curves calculated from the LVG models which match the observations of the $4_{04}$ - $3_{03}$ and $5_{05}$ - $4_{04}$ transitions of $HOCO^+$.  Calculations for Sgr A and Sgr B2 include the effect of a 10 K radiation field.  Each center line is for the observed antenna temperature ($T_A^*/\eta_B$) and the other two lines for corresponding 3 $\sigma$ values.  (a) Sgr A (M-0.13-0.08). Contours are 0.46, 0.53, and 0.61 K for the $4_{04}$ - $3_{03}$ line, and 0.39, 0.50, and 0.62 K for the $5_{05}$ - $4_{04}$ line.  (b) Sgr B2(2N). 1.30, 1.46, and 1.62 for the $4_{04}$ - $3_{03}$ line, and 1.23, 1.37, and 1.51 for the $5_{05}$ - $4_{04}$ line.  (c) Sgr B2(M).  0.46, 0.59, and 0.72 for the $4_{04}$ - $3_{03}$ line, and 0.63, 0.75, and 0.87 for the $5_{05}$ - $4_{04}$ line.  (d) TMC-1.  0.09 for the $4_{04}$ - $3_{03}$ line and 0.10 for the $1_{01}$ - $0_{00}$ line.

SgrA(M−0.13−0.08)

$4_{04} - 3_{03}$
$5_{05} - 4_{04}$

$\log(n(\text{HOCO}^+)/dV/dr)$

$\log(n(\text{H}_2))$

(a)

(b)

SgrB2(M)

$4_{04} - 3_{03}$

$5_{05} - 4_{04}$

$\log(n(\text{HOCO}^+)/dV/dr)$

$\log(n(\text{H}_2))$

155

(c)

SgrB2(2N)

$4_{04} - 3_{03}$

$5_{05} - 4_{04}$

x-axis: $\log(n(HOCO^+)/dV/dr)$

y-axis: $\log(n(H_2))$
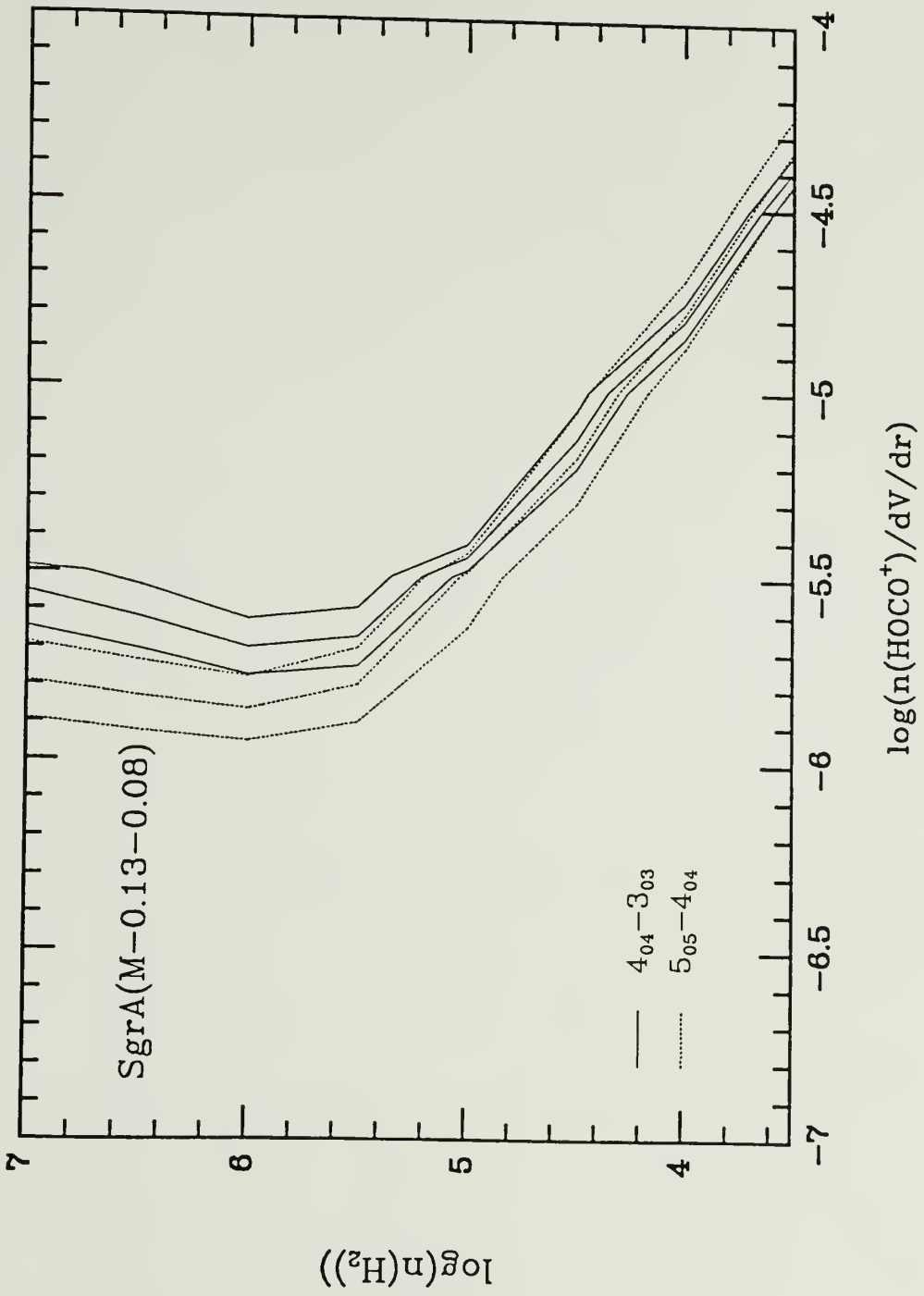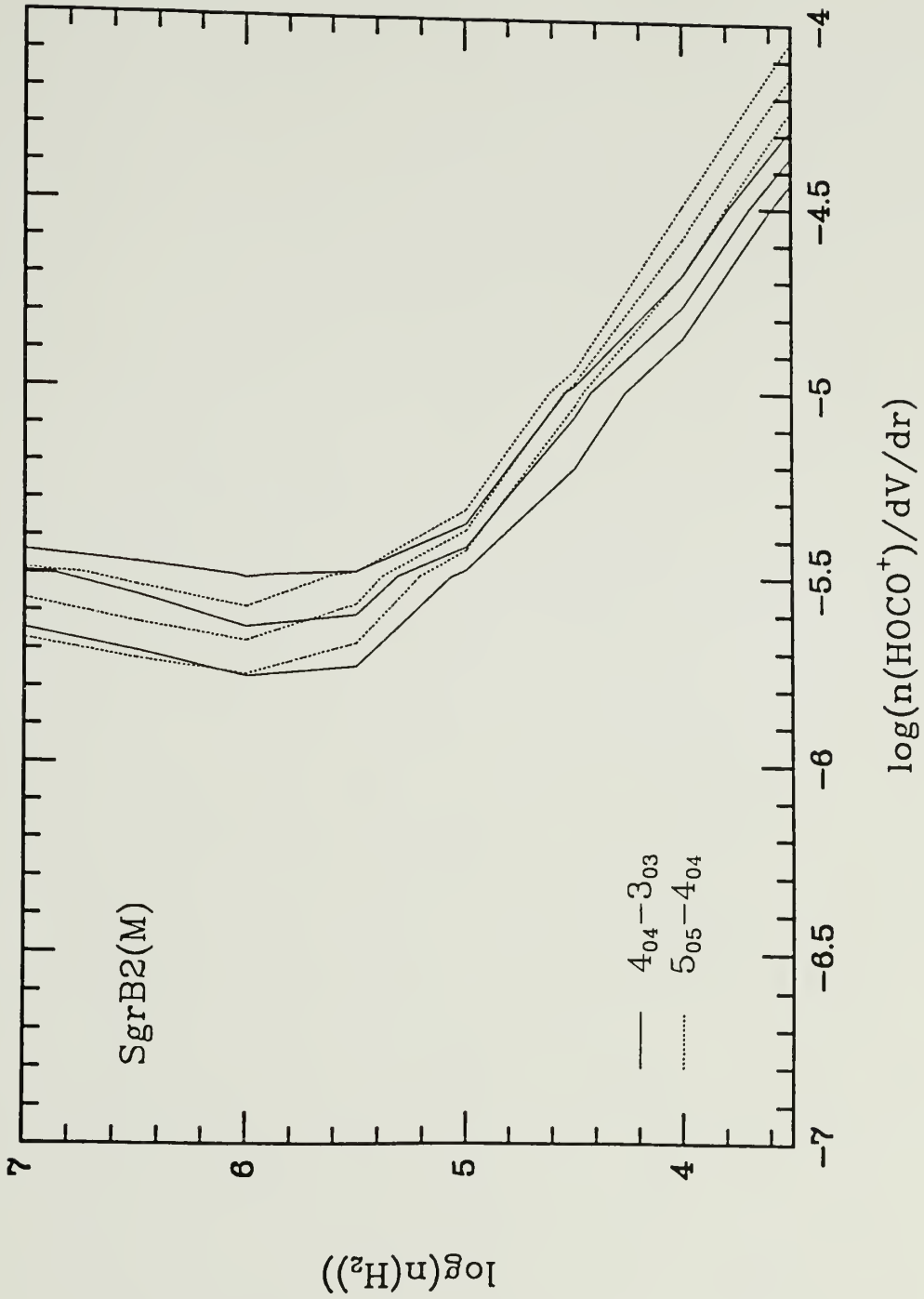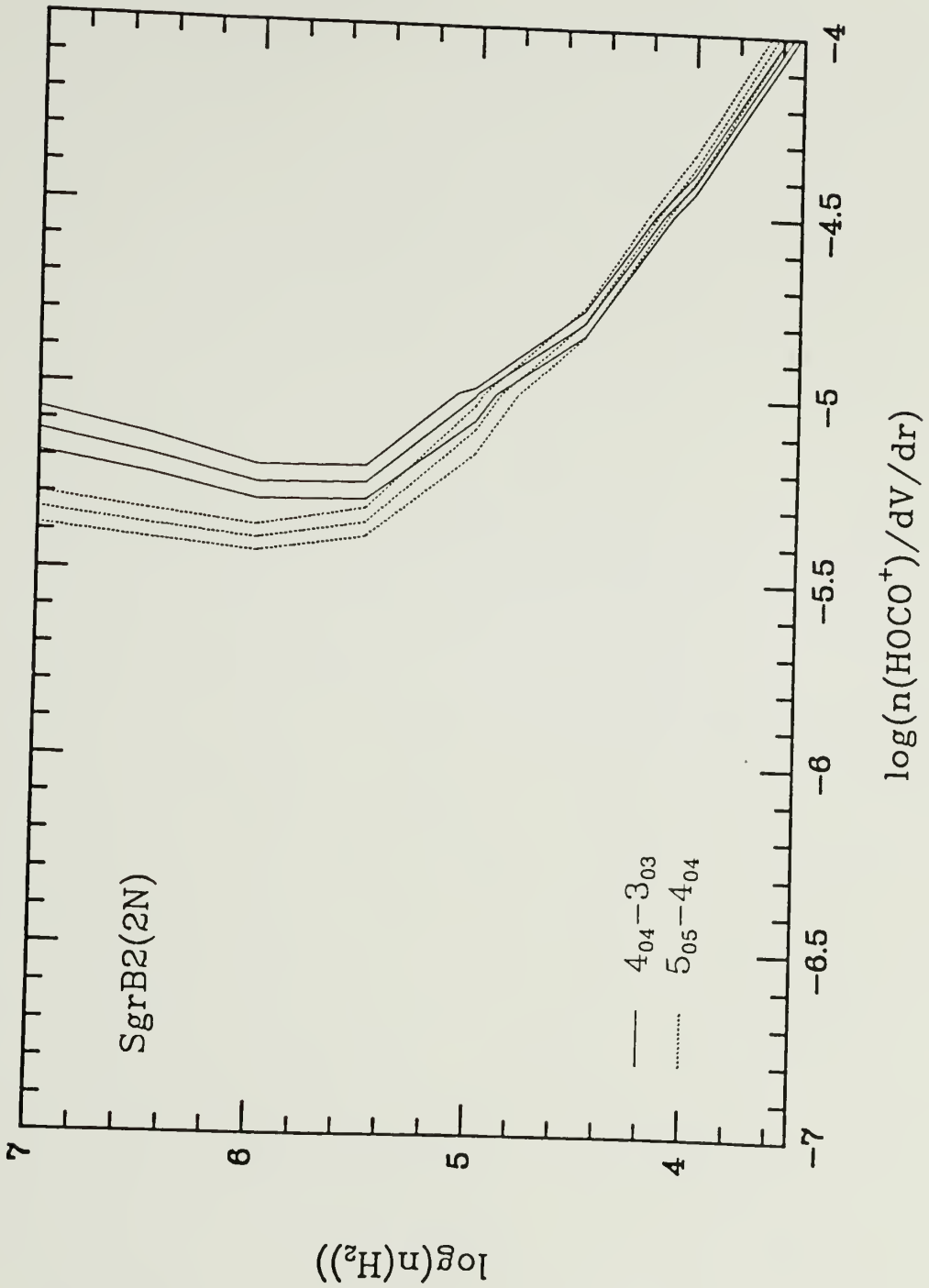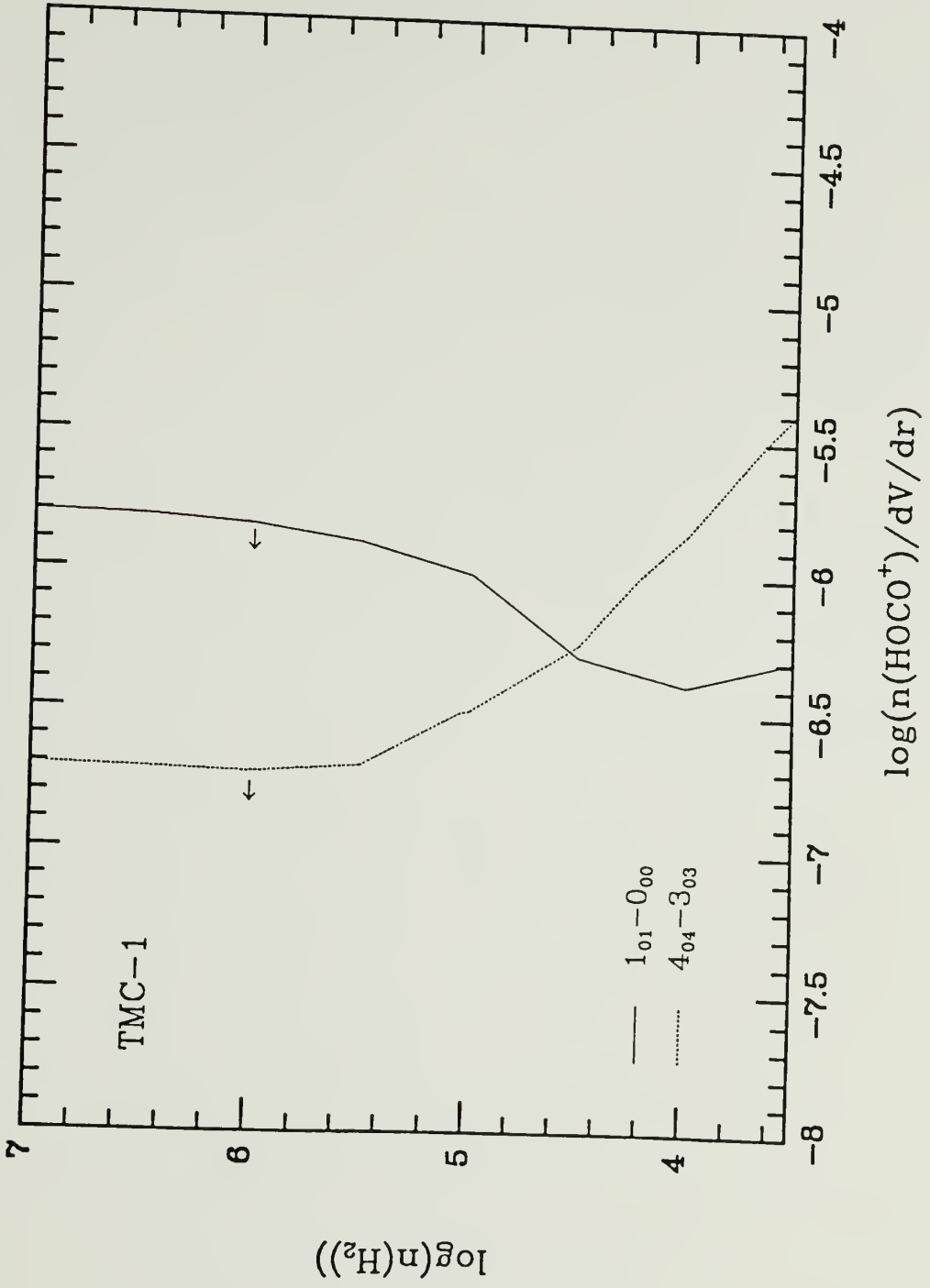
(d)

Since our two observed transitions typically do not well constrain both $n(H_2)$ and the abundance of $HOCO^+$ in the sources studied, we pick a range of values for $n(H_2)$ based on data for other molecules. The density distribution of the Sgr B2 molecular cloud has been modelled recently by Lis (1989), who derives $n(H_2) \sim 6 \times 10^5$ cm$^{-3}$ for the core component at the center with a radial exponent -2, which gives $n(H_2) \sim 4 \times 10^4$ cm$^{-3}$ at 2 arcminute north. In Sgr A (M-0.13-0.08), $n(H_2) \sim 1 \times 10^5$ cm$^{-3}$ has been derived from the $H_2CO$ analysis by Güsten and Henkel (1983), and $\sim 0.2 - 1 \times 10^5$ cm$^{-3}$ from virial masses by Armstrong and Barrett (1987). We use $n(H_2) \sim 0.5$-$5 \times 10^5$ cm$^{-3}$ for Sgr B2(M), and $1$-$5 \times 10^4$ cm$^{-3}$ for Sgr B2(2N) and the core of M-0.13-0.08, the peak position for the $4_{04}$ - $3_{03}$ transition observed in Sgr A. For the cold dark clouds TMC-1 and L134N, we use the maximum upper limits determined from the 3 $\sigma$ values for the two observed $HOCO^+$ transitions, $4_{04}$ - $3_{03}$ and $1_{01}$ - $0_{00}$ (see Figure 8.4d). The calculated results are normalized to a velocity gradient $dV/dr = 1$ km s$^{-1}$ pc$^{-1}$, and the abundances derived from this LVG analysis are given in Table 8.3. Note that the Sgr A position in Table 8.3 is the peak of the $HOCO^+$ $4_{04}$ - $3_{03}$ emission (offset $(\Delta l, \Delta b) = (1.4', 0.4')$ from the nominal position of M-0.13-0.08), while that in Paper 1 is offset $\sim 2'$ from this peak position toward Sgr A(West). The $HOCO^+$ column density in Sgr A has been increased by a factor of $\sim 50$ relative to that in Paper 1, which results from the difference in line intensity between the two

TABLE 8.3

Abundances of $HOCO^+$

| Source[a] | $N(HOCO^+)$ (cm$^{-2}$) | $\dfrac{f(HOCO^+)^{[b]}}{dV/dr}$ (km s$^{-1}$pc$^{-1}$)$^{-1}$ | $\dfrac{[HOCO^+]^{[c]}}{[H_2]}$ | $\dfrac{[HOCO^+]^{[d]}}{[HCO^+]}$ | $\dfrac{[CO_2]^{[e]}}{[CO]}$ |
|---|---|---|---|---|---|
| SgrA | 0.3-1.0 (15) | 4(-10) | 8(-9) | 3 | 1 |
| SgrB2(2N) | 0.9-3.1 (15) | 5(-10) | 4(-9) | 4 | 0.6 |
| SgrB2(M) | ≥ 1.4 (14) | ≥ 4(-12) | ≥ 1(-10) | ≥ 0.1 | ≥ 0.3 |
| TMC-1 | ≤ 1.1 (12) | — | ≤ 1(-10) | ≤ 1(-2) | ≤ 3(-2) |
| L134N | ≤ 1.0 (12) | — | ≤ 1(-10) | ≤ 1(-2) | ≤ 3(-2) |

Numbers in parentheses are powers of 10.

[a] For Sgr A at the peak position of the $HOCO^+$ $4_{04}$ - $3_{03}$ emission:

Offset $(\Delta l, \Delta b)$ = (1.4′, 0.4′) from the core of the M-0.13-0.08

condensation ; Other positions given in Paper 1.

[b] Fractional abundance of $HOCO^+$ divided by velocity gradient,

derived by the LVG analysis.

[c] SgrA: $N(H_2) \sim 7.8 \times 10^{22}$ cm$^{-2}$ (from $N(^{13}CO) \sim 2.7 \times 10^{17}$ cm$^{-2}$ at

the core of M-0.13-0.08 (Armstrong and Barrett 1987), $[^{12}CO]/[^{13}CO]$

$\sim$ 23 (Penzias 1980), and $[^{12}CO]/[H_2] \sim 8 \times 10^{-5}$); Sgr B2(M): $N(H_2) \sim$

$1.3 \times 10^{24}$ cm$^{-2}$ (Lis 1989); SgrB2(2N): $N(H_2) \sim 5.0 \times 10^{23}$ cm$^{-2}$ (from

(Continued on next page)

TABLE 8.3

(Continued)

$C^{18}O$: Lis 1989); TMC-1: $N(H_2) \sim 1 \times 10^{22}$ cm$^{-2}$ (Irvine *et al.* 1987; Friberg and Hjalmarson 1989); L134N: $N(H_2) \sim 8.2 \times 10^{21}$ cm$^{-2}$ (Swade 1987).

[d] SgrA: $N(HCO^+) \sim 2.8 \times 10^{14}$ cm$^{-2}$ (at the core of M-0.13-0.08 from the unpublished data of $HC^{13}O^+$ of Minh and Irvine, and $[HCO^+]/[H^{13}CO^+] \sim 23$); SgrB2(M): $N(HCO^+) \sim 1.3 \times 10^{15}$ cm$^{-2}$ (from the unpublished $HC^{18}O^+$ data of Minh and Irvine, assuming $[HCO^+]/[HC^{18}O^+] \sim 230$); SgrB2(2N): $N(HCO^+) \sim 4.7 \times 10^{14}$ cm$^{-2}$ (same as for SgrB2(M)); TMC-1 and L134N: $N(HCO^+) \sim 8 \times 10^{13}$ cm$^{-2}$ (Irvine, Goldsmith, and Hjalmarson 1987).

[e] From the equation of Herbst *et al.* (1977) (see also Paper 1).

observed positions (about a factor of 5) and the inclusion of the
background radiation effect (about a factor of 10).

## 8.5 Discussion

### 8.5.1 $HOCO^+$ Abundances

We derive fractional abundances of $HOCO^+$ relative to $H_2$ of
$f(HOCO^+) \geq 1 \times 10^{-9}$ in the Galactic center, which is about three
orders of magnitude greater than predicted by quiescent ion-molecule
gas-phase chemistry (Herbst and Leung 1986).    The non-detection of
$HOCO^+$ in the "typical" molecular clouds outside the Galactic center
(Paper 1) may indicate that the $HOCO^+$ chemistry in the Galactic
center is unique, although better rms values should be obtained for
other sources.

If the Galactic center environment produces an unusual
chemistry, this may be particularly prominent in Sgr A.    The
distribution of $HOCO^+$ looks quite similar to that of $NH_3$ (Güsten,
Walmsley, and Pauls 1981) and HNCO (Armstrong and Barrett 1984).
The fractional abundances of $HOCO^+$ in Sgr A appear to be in the
range $1$-$10 \times 10^{-9}$ relative to $H_2$, for values of $n(H_2)$ derived from
the $N(^{13}CO + C^{18}O)$ map of Armstrong and Barrett (1984) (assuming
$[^{12}CO]/[^{13}CO] \sim 23$ (Penzias 1980); $[CO]/[H_2] \sim 8 \times 10^{-5}$), with the
largest values ($\sim 10^{-8}$) for the centers of M-0.13-0.08 (Table 8.3)
and M 0.11-0.08.    In the third column of Table 8.3 we include

$f(HOCO^+)/dV/dr$ values derived in the model calculations. If we apply an estimated source size (~ 7 - 10 pc for M-0.13-0.08 from Figure 8.1) and the $HOCO^+$ line width (~ 17 km s$^{-1}$), we obtain $dV/dr$ ~ 2 km s$^{-1}$ pc$^{-1}$, which gives $f(HOCO^+)$ ~ $10^{-9}$. Although this value is about a factor of 10 less than that found by comparing the column density of $HOCO^+$ with the H$_2$ column density derived from other molecular data, it is still in the range we mentioned above. The model calculations, moreover, employ a simplfied radiative transfer analysis (cf. Irvine *et al.* 1985), and the actual $dV/dr$ in the region is quite uncertain; in addition, there may be an uncertain scaling factor in the collisional cross sections of $HOCO^+$ which were assumed to be the same as those of HNCO. Therefore we believe the fractional abundance derived by comparing the column density with other molecular data is more reliable than that found from the *in situ* $HOCO^+$ abundance in the model calculations.

Since upper limits for the $HOCO^+$ abundance in the cold dark clouds TMC-1 and L134N are much larger than the abundance predicted by quiescent ion-molecule chemistry (e.g. Herbst and Leung 1986), it is difficult to test the chemical models for $HOCO^+$. However, the fractional abundances for cold dark clouds are less by about a factor of 10 than those for the Galactic center clouds. Therefore, we expect that the formation processes of $HOCO^+$ must be efficient in the Galactic center region.

## 8.5.2 Chemistry related to HOCO[+]

Herbst *et al.* (1977) have suggested that HOCO[+] traces interstellar $CO_2$, and using major formation and destruction processes suggested that an abundance ratio $[HOCO^+]/[CO_2] \sim 10^{-5}$ (Herd, Adams, and Smith 1989) would be typical in molecular clouds. This implies a high abundance of $CO_2$ in the Galactic center. Pineau des Forêts, Roueff, and Flower (1989; hereafter PRF), however, suggested that the endothermic reaction $HCO^+ + O_2$ can form HOCO[+] in MHD shocks; in this case, HOCO[+] does not trace $CO_2$.

The chemical abundances in a shocked region largely depend on the initial abundances and shock conditions. The abundance ratios of $[HOCO^+]/[HCO^+]$ and $[CO_2]/[CO]$ are increased in the MHD shock model of PRF relative to preshock values by four and three orders of magnitude, respectively, (to ~ 0.1 for both ratios), by adding the reaction $HCO^+ + O_2 \rightarrow HOCO^+ + O$. The observed abundance ratio of $[HOCO^+]/[HCO^+]$ in the Galactic center clouds is, however, about an order of magnitude larger still (Table 8.3). In addition, the $HOCO^+$ $4_{04} - 3_{03}$ line has been observed to be fairly extended in Sgr B2 (Paper 1) and Sgr A (Figure 8.1). Although shocks may be prevalent in the Galactic center, it is not certain that the whole neutral gas complex has been in MHD shocks, which occupy relatively thin slabs (linear dimension $\leq 0.2$ pc; PRF). Therefore it may be difficult to explain the overall HOCO[+] abundance throughout the Galactic center clouds as a result of MHD shocks.

Another possible pathway for the formation of $CO_2$ is grain surface reactions. Grain-surface reactions alone form primarily simple, saturated hydrides, but UV photolysis may convert these into various other components. $H_2O$ ice is the most abundant molecule in grain mantles, and UV photolysis of $H_2O$ has been suggested to lead to the formation of $CO_2$, $H_2CO$, and $CH_3OH$ by reaction between photolysis products and neighboring simple species such as CO (cf. Tielens and Allamandola 1987; and see references therein), which itself has been identified as a major constituent in grain mantles (> 20 % of $H_2O$ toward NGC7538/IRS9 and Elias 16; see references in Grim and Greenberg 1987). This conjecture is supported by laboratory data: When a mixture of CO and $H_2O$ is irradiated by UV radiation, an observable amount of $CO_2$ is formed (Greenberg 1989). Inside a dense and quiescent cloud, this process may not be important because of a lack of UV photons, but in typical star-forming regions UV photons generated by newly formed stars could both process icy mantle material and warm up the grains to a high temperature, resulting in the evaporation of the grain mantles. In a region like the hot core component of Orion(KL), grain-related processes induced by radiative heating from the luminous IRc 2 are prominent, but the high density and temperature of the hot core leads to a low fractional ionization, which results in very inefficient ion-molecule chemistry (Blake *et al.* 1987). Since $HOCO^+$ forms mainly by the ion-molecule reaction between $H_3^+$ and $CO_2$, it is not certain whether the non-detection of $HOCO^+$ toward

Orion(KL) (Paper 1) indicates a small $CO_2$ abundance or inefficient ion-molecule chemistry of the region. In the Galactic center, however, the strong activities and shocks can generate a large abundance of UV photons in the extended region, which may result in effective UV photolysis of grain mantles and, consequently, a large abundance of $CO_2$ and hence of $HOCO^+$ in the extended region.

The grain surface chemical models are still in a formative stage, and UV photolysis processing is quite uncertain, partly because the UV photon density is not well known. Here we simply suggest an alternate route to explain the putative $CO_2$ abundance and consequently the $HOCO^+$ abundance in the Galactic center. The gas-phase reactions leading to formation of $HOCO^+$ and $CO_2$ should also be studied further.

CHAPTER 9


CONCLUSIONS


9.1 Summary


We have carried out radio observations for the interstellar

molecules $H_2S$, $H_2CS$, ethyl cyanide ($CH_3CH_2CN$), and $HOCO^+$, the

chemistry of which might be related to grain processes, either

directly or indirectly. Abundances of these species and chemical

implications for gas phase processes and grain-related processes

have been discussed in each chapter, and here we summarize the

conclusions.

In Chapters 2 - 4, we report the results for $H_2S$ observed

towards the cold dark clouds L134N and TMC-1 (Chapter 2), OMC-1

(Chapter 3), and other star-forming regions (Chapter 4). The

fractional abundances of $H_2S$ have been observed to be ~ $10^{-9}$

relative to $H_2$ towards L134N and quiescent warm clouds such as the

Orion extended ridge, and ~ $10^{-8}$ - $10^{-9}$ towards several active

star-forming regions. On the other hand, its abundance is enhanced

by a factor of 1000 in the Orion hot core and the plateau. We

conclude that $H_2S$ may be evaporating from the grain mantles in the

hot core. Even in the cold dark clouds, gas phase reactions may

not be able to produce the observed abundances, so that grain

surface reactions may be ultimately responsible for the gas phase

$H_2S$ abundances.    For these reasons $H_2S$ may be a good candidate to trace grain processes.

Our results for $H_2CS$ ortho-to-para ratios (Chapter 5) and ethyl cyanide abundances (Chapter 6) may contradict each other concerning the role of grains in dark cloud chemistry.    The ortho-to-para ratio of ~ 1.8 for $H_2CS$ in TMC-1 seems to indicate thermalization on ~ 10 K grain surfaces and imply continuous interactions between gas and grains: i.e. continuous adsorption and desorption.    On the other hand, the upper limit on the abundance of ethyl cyanide in TMC-1 may suggest that desorption processes are quite inefficient in cold dark clouds and the hydrogenation of $HC_3N$ on grain surfaces does not affect the gas phase abundances.    Perhaps the difference between these results is related to the larger molecular weight of $CH_3CH_2CN$ relative to $H_2CS$, and a consequent lower desorption probability.

In Chapters 7 and 8, we have presented the results for $HOCO^+$. We derive $HOCO^+$ fractional abundances ~ $10^{-8}$ - $10^{-9}$ relative to molecular hydrogen towards the Galactic center sources Sgr A and Sgr B2, which are about three orders of magnitude larger than those predicted by quiescent ion-molecule chemistry and about an order of magnitude larger than predicted by a MHD shock model.    If $HOCO^+$ traces interstellar $CO_2$, the high abundance of the latter ($[CO_2]$ ~ $[CO]$) in the Galactic center may result from the UV photolysis of grain mantles.    On the other hand, the $HOCO^+$ $4_{04} - 3_{03}$ line has not been detected in our survey of other Galactic sources.    Therefore,

gas phase $CO_2$ seems not to be an important carbon and oxygen reservoir in typical molecular clouds.

Quite recently d'Hendecourt and Muizon (1989) have claimed the discovery of interstellar carbon dioxide ($CO_2$) towards three infrared stars and suggested again the usage of $HOCO^+$ as a tracer of $CO_2$. Our results for $HOCO^+$ in the Galactic center and other molecular clouds could give some constraints on the grain surface chemistry for the formation of $CO_2$.

## 9.2 Implications for Interstellar Chemistry

The role of grains in interstellar chemistry has been often de-emphasized, except as a catalyst for the formation of $H_2$ molecules, largely because of the reasonable agreement between observational abundances and gas-phase calculations, at least for simple molecules (Irvine et al. 1985; Irvine and Knacke 1989). Although grain chemistry is highly uncertain compared with gas phase chemistry, and the grains constitute only about 1 % by mass of molecular clouds, the elements heavier than helium may exist in grains with comparable to or even greater abundances than the amounts in the gas phase, at least for certain elements (Irvine and Knacke 1989). Moreover, several molecules have been identified in grain mantles directly by infrared spectroscopy towards protostars embedded in molecular clouds (e.g. Hagen, Allamandola, and Greenberg

1980; Wilner 1984; Lacy *et al.* 1984).  $H_2O$ and CO, for example, have been identified in both the interstellar gas and solid phases.

Infrared spectroscopy of interstellar grains, however, has some limitations, because solid state spectra are not yet available except for a few simple molecules studied in the laboratory, because the interpretation of the broad spectral features attributed to interstellar grains is controversal, and above all, because observable sources are limited to a few protostars deeply embedded in molecular clouds.  While radio observations of interstellar molecules identified clearly through their rotational spectra have many advantages compared to infrared spectroscopy, they are limited to gas phase species and there are few such molecules which trace purely grain processes.  Consequently, there have been very few radio observations which clearly support grain processes.  Our radio observations of interstellar molecules mentioned in previous chapters may be useful in this connection.

Our results for $H_2S$ suggest that we may include $H_2S$ as a candidate for production by grain surface processes.  Although desorption should have to occur even in cold dark clouds to preserve the gas phase component, there has been little prior evidence for this phenomenon.  However, the abundance of $H_2S$ in quiescent clouds could be explained easily by grain surface formation followed by the desorption of the species, and the very high abundances in the Orion hot core and plateau strongly suggest evaporation of grain mantles. Our results for the $H_2CS$ ortho/para ratios also suggest an efficient

exchange of material between grain surfaces and the gas phase in cold dark clouds. On the other hand, the upper limits for the ethyl cyanide abundance may indicate a lower desorption probability in cold dark clouds, at least for heavy molecules like $CH_3CH_2CN$ and $CH_2CHCN$. Finally, we expect our $HOCO^+$ observations may give indirect evidence for energetic grain surface processes as well as some constraints on the gas phase chemistry.

We conclude that radio observations may be very useful for the study not only of gas phase processes but also of grain-related processes. They may at least give some constraints on highly uncertain grain processes, including accretion and desorption, surface reactions, evaporation of grain mantles, UV processing of grain mantles, and grain disruption by shocks. The understanding of interstellar grains would be increased most rapidly by carrying out studies of infrared spectroscopy, laboratory experiments, and radio observations simultaneously.

## 9.3 Future Observations

We plan to study $H_2S$ further with higher angular resolution and sensitivity towards various types of sources, especially towards a region like Orion(KL) where the $H_2S$ source sizes are estimated to be ~ 3" and ~ 7" for the hot core and the plateau, respectively. A map of the $H_2S$ emission in Sgr B2 would reveal whether there exist actually two different velocity components as was suggested by $H_2S$

and $H_2^{34}S$ lines.     This study could be interesting if $H_2S$ traces active regions inside a dense molecular cloud.

The distributions of $H_2S$ and $H_2CS$ in cold dark clouds could be useful for studing abundance gradients within such clouds. Moreover, the $H_2CS$ lines in the 3 mm region appear to be optically thin in most cases, and ortho-to-para ratios could be measured in a larger source sample as well as in several positions in a cloud. This ratio could also be measured using other molecules such as $H_2S$ and $H_2CCO$.

Better upper limits for the abundances of HDS in Orion(KL), of $H_2S$ in IC443B, and of $HOCO^+$ in molecular clouds outside the Galactic center would sharpen the arguments for their chemistry.     Especially since interstellar $CO_2$ has been tentatively identified towards a few protostars (d'Hendecourt and Muizon 1989), $HOCO^+$ observations towards these sources would be useful for studying its chemistry.

Statistical Equilibrium and LVG Models

## A.1 <u>Cloud</u> <u>Model</u>

The cloud model includes two coupled equations, the equations
of statistical equilibrium and the equation of radiative transfer.
The population of the energy levels of a molecule is determined by
the statistical equilibrium equations, while the radiative transfer
equation determines the radiation field inside the cloud, which is
necessary to determine the radiative rates in the statistical
equilibrium equations, and the emergent intensity from the cloud.

In statistical equilibrium, the rate of transitions that
populate an energy level i is exactly balanced by the rate of
transitions that depopulate the ith level.   For a k-level molecule
there are k equations of the form,

$$n_i \sum_j R_{ij} = \sum_j n_j R_{ji},$$

where $n_i$ and $n_j$ are the populations of the ith ($E_i$) and jth ($E_j$)
levels, respectively.    $R_{ij}$ is the rate of any transition that
changes the molecule's excitation from the ith level to the jth
level.   With $E_i > E_j$ the transition rates are given by

$$R_{ij} = A_{ij} + B_{ij} J + C_{ij} n$$
$$R_{ji} = B_{ji} J + C_{ji} n .$$

The $A_{ij}$, $B_{ij}$, $B_{ji}$ are the Einstein radiative rate coefficients, J is the intensity of the radiation field, $C_{ij}$ the collision rate coefficients, and n the space density of collision partners. If the transitions are optically thin and the only continuum background is the cosmic black-body radiation, the radiation intensity J can be approximated by a black-body at $T_{bg}$ ~ 2.7 K. However, if the transitions are optically thick, we have to solve the equation of radiative transfer to determine the radiation intensity at each point.

The radiative transfer equation is more difficult to solve, but it is simplfied considerably in the presence of systematic motion (Sobolev 1960; Castor 1970; Goldreich and Kwan 1974; Scoville and Solomon 1974; deJong, Chu, and Dalgarno 1975). If the velocity gradient is sufficiently large, an emitted photon travels a short distance compared with the cloud size before it is a Doppler width away from the velocity of the local material. The LVG approximation is valid for a cloud of radius R characterized by a local random motion $\Delta V_r$ of thermal or nonthermal origin if the velocity gradient $dV/dr$ satisfies,

$$\Delta V_r / dV/dr \ll R .$$

A velocity gradient of ~ 1 km s$^{-1}$ pc$^{-1}$ easily satisfies this relation for dark clouds (Snell 1981). In the LVG approximation, the mean intensity of the radiation field at any point is determined by the local conditions at that point, which fix the local source function and the escape probability of a photon from the cloud. We consider here a spherically symmetric cloud with a velocity field of $v = \alpha \cdot r$ . The input parameters necessary for the models to be considered here are the H$_2$ density, the kinetic temperature, and the molecular abundance of interest relative to H$_2$. The model solutions then give the line intensity, the optical depth, and the excitation temperature for the transitions included in the models. The input parameter values used for the models of H$_2$CS and HOCO$^+$ are given in the following section.

A.2 <u>Results for H$_2$CS</u>

We used the H$_2$CO collisional de-excitation rates (Green $et$ $al.$ 1978) for the corresponding H$_2$CS levels since those for H$_2$CS are not available, and collisional excitation rates have been calculated by assuming detailed balance. LVG models have been calculated for kinetic temperatures of 10 K (TMC-1), 20 K (Orion 3N1E), and 100 K (Orion KL). The input value ranges for the H$_2$ density and the H$_2$CS fractional abundance relative to H$_2$ are n(H$_2$) = 10$^{2.5}$ - 10$^6$ cm$^3$ and $f$(H$_2$CS) = 10$^{-5.5}$ - 10$^{-13}$, respectively. The calculations for T$_{kin}$ ~ 10 K and 20 K include 16 levels for ortho-H$_2$CS and 15 levels for
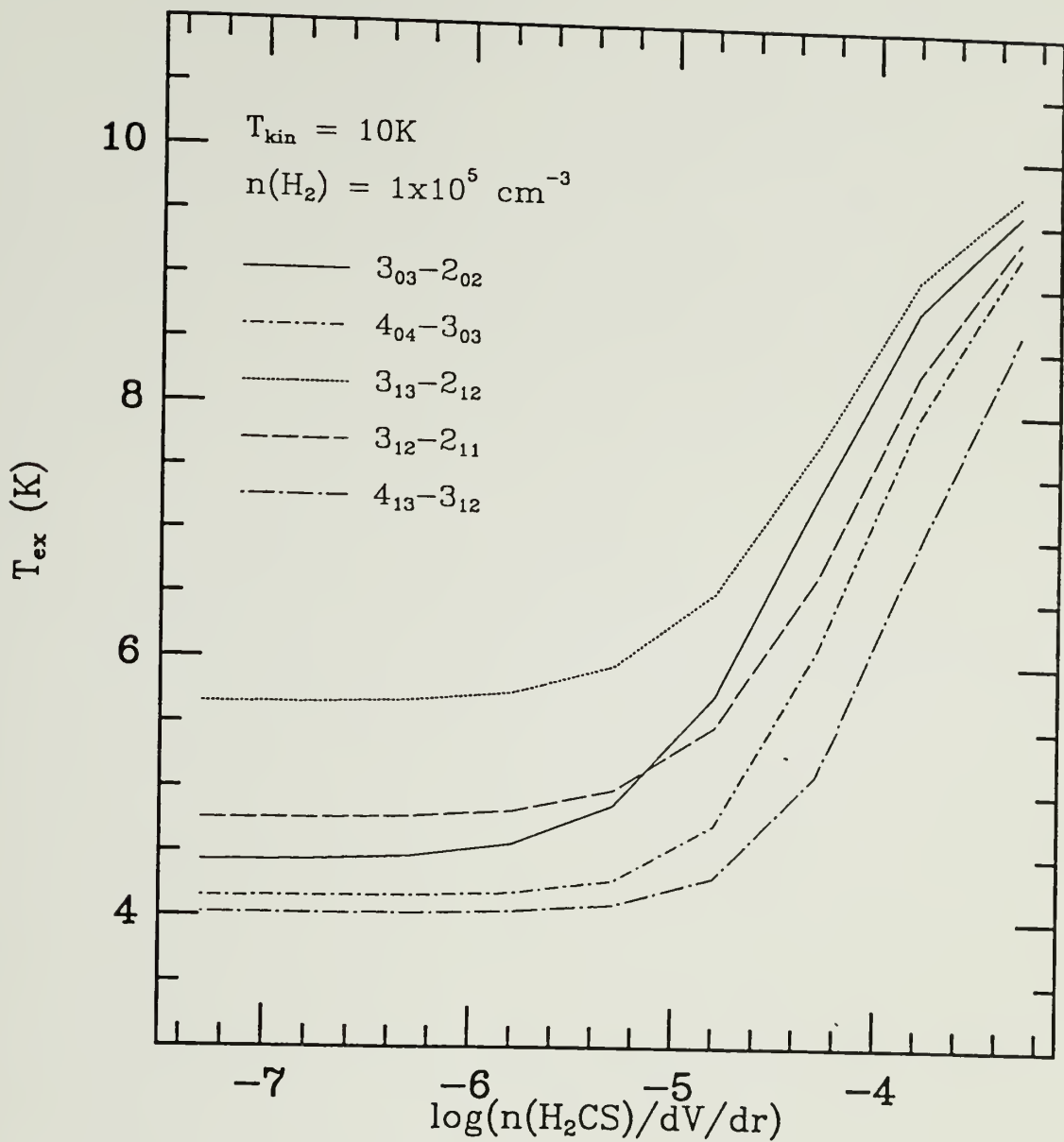
para-$H_2CS$ up to energy levels 70 K above the ground state, while for $T_{kin} \sim 100$ K, we have extrapolated the $H_2CO$ collisional de-excitation rates up to energy levels of 300 K (the collisional de-excitation rates are not sensitive to kinetic temperatures or $\Delta J$ values) and included 60 levels of ortho-$H_2CS$ and 49 levels of para-$H_2CS$. We have carried out calculations using a velocity gradient $dV/dr = 1$ km s$^{-1}$ pc$^{-1}$ but since the quantity of significance in the calculations is the total column density divided by the line width, $N(H_2CS)/\Delta V$ ($= n(H_2CS)/dV/dr$), we have shown the calculation results as a function of $n(H_2CS)/dV/dr$. The results are shown in Figures A.1 to A.3.

## A.3 Results for $HOCO^+$

We used the HNCO collisional de-excitation rates (S. Green, private communication ) for the corresponding $HOCO^+$ levels since those for $HOCO^+$ are not available and both $HOCO^+$ and HNCO have similar molecular constants and structures. The collisional excitation rates have been calculated by assuming detailed balance. We include a total of 72 levels up to energies of 200 K above the ground state in the $K_a = 0$, 1, and 2 ladders, and calculate for five different kintic temperatures (10 - 50 K) and for five different apparent background radiation temperatures (2.7 - 40 K). The apparent background radiation temperature is the temperature inferred from the background radiation intensity observed at the

point concerned in the LVG models.    LVG models have been
calculated for each kinetic temperature and background radiation
temperature, and the input values of the $H_2$ density, $n(H_2) = 10^{3.5}$ -
$10^7$ $cm^3$, and the $HOCO^+$ fractional abundance relative to $H_2$, $f(HOCO^+)$
$= 10^{-7.5} - 10^{-15}$.    We have carried out calculations using a
velocity gradient $dV/dr = 1$ km $s^{-1}$ $pc^{-1}$.    For the same reason we
mentioned above for $H_2CS$, we have shown the calculation results as a
function of $n(HOCO^+)/dV/dr$ ($= N(HOCO^+)/\Delta V$), and some of them are
illustrated in Figures A.4 to A.6.

Figure A.1a - c    Excitation temperature ($T_{ex}$) versus

$\log(n(H_2CS)/dV/dr)$ for $n(H_2) = 1 \times 10^5$ cm$^{-3}$.    Transitions are

indicated in the figures.    (a) for $T_{kin} = 10$ K.    (b) for

$T_{kin} = 20$ K.    (c) for $T_{kin} = 100$ K.

(a)

(b)

179

(c)

$T_{kin} = 100K$

$n(H_2) = 1\times10^5 \ cm^{-3}$

——— $3_{03}-2_{02}$

·—·—·— $3_{21}-2_{20}$

········· $3_{13}-2_{12}$

— — — $3_{12}-2_{11}$

Tau

$\log(n(H_2CS)/dV/dr)$

-7    -6    -5    -4

1    .8    .6    .4    .2    0

(c)

184
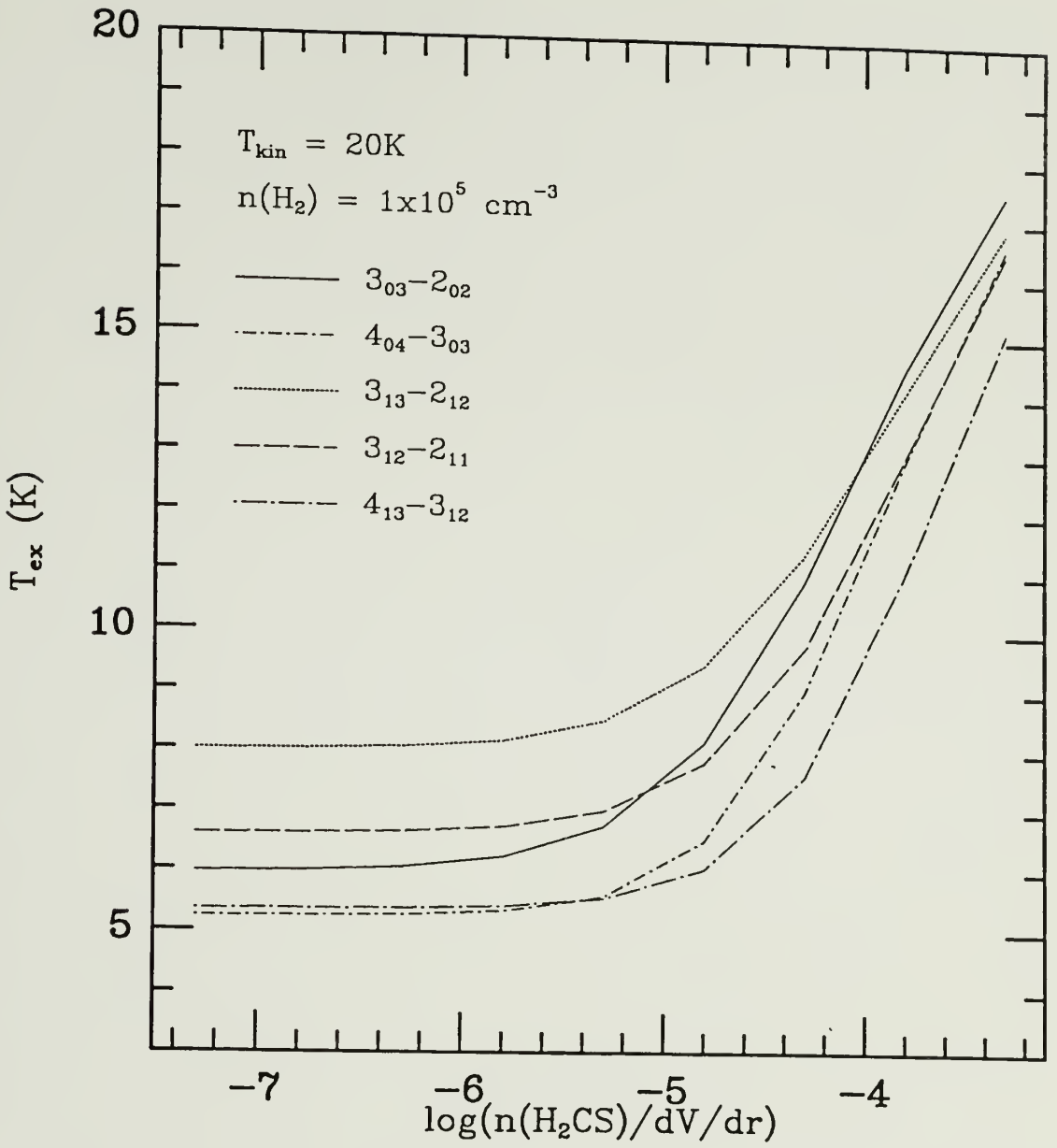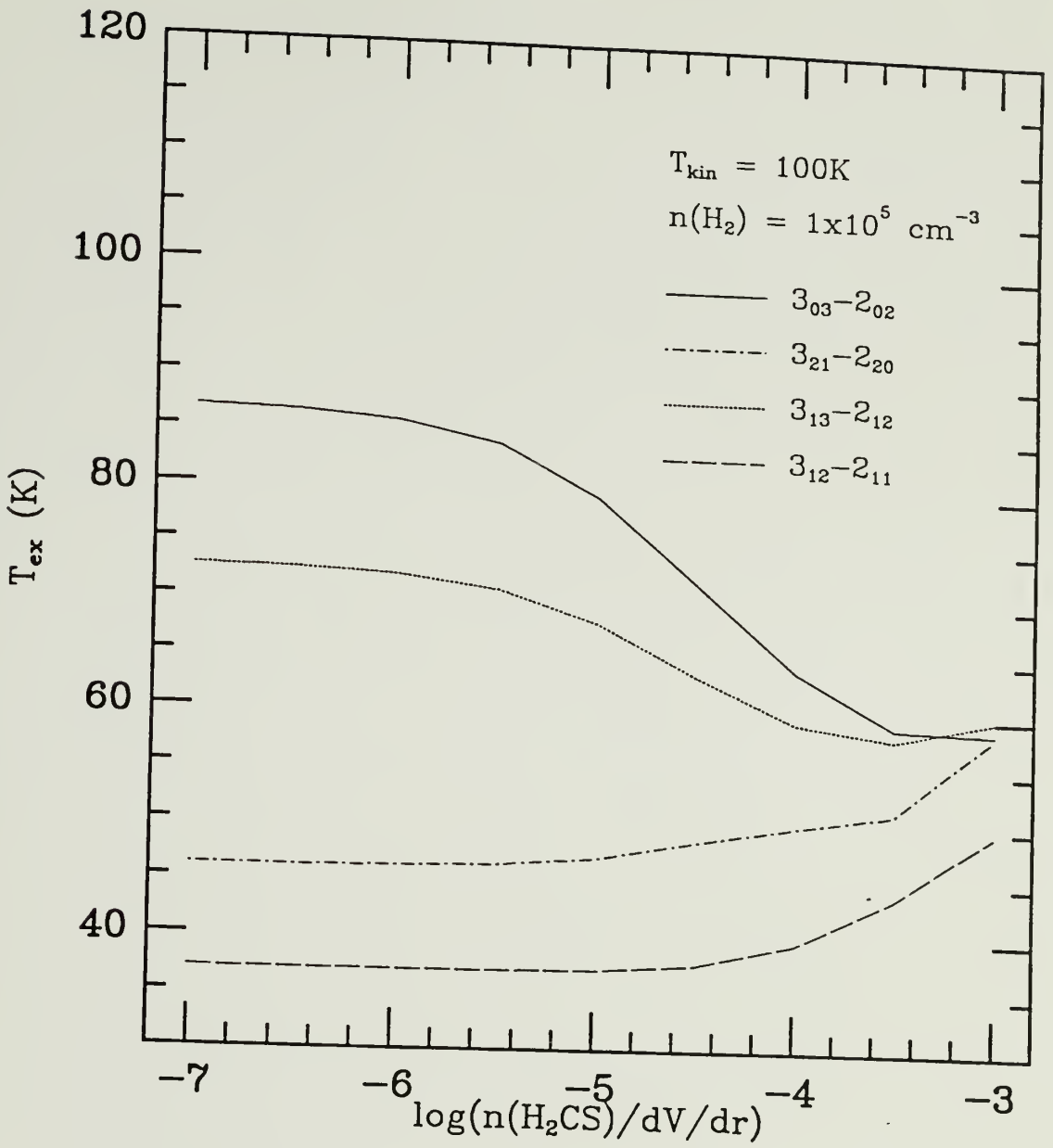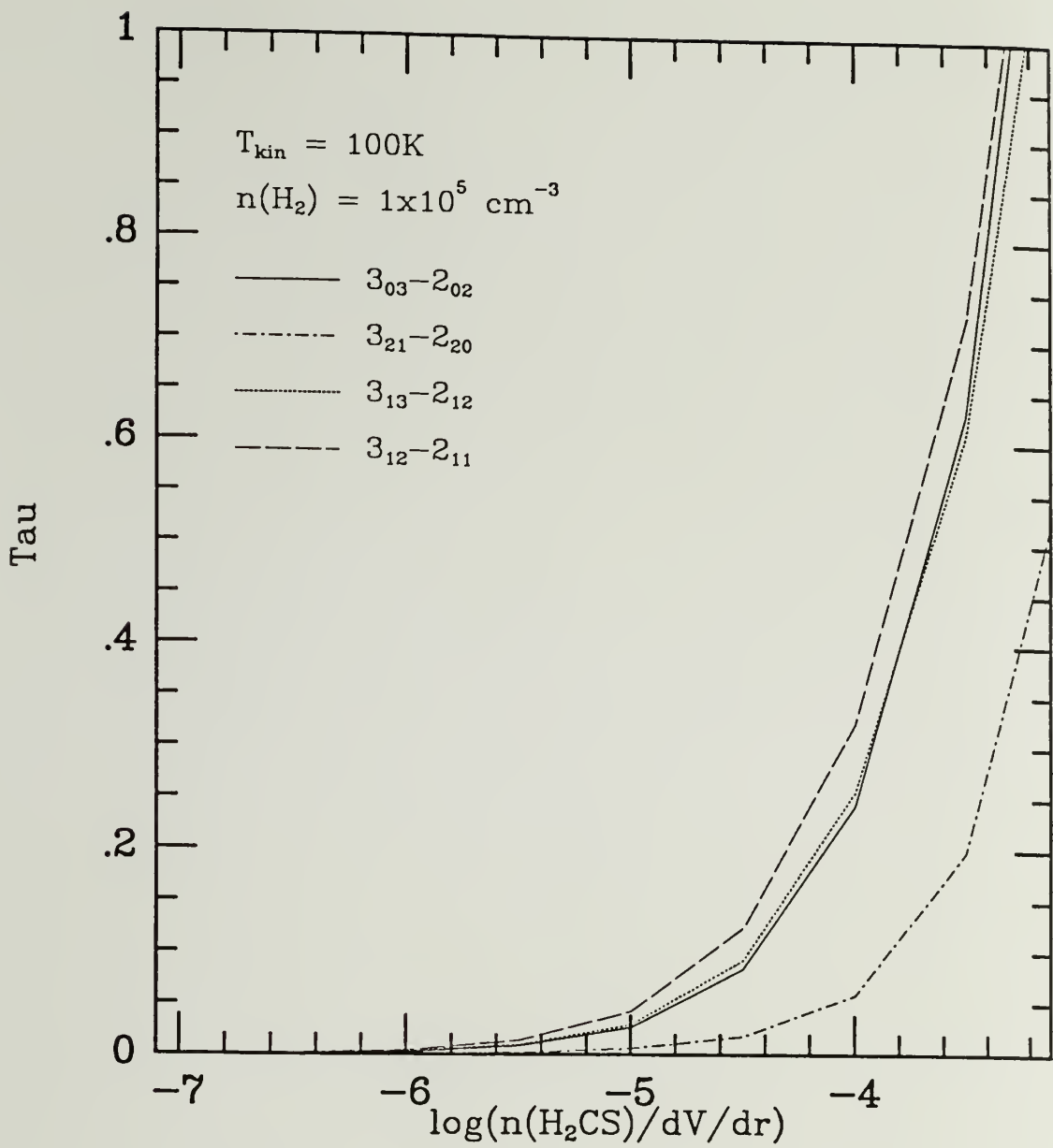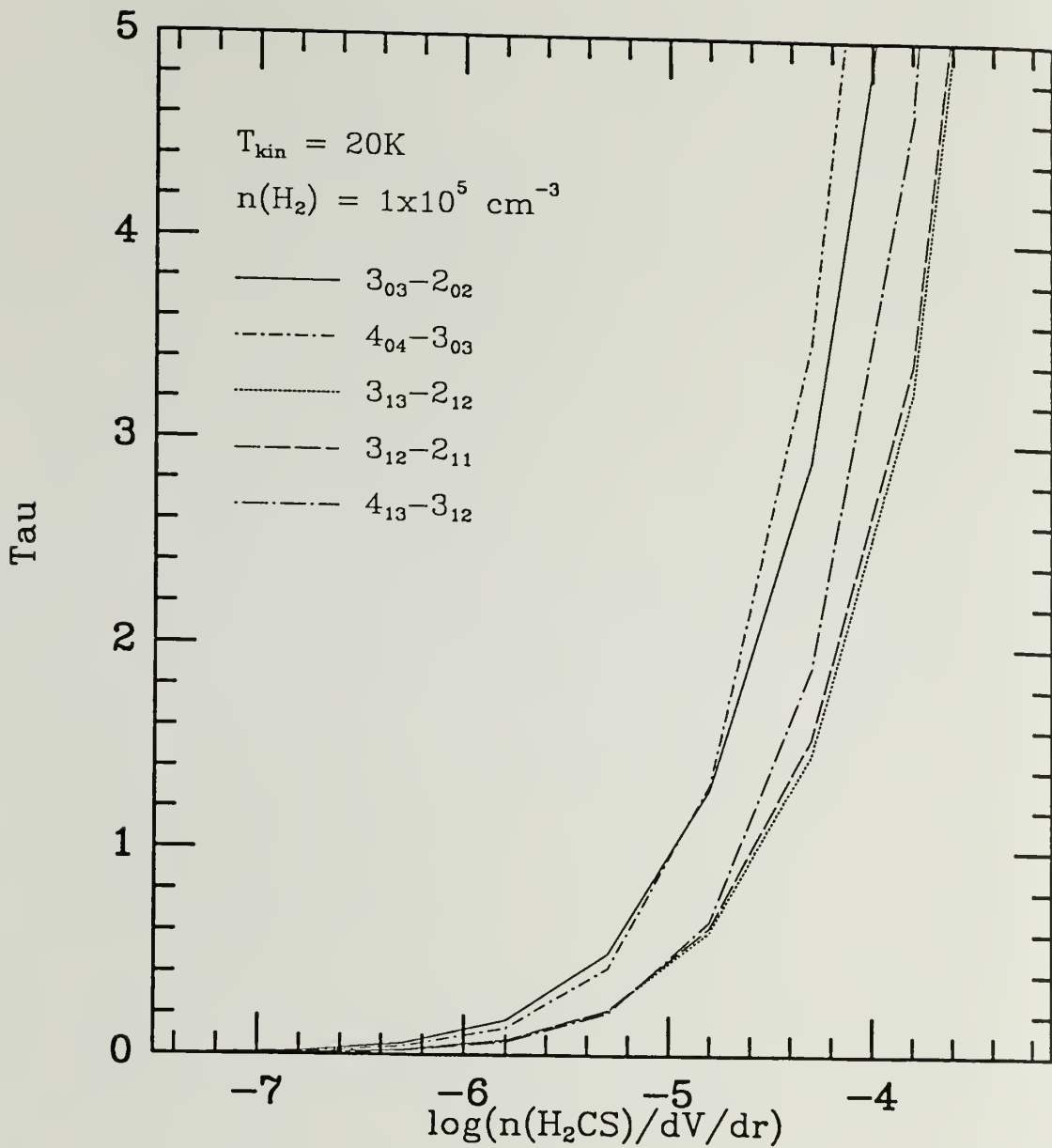
(b)
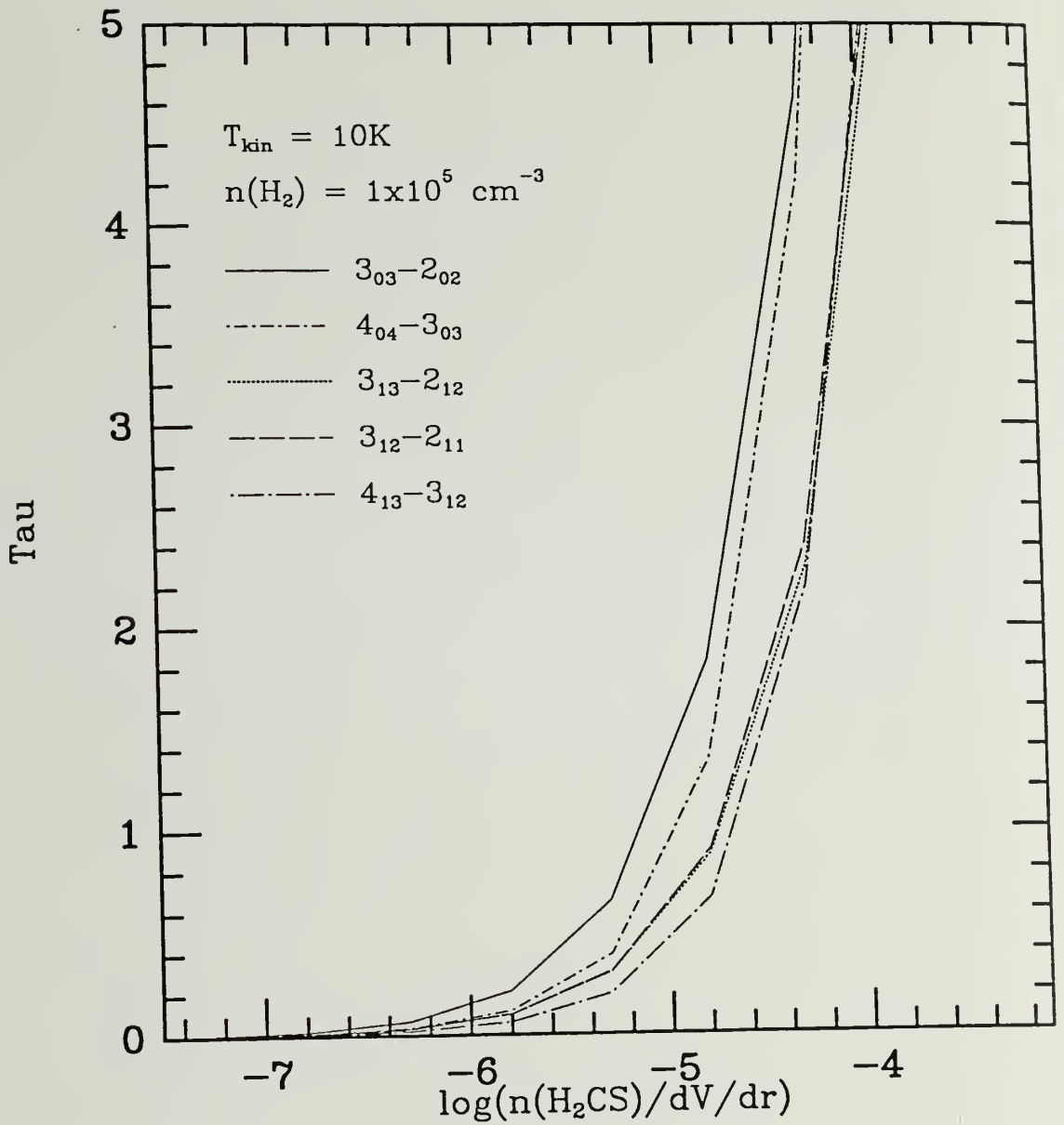
(a)

Figure A.2a - c    Optical depth (Tau) versus
$\log(n(H_2CS)/dV/dr)$ for $n(H_2) = 1 \times 10^5$ cm$^{-3}$.    Transitions are
indicated in the figures.    (a) for $T_{kin} = 10$ K.    (b) for
$T_{kin} = 20$ K.    (c) for $T_{kin} = 100$ K.

(f)

191

(e)

(d)

(c)

188
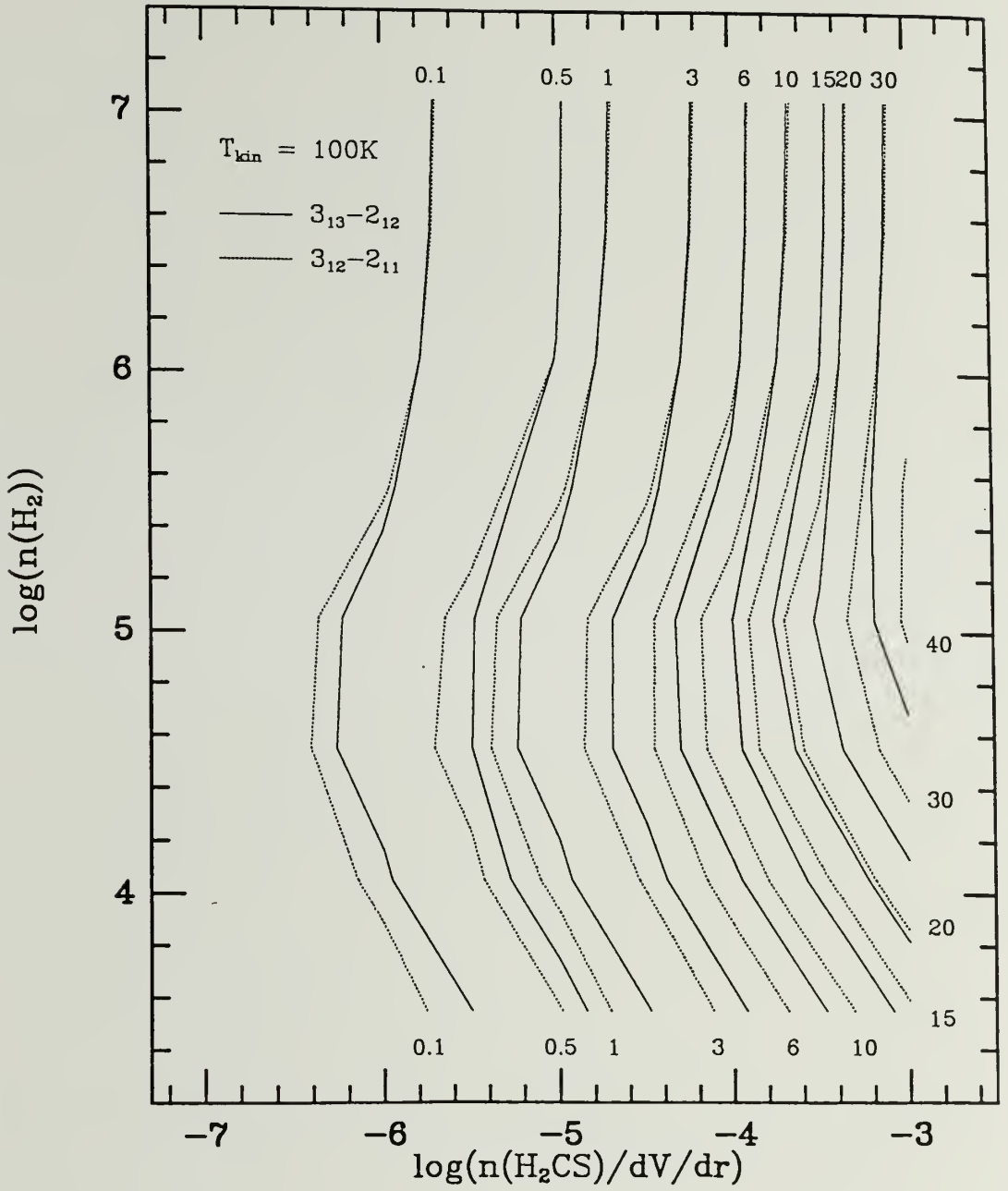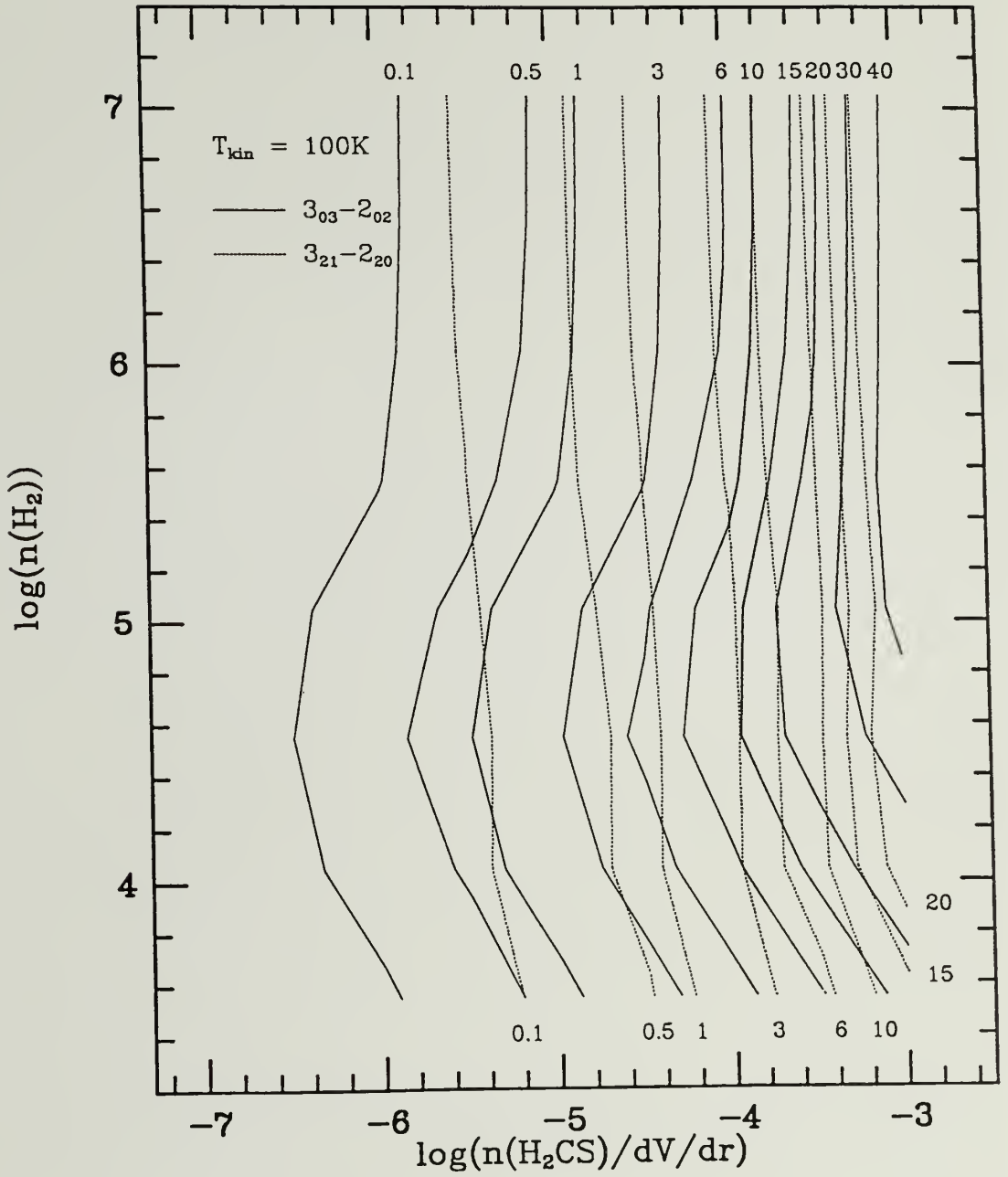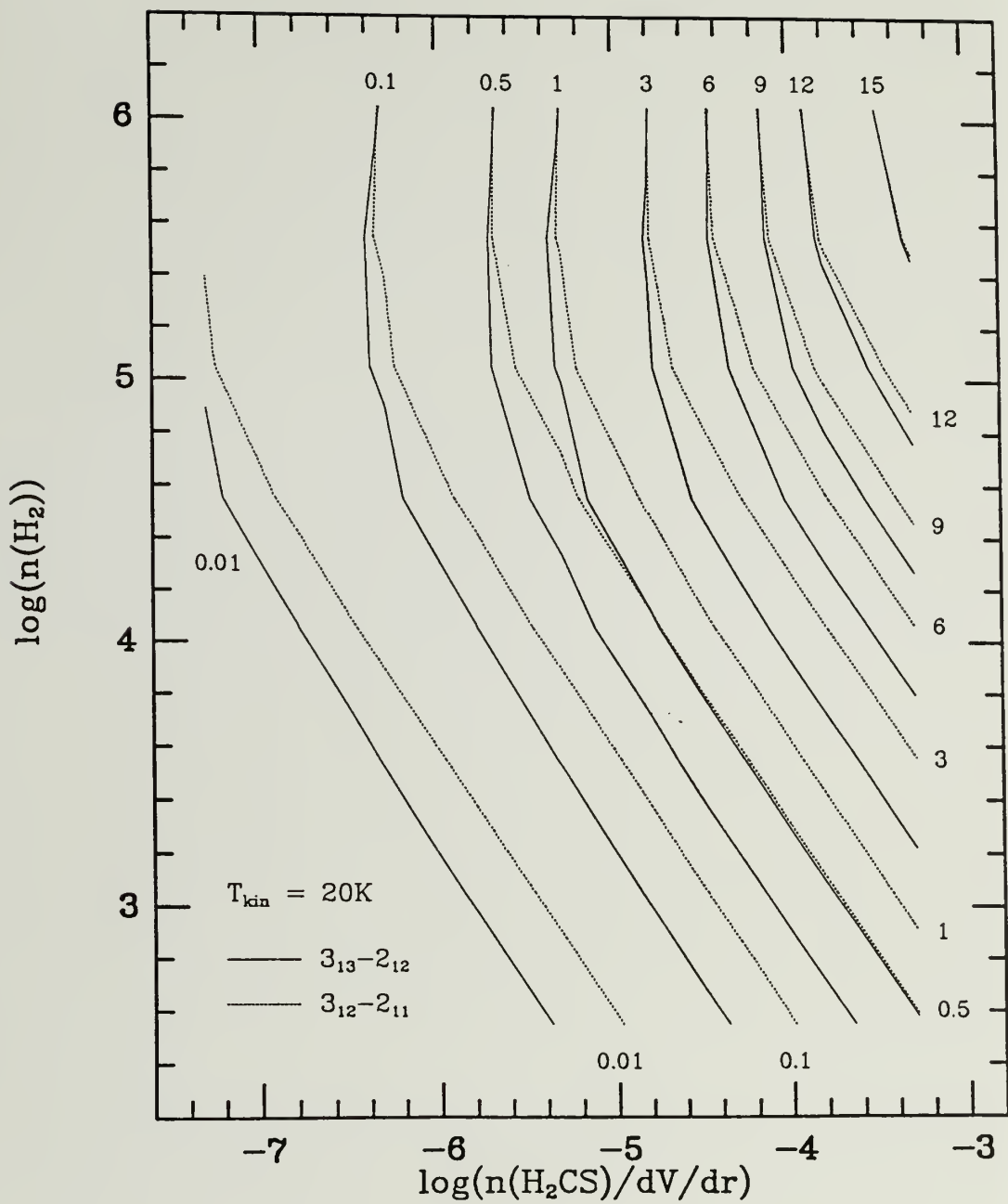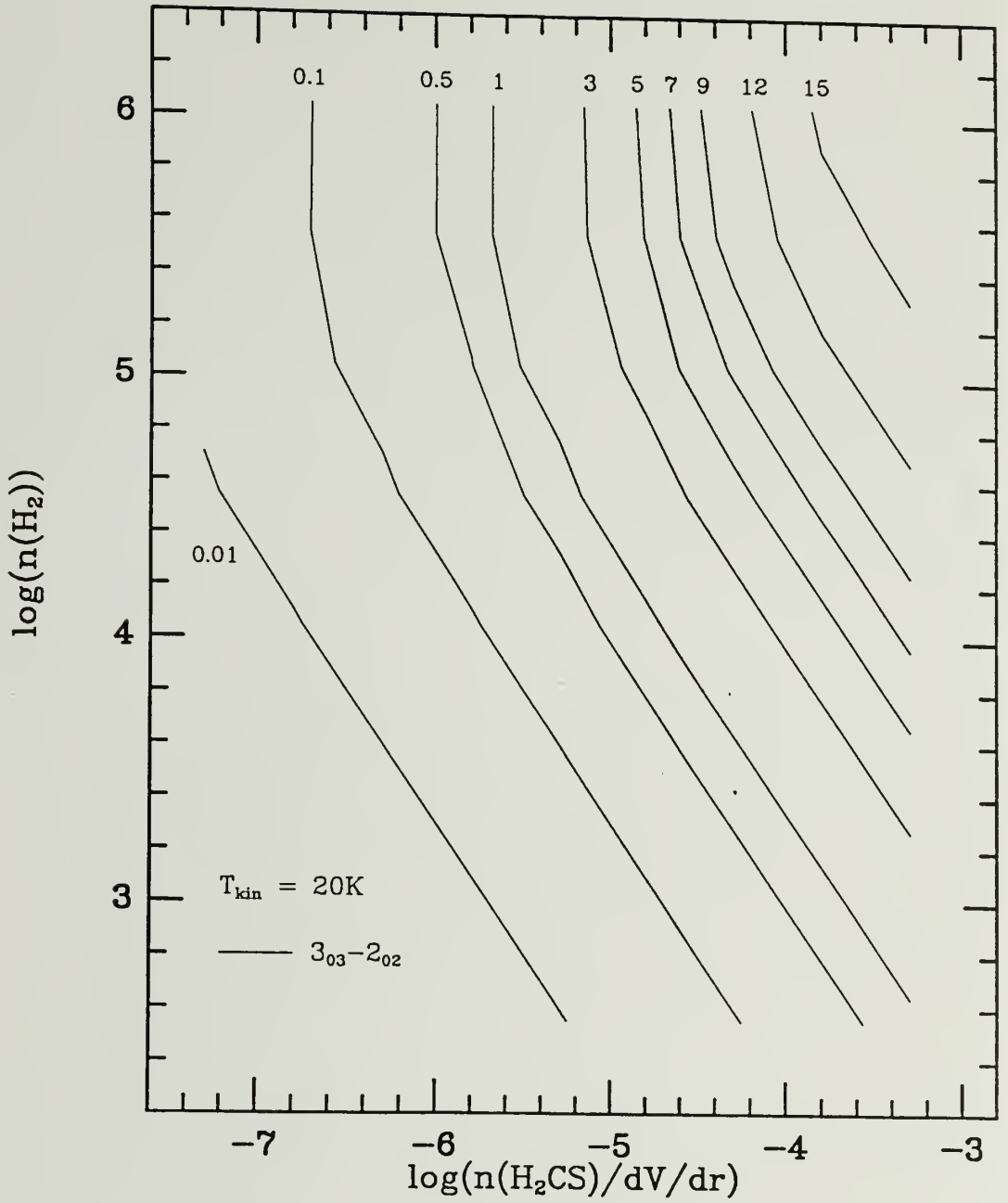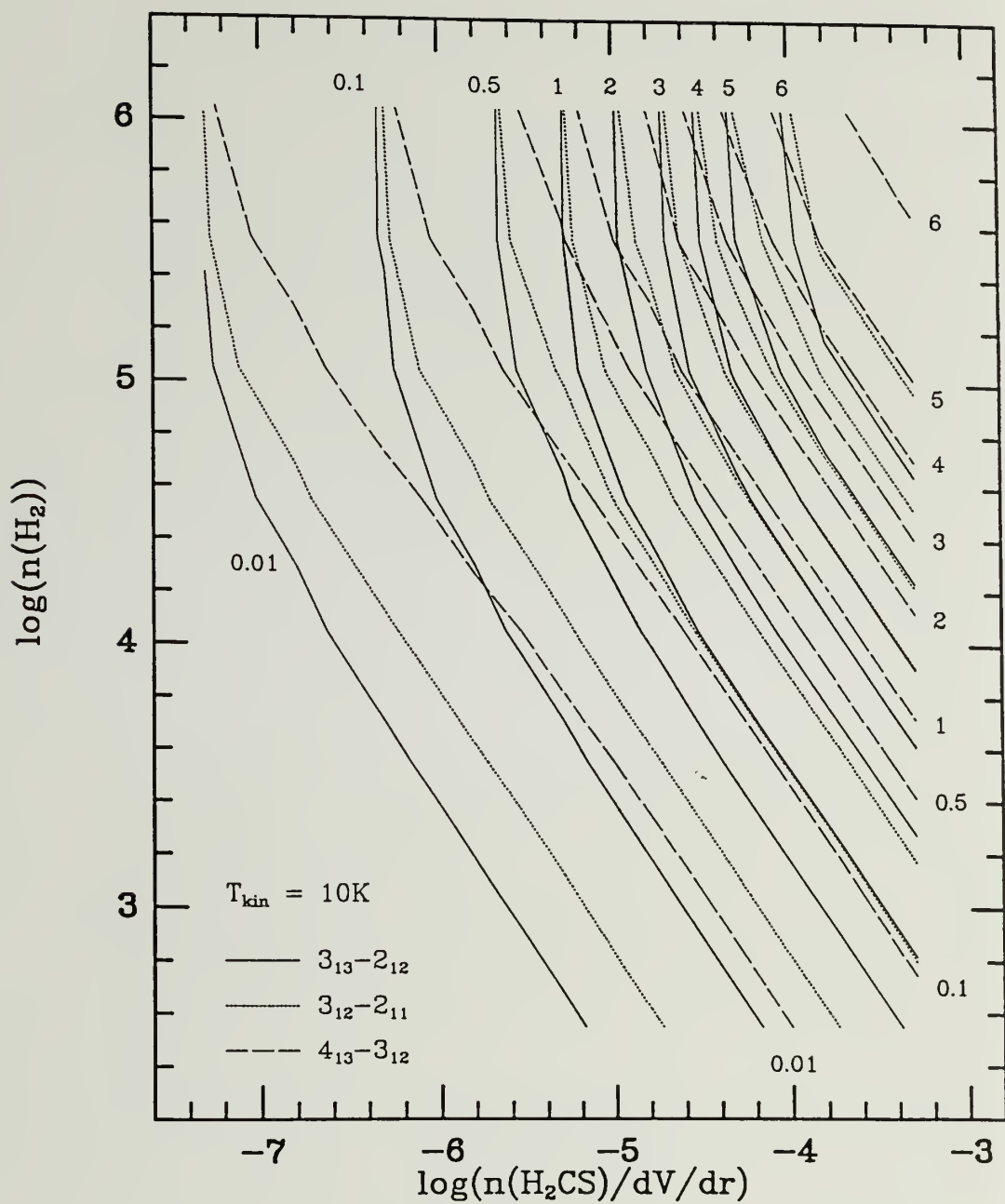
(b)
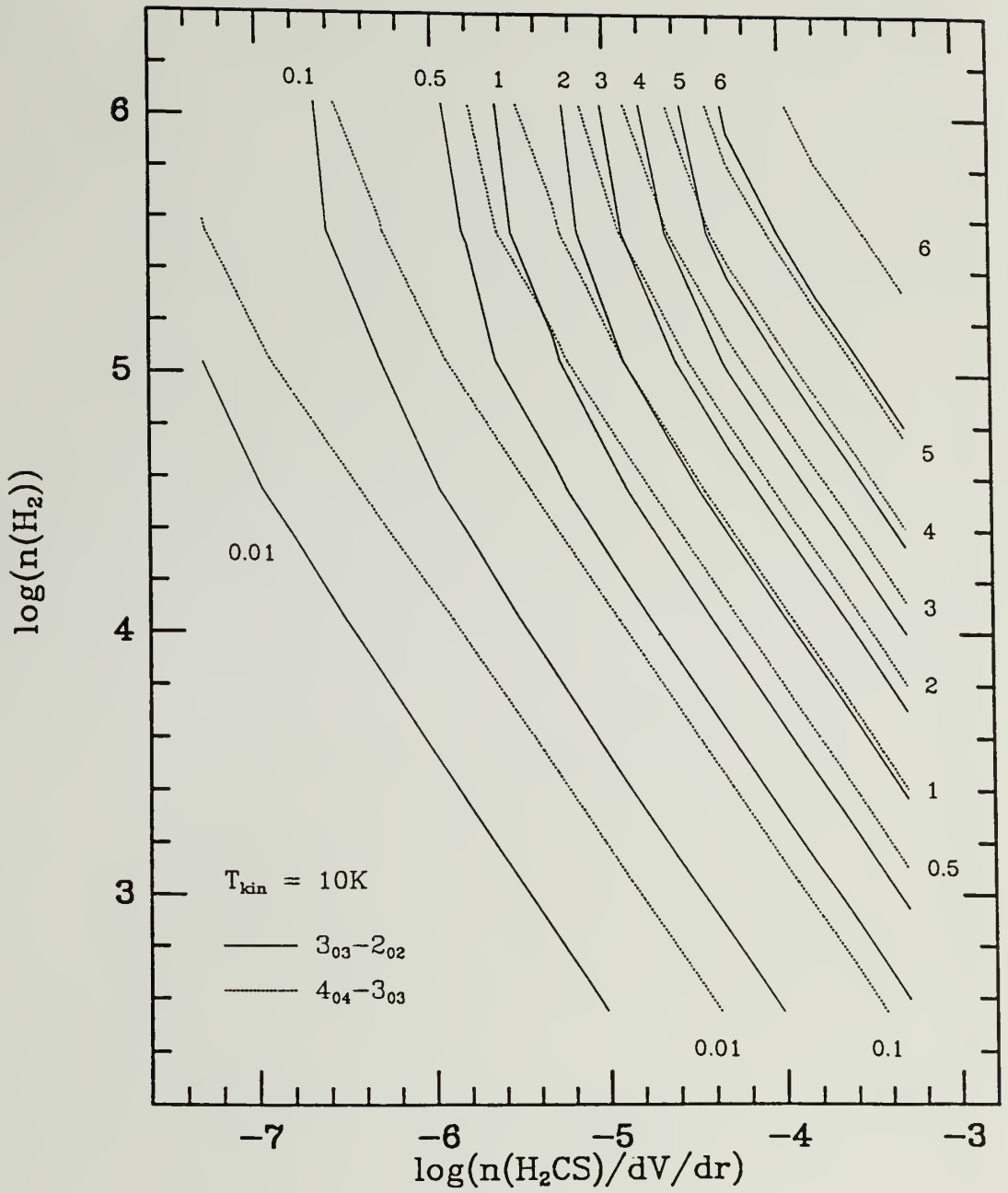
(a)

Figure A.3a - f   Constant antenna temperature curves.
Contour levels are indicated in the figures.   (a), (c), and
(e) for para transitions for $T_{kin}$ = 10, 20, and 100 K,
respectively.   (b), (d), and (f) for ortho transitions for
$T_{kin}$ = 10, 20, and 100 K, respectively.

Figure A.5a - b  Optical depth (Tau) versus

$\log(n(HOCO^+)/dV/dr)$ for $n(H_2) = 3.2 \times 10^4$ cm$^{-3}$.   (a) for $T_{kin}$

$= 10$ K and $T_{bg} = 2.7$ K.   (b) for $T_{kin} = 50$ K and $T_{bg} = 10$ K.

(b)

194

$T_{kin} = 10K$

$T_{bg} = 2.7K$

$n(H_2) = 3.2 \times 10^{-4}$ cm$^{-3}$

——————— $4_{04}-3_{03}$

················· $5_{05}-4_{04}$

– – – – – $4_{14}-3_{13}$

$T_{ex}$ (K)

$\log(n(HOCO^+)/dV/dr)$

(a)

193
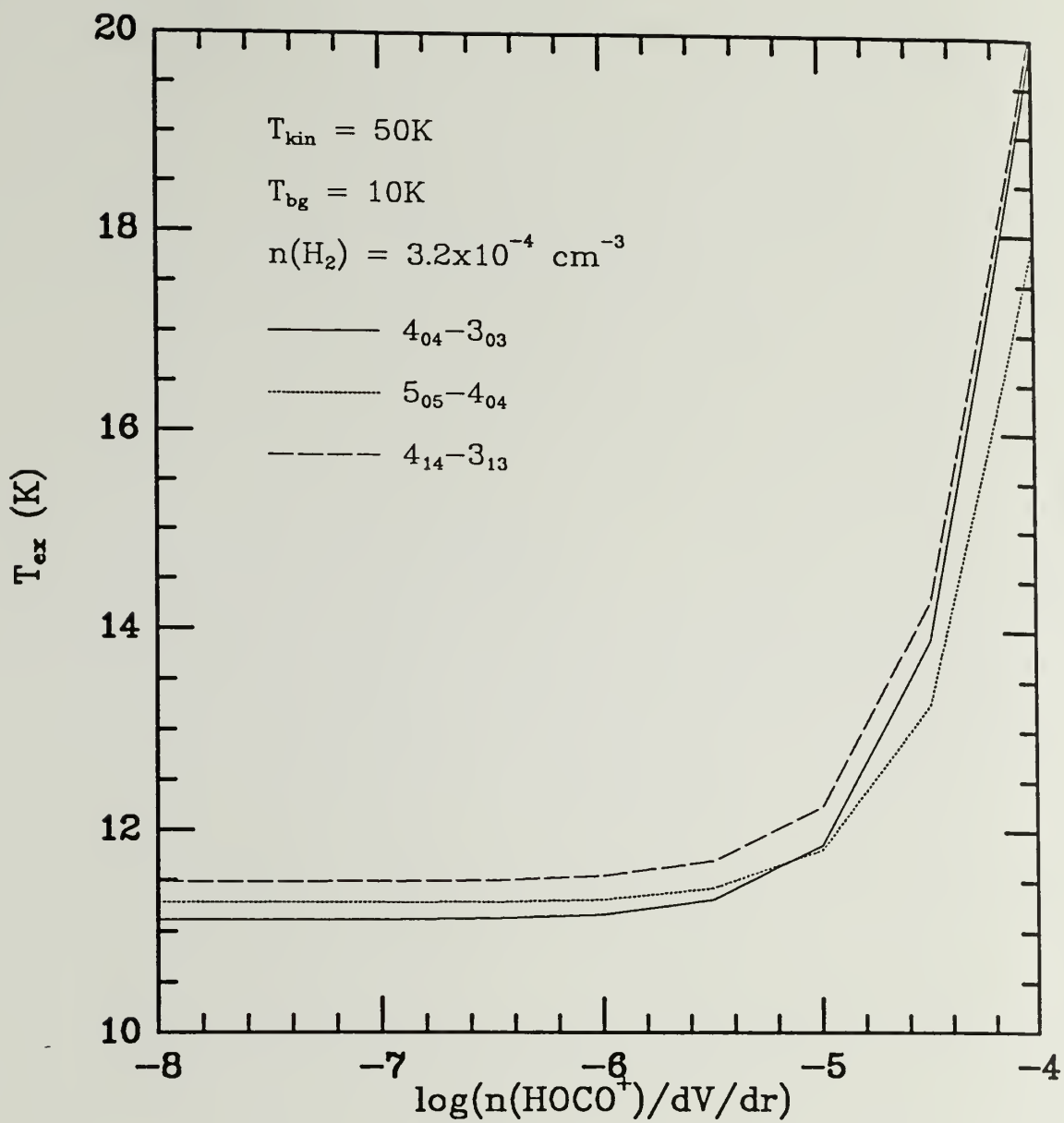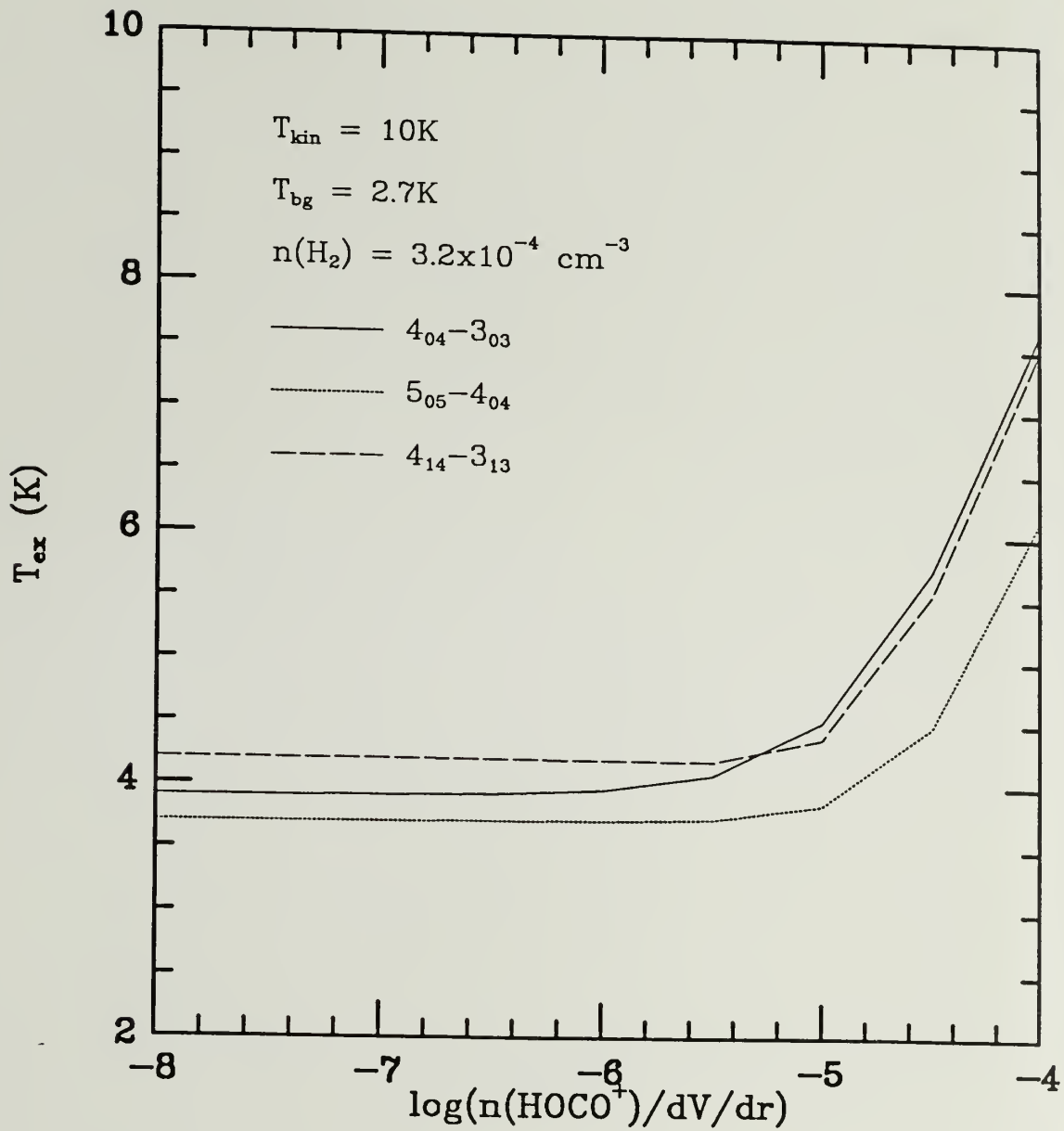
Figure A.4a - b    Excitation temperature ($T_{ex}$) versus $\log(n(HOCO^+)/dV/dr)$ for the volumn density $n(H_2) = 3.2 \times 10^4$ $cm^{-3}$.    (a) for the kinetic temperature $T_{kin} = 10$ K and the background temperature $T_{bg} = 2.7$ K.    (b) for $T_{kin} = 50$ K and $T_{bg} = 10$ K.

$T_{kin} = 10K$

$T_{bg} = 2.7K$

$n(H_2) = 3.2 \times 10^{-4} \ cm^{-3}$

——— $4_{04}-3_{03}$

·········· $5_{05}-4_{04}$

$\log(n(HOCO^+)/dV/dr)$

(a)

$T_{kin} = 50K$

$T_{bg} = 10K$

$n(H_2) = 3.2 \times 10^{-4} \ cm^{-3}$

—————— $4_{04} - 3_{03}$

·············· $5_{05} - 4_{04}$

— — — $4_{14} - 3_{13}$

Tau

$\log(n(HOCO^+)/dV/dr)$

(b)

197
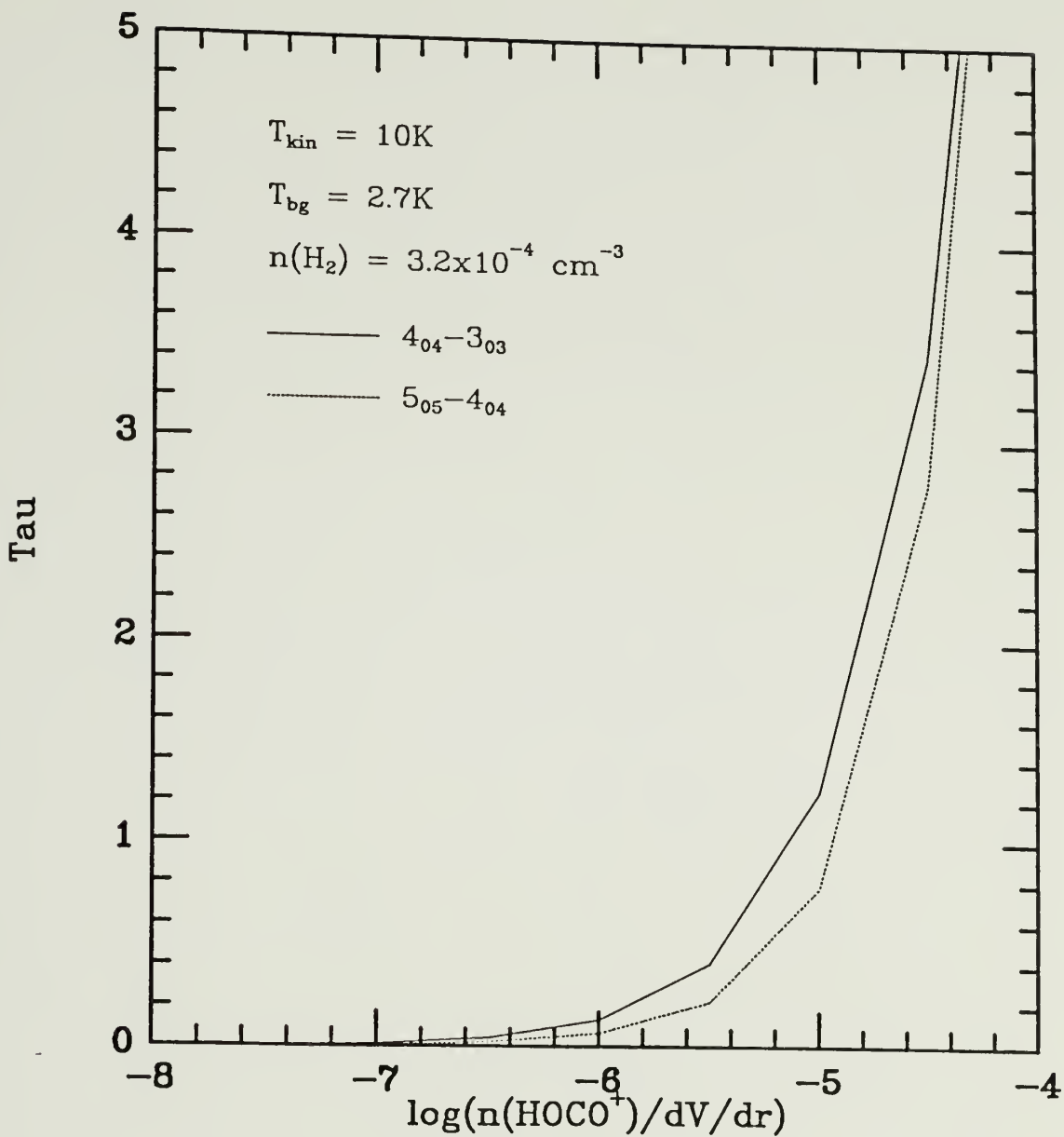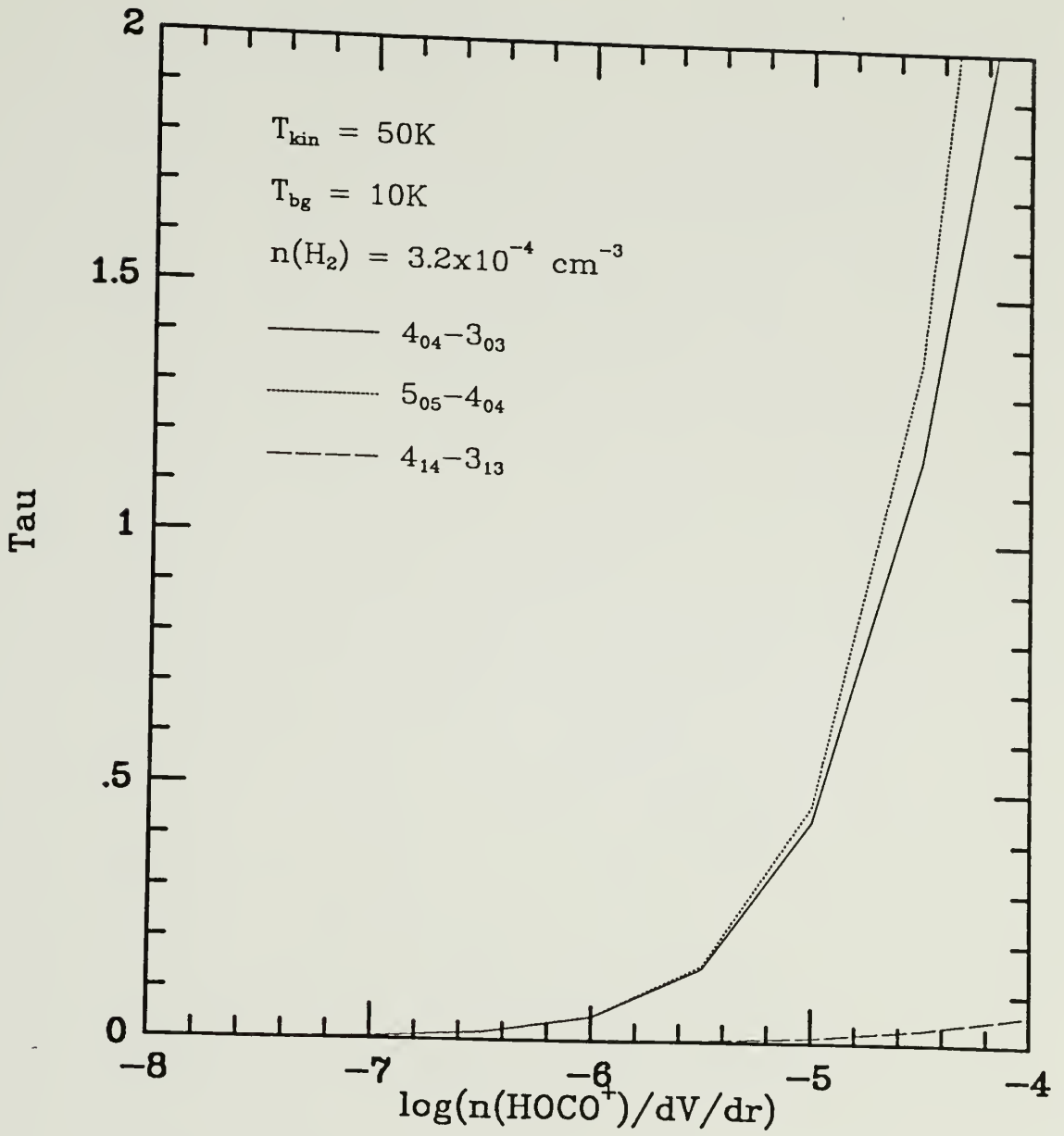
Figure A.6a - d    Constant antenna temperature curves.

Contour levels (K) are indicated in the figures.    (a) for the

$1_{01}$ - $0_{00}$ transition for $T_{kin}$ = 10 K and $T_{bg}$ = 2.7 K.    (b)

for the $4_{04}$ - $3_{03}$, $5_{05}$ - $4_{04}$, and $4_{14}$ - $3_{13}$ transitions for

$T_{kin}$ = 10 K and $T_{bg}$ = 2.7 K.    (c) for same transitions as in

(b) for $T_{kin}$ = 50 K and $T_{bg}$ = 10 K.    (d) for same transitions

as in (b) for $T_{kin}$ = 50 K and $T_{bg}$ = 20 K.

0.01     0.1     0.5   1     3

$T_{kin} = 10K$

$T_{bg} = 2.7K$

— $1_{01}-0_{00}$

7

6

5

4

$\log(n(H_2))$

5

7

−8     −7     −6     −5     −4

$\log(n(HOCO^+)/dV/dr)$

(a)

(b)

200

(c)

201

(d)

202
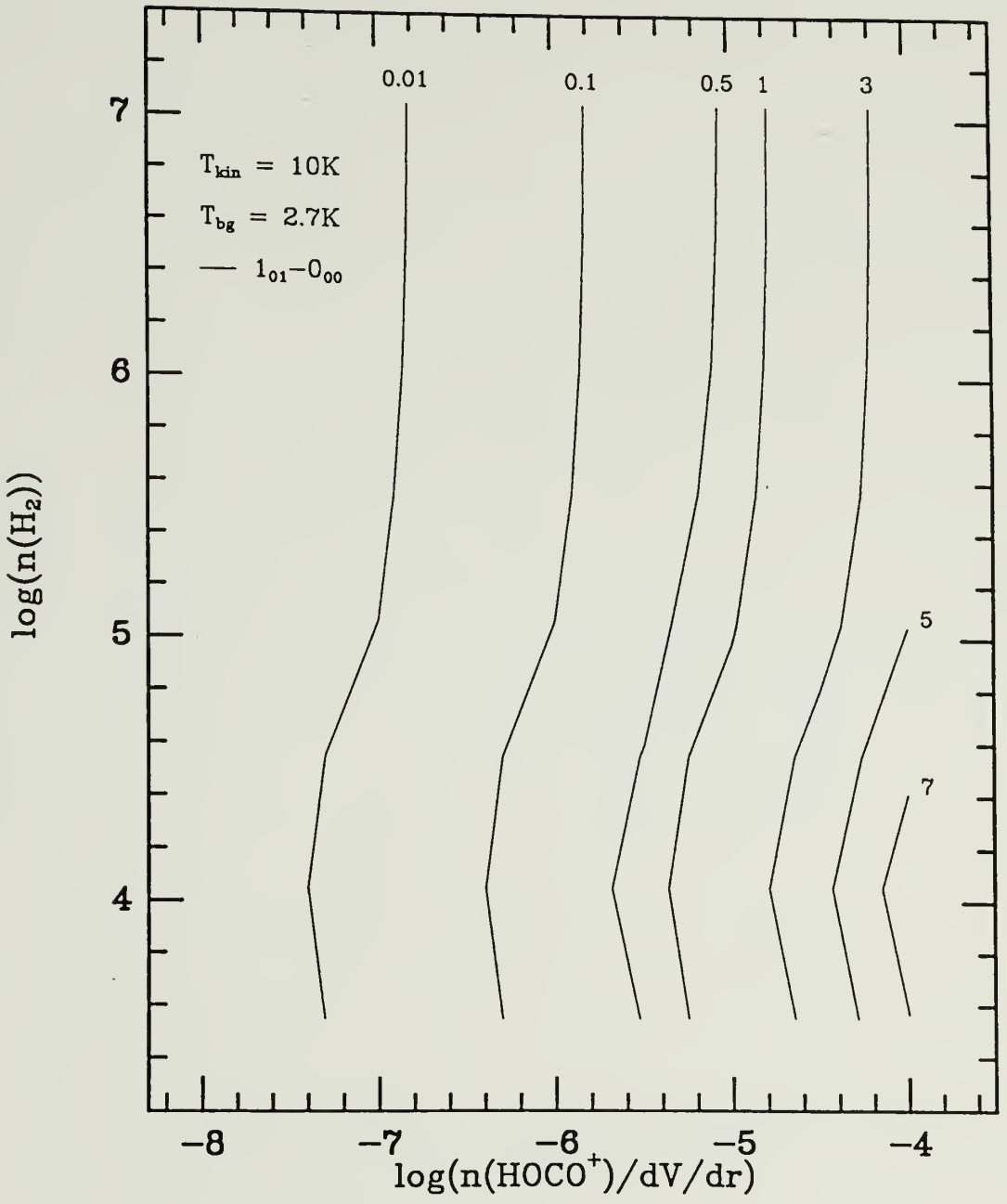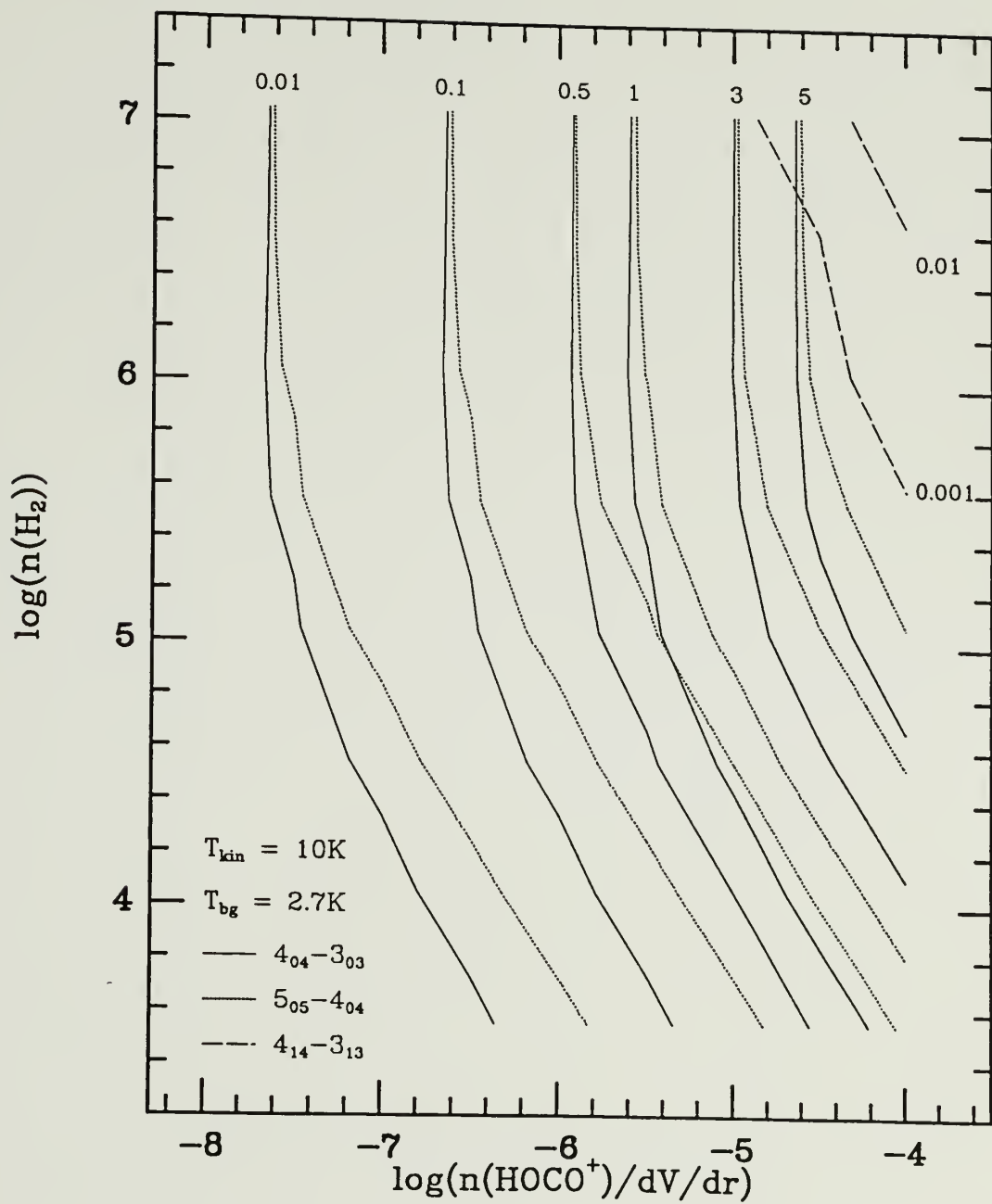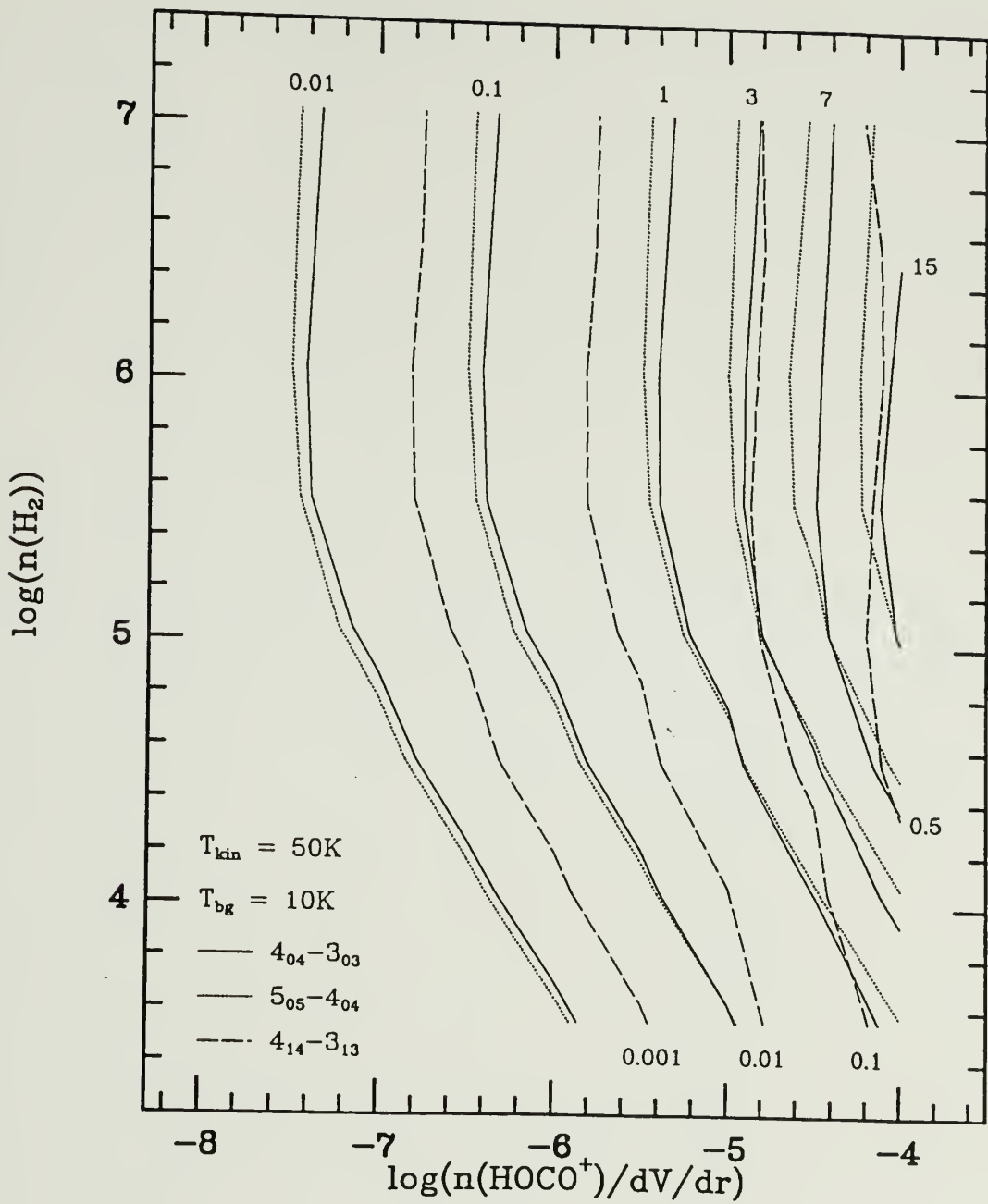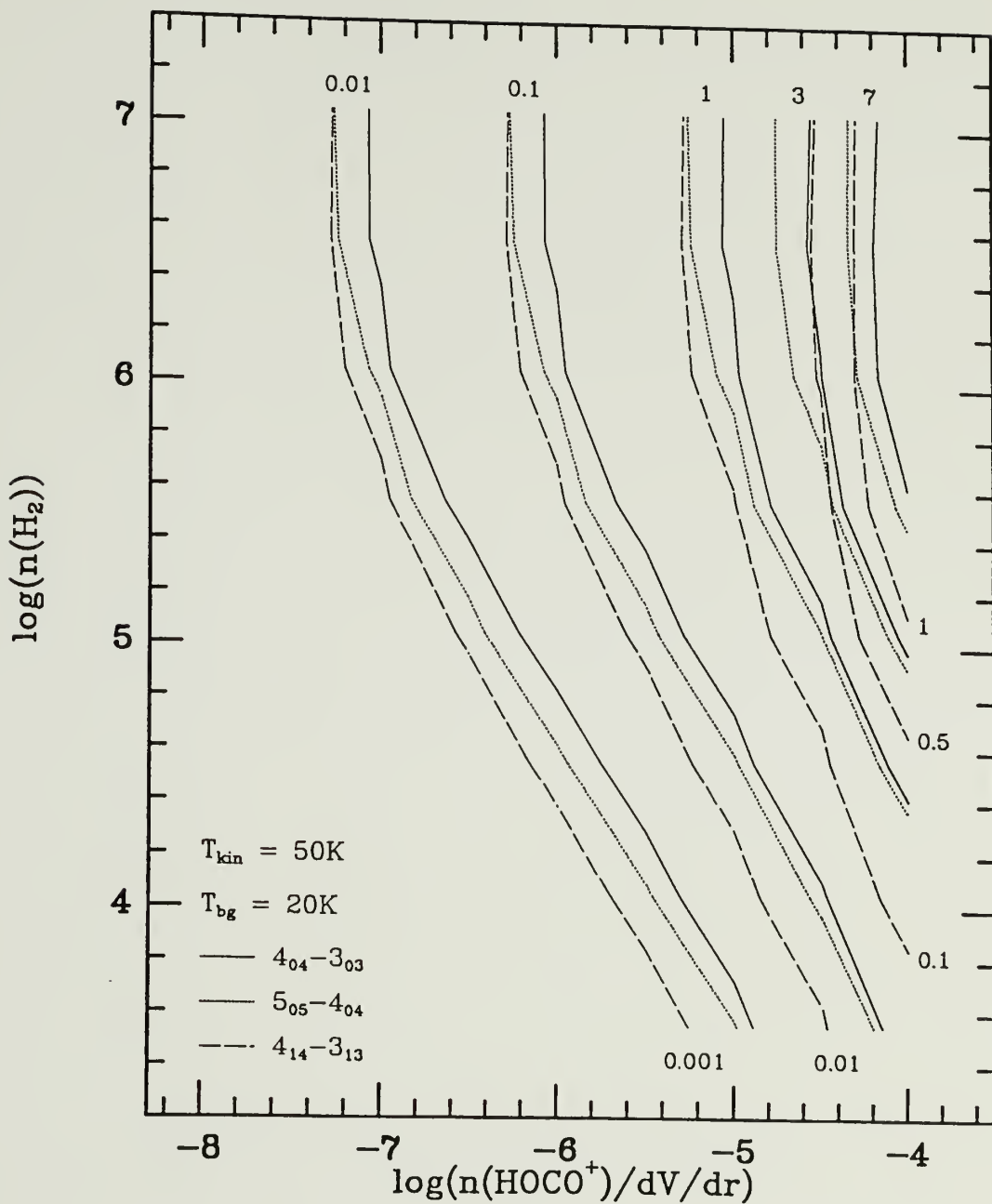
APPENDIX B


Abundances of Molecules in the Sgr A Cloud Complex


Data were obtained in 1988 June with the Swedish-ESO 15 m
telescope in Chile, together with the observations of the $HOCO^+$ $4_{04}$
- $3_{03}$ and $5_{05}$ - $4_{04}$ transitions described in Chapter 8.   Telescope
parameters are given in Table 8.1 and observing methods in § 8.3.
Observed molecules, transitions, and rest frequencies are included
in Table B.1, and observed line parameters toward the cores of
condensations in Sgr A (see Figure 8.1) are included in Table B.2.
Each condensation is labeled A - G for convenience, as indicated in
Table B.2.   The Cloud A/S position is offset $(\Delta l, \Delta b) = (1.4'$,
$0.4')$ from the nominal position implied by M-0.13-0.08 (Cloud A).
Sample spectra are shown in Figure B.1, including the $HOCO^+$ lines.

The column densities were determined from the following
equation, assuming optically thin emission and neglecting any
background radiation :

$$N_{molecule}(cm^{-2}) = 2 \pi \nu^2 k \Delta V T_R / h c^3 f A$$

where $\nu$ is the line frequency, $\Delta V$ the FWHP line width, $T_R$ the
brightness temperature assuming the source fills the main beam, $f$
the fractional population in the upper level of the transition, and
$A$ the Einstein spontaneous emission coefficient.

To derive the total column density of HCO, we used the normalized theoretical relative intensities of 42 : 25 : 25 : 8 for (J=3/2-1/2 F=2-1) : (J=3/2-1/2 F=1-0) : (J=1/2-1/2 F=1-1) : (J=1/2-1/2 F=1-0) (Schenewerk, Snyder, and Hjalmarson 1986).

Methyl acetylene ($CH_3CCH$) has been observed via its J=5-4 and 6-5 transitions. However, since the K = 0, 1, and 2 components overlap with each other, we fit to gaussians by assuming the same $V_{LSR}$ for each component. The gaussian fit results are given in Table B.3. Rotation temperatures of $CH_3CCH$ have been derived from the rotation diagrams in Figure B.2. Askne *et al.* (1984) have suggested that methyl acetylene is an excellent kinetic temperature probe and a simple rotation diagram can be used to determine the kinetic temperature.

The molecular abundances have been calculated by assuming $T_{ROT}$ and an LTE population distribution. We have used the rotation diagrams for $CH_3CCH$ to derive its column densities and assumed $T_{ROT}$ = 50 K for OCS since both species have similar electric dipole moments of less than 1 Debye (see Table B.1). We used $T_{ROT}$ = 20 K for other molecules in Table B.1, whose electric dipole moments are greater than 1 Debye. We did not derive the column density for methanol because of its probable non-Boltzmann excitation. The calculated abundances for molecules are given in Table B.4 toward each core. In Table B.5 we list the fractional abundances relative to $H_2$ for the molecules observed in Sgr A, with those for TMC-1 and Sgr B2 from the tabulation of Irvine, Goldsmith, and Hjalmarson

(1987) for comparison. The molecular hydrogen column densities were derived from $N(^{13}CO)$ for each position from the map of Armstrong and Barrett (1984) assuming $[CO]/[^{13}CO] = 23$ and $[CO]/[H_2] = 10^{-4}$ (Penzias 1980).

TABLE B.1

Observed Molecules in Sgr A

| Molecule | Transition | Rest Frequency[a] (GHz) | Dipole Moment[b] (Debye) |
|---|---|---|---|
| $H^{13}CO^+$ | 1 - 0 | 86.75429 | 4.48 |
| $HC^{18}O^+$ | 1 - 0 | 85.16226 | 4.48 |
| HCO | $1_{01} - 0_{00}$ [c] | 86.67082 | 1.36 |
| $HCS^+$ | 2 - 1 | 85.34790 | 1.86 |
| OCS | 7 - 6 | 85.13911 | 0.72 |
| $C_3H_2$ | $2_{12} - 1_{01}$ | 85.33889 | 3.30 |
| SiO | 2 - 1 | 86.84700 | 3.10 |
| $^{29}SiO$ | 2 - 1 | 85.75913 | 3.10 |
| $HC_5N$ | 32 - 31 | 85.20135 | 4.33 |
| $CH_3OH$ | $3_1 - 4_0 A^+$ | 107.01385 | 0.89 |
| HCOOH | $4_{14} - 3_{13}$ | 86.54613 | 1.40 |
| $CH_3CH_2OH$ | $6_{06} - 5_{15}$ | 85.26547 | 1.44 |
| $CH_3CCH$ | 5 - 4 K=0 | 85.45730 | 0.75 |
| | K=1 | 85.45567 | |
| | K=2 | 85.45077 | |
| | K=3 | 85.44260 | |
| | K=4 | 85.43117 | |
| | 6 - 5 K=0 | 102.54798 | |
| | K=1 | 102.54602 | |
| | K=2 | 102.54014 | |
| | K=3 | 102.53035 | |
| | K=4 | 102.49902 | |

[a] From the tabulation of Lovas (1986).

[b] From the table of Blake *et al*. (1987).

[c] For the J = 3/2 - 1/2, F = 2 - 1 transition.

Figure B.1    Sample spectra obtained toward the core of

M-0.13-0.08.    I-bars indicate the observed antenna

temperature scale of each spectrum.    The spectrum of $CH_3OH$ is

reversed in this figure for ease of presentation (the line is

actually in absorption).    The spectra have a resolution of

0.69 MHz.

M−0.13−0.08
(Cloud A)

$HOCO^+$ $(4_{04}-3_{03})$

$HOCO^+$ $(5_{05}-4_{04})$

$H^{13}CO^+$ (1−0)

$HC^{18}O^+$
(1−0)

OCS (7−6)

$HCS^+$
(2−1)

$C_3H_2$ $(2_{12}-1_{01})$

SiO (2−1)

$^{29}SiO$ (2−1)

$HC_5N$ (32−31)

HCO $(1_{01}-0_{00})$
J=3/2−1/2
F=2−1

F=1−0

$CH_3OH$
$(3_1-4_0\ A^+)$

$CH_3CCH$ (J=5−4)

$CH_3CCH$ (J=6−5)

$CH_3CH_2OH$ $(6_{06}-5_{15})$

.1K

.1K

.1K

.1K

.1K

.2K

.1K

.1K

.05K

.1K

.1K

.1K

.1K

Antenna Temperature, $T_A^*$ (K)

$V_{LSR}$ (km/s)

−200    −100    0    100    200
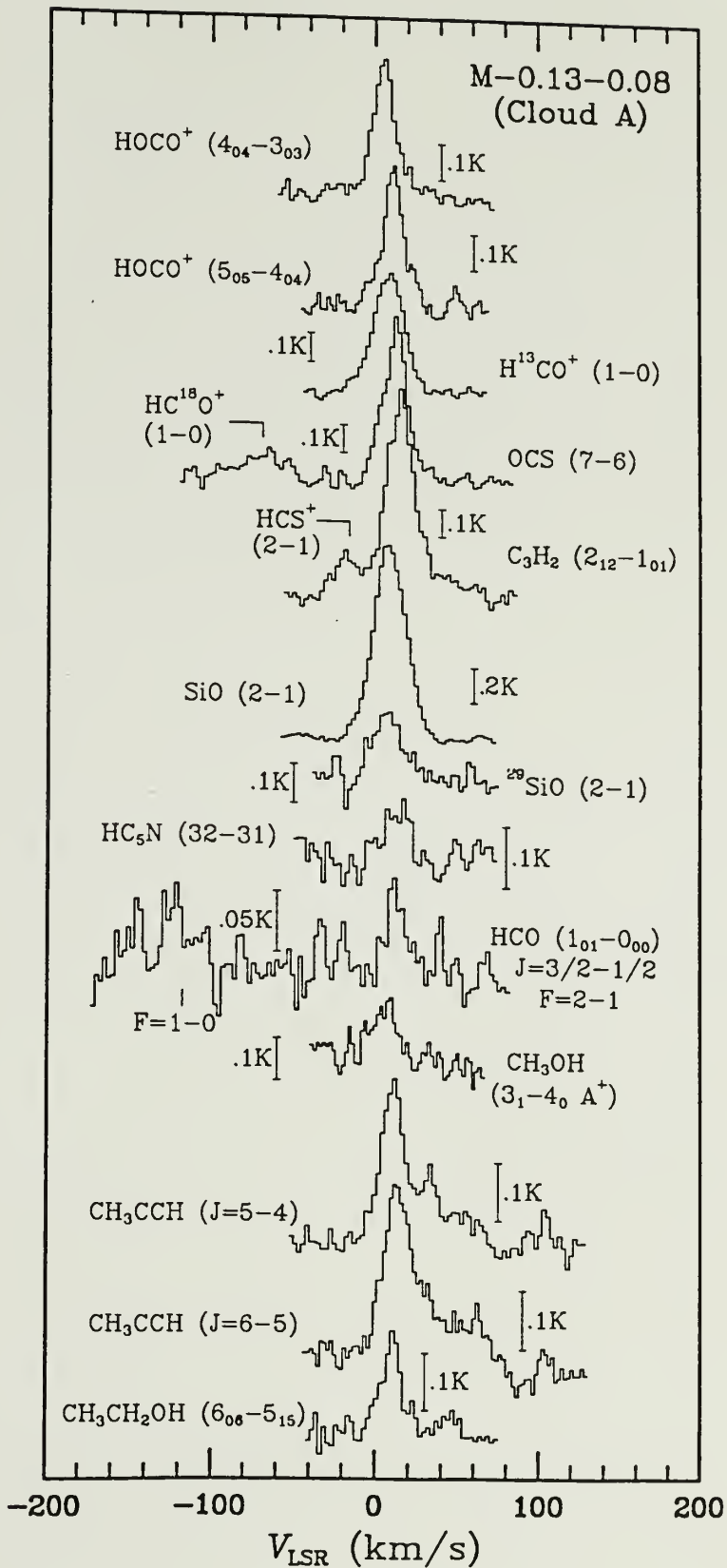
Line Parameters for the Observed Transitions

| Molecule | (Transition) | $T_A^*$ (K) | $\int T_A^* dV$ (K km s$^{-1}$) | $V_{LSR}$ (km s$^{-1}$) |
|---|---|---|---|---|
| | | M-0.13-0.08 (Cloud A) | | |
| $H^{13}CO^+$ | (1 - 0) | 0.41 | 10.4 | 9.1 |
| $HC^{18}O^+$ | (1 - 0) | 0.11 | 2.3 | 10.9 |
| HCO | $(1_{01} - 0_{00})^a$ | 0.09 | 1.0 | 11.7 |
| $HCS^+$ | (2 - 1) | 0.16 | 1.7 | 13.2 |
| OCS | (7 - 6) | 0.60 | 10.4 | 12.1 |
| $C_3H_2$ | $(2_{12} - 1_{01})$ | 0.74 | 15.9 | 15.2 |
| SiO | (2 - 1) | 1.10 | 30.5 | 7.8 |
| $^{29}SiO$ | (2 - 1) | 0.19 | 4.3 | 8.7 |
| $HC_5N$ | (32 - 31) | 0.11 | 1.8 | 12.2 |
| $CH_3OH$ | $(3_1 - 4_0\ A^+)$ | -0.15 | -2.5 | 9.6 |
| HCOOH | $(4_{14} - 3_{13})$ | ≤ 0.06 | — | — |
| $CH_3CH_2OH$ | $(6_{06} - 5_{15})$ | 0.20 | 3.2 | 10.7 |
| | | M-0.13-0.08 (Cloud A/S) | | |
| $H^{13}CO^+$ | (1 - 0) | 0.56 | 12.4 | 18.6 |
| $HC^{18}O^+$ | (1 - 0) | 0.10 | 1.7 | 20.6 |
| HCO | $(1_{01} - 0_{00})^a$ | 0.05 | 1.0 | 19.0 |
| $HCS^+$ | (2 - 1) | 0.15 | 1.7 | 27.4 |
| OCS | (7 - 6) | 0.64 | 13.4 | 19.4 |
| $C_3H_2$ | $(2_{12} - 1_{01})$ | 0.68 | 13.4 | 19.4 |
| SiO | (2 - 1) | 1.71 | 40.2 | 15.0 |
| $^{29}SiO$ | (2 - 1) | 0.21 | 3.5 | 20.8 |
| $HC_5N$ | (32 - 31) | 0.10 | 2.0 | 15.0 |
| $CH_3OH$ | $(3_1 - 4_0\ A^+)$ | -0.14 | -2.2 | 23.1 |
| HCOOH | $(4_{14} - 3_{13})$ | 0.11 | 2.2 | 23.3 |
| $CH_3CH_2OH$ | $(6_{06} - 5_{15})$ | 0.22 | 3.3 | 18.0 |

| Molecule | (Transition) | $T_A^*$ (K) | $\int T_A^* dV$ (K km s$^{-1}$) | $V_{LSR}$ (km s$^{-1}$) |
|---|---|---|---|---|
| M-0.02-0.07 (Cloud B) | | | | |
| $H^{13}CO^+$ | (1 - 0) | 0.38 | 11.2 | 47.1 |
| $HC^{18}O^+$ | (1 - 0) | 0.10 | 1.8 | 54.5 |
| HCO | $(1_{01} - 0_{00})$ | 0.04 | 0.7 | 49.5 |
| $HCS^+$ | (2 - 1) | 0.32 | 4.3 | 51.5 |
| OCS | (7 - 6) | 0.50 | 12.3 | 46.1 |
| $C_3H_2$ | $(2_{12} - 1_{01})$ | 0.45 | 13.1 | 51.4 |
| SiO | (2 - 1) | 1.44 | 46.4 | 41.2 |
| $^{29}SiO$ | (2 - 1) | 0.20 | 5.6 | 47.3 |
| $HC_5N$ | (32 - 31) | 0.08 | 1.4 | 46.7 |
| $CH_3OH$ | $(3_1 - 4_0\ A^+)$ | -0.12 | -2.3 | 44.2 |
| HCOOH | $(4_{14} - 3_{13})$ | 0.05 | 1.0 | 47.4 |
| $CH_3CH_2OH$ | $(6_{06} - 5_{15})$ | 0.16 | 3.9 | 47.1 |
| M 0.06-0.04 (Cloud C) | | | | |
| $H^{13}CO^+$ | (1 - 0) | 0.17 | 4.2 | 44.8 |
| $HC^{18}O^+$ | (1 - 0) | ≤ 0.05 | — | — |
| HCO | $(1_{01} - 0_{00})$ | ≤ 0.04 | — | — |
| $HCS^+$ | (2 - 1) | 0.09 | 0.8 | 46.6 |
| OCS | (7 - 6) | 0.18 | 3.4 | 46.1 |
| $C_3H_2$ | $(2_{12} - 1_{01})$ | 0.20 | 4.0 | 49.0 |
| SiO | (2 - 1) | 0.58 | 11.4 | 41.2 |
| $^{29}SiO$ | (2 - 1) | ≤ 0.05 | — | — |
| $HC_5N$ | (32 - 31) | 0.06 | 0.8 | 50.5 |
| $CH_3OH$ | $(3_1 - 4_0\ A^+)$ | -0.09 | -1.6 | 42.3 |
| HCOOH | $(4_{14} - 3_{13})$ | ≤ 0.05 | — | — |
| $CH_3CH_2OH$ | $(6_{06} - 5_{15})$ | 0.08 | 1.8 | 47.1 |

| Molecule | (Transition) | $T_A^*$ (K) | $\int T_A^* dV$ (K km s$^{-1}$) | $V_{LSR}$ (km s$^{-1}$) |
|---|---|---|---|---|
| M 0.07-0.08 (Cloud D) | | | | |
| H$^{13}$CO$^+$ | $(1 - 0)$ | 0.42 | 11.2 | 47.0 |
| HC$^{18}$O$^+$ | $(1 - 0)$ | 0.07 | 1.0 | 53.5 |
| HCO | $(1_{01} - 0_{00})$ | $\leq 0.06$ | — | — |
| HCS$^+$ | $(2 - 1)$ | 0.11 | 1.6 | 56.7 |
| OCS | $(7 - 6)$ | 0.29 | 5.1 | 50.9 |
| C$_3$H$_2$ | $(2_{12} - 1_{01})$ | 0.38 | 8.8 | 56.3 |
| SiO | $(2 - 1)$ | 1.00 | 28.1 | 48.3 |
| $^{29}$SiO | $(2 - 1)$ | 0.18 | 2.4 | 44.9 |
| HC$_5$N | $(32 - 31)$ | 0.05 | 0.7 | 46.0 |
| CH$_3$OH | $(3_1 - 4_0$ A$^+)$ | -0.18 | -2.5 | 46.2 |
| HCOOH | $(4_{14} - 3_{13})$ | $\leq 0.05$ | — | — |
| CH$_3$CH$_2$OH | $(6_{06} - 5_{15})$ | 0.10 | 1.8 | 54.3 |
| M 0.10-0.01 (Cloud E) | | | | |
| H$^{13}$CO$^+$ | $(1 - 0)$ | 0.26 | 4.7 | 44.8 |
| HC$^{18}$O$^+$ | $(1 - 0)$ | 0.06 | 1.1 | 41.4 |
| HCO | $(1_{01} - 0_{00})$ | $\leq 0.04$ | — | — |
| HCS$^+$ | $(2 - 1)$ | 0.17 | 1.8 | 48.0 |
| OCS | $(7 - 6)$ | 0.23 | 4.8 | 48.5 |
| C$_3$H$_2$ | $(2_{12} - 1_{01})$ | 0.23 | 6.3 | 53.9 |
| SiO | $(2 - 1)$ | 0.70 | 12.9 | 48.3 |
| $^{29}$SiO | $(2 - 1)$ | 0.10 | 1.5 | 41.6 |
| HC$_5$N | $(32 - 31)$ | 0.06 | 0.8 | 43.6 |
| CH$_3$OH | $(3_1 - 4_0$ A$^+)$ | -0.18 | -2.5 | 46.2 |
| HCOOH | $(4_{14} - 3_{13})$ | $\leq 0.06$ | — | — |
| CH$_3$CH$_2$OH | $(6_{06} - 5_{15})$ | 0.14 | 1.9 | 44.6 |

| Molecule | (Transition) | $T_A^*$ (K) | $\int T_A^* dV$ (K km s$^{-1}$) | $V_{LSR}$ (km s$^{-1}$) |
|---|---|---|---|---|
| M 0.11-0.08 (Cloud F) | | | | |
| $H^{13}CO^+$ | (1 - 0) | 0.49 | 11.5 | 51.9 |
| $HC^{18}O^+$ | (1 - 0) | 0.12 | 1.5 | 46.6 |
| HCO | $(1_{01} - 0_{00})$ | 0.07 | 0.7 | 55.1 |
| $HCS^+$ | (2 - 1) | 0.16 | 1.5 | 58.4 |
| OCS | (7 - 6) | 0.50 | 11.9 | 50.9 |
| $C_3H_2$ | $(2_{12} - 1_{01})$ | 0.36 | 7.2 | 58.7 |
| SiO | (2 - 1) | 1.47 | 44.8 | 53.1 |
| $^{29}$SiO | (2 - 1) | 0.24 | 5.6 | 49.7 |
| $HC_5N$ | (32 - 31) | 0.10 | 1.6 | 48.5 |
| $CH_3OH$ | $(3_1 - 4_0\ A^+)$ | -0.13 | -3.1 | 42.3 |
| HCOOH | $(4_{14} - 3_{13})$ | 0.08 | 1.0 | 54.6 |
| $CH_3CH_2OH$ | $(6_{06} - 5_{15})$ | 0.15 | 3.2 | 49.5 |
| M 0.25+0.01 (Cloud G) | | | | |
| $H^{13}CO^+$ | (1 - 0) | 0.22 | 5.6 | 35.2 |
| $HC^{18}O^+$ | (1 - 0) | 0.06 | 0.8 | 37.1 |
| HCO | $(1_{01} - 0_{00})$ | ≤ 0.05 | — | — |
| $HCS^+$ | (2 - 1) | 0.08 | 1.5 | 36.0 |
| OCS | (7 - 6) | 0.15 | 5.9 | 36.7 |
| $C_3H_2$ | $(2_{12} - 1_{01})$ | 0.19 | 7.5 | 39.4 |
| SiO | (2 - 1) | 0.52 | 19.0 | 31.6 |
| $^{29}$SiO | (2 - 1) | 0.12 | 1.6 | 31.7 |
| $HC_5N$ | (32 - 31) | 0.09 | 0.6 | 19.7 |
| $CH_3OH$ | $(3_1 - 4_0\ A^+)$ | -0.17 | -3.4 | 25.0 |
| HCOOH | $(4_{14} - 3_{13})$ | 0.09 | 1.1 | 39.0 |
| $CH_3CH_2OH$ | $(6_{06} - 5_{15})$ | 0.10 | 2.0 | 42.5 |

[a] For $J = 3/2 - 1/2$, $F = 2 - 1$.  NOTE.- Upper limits are 3 $\sigma$.
Spectral resolution is 0.69 MHz and the typical rms value is ~20 mK.

TABLE B.3

Gaussian Fit Parameters for CH$_3$CCH

| Transition | | Cloud A | | Cloud A/S | | Cloud B | |
|---|---|---|---|---|---|---|---|
| | | $T_A^*$ (K) | $\Delta V$ (km s$^{-1}$) | $T_A^*$ (K) | $\Delta V$ (km s$^{-1}$) | $T_A^*$ (K) | $\Delta V$ (km s$^{-1}$) |
| J=5-4 | K=0 | 0.16 | 18.8 | 0.11 | 20.6 | 0.14 | 19.7 |
| | K=1 | 0.15 | 11.5 | 0.10 | 17.0 | 0.15 | 24.9 |
| | K=2 | 0.12 | 16.0 | 0.07 | 15.4 | 0.09 | 16.9 |
| | K=3 | 0.06 | 21.8 | 0.08 | 17.0 | 0.08 | 20.4 |
| | K=4 | 0.04 | 19.2 | 0.04 | 17.0 | 0.04 | 14.6 |
| J=6-5 | K=0 | 0.19 | 17.2 | 0.16 | 23.7 | 0.18 | 20.9 |
| | K=1 | 0.13 | 19.0 | 0.18 | 14.7 | 0.16 | 21.1 |
| | K=2 | 0.09 | 16.6 | 0.09 | 14.6 | 0.13 | 17.7 |
| | K=3 | 0.09 | 15.0 | 0.10 | 15.8 | 0.11 | 18.0 |
| | K=4 | ≤0.02 | — | 0.03 | 9.0 | 0.05 | 16.9 |

| Transition | | Cloud C | | Cloud D | | Cloud E | |
|---|---|---|---|---|---|---|---|
| | | $T_A^*$ (K) | $\Delta V$ (km s$^{-1}$) | $T_A^*$ (K) | $\Delta V$ (km s$^{-1}$) | $T_A^*$ (K) | $\Delta V$ (km s$^{-1}$) |
| J=5-4 | K=0 | 0.05 | 16.3 | 0.07 | 23.7 | 0.07 | 17.9 |
| | K=1 | 0.07 | 10.7 | 0.10 | 15.6 | 0.06 | 25.1 |
| | K=2 | 0.02 | 14.8 | 0.05 | 14.7 | 0.09 | 14.5 |
| | K=3 | 0.04 | 19.5 | 0.05 | 18.5 | 0.07 | 18.8 |
| | K=4 | 0.02 | 10.2 | ≤0.02 | — | 0.05 | 16.0 |
| J=6-5 | K=0 | 0.06 | 17.2 | 0.11 | 15.7 | 0.08 | 20.5 |
| | K=1 | 0.07 | 15.0 | 0.12 | 13.9 | 0.10 | 17.0 |
| | K=2 | 0.04 | 10.3 | 0.08 | 13.1 | 0.07 | 19.7 |
| | K=3 | 0.05 | 13.0 | 0.10 | 10.6 | 0.05 | 21.5 |
| | K=4 | 0.02 | 10.0 | 0.03 | 14.3 | ≤0.02 | — |

TABLE B.3

(Continued)

| Transition | | Cloud F | | Cloud G | |
|---|---|---|---|---|---|
| | | $T_A^*$ (K) | $\Delta V$ (km s$^{-1}$) | $T_A^*$ (K) | $\Delta V$ (km s$^{-1}$) |
| J=5-4 | K=0 | 0.10 | 25.2 | 0.14 | 21.4 |
| | K=1 | 0.08 | 19.4 | 0.14 | 16.1 |
| | K=2 | 0.08 | 14.6 | 0.08 | 18.8 |
| | K=3 | 0.07 | 17.9 | 0.11 | 15.9 |
| | K=4 | 0.03 | 13.1 | ≤0.02 | — |
| J=6-5 | K=0 | 0.11 | 18.6 | 0.15 | 21.7 |
| | K=1 | 0.10 | 14.5 | 0.16 | 21.4 |
| | K=2 | 0.06 | 15.8 | 0.12 | 12.2 |
| | K=3 | 0.10 | 19.3 | 0.10 | 15.0 |
| | K=4 | 0.03 | 14.2 | 0.03 | 14.2 |

Figure B.2    Rotation diagrams for $CH_3CCH$ J = 5 - 4 and 6 - 5

transitions obtained at the center of each Cloud.    Data are

listed in Table B.3 and error bars indicate 3 $\sigma$ values.

$I$ in the ordinate is $I$ =

$$[3k \ (J+1) \ S(I,0) \ / \ 8\pi^3 \ \nu \ \mu^2 \ \{(J+1)^2 - K^2\} \ S(I,K)] \int T_A^* dV \ / \ \eta_B,$$

and see the notation in Hollis *et al.* (1981).
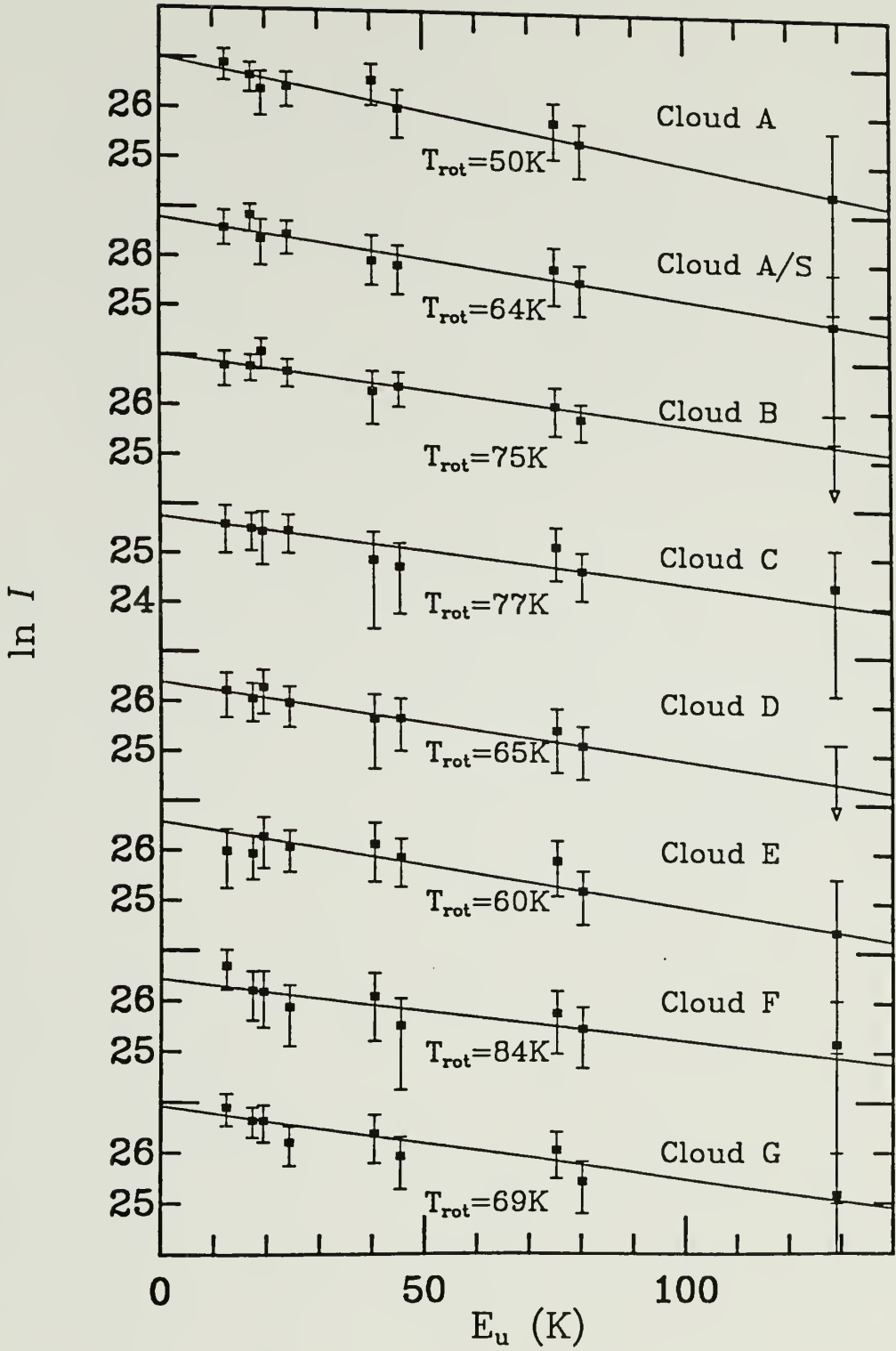
TABLE B.4

Column Densities of Observed Molecules ($cm^{-2}$)

| Cloud / Molecule | A/S | B | C | D | E | F | G |
|---|---|---|---|---|---|---|---|
| $H^{13}CO^+$ | 2(13) | 2(13) | 7(12) | 2(13) | 7(12) | 2(13) | 9(12) |
| $HC^{18}O^+$ | 3(12) | 3(12) | ≤2(12) | 2(12) | 2(12) | 2(12) | 1(12) |
| HCO | 9(13) | 6(13) | ≤8(13) | ≤1(14) | ≤7(13) | 6(13) | ≤9(13) |
| $HCS^+$ | 2(13) | 4(13) | 8(12) | 2(13) | 2(13) | 2(13) | 2(13) |
| OCS | 2(15) | 2(15) | 6(14) | 9(14) | 9(14) | 2(15) | 1(15) |
| $C_3H_2$ | 2(14) | 2(14) | 6(13) | 1(14) | 9(13) | 1(14) | 1(14) |
| SiO | 1(14) | 2(14) | 4(13) | 1(14) | 5(13) | 2(14) | 7(13) |
| $^{29}SiO$ | 2(13) | 3(13) | ≤5(12) | 1(13) | 7(12) | 3(13) | 7(12) |
| $HC_5N$ | 8(13) | 6(13) | 3(13) | 3(13) | 3(13) | 7(13) | 3(13) |
| $CH_3CCH$ | 1(15) | 2(15) | 6(14) | 1(15) | 1(15) | 2(15) | 2(15) |
| HCOOH | 2(14) | 1(14) | ≤1(14) | ≤1(14) | ≤1(14) | 1(14) | 1(14) |
| $CH_3CH_2OH$ | 9(14) | 1(15) | 5(14) | 5(14) | 5(14) | 9(14) | 5(14) |

NOTE. - Numbers in parentheses are powers of 10. Positions given in Table B.2. Assumes optically thin emission and Boltzmann population distributions.

TABLE B.5

Comparison of Fractional Abundances relative to Molecular Hydrogen

| Molecule | Sgr A | Sgr B2 | TMC-1 |
|---|---|---|---|
| $HCO^+$ | — | 8 (-9) | 1 (-8) |
| $H^{13}CO^+$ | 3 (-10) | — | — |
| $HC^{18}O^+$ | 3 (-11) | — | — |
| HCO | 1 (-9 ) | — | — |
| $HCS^+$ | 2 (-10) | 2 (-10) | 6 (-10) |
| OCS | 2 (-8) | 1 (-8) | 2 (-9) |
| $C_3H_2$ | 2 (-9) | 1 (-9) | 2 (-8) |
| SiO | 2 (-9) | 4 (-10) | $\leq$ 5 (-12) |
| $^{29}SiO$ | 3 (-10) | — | — |
| $HC_5N$ | 5 (-10) | 4 (-10) | 3 (-9) |
| $CH_3CCH$ | 2 (-8) | 4 (-9) | 6 (-9) |
| HCOOH | 1 (-9) | 2 (-9) | — |
| $CH_3CH_2OH$ | 1 (-8) | 3 (-9) | — |

NOTE.- Numbers in parentheses are powers of 10.   Data for Sgr B2
and TMC-1 were adopted from the table of Irvine, Goldsmith, and
Hjalmarson (1987).

BIBLIOGRAPHY

Allen, M. and Robinson, G. W. 1975, *Ap. J.*, 195, 81.

Allen, M. and Robinson, G. W. 1977, *Ap. J.*, 212, 396.

Andersson, M. 1985, in *(Sub)Millimeter Astronomy*, eds. P. A. Shaver and K. Kjar, ESO Conf. Workshop Proc. No.22, p. 353.

Armstrong, J. T., and Barrett, A. H. 1984, *Ap. J. Suppl.*, 57, 535.

Askne, J., Hoglund, B., Hjalmarson, A., and Irvine, W. M. 1984, *Astr. Ap.*, 130, 311.

Batrla, W., Wilson, T. L., Bastien, P., and Ruf, K. 1983, *Astr. Ap.*, 128, 279.

Becklin, E. E., Gatley, I., and Werner, M. W. 1982, *Ap. J.*, 258, 134.

Bogey, M., Demuynck, C., Destombes, J. L. 1984, *Astr. Ap.*, 138, L11.

Booth, R. S. *et al.* 1989, *Astr. Ap.*, 216, 315.

Brown, R. L. and Liszt, H. S. 1984, *Ann. Rev. Astr. Ap.*, 22, 223.

Brown, P. D. and Millar, T. J. 1989, *M. N. R. A. S.*, 237, 661.

Blake, G. A., Sutton, E. C., Masson, C. R., and Phillips, T. G. 1987, *Ap. J.*, 315, 621.

Campell, B. and Thompson, R. I. 1984, *Ap. J.*, 279, 650.

Castor, J. I. 1970, *M. N. R. A. S.*, 149, 111.

Charnley, S. B., Dyson, J. E., Hartquist, T. W., and Williams, D. A. 1988, *M. N. R. A. S.*, 231, 269.

Churchwell, E., and Hollis, J. M. 1983, *Ap. J.*, 272, 591.

Churchwell, E., Wood, D., Myers, P. C., and Myers, R. V. 1986, *Ap. J.*, 305, 405.

Cummins, S. E., Linke, R. A., and Thaddeus, P. 1986, *Ap. J. Suppl.*, 60, 819.

Cupp, R. E., Kempf, R. A., and Gallagher, J. J. 1968, *Phys. Rev.*, 171, 60.

Dalgarno, A., Black, J. H., and Weisheit, J. C. 1973, *Ap. Letters*, 14, 77.

Davis, D. S., Larson, H. P., and Smith, H. A. 1982, *Ap. J.*, 259, 166.

deJong, T., Chu, S. -L., and Dalgarno, A. 1975, *Ap. J.*, 199, 69.

DeNoyer, L. K. and Frerking, M. A. 1981, *Ap. J. (Letters)*, 246, L37.

Dent, W. A., Werner, M. W., Gately, I., Becklin, E. E., Hildebrand, R. H., Keene, J., and Whitcomb, S. E. 1982, in *The Galactic Center*, eds. G. R. Riegler and R. D. Blandford (New York: Am. Inst. Phys.), p. 33.

d'Hendecourt, L. B., Allamandola, L. J., and Greenberg, J. M. 1985, *Astr. Ap.*, 152, 130.

d'Hendecourt, L. B. and Muizon, Jourdain de, M. 1989, *Astr. Ap.*, in press.

Dopita, M. A. 1977, *Astr. Ap.*, 56, 303.

Drain, B. T. and Salpeter, E. E. 1979, *Ap. J.*, 231, 77.

Duley, W. W., Millar, T. J., and  Williams, D. A. 1980, *M. N. R. A. S.*, 192, 945.

Evans, II, N. J. and Blair, G. N. 1981, *Ap. J.*, 246, 394.

Friberg, P. and Hjalmarson, A. 1989, in *Molecular Astrophysics*, ed. T. Hartquist (Cambridge: Cambridge University Press), in press.

Gardner, F. F., Höglund,B., Shukre, C., Stark, A. A., and Wilson, T. L. 1985, *Astr. Ap.*, 146, 303.

Gatley, I., Becklin, E. E., Werner, M. W., and Harper, D. A. 1978, *Ap. J.*, 220, 822.

Gately, I., Hasegawa, T., Suzuki, H., Garden, R., Brand, P., Lightfoot, J., Glencross, W., Okuda, H., and Nagata, T. 1987, *Ap. J. (Letters)*, 318, L73.

Geballe, T. R., Baas, F., Greenberg, J. M., and Schutte, W. 1985, *Astr. Ap.*, 146, L6.

Genzel, R. *et al.* 1978, *Astr. Ap.*, 66, 13.

Genzel, R. and Downes, D. 1977, *Astr. Ap.*, 61, 117.

Genzel, R. and Downes, D. 1982, in *Regions of Recent Star Formation*, eds. R. S. Roger and P. E. Dewdney (Dordrecht: Reidel), p. 251.

Genzel, R., Downes, D., Ho, P. T. P., and Bieging, J. H. 1982, *Ap. J. (Letters)*, 259, L103.

Genzel, R., Watson, D. M., Townes, C. H., Dinerstein, H. L., Hollenbach, D., Lester, D. F., and Werner, M. 1984, *Ap. J.*, 276, 551.

Gerry, M. C. L., Yamada, K., and Winnewisser, G. 1979, *J. Phys. Chem. Ref. Data*, 8, 107.

Goldreich, P. and Kwan, J. 1974, *Ap. J.*, 189, 441.

Goldsmith, P. F. and Mao, X.- J. 1983, *Ap. J.*, 265, 791.

Goldsmith, P. F., Irvine, W. M., Hjalmarson, A., Elldér, J. 1986, *Ap. J.*, 310, 383.

Goldsmith, P. F., Krotkov, R., Snell, R. L., Brown, R. D., and Godfrey, P. 1983, *Ap. J.*, 274, 184.

Goldsmith, P. F., Snell, R. L., Hasegawa, T., and Ukita, N. 1987, *Ap. J.*, 314, 525.

Graff, M. M., and Dalgarno, A. 1987, *Ap. J.*, 317, 432.

Green, S., Garrison, B. J., Lester, Jr.,W. A., and Miller, W. H. 1978, *Ap. J. Suppl.*, 37, 321.

Green, S., Schor, H., Siegbahn, P., and Thaddeus, P. 1976, *Chem. Phys.*, 17, 479.

Greenberg, J. M. 1963, *Ann. Rev. Astr. Ap.*, 15, 267.

Greenberg, J. M. 1989, in *Chemistry in Space*, eds. J. M. Greenberg and V. Pirronello (Dordrecht: Kluwer Academic Press), in press.

Greenberg, J. M., Allamandola, L. J., Hagen, W., van de Bult, C. E. P., and Baas, F. 1980, in *Interstellar Molecules*, ed. B. H. Andrew (Dordrecht: Reidel), p. 355.

Grim, R. J. A. and Greenberg, J. M. 1987, *Astr. Ap.*, 181, 168.

Guélin, M., and Cernicharo, J. 1989, in *The Physics and Chemistry of Interstellar Molecular Clouds*, ed. G. Winnewisser (Berlin: Springer-Verlag), in press.

Güsten, R., and Henkel, C. 1983, *Astr. Ap.*, 126, 136.

Güsten, R., Walmsley, C. M., and Pauls, T. 1981, *Astr. Ap.*, 103, 197.

Hagen, W., Allamandola, L. J., and Greenberg, J. M. 1980, *Astr. Ap.*, 86, L3.

Harris, A. Townes, C. H., Matsakis, D. N., and Palmer, P. 1983, *Ap. J. (Letters)*, 265, L63.

Hartquist, T. W., Oppenheimer, M., and Dalgarno, A. 1980, *Ap. J.*, 236, 182.

Hasegawa, T., Gately, I., Garden, R. P., Brand, P., Ohishi, M., Hayashi, M., and Kaifu, N. 1987, *Ap. J. (Letters)*, 318, L77.

Helminger, P., De Lucia, F. C., and Kirchhoff, W. H. 1973, *J. Phys. Chem. Ref. Data*, 2, 215.

Herbst, E., Adams, N. G., and Smith, D. 1983, *Ap. J.*, 269, 329.

Herbst, E., DeFrees, D. J., and Koch, W. 1989, *M. N. R. A. S.*, 237, 1057.

Herbst, E., Green, S., Thaddeus, P., and Klemperer, W. 1977, *Ap. J.* 215, 503.

Herbst, E. and Leung, C. M. 1986a, *M. N. R. A. S.*, 222, 689.

Herbst, E. and Leung, C. M. 1986b, *Ap. J.*, 310, 378.

Herd, C. R., Adams, N. G., and Smith, D. 1989, preprint.

Hildebrand, R. H., Whitcomb, S. E., Winston, R., Stiening, R. F., Harper, D. A., and Moseley, S. H. 1978, *Ap. J. (Letters)*, 219, L101.

Hollenbach, D. J. and Salpeter, E. E. 1971, *Ap. J.*, 163, 155.

Hollis, J. M., Snyder, L. E., Blake, D. H., Lovas, F. J., Suenram, R. D., and Ulich, B. L. 1981, *Ap. J.*, 251, 541.

Huang, Y.-L., Dickman, R. L., and Snell, R. L. 1986, *Ap. J. (Letters)*, 302, L63.

Irvine, W. M., Avery, L. W., Friberg, P., Matthews, H. E., and Ziurys, L. M. 1987, in *Interstellar Matter*, eds. J. M. Moran and P. T. P. Ho (New York: Gordon and Breach), p. 15.

Irvine, W. M., Friberg, P., Kaifu, N., Kawaguchi, K., Kitamura, Y.,
    Matthews, H. E., Minh, Y. C., Saito, S., Ukita, N., and
    Yamamoto, S. 1989, *Ap. J.*, 342, 871.

Irvine, W. M., Goldsmith, P. F., and Hjalmarson, Á. 1987, in
    *Interstellar Processes*, eds. D. J. Hollenbach and H. A.
    Thronson, Jr. (Dordrecht: Reidel), p. 561.

Irvine, W. M., Good, J. C., and Schloerb, F. P. 1983, *Astr. Ap.*,
    127, L10.

Irvine, W. M. and Hjalmarson, A. 1984, *Origins Life*, 14, 15.

Irvine, W. M., and Knacke, R. F. 1989, in *The Origin and Evolution
    of Planetary Atmospheres*, eds. S. K. Atreya, J. B. Pollack, and
    M. S. Matthews (Tucson: U.Arizona), p.3.

Irvine, W. M. and Schloerb, F. P. 1984, *Ap. J.*, 282, 516.

Irvine, W. M., Schloerb, F. P., Hjalmarson, Â., and Herbst E. 1985,
    in *Protostars and Planets II*, eds. D. C. Black and M. S.
    Matthews (Tucson: U. Arizona), p. 579.

Johansson, L. E. B., Andersson, C., Elldér, J., Friberg, P.,
    Hjalmarson, A., Höglund, B., Irvine, W. M., Olofsson, H., and
    Rydbeck, G. 1984, *Astr. Ap.*, 130, 227.

Kahane, C., Frerking, M. A., Langer, W. D., Encrenaz, P., and
    Lucas, R. 1984, *Astr. Ap.*, 137, 211.

Kameya, O., Hasegawa, T. I., Hirano, N., Takakubo, K. 1989, *Ap. J.*,
    339, 222.

Knacke, R. F., Geballe, T. R., Noll, K. S., and Tokunaga, A. T.
    1985, *Ap. J. (Letters)*, 298, L67.

Knacke, R. F., McCorkle, S., Puetter, R. C., Erickson, E. F.,
    and Kratschmer, W. 1982, *Ap. J.*, 260, 141.

Knowles, S. H., Johnston, K. J., Moran, J. M., Burke, B. F., Lo,
    K. Y., and Papadopoulos, G. D. 1974, *Ap. J.*, 79, 925.

Krugel, E., Stenholm, L. G., Steppe, H.,and Sherwood, W. A. 1983,
    *Astr. Ap.*, 127, 195.

Lacy, J. H., Baas, F., Allamandolar, L. J., Persson, S. E.,
    McGregor, P. J., Lonsdale, C. J., Geballe, T. R., and van de
    Bult, C. E. P. 1984, *Ap. J.*, 276, 533.

Leger, A., Jura, M., and Omont, A. 1985, *Astr. Ap.*, 144, 147.

Lester, D. F., Werner, M. W., Storey, J. W. V., Watson, D. M., and Townes, C. H. 1981, *Ap. J. (Letters)*, 248, L109.

Leung, C. M., Herbst, E., and Huebner, W. F. 1984, *Ap. J. Suppl.*, 56, 231.

Linke, R. A., Guelin, M., and Langer, W. D. 1983, *Ap. J. (Letters)*, 271, L85.

Linke, R. A., Stark, A. A., Frerking, M. A. 1981, *Ap. J.*, 243, 147.

Lis, D. L. 1989, Ph. D. Thesis. University of Massachusetts.

Liszt, H. S. 1978, *Ap. J.*, 219, 454.

Liszt, H. S. and Vanden Bout, P. A. 1985, *Ap. J.*, 291, 178.

Loren, R. B. 1984, *MWO Spectral Line Detections from 128 to 357 GHz, 1979-1984*, Tech. Rept. AST 8116403-7.

Lovas, F. J. 1982, *J. Phys. Chem. Ref. Data*, 11, 251.

Lovas, F. J. 1986, *J. Phys. Chem. Ref. Data*, 15, 251.

Lovas, F. J. 1989, *Recommended Frequencies of the Interstellar Molecules*.

Matthews, H. E. and Sears, T. J. 1983a, *Ap. J. (Letters)*, 267, L53.

Matthews, H. E. and Sears, T. J. 1983b, *Ap. J.*, 272, 149.

Millar, T. J. 1982, *M. N. R. A. S.*, 199, 309.

Millar, T. J., Adams, N. G., Smith, D., Lindinger, W., and Villinger, H. 1986, *M. N. R. A. S.*, 221, 673.

Millar, T. J., Bennett, A., and Herbst, E. 1989, *Ap. J.*, 340, 906.

Millar, T. J. and Nejad, L. A. M. 1985, *M. N. R. A. S.*, 217, 507.

Mitchell, G. F. 1984, *Ap. J.*, 287, 665.

Minh, Y. C. and Irvine, W. M. 1989, in preparation.

Minh, Y. C., Irvine, W. M., and Ziurys, L. M. 1988, *Ap. J.*, 334, 175.

Minh, Y. C., Irvine, W. M., and Ziurys, L. M. 1989, *Ap. J. (Letters)*, 345, L63.

Minh, Y. C., Irvine, W. M., Ziurys, L. M., and McGonagle, D. 1989, in preparation.

Morris, M., Polish, N., Zuckerman, B., and Kaifu, N. 1983, *A. J.*, **88**, 1228.

Olano, C. A., Walmsley, C. M., and Wilson, T. L. 1988, *Astr. Ap.*, **196**, 194.

Oort, J. H. 1977, *Ann. Rev. Astr. Ap.*, **15**, 295.

Penzias, A. A. 1980, *Science*, **208**, 663.

Pineau des Forets, G., Roueff, E., and Flower, D. R. 1986, *M. N. R. A. S.*, **220**, 801.

Pineau des Forets, G., Roueff, E., and Flower, D. R. 1989, preprint.

Plambeck, R. L. and Wright, M. C. H. 1987, *Ap. J. (Letters)*, **330**, L61.

Plambeck, R. L., Wright, M. C. H., Welch, W. J., Bieging, J. H., Baud, B., Ho, P. T. P., and Vogel, S. N. 1982, *Ap. J.*, **259**, 617.

Poynter, R. L. and Pickett, H. M. 1984, *Submillimeter, Millimeter, and Microwave Spectral Line Catalogue* (JPL Pub. 80-23, Rev. 2).

Prasad, S. S. and Huntress, Jr., W. T. 1979, *Ap. J.*, **228**, 123.

Prasad, S. S. and Huntress, Jr., W. T. 1982, *Ap. J.*, **260**, 590.

Prasad, S. S., Tarafdar, S. P., Villere, K. R., and Huntress, Jr., W. T. 1987, in *Interstellar Processes*, eds. D. J. Hollenbach and H. A. Thronson, Jr. (Dordrecht: Reidel), p. 631.

Righini, G., Simon, M., and Joyce, R. R. 1976, *Ap. J.*, **207**, 119.

Saito, S., Kawaguchi, K., Yamamoto, S., Ohishi, M., Suzuki, H., and Kaifu, N. 1987, *Ap. J. (Letters)*, **317**, L115.

Schenewerk, M. S., Snyder, L. E., and Hjalmarson, A. 1986, *Ap. J. (Letters)*, **303**, L71.

Schloerb, F. P., Friberg, P., Hjalmarson, Á., Höglund, B., and Irvine, W. M. 1983, *Ap. J.*, **264**, 161.

Schloerb, F. P., Snell, R. L.,and Young, J. S. 1983, *Ap. J.*, **267**, 163.

Schmid-Burgk, J., Densing, R., Krugel, E., Nett, H., Roser, H. P., Schafer, F., Schwaab, G., van der Wal, P., and Wattenbach, R. 1989, *Astr. Ap.*, **215**, 150.

Scoville, N. Z., Sargent, A. I., Sanders, D. B., Claussen, M. J., Masson, C. R., Lo, K. Y., and Phillips, T. G. 1986, *Ap. J.*, **303**, 416.

Scoville, N. Z. and Solomon, P. M. 1973, *Ap. J.*, **180**, 31.

Scoville, N. Z. and Solomon, P. M. 1974, *Ap. J. (Letters)*, **187**, L67.

Scoville, N. Z., Solomon, P. M., and Penzias, A. A. 1975, *Ap. J.*, **201**, 352.

Sinclair, M. W., Fourikis, N., Ribes, J. C., Robinson, B. J., Brown, R. D., and Godfrey, P. D. 1973, *Australian J. Phys.*, **26**, 85.

Snell, R. L. and Wootten, A. 1979, *Ap. J.*, **228**, 748.

Smith, I. W. M. 1988, *M. N. R. A. S.*, **234**, 1059.

Smith, D., and Adams, N. G. 1985, in *Molecular Astrophsics*, eds. G. H. F. Diercksen *et al*. (Dordrecht: Reidel), p. 453.

Smith, J., Lynch, D. K., Cudaback, D., and Werner, M. 1979, *Ap. J.*, **234**, 902.

Snell, R. L. 1981, *Ap. J. Suppl.*, **45**, 121.

Sobolov, V. V. 1960, *Moving Envelopes of Stars* (Cambridge: Harvard University Press).

Spitzer, L., Drake, J. F., Jenkins, E. B., Morton, D. C., Rogerson, J. B., and York, D. G. 1973, *Ap. J. (Letters)*, **181**, L116.

Sutton, E. C., Blake, G. A., Masson, C. R., and Phillips, T. G. 1985, *Ap. J. Suppl.*, **58**, 341.

Swade, D. A. 1987, Ph. D. Thesis, University of Massachusetts.

Swade, D. A. 1989, *Ap. J. Suppl.*, **71**, 219.

Sweitzer, J. S. 1978, *Ap. J.*, **225**, 116.

Takayanagi, K., Sakimoto, K., and Onda, K. 1987, *Ap. J. (Letters)*, **318**, L81.

Thaddeus, P., Gûelin, M., and Linke, R. A. 1981, *Ap. J. (Letters)*, **246**, L41.

Thaddeus, P., Kutner, M. L., Penzias, A. A., Wilson, R. W., and Jefferts, K. B. 1972, *Ap. J. (Letters)*, 176, L73.

Tielens, A. G. G. M. and Allamandola, L. J. 1987, in *Interstellar Processes*, eds. D. Hollenbach and H. Thronson (Dordrecht: Reidel), p. 397.

Tielens, A. G. G. M. and Allamandola, L. J., Bregman, J., Goebel, J., d'Hendecourt, L. B., and Witteborn, F. C. 1984, *Ap. J.*, 287, 697.

Tielens, A. G. G. M. and Hagen, W. 1982, *Astr. Ap.*, 114, 245.

Turner, B. E.,and Thaddeus, P. 1977, *Ap. J.*, 211, 755.

Vanden Bout, P. A., Loren, R. B., Snell, R. L., and Wootten, A. 1983, *Ap. J.*, 271, 161.

Van Dishoeck, E. F., and Black, J. H. 1988, in *Physical Processes in Interstellar Clouds*, ed. M.Scholer (Dordrecht: Reidel),in press.

Vogel, S. N., Wright, M. C. H., Plambeck, R. L., and Welch, W. J. 1984, *Ap. J.*, 283, 655.

Walmsley, C. M., Hermsen, W., Henkel, C, Mauersberger, R., and Wilson, T. L. 1987, *Astr. Ap.*, 172, 311.

Watson, W. D. and Salpeter, E. E. 1972, *Ap. J.*, 174, 321.

Watson, W. D. and Walmsley, C. M. 1982, in *Regions of Recent Star Formation*, eds. R. S. Roger and P. E. Dewdney (Dordrecht: Reidel), p. 357.

Werner, M. W., Becklin, E. E., Gatley, I., Matthews, K., and Neugebaur, C. G. 1979. *M. N. R. A. S.*, 188, 463.

Wilner, S. P. 1984, in *Galactic and Extragalactic Infrared Spectroscopy*, eds. M. F. Kessler and J. P. Phillips (Dordrecht: Reidel), p. 37.

Wilson, T. L. and Walmsley, C. M. 1989, *Astr. Ap. Rev.*, 1, 141.

Winnewisser, G. and Herbst, E. 1987, *Topics in Current Chemistry*, 139, 119.

Wootten, A., Snell, R., and Evans II, N. J. 1980, *Ap. J.*, 240, 532.

Wynn-Williams, C. G., Becklin, E. E., and Neugebaur, G. 1974, *Ap. J.*, 187, 473.

Wynn-Williams, C. G., Werner, M. W., and Wilson, W. J. 1974, *Ap. J.*, **187**, 41.

Yamamoto, S., Saito, S., Kawaguchi, K., Kaifu, N., Suzuki, H., and Ohishi, M. 1987, *Ap. J. (Letters)*, **317**, L119.

Ziurys, L. M., Erickson, N. R., and Grosslein, R. M. 1988, in *Interstellar Matter*, eds. J. M. Moran and P. T. P. Ho (New York: Gordon and Breach), p. 255.

Ziurys, L. M. and Friberg, P. 1987, *Ap. J. (Letters)*, **314**, L49.

Ziurys, L. M., Snell, R. L., and Dickman, R. L. 1988, in *Molecular Clouds in the Milky Way and External Galaxies*, eds. R. L. Dickman, R. L. Snell, and J. S. Young (Berlin: Springer-Verlag), p. 184.

Ziurys, L. M., Wilson, T. L., and Mauersberger R. 1989, preprint.